An investigation into protein and lipid binding by the phosphatidylinositol transfer protein RdgBβ

Kathryn Lucy Garner

A thesis submitted to University College London for the degree of Doctor of Philosophy

June 2012

Department of Neuroscience, Physiology and Pharmacology,
University College London

I, Kathryn Lucy Garner, confirm that the work presented in this thesis is my own. Where information has been derived from other sources, I confirm that this has been indicated in the thesis.

Signed .....

For my nan

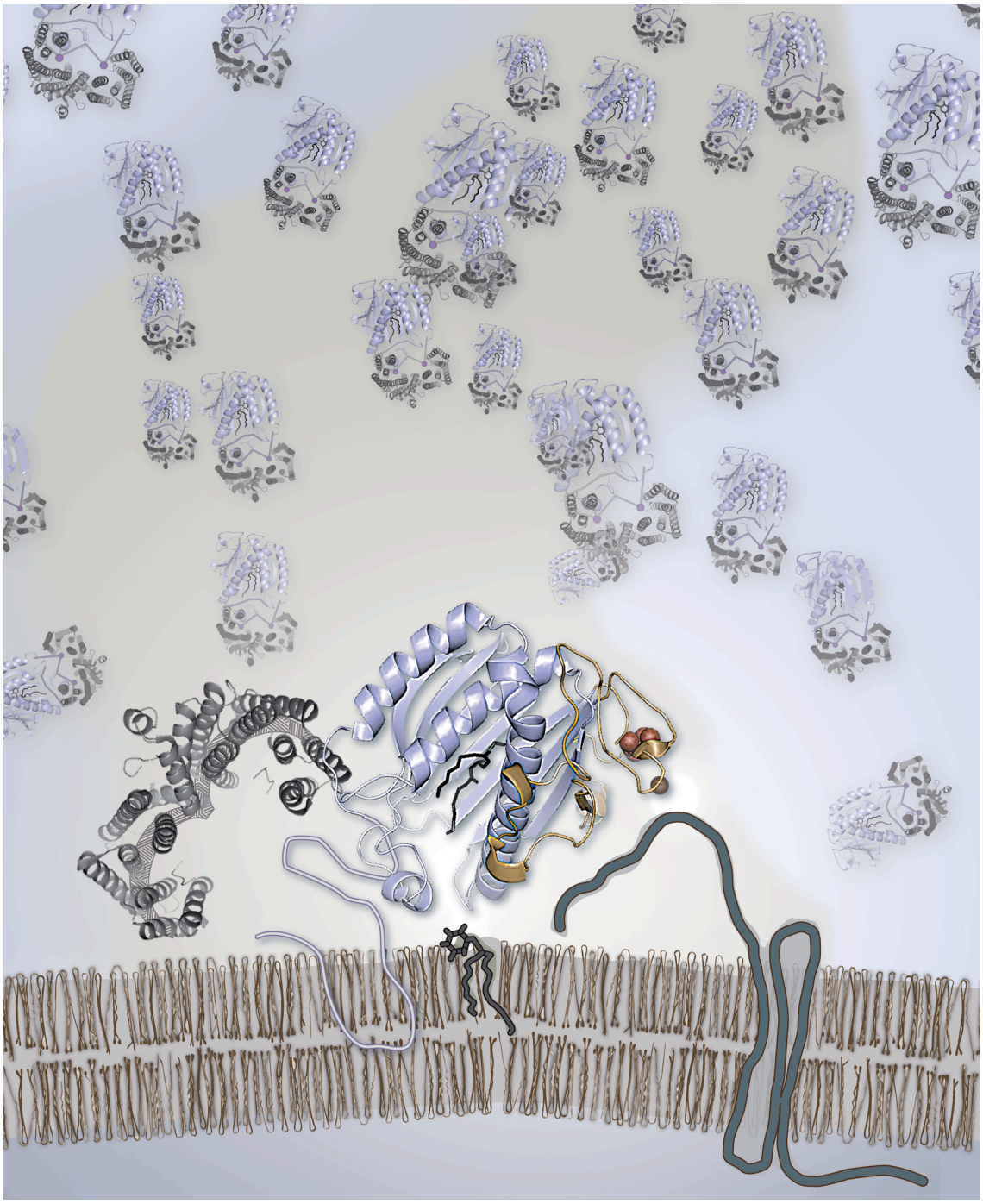

K & H Garner, 2012.

Abstract

The phosphatidylinositol transfer proteins (PITPs) are a family of lipid carrier proteins that bind and transfer phosphatidylinositol (PI) and phosphatidylcholine (PC) between membranes. PITPs are commonly involved in phosphoinositide-requiring processes, including phospholipase C and PI 3-kinase signalling, and membrane trafficking. In this study I focus on the uncharacterised soluble PITP, RdgBβ (*PITPNC1*). The lipid binding and transfer properties of RdgBβ have scarcely been characterised, and the function of RdgBβ is completely unknown. I uncover that RdgBβ interacts with 14-3-3 through its long, disordered C-terminus. RdgBβ is ubiquitinated and subject to rapid degradation in cells, and binding of 14-3-3 via two phosphorylated residues may serve to protect the protein from protease digestion. Whereas RdgBβ binds 14-3-3 under basal conditions, I deduce that, upon stimulation of cells with phorbol ester, RdgBβ binds the Angiotensin II receptor (AT_1R)-associated protein, ATRAP, via its N-terminal PITP domain. Others have shown that ATRAP suppresses Angiotensin II signalling by uncoupling AT_1R from G proteins and promoting AT_1R internalisation. I find that the RdgBβ-ATRAP interaction is blocked by inhibition of protein kinase C or protein synthesis, and may function to re-localise RdgBβ to the membrane in stimulated cells. Unexpectedly, I find that RdgBβ binds PI and phosphatic acid (PA), rather than PI and PC, and that binding of PA is increased by stimulation of cells with GTPγS. Mass spectrometry is used to analyse the molecular species of PI and PA bound by RdgBβ, and reveals that whereas RdgBβ is non-selective in its binding of PI, it selects short-chain monounsaturated or saturated PA species, likely derived from the hydrolysis of PC by phospholipase D.

Acknowledgements

I'd like to thank Michelle Li for the technical support and companionship in the lab. All of the mass spectrometry was carried out and data analysed by our collaborators, Dr. Alan Hunt and Grielof Koster at the University of Southampton. Dr. Andrew Martin gave me guidance for producing the comparative model of the RdgBβ PITP domain and subsequent mapping of the lipid-binding cavity. Dr. Julie Pitcher provided the immunoprecipitation protocol and guided me on the design of my first experiment.

On a personal note I'd like to thank my husband, Hugh Garner, for his unrelenting belief in me and my abilities. He never complained when I returned home late from the lab or woke up early at the weekends to study. (Well, except once, when his foot was in plaster.) I'd also like to thank my auntie, Ruth Leman, for her incredible support, particularly during the latter part of this project. Dr. Sandip Patel (now Prof.), Dr. Dev Churamani and Robert Hooper (now Dr.) kept me entertained for hours outside of the lab and participated in useful discussions about science in their more sober moments.

Last, but by no means least, I wish to thank my supervisor, Prof. Shamshad Cockcroft, for making this project possible and for pushing me and the project forward. She always encouraged me to ask the big questions and without her I would not have had the courage to do the crazy 'look-see' experiments, which have in no doubt yielded the most interesting results.

This work was funded by the British Heart Foundation, to whom I am enormously thankful.

Contents

List of Figures

List of Tables

Publications

Garner K, Hunt A N, Koster G, Somerharju P, Groves E, Li M, Padinjat R, Holic R and Cockcroft S (2012). RdgBβ (PITPNC1) of the class II PITP family binds and transfers Phosphatidic Acid. *Submitted to the Journal of Biological Chemistry.*

Cockcroft S and Garner K (2012). 14-3-3 and ATRAP bind to the soluble Class IIB phosphatidylinositol transfer protein RdgBβ at distinct sites. Biochemical Society Transactions. *40* (2): 451-6. PMID: 22435829. *Review.*

Garner K, Li M, Ugwuanya N and Cockcroft S (2011). The phosphatidylinositol transfer protein, RdgBβ binds 14-3-3 via its unstructured C-terminus, whereas its lipid binding domain interacts with the integral membrane protein, ATRAP (Angiotensin II Type I Receptor-associated Protein). Biochemical Journal. *439* (1): 97-111. PMID: 21728994.

Cockcroft S and Garner K (2011). 'Function of the phosphatidylinositol transfer protein gene family: is phosphatidylinositol transfer the mechanism of action?' Critical Reviews in Biochemistry and Molecular Biology. *46* (2): 89-117. PMID: 21275878. *Review*.

Abbreviations

aa	Amino acids
APS	Ammonium persulphate
ARF	Adenosine diphosphate-ribosylation factor
AT_1R	Angiotensin II type 1 receptor
ATP	Adenosine triphosphate
ATRAP	Angiotensin II receptor-associated protein
AVP	Another void program
BCA	Bicinchoninic acid
BDNF	Brain-derived neurotrophic factor
BIM-I	Bisindolylmaleimide I, PKC inhibitor
BOPIDY	Boron-dipyrromethene, fluorescent dye
bp	Base pairs
BSA	Bovine serum albumin
CAML	Calcium-modulating cyclophilin ligand
cDNA	Complementary deoxyribonucleic acid
CDP	Cytidine diphosphate
cds	*Drosophila* CDP-DAG synthase mutant
CERT	Ceramide transporter
CHX	Cycloheximide
CL	Cardiolipin
CMV	Cytomegalovirus
COPI	Coat protein complex I
COS-7	CV-1 (simian) in origin carrying the SV40 genetic material, cell line
DAG	Diacylglycerol
DCC	Deleted in colorectal cancer
DDK	Protein tag composed of aspartic acid and lysine residues (FLAG)
DGK	Diacylglycerol kinase
DIG	Digoxigenin
Dm	*Drosophila melanogaster*
DMEM	Dulbecco's modified Eagle's medium
DMSO	Dimethyl sulfoxide
DOPE	Discrete optimised protein energy
dpm	Disintegrations per minute
dsDNA	Double-stranded deoxyribonucleic acid
DSS	Disuccinimidyl suberate

ECFP	Enhanced cyan fluorescent protein
ECL	Enhanced chemoluminescence
EDTA	Ethylenediaminetetraacetic acid
EGF	Epidermal growth factor
EGFP	Enhanced green fluorescent protein
ENTH	Epsin N-terminal homology
ER	Endoplasmic reticulum
ERG	Electroretinogram
ERGIC	ER-Golgi intermediate compartment
ERK1/2	Extracellular signal-related kinase 1/2
ESI-MS/MS	Tandem electrospray ionisation mass spectrometry
FCS	Foetal calf serum
FLAG	Protein tag composed of aspartic acid and lysine residues (DDK)
FYVE	Fab1, YOTB, Vac1 and EEA1
GBF1	Golgi-specific brefeldin A-resistant guanine nucleotide exchange factor 1
GFP	Green fluorescent protein
GPCR	G protein-coupled receptor
GRK	G protein-coupled receptor kinase
GST	Glutathione *S*-transferase
GTP	Guanosine triphosphate
GTPγS	Guanosine 5'-O-[gamma-thio]triphosphate
HA	Haemagglutinin
HEK293	Human embryonic kidney cell line
HEPES	4-(2-hydroxyethyl)-1-piperazineethanesulfonic acid
HI	Heat-inactivated
HL60	Human (promyelocytic) leukaemia cell line
HRP	Horseradish peroxidase
IP	Immunoprecipitate/Immunoprecipitation
IP_3	Inositol trisphosphate; $I(1,4,5)P_3$
IPTG	Isopropyl β-*D*-1-thiogalactopyranoside
kb	Kilo base pairs
KDEL	Lysine, aspartic acid, glutamic acid and leucine amino acid motif
LB	Luria broth
LY	LY294002
MAP	Mitogen-activated protein
MCS	Multiple cloning site
mRNA	Messenger ribonucleic acid

Myc	Myelocytomatosis
NEB	New England Biolabs
NEM	*N*-ethylmaleimide
OSBP	Oxysterol-binding protein
PA	Phosphatidic acid
PAP	Phosphatidic acid phosphatase
PBD	Polo box domain
PBS(-T)	Phosphate-buffered saline(-tween)
PC	Phosphatidylcholine
PC12	Pheochromocytoma, neuroendocrine cell line
pcDNA	Plasmid complementary deoxyribonucleic acid
PCR	Polymerase chain reaction
PDB	Protein databank
PDME	Phosphatidyl-*N*,*N*-dimethylethanolamine
PE	Phosphatidylethanolamine
PEST	Protein sequence rich in proline, glutamic acid, serine and threonine residues
PG	Phosphatidylglycerol
PH	Pleckstrin homology
PI	Phosphatidylinositol
PI3K	Phosphatidylinositol 3-kinase
PI4K	Phosphatidylinositol 4-kinase
PI4P-5-K	Phosphatidylinositol-4-phosphate 5-kinase
PIP	Phosphatidylinositol phosphate; PI(3)P, PI(4)P, PI(4)P
PIP_2	Phosphatidylinositol bisphosphate; $PI(4,5)P_2$, $PI(3,5)P_2$, $PI(3,4)P_2$
PIP_3	Phosphatidylinositol trisphosphate; $PI(3,4,5)P_3$
PIPES	1,4-Piperazinediethanesulfonic acid
PIS	Phosphatidylinositol synthase
PITP	Phosphatidylinositol transfer protein
PKA	Protein kinase A
PKB	Protein kinase B (Akt)
PKC	Protein kinase C
PKD	Protein kinase D
PLC	Phospholipase C
PLD	Phospholipase D
Plk1	Polo-like kinase 1
PMA	Phorbol 12-myristate 13-acetate

PMME	Phosphatidyl-*N*-monomethylamine
PS	Phosphatidylserine
PTEN	Phosphatase and tensin homologue
PVDF	Polyvinylidene fluoride
RACK1	Receptor for activated C kinase
RdgB	Retinal degeneration B
RIPA	Radioimmunoprecipitation assay
RNAi	Ribonucleic acid interference
RPMI	Roswell Park Memorial Institute
RT	Room temperature
RT-PCR	Reverse transcription-polymerase chain reaction
SD	Standard deviation
SDS	Sodium dodecyl sulphate
SDS-PAGE	Sodium dodecyl sulphate-polyacrylamide gel electrophoresis
SEM	Standard error of the mean
SET	Sucrose-EDTA-Tris
siRNA	Small interfering ribonucleic acid
SLO	Streptolysin O
SM	Sphingomyelin
SRC	Subrhabdomeric cisternae
StAR	Steroidogenic acute regulatory protein
START	StAR-related lipid transfer
TAE	Tris-acetate-EDTA
TBS(-T)	Tris-buffered saline(-tween)
TEMED	*N,N,N',N'*-tetramethylethylenediamine
TGN	*Trans*-Golgi network
TLC	Thin layer chromatography
T_m	Melting temperature
TNP-PE	*N*-trinitrophenyl-phosphatidylethanolamine
TX-100	Triton X-100
VAP	(Vesicle-associated membrane protein) VAMP-associated protein
VSMC	Vascular smooth muscle cells
VSV	Vesicular stomatitis virus
WB	Western blot
WT	Wild-type
WW	Two conserved tryptophan proline-rich peptide binding motif

CHAPTER 1: Introduction

1.1: Phosphoinositides and phosphatidylinositol transfer proteins

Phosphoinositides are essential components of all eukaryotic cell membranes. They are derived from the phosphorylation of the phospholipid, phosphatidylinositol (PI), at positions 3, 4 and 5 of its inositol head group (Figure 1.1), to produce seven phosphorylated derivatives. Whereas PI itself only constitutes ~5-7% of the total cellular lipids, the phosphoinositides make up just over a tenth of this amount, the major bulk of which is PI(4)P and PI(4,5)P_2. Phosphoinositides form docking sites for protein effectors containing membrane-interaction domains, such as PH, FYVE and ENTH domains, and act as precursors of many second messengers. Different species of phosphoinositide have unique distributions across intracellular membranes, brought about partly by the differential distribution of the enzymes that generate or modify them. Phosphoinositides form part of a dynamic protein-lipid interaction network capable of regulating a multitude of cellular processes, including cell growth and survival through signal transduction and ion channel modulation, cytoskeletal dynamics and membrane trafficking. Almost all of the structural lipids or their precursors are synthesised at the endoplasmic reticulum (ER), and so the phosphoinositides must reach their destination either via vesicular transport, or with the help of lipid carrier proteins (Figure 1.2). One such lipid carrier, a key regulator in the distribution of phosphoinositides, is the phosphatidylinositol transfer protein (PITP).

There are five members of the PITP family in humans (Figure 1.3 A, p. 49): three members of the family are small, soluble proteins (PITPα, PITPβ and RdgBβ), whereas the RdgBα I and II proteins are large, multi-domain, membrane-associated proteins. The PITPs are characterised by the presence of a PITP domain at their N-terminus; the class I proteins, PITPα and PITPβ, bind a single molecule of either PI or phosphatidylcholine (PC) in the lipid-binding cavity of this domain (Figure 1.3 B). It is becoming clear that the PI-binding and transfer activity of distinct PITPs is vital in almost all processes involving phosphoinositides. I begin this section by discussing the role of phosphoinositides in particular biological processes with respect to PITPs, and then

progress to an analysis of PITP function at the molecular level. An emerging theme is one in which PITP presents PI to PI kinases for phosphorylation to PI(3)P or PI(4)P.

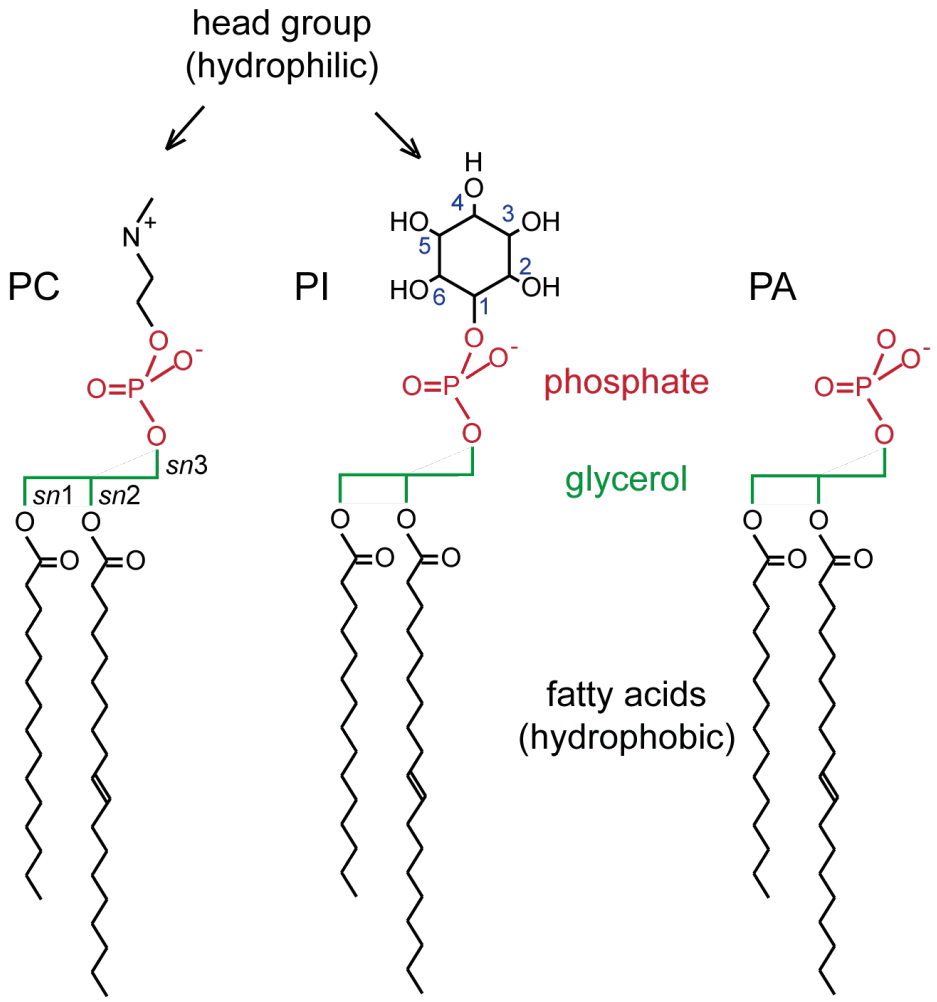

Figure 1.1: The structure of key phospholipids: PC, PI and PA.

Molecular structures of PC, PI and phosphatidic acid (PA). The head groups of PC and PI are indicated beyond the phosphate group, which is in red; the glycerol backbone is indicated in green, and the fatty acid/acyl chains indicated, attached to positions *sn*1 and *sn*2 of the glycerol moiety. The numbering of the inositol head group hydroxyl groups is indicated in blue.

1.1.1: PITP and Signal Transduction: PLC and PI3K

Reconstitution of PLC activity in permeabilised cell assays

Multiple studies report roles for PITP family members in phospholipase C (PLC) signalling (Figure 1.2). The first mammalian PITP was purified from bovine brain cytosol in 1974 (Helmkamp et al., 1974). When the second PITP was cloned in 1994 (Tanaka and Hosaka, 1994), the first PITP was renamed PITPα, and the second, PITPβ. Prior to this, in 1993, a requirement of PITP for PLC activity was established (Thomas et al., 1993). When HL60 cells were permeabilised by streptolysin O (SLO), which forms large lesions in the cell membrane by sequestering cholesterol, cytosolic proteins were observed to leak out (Stutchfield and Cockcroft, 1988). By 10-15 mins, the ability of GTPγS to activate PLCβ was greatly diminished (Thomas et al., 1991). There are six families of PLC enzymes in mammalian cells (PLCβ, γ, δ, ε ζ and η), each with differing characteristics and activation requirements. The predominant PLC isoforms in HL60 cells washed of cytosol were found to be PLC-β2 and PLC-β3 (Thomas et al., 1993). GTPγS is a poorly-hydrolysable analogue of GTP and therefore is a potent activator of G proteins. PLCβ isoforms are activated by α or βγ subunits of the $G_{q/11}$ family of heterotrimeric G proteins (specificity varies according to the PLCβ isoform), and therefore are activated downstream of GTPγS. It was identified that bovine brain cytosol was able to reconstitute PLC activity, and the reconstituting factor was purified, sequence determined and protein identified as PITP (Thomas et al., 1993). Since PITP transfers PI between membranes *in vitro*, it was proposed that PITP delivers PI from its site of synthesis at the ER to the plasma membrane for phosphorylation by lipid kinases to $PI(4,5)P_2$, the substrate of PLC (Figure 1.2). In these experiments, PITP was essential for the sustained activity of PLCβ, and reconstitution increased linearly as more PITP was added.

(Facing page) Figure 1.2: Phosphoinositide metabolism and the PI cycle.

PI is synthesised at the ER and transported to distal intracellular membranes by PITPs or vesicular transport. PI is phosphorylated by lipid kinases such as PI 4-kinase (PI4K) and PI4P 5-kinase (PI4P-5-K). PI(4,5)P_2 has many functions, including hydrolysis by PLC in response to an appropriate stimulus, to produce the second messengers, diacylglycerol (DAG) and inositol trisphosphate (IP_3). IP_3 promotes Ca^{2+} release from intracellular stores, and this Ca^{2+}, together with DAG, activates protein kinase C (PKC). DAG may then be phosphorylated to PA by DAG kinase (DGK). PA is also produced by the hydrolysis of PC by phospholipase D (PLD). PI re-synthesis occurs at the ER, the location of the two key enzymes in this process, cytidine diphosphate (CDP)-DAG synthase and PI synthase (PIS), and therefore either DAG or, more likely, PA, must be transferred back to the ER (mechanism unknown). PAP, PA phosphatase.

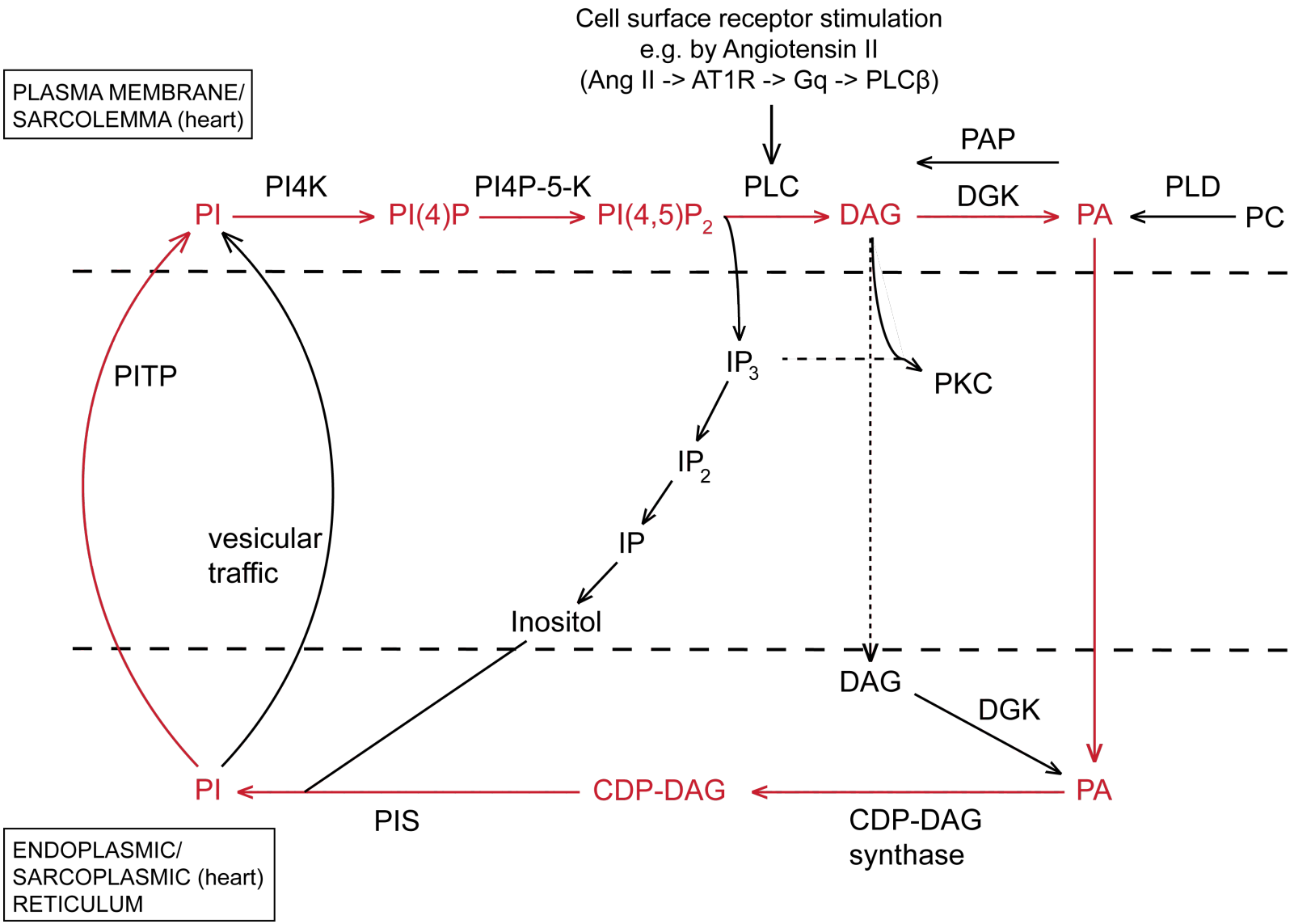
Cell surface receptor stimulation
e.g. by Angiotensin II
(Ang II -> AT1R -> Gq -> PLCβ)
PLASMA MEMBRANE/
SARCOLEMMA (heart)
PAP
PI4K
PI4P-5-K
PLC
DGK
PLD
PI
PI(4)P
PI(4,5)P2
DAG
PA
PC
IP3
PKC
PITP
IP2
IP
vesicular
traffic
Inositol
DAG
DGK
PI
CDP-DAG
PA
PIS
CDP-DAG
synthase
ENDOPLASMIC/
SARCOPLASMIC (heart)
RETICULUM

PLCγ is activated downstream of tyrosine kinases, such as the receptor tyrosine kinase, epidermal growth factor (EGF) receptor, as well as non-receptor tyrosine kinases of the Src family, such as Lyn and Syk. PLCγ is a soluble protein, recruited to activated membrane proteins by binding to phospho-tyrosine residues via its SH2 domains. Since PLCγ would be lost during permeabilisation with SLO, examination of the effect of PITP on PLCγ activity in permeabilised cells required that purified PLCγ be titrated back into the system, along with appropriate stimulus and recombinant PITP. As for GTPγS-stimulated PLCβ in HL60 cells, PITP was found to be required for the reconstitution of receptor tyrosine kinase (EGF)-stimulated PLC activity in SLO-permeabilised A431 human epidermoid carcinoma cells; the addition of EGF and PLCγ alone was insufficient for restoration of the activity (Kauffmann-Zeh et al., 1995). A similar requirement for PITP was demonstrated in antigen-stimulated RBL-2H3 cells, where PLCγ is activated downstream of the Fc receptor via non-receptor tyrosine kinases (Cunningham et al., 1996). The ability of PITP to reconstitute the activity of both PLCβ and PLCγ indicates a PLC isoform-independent function for PITP.

It was initially assumed that PLC would use up all available PIP_2 in the local membrane, and that PITP would only be required to deliver more PI from the ER once the signalling membrane PIP_2 (and therefore PI and PIP) stocks had been exhausted. One study estimated that there was sufficient PI in the plasma membrane of permeabilised HL60 cells to maintain PLC activity linearly for 20 min when the cells were stimulated with GTPγS (Cunningham et al., 1995). It was therefore expected that PITP addition would not affect the initial rate of inositol lipid hydrolysis (at <20 min), only the ability of PLC to sustain this rate. However, upon addition of PITP, the initial rate of inositol phosphate production was greatly increased in response to 10 μM GTPγS, in contrast to GTPγS alone (Cunningham et al., 1995). Another experiment monitored the decline in inositol lipid hydrolysis upon permeabilisation. The decline was observed to exactly match the exit of PITP from the cytosol (Cunningham et al., 1995).

The amount of inositol trisphosphate (IP_3) made upon stimulation with GTPγS in the presence of PITP is far greater than the amount of PIP_2 present in cells, indicating that the lipid kinases, PI 4-kinase (PI4K), which phosphorylates PI at the 4'-OH position of

the inositol head group to PI(4)P, and PI4-P 5-kinase (PI4P-5-K), which phosphorylates PI(4)P at the 5'-OH position to PI(4,5)P_2, must be able to carry out their functions on demand. In cells permeabilised in the presence of 100 μM Mg-ATP and 10 μCi [γ-^{32}P]-ATP, stimulation with GTPγS increased the amount of radioactivity associated with PIP_2 more rapidly than in control cells (Cunningham et al., 1995), indicating the ability of GTPγS to stimulate lipid kinase activity. Here the activity of both kinases, PI4K and PI4P-5-K, was found to be associated with membranes and therefore not lost upon permeabilisation. Upon permeabilisation of the HL60 cells to remove endogenous PITP prior to the addition of GTPγS, synthesis of PIP_2 was impaired, and was only regained upon addition of exogenous PITP (Cunningham et al., 1995). The authors interpret this observation as PITP exerting a direct effect on lipid kinase activity, which they say explains why reconstitution of PLC signalling by PITP is absolutely dependent on the presence of Mg-ATP (Thomas et al., 1993). These interpretations gave rise to the 'Lipid Presentation' model of PITP function (Figure 1.5 B, p. 61) (Cunningham et al., 1995).

As in HL60 cells, the PI4K regulated by EGF in A431 cells is membrane-associated and therefore not lost from cells during permeabilisation. The activity of endogenous PI4K was measured in response to differing combinations of exogenously-added EGF, PITP and PLCγ. Addition of each component individually did not increase PI4K activity, only the addition of EGF and PITP together increased the amount of phosphorylated PI (PIP and PIP_2) present (Kauffmann-Zeh et al., 1995). The further addition of PLCγ resulted in the phosphorylated PI species being barely detectable, likely due to the rapid hydrolysis of PIP_2 by PLCγ. That PITP is required for PI4K activity as well as PLC activity, and that the dose response of PLCγ activity to PITP is similar to that of PI phosphorylation by PI4K, again indicates that the target of PITPs might be PI4K rather than the PLC itself.

RdgBα and PLC signalling in the fly eye

The *rdgB* mutant was one of the first *Drosophila* retinal degeneration mutants identified (Hotta and Benzer, 1969), characterised by an abnormal termination of the light response in the photoreceptor cells of the eye and a profound loss of the electroretinogram (ERG) amplitude shortly after initial light exposure. The mutant fly

also suffered light-enhanced retinal degeneration. The gene responsible was identified in 1991 (Vihtelic et al., 1991), and subsequent analysis of the protein product revealed a 160 kDa membrane-associated protein with 281 N-terminal residues that shared >40% identity to the rat brain PITP (Vihtelic et al., 1993). The identification of this protein founded the class II PITPs, and gave them their alternate name, Retinal degeneration type B (RdgB) (Figure 1.3 A, p. 49).

The *Drosophila* photoreceptor cell is a giant polarized cell whose apical domain forms the specialised light-sensing organelle, known as the rhabdomere. This organelle consists of closely packed photoreceptive microvilli. In the *rdgB* mutant, the rhabdomeric membrane undergoes vesiculation and is internalised and lost, resulting in a reduction in the size of the apical membrane. *Drosophila melanogaster* (*Dm*)-RdgBα localises to the region immediately beneath the light-sensing rhabdomeric membrane, the subrhabdomeric cisternae (SRC), as well as to the adjacent plasma membrane (Vihtelic et al., 1993). This subrhabdomeric region is continuous with the main ER system of the photoreceptor, the site where PI synthesis occurs. Visual transduction is mediated by the PLC-catalysed hydrolysis of $PI(4,5)P_2$, and mutation of enzymes involved in PI re-synthesis all lead to retinal degeneration. This includes mutation of CDP-DAG synthase in the *cds* mutant, which is unable to sustain a light-activated current (Wu et al., 1995). Furthermore, neither the *rdgB* nor the *cds* mutant was able to promote recovery from inactivation for the *trp* (*transient receptor potential*) mutant phenotype, in which Ca^{2+} entry into the rhabdomere is prevented (Hardie et al., 2001). It is understood that Ca^{2+} inhibits PIP_2 hydrolysis, and so a functioning PI re-synthesis pathway is required to overcome this defect.

Detection of light by the G protein-coupled receptor (GPCR) rhodopsin leads to the activation of PLCβ (NorpA) via the heterotrimeric G protein, G_q. Since the SRC lies in such close proximity to the rhabdomeric membrane above (~10 nm), it is hypothesised that Dm-RdgBα remains associated with the SRC via hydrophobic regions of its sequence, whilst its N-terminal PITP domain 'swings' between the SRC and the rhabdomere to deliver PI. The membrane-anchoring domains are not essential for its function, however, as expression of the Dm-RdgBα PITP domain in *rdgB* mutant flies

was sufficient to restore the wild-type electrophysiological light response and prevent degeneration (Milligan et al., 1997).

PITPα, PLC and PI3K in axonal outgrowth

PITPα plays a crucial role in the developing nervous system: mutation of the gene encoding PITPα, *PITPNA*, was found to be responsible for the *vibrator* mouse mutant phenotype (Hamilton et al., 1997). This mouse had a rapid action tremor and died within 30 days of birth (<P30). Neurones of the spinal cord, dorsal root ganglia, brainstem and cerebellum showed progressive degeneration, with dilated ER in the neurone cell bodies, dendrites and axons, eventually progressing to severe intracellular vacuolation and some cell death (Weimar et al., 1982).

Wiring of the nervous system is informed by extracellular guidance factors, which attract or repel the growth cones at the tips of developing neurones. Attracting substances include growth factors, such as netrin-1 and brain-derived neurotrophic factor (BDNF), and components of the extracellular matrix, such as laminin. Cortical explants derived from E15 *vibrator* mice (PITPα^{vb} mice), shown to have a 5-fold reduction in PITPα protein expression, extended only a few short processes under basal conditions, similar to wild-type neurones. However, the number and length of processes was significantly reduced relative to wild-type explants when growth was stimulated by netrin-1 (Xie et al., 2005). Process elongation induced by BDNF was also attenuated. Similarly, hippocampal neurones grown on poly-L-lysine (a non-stimulatory substratum) and treated with *PITPNA* siRNA, which reduced PITPα protein levels by ~70%, exhibited a morphology comparable to control neurones. When the same neurones were grown on laminin, however, a significant reduction in axonal length was observed for the PITPα-knockdown cells (Cosker et al., 2008).

PITPα expression is enriched in the brain. An analysis of developing rat E18 hippocampal neurones indicated the specific presence of PITPα protein in the axonal processes, including growth cones, and its expression was found to increase during the first few days of development (Cosker et al., 2008). This localisation contrasts with that reported in COS-7 cells, in which PITPα was observed throughout the cytoplasm and

nucleus (Larijani et al., 2003), indicating that PITPα could have specific binding partners in axons which determine its discrete localisation.

DCC ('Deleted in colorectal cancer'), and the closely-related protein, neogenin, are cell surface receptors that bind netrin-1 through their extracellular domains. They are transmembrane proteins, yet lack any discernible catalytic activity, and so it was initially unclear how the netrin-1 signal is transmitted into the cell interior. A yeast two-hybrid screen identified PITPα as a binding partner of DCC and neogenin, the interaction confirmed in neuronal lysates, and further experiments deduced that PITPα interacts with the P3 domain of both proteins (Xie et al., 2005). The amount of PITPα associated with DCC (or neogenin) increased 4-fold after stimulation of the neurones with netrin-1. This event was also observed in HEK-293 cells expressing DCC (or neogenin) and PITPα.

Growth cone guidance in response to netrin-1 or BDNF requires co-activation of the PLCγ and PI 3-kinase (PI3K) signalling pathways (Ming et al., 1999). In cultured wild-type cortical neurones, netrin-1 stimulated PIP_2 hydrolysis in a time-dependent manner. However, this agonist failed to induce PIP_2 hydrolysis in neurones from homozygous PITPα^{vb} mice (Xie et al., 2005). Like PLC, the substrate of PI3K is $PI(4,5)P_2$, but rather than hydrolysing it, PI3K phosphorylates PIP_2 at the 3'-OH position of its inositol ring to form $PI(3,4,5)P_3$. PI3K activity is specifically activated at the tip of the elongating axon in response to laminin stimulation. On this substratum, the effect of PITPα over-expression on axonal extension was found to be blocked by treatment with the PI 3-kinase inhibitor, LY294002 (Cosker et al., 2008). Similarly, the application of BDNF to hippocampal neurones resulted in an increase in axonal length; this effect was also attenuated by inhibition of PI3K or PITPα knockdown (Cosker et al., 2008).

The activity of PI3K activates the serine/threonine protein kinase, protein kinase B (PKB) through the local provision of $PI(3,4,5)P_3$. Stimulation of hippocampal neurones with BDNF for 1 hr or 15 hrs was observed to promote activation of PKB, as did expression of GFP-PITPα. The quantity of phosphorylated (active) PKB was ~50% higher in whole cell lysates derived from cells over-expressing PITPα compared with control-transfected cells, and immunocytochemistry revealed that the quantity of

phospho-PKB was significantly increased in the axonal growth cones (Cosker et al., 2008). Co-expression of GFP-PITPα with a dominant-negative PKB mutant, K179M, in hippocampal cells grown on laminin suppressed PITPα-promoted axonal elongation.

Together, these studies indicate a requirement for PITPα in axonal outgrowth under stimulation from netrin-1, BDNF or laminin. PITPα is specifically involved in signal transduction upstream of PIP_2 hydrolysis by PLC, and upstream of PI3K activity. Since both enzymes use the substrate $PI(4,5)P_2$, this implies that PITPα functions in the delivery of PI to the signalling membrane.

The ability of PITPα to enhance the activity of a receptor-stimulated PI3K is consistent with a previous report, where PITPα was found to be required for the reconstitution of PI3Kγ activity stimulated by fMetLeuPhe (a G_i-coupled receptor) or GTPγS in SLO-permeabilised human neutrophils washed of cytosol (Kular et al., 1997).

RdgBα in *C. elegans* sensory systems

The nematode worm, *Caenorhabditis elegans*, has a compact nervous system consisting of 302 neurones. It detects chemicals with a limited number of sensory neurones, permitting the dissection of roles for each neurone by researchers. The sensory system exhibits a plastic behaviour that changes with experience (gustatory plasticity or salt chemotaxis learning); for example, NaCl is usually an attractive taste, but animals previously soaked in a buffer containing NaCl in the absence of food show an avoidance behaviour towards NaCl rather than attraction. The ASE taste sensory (gustatory) neurones, ASEL and ASER (bilaterally symmetrical pair, left and right, respectively), play a major role in salt-attraction behaviour.

ASEL and ASER are differentially activated by salt, and each expresses different sets of receptor-type guanylyl cyclases, which mediate these responses. The switch between attraction and avoidance to salt is reversible and involves the diacylglycerol (DAG)/ protein kinase C (PKC) (Figure 1.2) and PI3K/PKB signalling pathways, which act antagonistically to one another (Adachi et al., 2010). When DAG concentration/PKC activity is high, animals display an attractive behaviour to salt, whereas when DAG/

PKC is low, animals demonstrate avoidance. Constitutive attraction behaviour towards salt is observed when the DAG/PKC pathway is activated by genetic or pharmacological manipulation. Conversely, the PI3K/PKB pathway promotes salt avoidance. PTEN is a phosphatase which removes the 3'-phosphate from $PI(3,4,5)P_3$, terminating PI3K signalling. The *daf-18* mutant, which has a mutation in the gene encoding a homologue of PTEN, avoids salt under naïve conditions (Adachi et al., 2010). (The wild-type animal is attracted to salt under the same conditions.)

A *C. elegans* mutant, *pe1209*, was identified which displayed a reduced attraction to salt compared to wild-type animals under naïve conditions, and remained attracted to salt even after NaCl conditioning (i.e. exposure to NaCl in the absence of food). These animals were found to have a mutated *pitp-1* allele, the sole *C. elegans* orthologue of RdgBα (Iwata et al., 2011). Wild-type PITP-1 expression was observed in many neurones throughout the nervous system, including the sensory neurones, ASE and AWC. (AWC neurones are olfactory neurones, which sense odorants.) The re-expression of PITP-1 in the *pitp-1* mutant *C. elegans* fully restored the behavioral defects of attraction and plasticity in the whole animal, with only partial restoration when PITP-1 re-expression was confined to ASE neurones (Iwata et al., 2011).

In contrast to the fly *rdgB* and mouse *vibrator* mutants, *C. elegans pitp-1* mutants suffered no cell morphological defects. Further to the defective salt attraction phenotype, *pitp-1* mutants were found to be deficient in chemotaxis towards odorants sensed by the AWC neurone, benzaldehyde and isoamyl alcohol, and displayed minor defects in chemotaxis to the AWA-sensed odorants, diacetyl and pyrazine. The *pitp-1* mutants also suffered from inadequate osmotic avoidance, which is mediated by the ASH sensory neurones (Iwata et al., 2011).

In the wild-type ASER neurone, PITP-1 was found mainly in a punctate pattern along the axon and cell body. It co-localised with the synaptic vesicle marker, mCherry-RAB-3 in the axon, indicating that PITP-1 is localised to pre-synaptic sites (Iwata et al., 2011). UNC-104 (KIF1A) is essential for the trafficking of synaptic vesicles from the cell body to these sites in *C. elegans*; in *unc-104* mutants, PITP-1 localisation was decreased in the axon and increased in the dendrite and cell body (Iwata et al., 2011),

confirming a requirement for functional trafficking of synaptic vesicles for the proper localisation of PITP-1.

At pre-synaptic sites, $PI(4,5)P_2$ could be required intact for the assembly of proteins involved in synaptic vesicle release at the membrane. Alternatively, its hydrolysis by PLC may be required to produce DAG, which binds Unc13 in *C. elegans*, a protein required for synaptic vesicle priming. Loss-of-function mutations in *dgk-1*, encoding DAG kinase (DGK), exhibit enhanced neurotransmission at the neuromuscular junction due to the accumulation of DAG (Miller et al., 1999; Nurrish et al., 1999). A loss-of-function mutation in *dgk-1* was observed to almost completely suppress the *pitp-1* defects in attraction to both salt and benzaldehyde, indicating the importance of DAG signalling in the promotion of attraction behaviour (Iwata et al., 2011). This suggests that PI delivered by PITP-1 to synaptic membranes is required for attraction to salt and benzaldehyde through $PI(4,5)P_2$ hydrolysis to DAG, rather than for the intact $PI(4,5)P_2$ itself.

The *dgk-1* mutation suppressed the reduced attraction phenotype, but was unable to suppress the defect in plasticity of salt chemotaxis. This indicates a requirement for other PI derivatives, $PI(4,5)P_2$ itself, $PI(3,4,5)P_3$ or IP_3 in the plasticity of chemotaxis. The involvement of the PI3K pathway in the function of PITP-1 was not examined. As in the *Drosophila rdgB* mutant, expression of the N-terminal PITP domain alone was able to rescue both behavioral phenotypes of the *pitp-1* mutant, which implies that the principle function of PITP-1 in neurotransmission and behavioral plasticity is performed by the PITP domain, and could therefore be its ability to bind and transfer PI.

In *C. elegans*, ASER does not require PITP-1 for the primary sensory response, since sensory transduction is mediated by guanylyl cyclases and cGMP-gated channels and does not require phosphoinositides. However, PITP-1 is required for the transmission of this sensory information at synapses and modulation of behaviour in response to pre-conditioning. The common feature is the involvement of RdgBα in processes involving phosphoinositides.

1.1.2: PITP and membrane trafficking

PITP in exocytosis

In secretory cells, a priming event (requiring ATP) and a triggering event (requiring Ca^{2+}) are necessary for the fusion of secretory granules with the plasma membrane. Rat brain cytosol was found to reconstitute this process in cytosol-depleted PC12 cells, and three priming-specific factors were isolated by gel filtration, PEP1-3. PEP3 was identified as PITP (Hay and Martin, 1993), whilst PEP1 was identified as a type 1 PIP 5-kinase (Hay et al., 1995). ATP is not required for PITP activity, but does provide the phosphate source for phosphorylation of PIP by PIP-5-K. Therefore, it was proposed that PITP delivered PI for phosphorylation by the type 1 PIP 5-kinase. PLC activity was found to be dispensable; here instead $PI(4,5)P_2$ is required for localisation of specific proteins to the plasma membrane to facilitate exocytosis.

In HL60 cells there is a requirement for GTP in Ca^{2+}-mediated secretion. Upon permeabilisation of these cells with SLO, the ability of GTPγS to stimulate Ca^{2+}-dependent secretion of the marker protein, hexosaminidase, was diminished as cytosolic proteins leaked from the cells. Whereas the small GTPase Rho remained associated with the HL60 cell membranes, ADP-ribosylation factor (ARF) GTPase was washed out with the other cytosolic proteins, and indeed ARF1 and ARF3 were purified as reconstitution factors for GTPγS-stimulated Ca^{2+}-mediated secretion in HL60 cells (Fensome et al., 1996). At low protein concentrations, the effect of recombinant PITP and ARF on secretion was additive, and absolutely required the presence of GTPγS. PA has been shown to activate type 1 PI4P-5-K (Jenkins et al., 1994), for the production of $PI(4,5)P_2$ from PI(4)P, and PA is a product of PC hydrolysis by phospholipase D (PLD) (Figure 1.2). In turn, ARF activates PLD, and ARF has been shown to stimulate PIP_2 production in a manner comparable to PITP (Fensome et al., 1996). It therefore seems that PITP and ARF work synergistically to make $PI(4,5)P_2$, required for the assembly of exocytosis effector proteins. PITP delivers PI to the plasma membrane for phosphorylation by PI4K to PI(4)P; meanwhile ARF GTPase activates PLD to produce PA, which stimulates a type 1 PI4P-5-K to phosphorylate PI(4)P to $PI(4,5)P_2$.

PITP in secretory vesicle formation

A cell-free post-*trans*-Golgi network (TGN) secretory vesicle formation assay has been described (Ohashi and Huttner, 1994). PC12 neuroendocrine cells were pulse-labelled with [^{35}S]-sulphate and the TGN membranes harvested by homogenisation and ultra-centrifugation steps. Cytosol ('post-nuclear supernatant'), from similar rounds of homogenisation and centrifugation of unlabelled PC12 cells was assessed for its ability to stimulate post-TGN vesicle formation. The transfer of marker proteins, heparan sulphate proteoglycan for constitutive secretory vesicles and secretogranin II for secretory granules, into the unlabelled cytosol was monitored (Ohashi and Huttner, 1994). The efficiency of post-TGN secretory vesicle formation decreased if the cytosol was diluted, indicating the requirement of a cytosolic factor for the formation of secretory vesicles from the TGN (Ohashi et al., 1995). The factor was isolated by fractionation, and was in fact found to be two proteins, PITPα and PITPβ. PITPα or PITPβ purified from bovine brain, or recombinant mouse PITPα, were each able to stimulate post-TGN secretory vesicle formation from the [^{35}S]-sulphate-labelled PC12 TGN membranes (Ohashi et al., 1995).

RdgBαI in the scission of vesicles from the TGN

The mammalian RdgBα protein was cloned as a mouse homologue of Dm-RdgBα, able to rescue the mutant fly *rdgB* phenotype (Chang et al., 1997). The mouse protein rescued both the retinal degeneration and the abnormal ERG. A second mammalian homologue, which shares 56% identical residues with the first protein, was subsequently identified (Lu et al., 1999a). The first protein was therefore renamed RdgBαI and the second, RdgBαII. Transgenic expression of RdgBαII also suppressed the retinal degeneration phenotype of the *rdgB* flies, yet unlike RdgBαI, was unable to restore the electrophysiological light responses. In mice, knock-out of the gene encoding RdgBαII, *PITPNM2*, appear normal, yet deletion of the gene encoding RdgBαI, *PITPNM1*, is embryonic lethal (Lu et al., 2001). This indicates that RdgBαI and RdgBαII perform distinct roles in mammalian cells, and that RdgBαI likely performs an essential, housekeeping role.

The RdgBα proteins were also independently identified as binding partners for the protein tyrosine kinase PYK2, and were consequently designated 'Nir' proteins (PYK2 N-terminal domain-interacting receptors) (Lev et al., 1999). There are three Nir proteins: Nir1 (*PITPNM3*) lacks the N-terminal PITP domain, Nir2 refers to RdgBαI (*PITPNM1*) and Nir3 is RdgBαII (*PITPNM2*).

RdgBα proteins are large, membrane-associated multi-domain proteins (Figure 1.3 A, p. 49). RdgBαI and Dm-RdgBα, when first cloned, were proposed to be integral membrane proteins consisting of six transmembrane domains (Vihtelic et al., 1993; Aikawa et al., 1999). However, subsequent biochemical analyses revealed that RdgBα is actually a peripheral membrane protein, which associates with the membrane through protein-protein interactions (Lu et al., 1999a; Litvak et al., 2002). For mammalian RdgBαII, 1 M NaCl, high pH and strong denaturants, known to disrupt protein-protein interactions, solubilised the protein completely. RdgBαII was not detected in either the TX-100-soluble or insoluble membrane fractions (Lu et al., 1999a).

RdgBαI localises mainly to the Golgi apparatus, and also to the ER (Aikawa et al., 1999; Litvak et al., 2002). In contrast, the PITP domain (1-257 aa) expressed alone displays cytosolic staining (Litvak et al., 2002), indicating that the Golgi and ER localisation is dependent on a sequence distinct from the PITP domain (Litvak et al., 2002). Depletion of RdgBαI from HeLa cells using RNAi resulted in a disorganised Golgi, with swollen cisternae and a re-distribution of Golgi markers (Litvak et al., 2005).

An assessment of trafficking to and from the Golgi indicated a defect in traffic through the secretory pathway, from the Golgi to the plasma membrane, in RdgBαI-knockdown cells. Control and knockdown cells were infected with a temperature-sensitive strain of vesicular stomatitis virus (tsO45 VSV), which contained a glycoprotein (VSV-G) which misfolds at 40°c and fails to exit the ER. Dropping the temperature to 32°c enabled rapid folding and transport of VSV-G from the ER. Cells were kept at 40°c for 3 hr to accumulate VSV-G in the ER, and then the temperature was shifted to 32°c for different time periods. In control cells, all of the VSV-G had reached the plasma membrane by 45 min at 32°c; in RdgBαI-knockdown cells, this took ~2 hrs (Litvak et al., 2005). In

RdgBαI-knockdown cells, expressed YFP-VSV-G was observed in highly dynamic, long, tubular structures emanating from the TGN, and only a few intermediate carriers detached from the Golgi. By contrast, in control cells, YFP-VSV-G appeared in various intermediate carriers that moved rapidly from the TGN towards the plasma membrane, indicating a defect in fission of vesicles from the Golgi apparatus in RdgBαI-knockdown cells (Litvak et al., 2005).

The level of DAG at the Golgi apparatus is critical for membrane tubule constriction and can therefore affect membrane transport from the TGN. Methods used to monitor DAG levels detected lower levels at the Golgi in RdgBαI-knockdown cells than in control cells (Litvak et al., 2005). A GFP-PKD reporter construct, which binds to DAG at the Golgi in control cells, re-localised to the cytosol in RdgBαI-knockdown cells. One pathway to DAG production is via sphingomyelin (SM) synthase, which uses ceramide and PC to produce SM and DAG. Inhibition of ceramide synthesis with fumonisin B1 (FB1), similarly re-localised the GFP-PKD reporter construct. Lastly, an *in vitro* DGK assay was used, and indicated that the DAG level in the Golgi of RdgBαI-knockdown cells and FB1-treated cells was reduced by ~40% and ~70% respectively, compared to control cells (Litvak et al., 2005). By contrast, RdgBαI-knockdown Golgi membranes had a much higher level of PC.

RdgBαI interacts with Vesicle-associated membrane protein (VAMP)-associated protein (VAP) through its FFAT motif (two phenylalanines (FF) in an acidic tract (Loewen et al., 2003)), at 349-355 aa (Amarilio et al., 2005) (Figure 1.3 A). Although VAP is an ER integral membrane protein, siRNA knockdown of VAP resulted in an unusual Golgi morphology, with long tubules emanating from a dispersed Golgi complex (Peretti et al., 2008). The ceramide transfer protein (CERT) and oxysterol binding protein (OSBP), also have VAP-binding FFAT motifs. In wild-type cells, binding of 25-hydroxycholesterol to OSBP promotes its translocation to the Golgi to enhance ceramide transport by CERT (Perry and Ridgway, 2006). However, CERT, OSBP and RdgBαI all re-localised to the cytosol upon VAP-knockdown. This re-localisation could be rescued, however, with over-expression of full-length RdgBαI, and only partially rescued with expression of the PITP domain only of RdgBαI, which lacks the FFAT motif (Peretti et al., 2008).

Both CERT and OSBP have PH domains that bind PI(4)P. VAP knockdown slightly reduced localisation of the GFP-OSBP-PH fusion protein to the Golgi, indicating a decline in PI(4)P levels (Peretti et al., 2008). Since RdgBαI has an N-terminal PITP domain, this points to a model in which RdgBαI binds VAP proteins at the ER via its FFAT motif, and its PITP domain swings between the ER and the Golgi at ER-Golgi membrane contact sites, delivering PI for phosphorylation to PI(4)P at the Golgi apparatus. Of note, a different study reported an interaction between RdgBαI and type III PI4K via 378 aa at the RdgBαI N-terminus, and PI4K activity was identified in RdgBαI immunoprecipitates (Aikawa et al., 1999). Since CERT transfers ceramide from the Golgi to the ER, it seems likely that it is the re-localisation of this protein upon VAP- or RdgBαI-knockdown that causes the decline in DAG levels, since SM synthase does not receive the ceramide it requires to synthesise DAG and SM. This also explains the increase in PC levels observed upon RdgBαI-knockdown, as PC is not used by SM synthase. Over-expression of RdgBαI alone was sufficient to restore all of the defects in VAP-knockdown cells, including PI(4)P levels, DAG levels, targeting of OSBP and CERT to the Golgi apparatus and protein transport from the TGN.

PITPβ in retrograde trafficking from the Golgi to the ER

Ablation of the *PITPNB* gene is embryonic lethal, yet ablation of *PITPNA*, the gene encoding PITPα, is not (Alb et al., 2002). This suggests that PITPβ carries out an essential house-keeping function in mammalian cells. There are two isoforms of PITPβ due to alternative splicing of the *PITPNB* mRNA. These isoforms differ in their C-termini. PITPβ is ubiquitously expressed in mammalian cells (Morgan et al., 2006), and localises to the Golgi in a variety of cell types (de Vries et al., 1995; 1996; Morgan et al., 2006; Shadan et al., 2008). More specifically, PITPβ has been reported to localise to the TGN, since it co-localises with the TGN38 marker (Phillips et al., 2006).

Major phosphorylation of PITPβ has been reported at Ser262, a residue unique to the C-terminus of PITPβ-sp1 (van Tiel et al., 2002). This group observed that phosphorylation of Ser262 was required for targeting of PITPβ to the Golgi in NIH3T3 fibroblast cells: the PITPβ S262A mutant was distributed throughout the cell, as was the wild-type

protein when cells were treated with a PKC inhibitor. In another study, the exchange of the C-terminal 28 residues between PITPα and PITPβ switched PITPα localisation to the Golgi apparatus and re-distributed PITPβ throughout the cytoplasm (Phillips et al., 2006). It should be noted, however, that two studies failed to demonstrate a requirement for Ser262 phosphorylation in targeting PITPβ to the Golgi (Morgan et al., 2006; Phillips et al., 2006). Furthermore, PITPβ-sp2, which lacks the Ser262 residue, was observed to localise to the Golgi in COS-7 cells (Morgan et al., 2006) and in PITPα$^{-/-}$ murine embryonic fibroblasts (Phillips et al., 2006).

Depletion of PITPβ from HeLa cells by RNAi results in a compacted Golgi apparatus and distorted nucleus. In addition, there is a specific defect in retrograde traffic from the Golgi to the ER mediated by coat protein complex I (COPI)-coated vesicles (Carvou et al., 2010). The KDEL receptor, important for retrieval of ER resident proteins from the Golgi in COPI-coated vesicles, is arrested at the Golgi in PITPβ-knockdown cells. ERGIC-53, which also cycles between the ER-Golgi intermediate compartment (ERGIC) and the ER in COPI-coated vesicles, is arrested at the ERGIC in PITPβ-knockdown cells.

The researchers report a reduction in PI(4)P by ~40% in PITPβ-knockdown cells, and mutants defective in PI binding and exchange were unable to rescue the PITPβ-knockdown phenotype (Carvou et al., 2010). An early event in the formation of trafficking vesicles is the activation of ARF1 by Golgi-specific brefeldin A-resistant guanine nucleotide exchange factor 1 (GBF1). PI(4)P, produced by phosphorylation of PI by the type IIIα PI4K, is required for the localisation of GBF1 to the *cis*-Golgi membrane (Dumaresq-Doiron et al., 2010). GBF1 then interacts with the γ-COP subunit of COPI, recruiting the COPI complex to the membrane prior to activation of ARF1 (Deng et al., 2009). Here, PITPβ appears to be presenting PI to PI4KIIIα to produce PI (4)P, required for the assembly of COPI-coated vesicles at the Golgi apparatus.

PITP and the endosomal trafficking pathway

The membranes of early endosomes and the internal vesicles of multi-vesicular endosomes are enriched in PI(3)P (Gillooly et al., 2000). Protein effectors bind to PI(3)

P using their FYVE domains; thus, PI(3)P regulates transport of cargo through the endosomal pathway. PI(3)P is formed by type II or III PI3Ks, which phosphorylate PI itself at the 3'-OH position of its inositol head group.

In yeast, the type III PI3K, Vps34p, exists in a complex with Vps15p, a 160 kDa serine/threonine protein kinase. Vps15p recruits Vps34p to the Golgi and enhances its PI3K activity. A human homologue of Vps15p was identified in anti-PI3K immunoprecipitates from Jurkat cells (Panaretou et al., 1997). Being a protein of 150 kDa, it was named 'p150'. p150 displayed serine/threonine protein kinase activity and increased the PI3K activity of the Vps34p human homologue, hVps34p, two-fold.

Furthermore, the GST-p150-PI3K complex expressed in Sf9 insect cells associated with PITPβ (Panaretou et al., 1997). PITP was immunoprecipitated from Jurkat cells using a mouse monoclonal anti-PITP antibody, and the immunoprecipitate monitored for its kinase activity towards PI. PITP did co-immunoprecipitate with lipid kinase activity, specifically with PI3K, not PI4K, activity. The addition of either recombinant PITPα or recombinant PITPβ, pre-incubated with 1 mM PI, to the GST-p150-PI3K complex, resulted in a dose-dependent increase in PI3K activity (Panaretou et al., 1997). This study indicates that PITP contributes to type III PI3K activity, and implicates a role for PITP in endosomal trafficking by providing PI for the local enrichment of endosomal membranes in PI(3)P.

Dm-PITP and cytokinesis

In contrast to mammalian cells, *Drosophila* has only a single class I PITP, Dm-PITP. Dm-PITP is 61-62% identical to mammalian PITPβ, and 59% identical to mammalian PITPα. Flies homozygous for a mutant allele of the *giotto* (*gio*) gene, which encodes the Dm-PITP protein, have been observed to frequently have multi-nucleate spermatids, indicative of failures in meiotic cytokinesis (the separation of the two daughter cells at the end of cell division) (Giansanti et al., 2006). Specifically, mutant *gio* spermatocytes were found to be defective in actomyosin ring constriction and furrow ingression. A similar phenotype was observed in mitotic cells (late telophase neuroblast cells in brain preparations from mutant flies).

Since PITPs have been implicated in the budding of secretory vesicles from the TGN, and in the process of vesicle fusion with the plasma membrane, the behaviour of Golgi-derived vesicles during meiotic division was analysed (Giansanti et al., 2006). In wild-type spermatocytes, the Golgi stacks were observed to disassemble into numerous vesicle-like structures at metaphase of meiosis I, when the chromosomes line up along the cell equator. During anaphase the spindles shorten, separating the sister chromatids and moving them towards the spindle poles. In telophase, the nuclear envelope reforms around each set of chromatids; at this time the Golgi-derived vesicles were concentrated near the spindle poles and excluded from the central region of the cell, where the cleavage furrow was beginning to form. By contrast, 61.7% of *gio* mutant spermatocytes displayed an abnormal localisation of vesicle-like structures at the cell equator (Giansanti et al., 2006). Cleavage furrow formation requires the addition of new membranes, and in the mutant spermatocytes the Golgi-derived vesicles failed to fuse with the invaginating furrow membrane, resulting in the observed abnormal accumulation of these structures at the centre of the cell.

A rabbit polyclonal antibody raised against the entire protein indicated that Dm-PITP accumulated both at the cell poles and at an elliptical structure that encircled the chromosomes, during metaphase and anaphase of meiosis I of wild-type primary spermatocytes. As the spermatocytes progressed to telophase, the protein was still visible at the spindle poles, but was now also enriched at the cleavage furrow (Giansanti et al., 2006).

Notably, a similar phenotype to the *gio* mutant was observed for the *four wheel drive* (*fwd*) mutant, in which the gene encoding a PI4K was found to be mutated. Like the *gio* mutant, the *fwd* mutants displayed a specific defect in actomyosin ring constriction (Giansanti et al., 2006). This indicates that Dm-PITP and a Dm-PI4K are required for the fusion of Golgi-derived vesicles with the invaginating cleavage furrow, an event required for actomyosin ring constriction during both meiotic and mitotic cytokinesis.

Dm-RdgBα and light-induced arrestin trafficking

Activation of a GPCR promotes its phosphorylation by a G protein-coupled receptor kinase (GRK) and the subsequent recruitment of the adaptor protein, arrestin. Arrestin binding uncouples the receptor from the G protein by steric hindrance, and promotes internalisation of the receptor by recruitment of endocytic vesicle coat proteins. The predominant arrestin in *Drosophila* photoreceptor cells is Arr2. The exposure of dark-adapted flies to a pulse of bright blue light maximally coverts the GPCR, rhodopsin, to its light-activated form, metarhodopsin. Under these conditions in wild-type flies, Arr2 translocates to the rhabdomere. If the flies are then exposed to the dark for 3 hrs, rhodopsin-Arr2 complexes undergo clathrin-dependent endocytosis and movement into the cell bodies.

In the *rdgB* and *cds* mutants, Arr2 was not localised to the rhabdomere following the pulse of bright blue light, but was instead diffusely distributed between the cell bodies and the rhabdomeres (Lee et al., 2003). Further analysis indicated that rather than being unable to traffic, Arr2 was much slower in reaching the rhabdomere in *rdgB* and *cds* mutants than in wild-type flies. The fact that these flies have absent or defective RdgBα and CDP-DAG synthase proteins, respectively, indicates an involvement of phosphoinositides in arrestin trafficking. Lipid binding experiments indicated that Arr2 did indeed bind phosphoinositides, most likely $PI(3,4,5)P_3$ (Lee et al., 2003).

Comparative modelling identified three lysine residues in a basic patch as a putative phosphoinositide-binding site. The mutation of these residues to glutamine produced the $Arr2^{3K/Q}$ mutant, which was unable to bind phosphoinositides. Like the wild-type Arr2 in *rdgB* and *cds* mutant flies, $Arr2^{3K/Q}$ was present diffusely throughout the cell bodies and rhabdomeres due to a delay in the light-dependent movement to the rhabdomeres (Lee et al., 2003). This defect occurred in both directions: in wild-type flies, 3 hrs in the dark re-distributed the rhodopsin-Arr2 complexes into the cell bodies; for the $Arr2^{3K/Q}$ mutant, this re-distribution was observed after 72 hrs. These experiments implicate RdgBα in PI delivery in *Drosophila* photoreceptor cells for production of $PI(3,4,5)P_3$, required for effective arrestin trafficking.

1.1.3: Summary

PITPs are implicated in a wide variety of cell signalling and membrane trafficking processes, and in all of these, a connection to phosphoinositides and the delivery of PI can be envisaged. In some, a clear connection can be observed between PITP and the stimulation of lipid kinase activity (Cunningham et al., 1995; Kauffmann-Zeh et al., 1995; Panaretou et al., 1997), rather than the passive transfer of PI down a PI chemical gradient (Currie et al., 1997).

1.2: The PITP domain

1.2.1: Structure of the PITP domain

The original purification of PITP from bovine brain yielded two subforms that could be distinguished on the basis of their isoelectric points (Helmkamp et al., 1974). Subsequent analysis revealed that these two subforms were the PI- and PC-loaded forms of PITP (van Paridon et al., 1987b), due to the different charges on the phospholipid molecules. X-ray crystal structures of the class I proteins bound to PI or PC have been reported (Yoder et al., 2001; Tilley et al., 2004; Vordtriede et al., 2005), and it appears that the charge imparted on the PITP by the phospholipid is the only difference between the PI- and PC-bound structures.

The PITP domain is composed of eight β-strands that form a large, concave sheet, together with three long, and four shorter, α-helices (Figure 1.3 B). A single molecule of lipid cargo occupies a space between the β-sheet and two of the long α-helices, αA and αF, in the lipid-binding cavity. A polar region of the cavity accommodates the phospholipid head group, whilst two hydrophobic channels house the *sn*1 and *sn*2 fatty acyl chains. The C-terminal region, 233-271 aa, consists of the αG helix and an 11 aa extension, the latter of which limits access to the lipid-binding cavity (Yoder et al., 2001) (also referred to as the cavity 'lid'). With the lid closed PITP is transport-ready; the phospholipid is completely enclosed within the protein, shielded from the aqueous cytosol.

(Facing page) Figure 1.3: The human PITP family and PITP domain structure

(A) Domain architecture of the human PITPs. Each family member has the defining PITP domain at its N-terminus, yet differs in its C-terminal residues. Sequence length in amino acids is indicated at the top-right of each protein. Gene names are given on the right. (B) X-ray crystal structure of PITPα with PI bound (PDB: 1uw5) ('closed' structure). Regulatory loop, blue (with Ser166 residue indicated); lipid exchange loop, green; αG helix and 11 aa C-terminal extension, red. WW203/204 are indicated, WW. (C) and (D) The apo-structure, devoid of lipid (PDB: 1kcm), shown as cartoon or surface, respectively. Numbering of secondary structural elements is indicated in (C), α-helices αA-αG, β-strands β1-β8. In (D), the upper image has been captured looking 'down' the cavity, through the smaller opening, and the lower image has been captured looking 'up', through the larger opening. (Directions 'up' and 'down' are relative to the structures shown in (B) and (C).) Inset images indicate the exposure of the Ser166 and Thr59 residues in the apo-structure. Exposure of Ser166 on the surface of the closed structure is shown for comparison. Thr59 is not exposed on the surface of the closed structure.

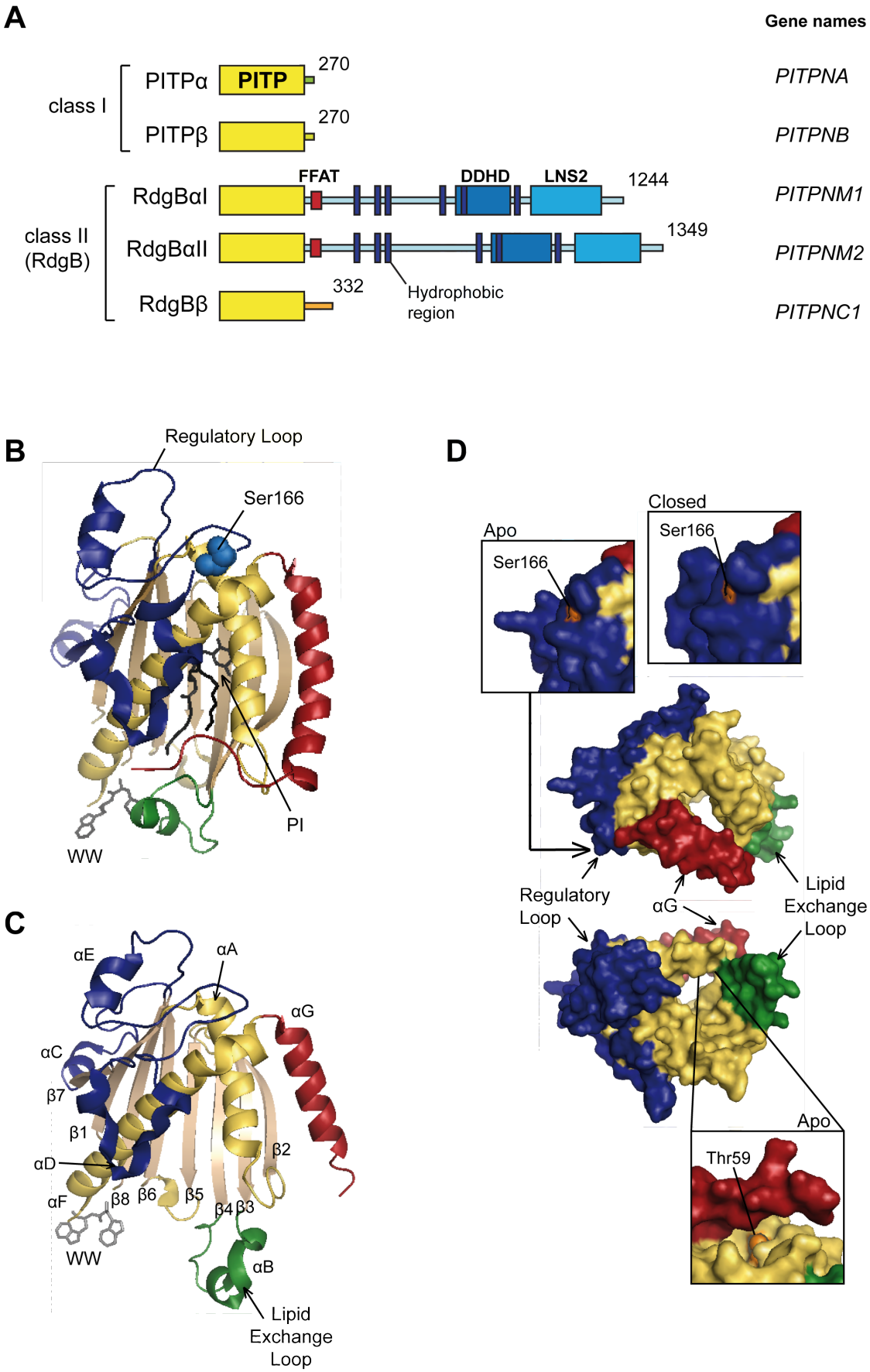
A
Gene names
class I
PITPα
PITP
270
PITPNA
PITPβ
270
PITPNB
class II
(RdgB)
RdgBαI
FFAT
DDHD
LNS2
1244
PITPNM1
RdgBαII
1349
PITPNM2
RdgBβ
332
Hydrophobic
region
PITPNC1
B
Regulatory Loop
Ser166
PI
WW
C
αE
αA
αG
αC
β7
β1
αD
β2
αF
β8
β6
β5
β4
β3
WW
αB
Lipid
Exchange
Loop
D
Apo
Ser166
Closed
Ser166
Regulatory
Loop
αG
Lipid
Exchange
Loop
Apo
Thr59

Yoder and colleagues also defined the 'regulatory loop', an extensive loop region between strands β6 and β8 (119-190 aa) (Yoder et al., 2001) (Figure 1.3 B). They speculated that this region would be required for the association of PITP with a wide variety of lipid- and protein-modifying enzymes (Figure 1.5 C).

1.2.2: Membrane Interaction

An open or 'apo' structure of PITPα has also been reported, devoid of lipid (Schouten et al., 2002) (Figure 1.3 C & D). Earlier studies using proteases to assess the conformation of PITP showed that PITPα was highly resistant to trypsin digestion alone, yet became susceptible to cleavage of its C-terminus when incubated with vesicles (Tremblay et al., 1996). This indicates that PITP adopts a tightly closed conformation when transporting lipid between membranes, and becomes more flexible, releasing its C-terminus, upon interaction with vesicles (Figure 1.5 A, p. 61). The apo-structure is therefore believed to only occur upon interaction with the membrane, when PITP is in the process of lipid exchange.

The apo-conformation of PITPα has been compared with its closed conformation to reveal that upon interaction with membranes, the lipid exchange loop swings outwards by ~90°. The C-terminal αG has moved outwards from the main structure by 20°, which is accompanied by a partial unwinding of residues 254-257 and a disordering of the C-terminal tail (258-271 aa) (Schouten et al., 2002). The lipid-binding core is largely unaffected: the peripheral β-strands, β2, β3 and β4, twist and flatten out. These conformational changes create a channel through the PITP protein (Figure 1.3 D), from a large opening between the β-sheet and the long helices, αA and αF. The channel terminates in a small hydrophobic opening between the N-terminus of helix αG and strands β2 and β3, near the phospholipid head group in the corresponding closed structure. It has been hypothesised that the small opening allows water molecules through, destabilising the hydrogen bond network holding the lipid head group in place, promoting deposition of the lipid cargo in the membrane (Wirtz et al., 2006). The large opening exposes a hydrophobic surface of ~1300 $Å^2$ (Schouten et al., 2002). Residues 70-78 aa of one lipid exchange loop insert into and shield the exposed hydrophobic

surface of another PITP, and consequently the apo-PITP structures form tight dimers in the crystal.

The finding that the lipid-binding cavity is closed by a lid comprising the C-terminal 11 aa (Yoder et al., 2001), and that upon membrane interaction the C-terminal αG swings out from the main structure, exposing the cavity so that PITP molecules dimerise to mask the hydrophobic surfaces (Schouten et al., 2002), supports earlier biochemical studies of the PITP C-terminus. Deletion of 5 or 10 amino acids (PITPα-Δ5 or -Δ10, respectively) reduced both the PI and PC transfer activity of PITPα, although near-wild-type PC transfer was retained at high protein concentrations (Hara et al., 1997). Neither the PITPα-Δ20 mutant nor the PITPα protein digested with the protease subtilisin, which removed 24 aa from the C-terminus, exhibited PI transfer activity (Hara et al., 1997; Prosser et al., 1997). The PITPα protein treated with subtilisin was observed to dimerise when analysed by gel filtration (Prosser et al., 1997). Other studies showed that removal of 5, 12 or 18 amino acids from the C-terminus of PITPα resulted in an increased affinity for vesicles and membranes (Tremblay et al., 1996; 1998; Larijani et al., 2003). It is therefore clear that the C-terminal deletion mutants exhibit a reduced lipid transfer activity because they have an increased affinity for the membrane. Some affinity of PITP for membranes is required, but if the affinity is too great, transfer activity will be greatly reduced or eliminated. This increased affinity comes from exposure of hydrophobic surfaces in the lipid-binding cavity.

Tryptophan 203 and 204

In the apo-structure of PITPα, Schouten and colleagues noted that the displacement of the C-terminal region and lipid exchange loop would allow the aromatic residues, Y103, W203 and W204, and positively-charged residues, K105, K202 and K209, to contact the membrane (Schouten et al., 2002).

In the class I PITPs, the two tryptophan residues, W203 and W204, are located at the tip of the loop between strand β8 and helix αF, facing the membrane interface (Figure 1.3 B). Mutation of these two residues to alanine led to a loss of lipid transfer and of membrane association (Tilley et al., 2004; Shadan et al., 2008), indicating that these two

residues insert into the membrane. Insertion of the tryptophan residues into the membrane could indirectly perturb the αG helix, via αF, causing a shifting of the C-terminal lid residues. The use of tryptophan residues in membrane interactions is a common feature of membrane-active proteins (Yau et al., 1998).

Y103 lies next to the opening of the lipid-binding cavity, on the loop between strands β5 and β6. Mutation of this site to an alanine residue produced a modest reduction in PI and PC transfer, yet no effect on lipid binding (Tilley et al., 2004). Therefore, the Y103 residue may interact with the membrane but its presence is not required for the interaction to take place, unlike WW203/204.

Dynamics of membrane interaction

The class I proteins, PITPα and PITPβ, have a cysteine residue (C95) in their lipid head group-binding pocket (Figure 1.4), which can be modified by the addition of a thiol modifying agent, such as *N*-ethylmaleimide (NEM). Since PITP only assumes its open conformation during interaction with a membrane, NEM is only able to modify C95 when PITP is in the process of lipid exchange. Modification by NEM is irreversible, and PITPs modified in this way either remain membrane-associated, or eventually fall off and dimerise to shield their internal hydrophobic surfaces. Lipid transfer activity is inhibited. NEM has therefore been used as a tool alongside gel filtration and immunofluorescence microscopy to investigate the dynamics of membrane interaction of PITPα and PITPβ (Shadan et al., 2008). Within 2 min of NEM treatment, the majority of PITPβ shifted to a higher-molecular weight fraction, not associated with lipid transfer activity, indicating that almost the entire pool of PITPβ had sampled a membrane within 2 min. By contrast, a substantial portion of PITPα remained in the lower-molecular weight fractions at 10 min, suggesting that it had not undergone the same conformational change and was therefore not modified by NEM (Shadan et al., 2008). These experiments were carried out in PC12 cells under basal conditions, perhaps indicating the presence of a distinct pool of PITPα that may require some sort of ‘activation signal’ before it undergoes lipid exchange.

An earlier study employed fluorescence lifetime imaging microscopy (FLIM) to examine fluorescence resonance energy transfer (FRET) between the EGFP-PITP donor fluorophore and BOPIDY-labelled phospholipid (PI or PC) acceptor fluorophore in COS-7 cells (Larijani et al., 2003). A reduction in EGFP lifetime indicated an interaction between PITP and phospholipid, as the energy was transferred to the acceptor fluorophore. In unstimulated cells, PITPα interacted with PI and PC similarly, at the plasma membrane and in the cytoplasm (includes ER). Upon EGF stimulation, the interaction between PITPα and either phospholipid was increased, most notably an increase of 30% was observed between PITPα and PI at the plasma membrane. For PITPβ, EGFP lifetime decreased at the Golgi apparatus and plasma membrane in unstimulated cells, and was further reduced in the Golgi, plasma membrane and the cytoplasm upon EGF stimulation. At the Golgi, the reduction in lifetime corresponded to a 40% increase in FRET efficiency. Using the related technique, fluorescence recovery after photobleaching (FRAP), cells were selectively bleached at the cytoplasm, plasma membrane or Golgi apparatus, as appropriate, and fluorescence recovery monitored as a measurement of PITP mobility at that membrane. Following stimulation with EGF, the mobile fraction of PITPα at the plasma membrane decreased from 91% to 68%, indicating a reduction in PITPα mobility at the plasma membrane in response to EGF stimulation. By contrast, the mobility of PITPβ was unchanged upon EGF stimulation (Larijani et al., 2003).

1.2.3: PI- and PC-binding

PITPα and PITPβ can bind either PI or PC. PITPα has a 16-fold higher affinity for binding to PI than it does to PC (van Paridon et al., 1987a). PC accounts for ~40% cellular phospholipids whereas PI only accounts for 2-12% in most mammalian cells. Thus, the higher affinity of PI binding compensates for its lower concentration. In general, when PITPα is purified from tissue, it is loaded with PI and PC in approximately equal quantities (Helmkamp et al., 1974; Thomas et al., 1993), and the same is true for PITPβ (Morgan et al., 2006). Comparison of the structures of the PI- and PC-bound PITPα reveals that both lipids occupy the same space in the lipid-binding cavity, and in fact the only difference is that the inositol head group makes more

hydrogen bonds with specific amino acid residues than does the choline moiety (Yoder et al., 2001; Tilley et al., 2004; Vordtriede et al., 2005) (Figure 1.4).

Phospholipid phosphate and acyl chain-binding

Residues that make contact with both PI and PC are those making contact with the phosphate group and the acyl chains. T97 and K195 form direct hydrogen bonds with oxygen atoms of the phosphate, and E218 and Y63 make direct hydrogen bond contact with the acyl chains (Figure 1.4).

PI inositol head group-binding

Five residues in the lipid-binding cavity make hydrogen bond contact with the inositol head group: Q22, T59, E86, K61 and N90 (Figure 1.4, left panel). Mutation of either K61 or N90 resulted in a complete loss of PI binding and transfer, but left PC binding and transfer unaffected (Tilley et al., 2004; Carvou et al., 2010). For E86, mutation to alanine reduced PI binding and transfer, with no effect on PC binding and transfer. However, the conservative mutation E86Q, was found to reduce both PI and PC binding (Tilley et al., 2004).

Threonine 59

Along with the side chain of K61, T59 forms a hydrogen bond with the 4'-OH on the inositol head group of PI (Figure 1.4, left panel). In the PC-bound structure of PITPα, T59 makes *van der Waals* contact with one of the methyl groups of PC (Yoder et al., 2001). Mutation of T59 to E, D, N or Q, abolishes PI transfer without a significant effect on PC transfer (Alb et al., 1995), whereas mutation of T59 to S, V or A retains some PI transfer activity (Tilley et al., 2004). Conceivably, the conservative substitution T59S might still be able to form a hydrogen bond with the inositol head group of PI. Valine and alanine are small, uncharged amino acids which might not interfere with inositol binding, but wouldn't encourage it either. The carboxylic acid functional groups of glutamic acid and aspartic acid could disrupt the local charge distribution and

disfavour inositol binding; likewise asparagine and glutamine, though uncharged, have a carboxyl group which could cause steric, as well as chemical, hindrance.

T59 belongs to a consensus site for phosphorylation by PKC (Alb et al., 1995; Morgan et al., 2004), and prior to resolution of the first PITP crystal structure it was widely thought that this residue was phosphorylated *in vivo*. My own inspection of the apo-structure indicates that T59 is exposed in the channel through the protein (Figure 1.3 D), yet is completely buried in the closed structure. Mutation of T59, including to the phospho-mimetic, T59E, does not affect PC transfer, implying that the closed-open-closed transition and PC-PC lipid exchange at membranes takes place. However, the RdgBαI T59E mutant associated with lipid droplets in HeLa cells (Litvak et al., 2002). In RdgBαI, perhaps PC-PC lipid exchange activity is not preserved. Instead RdgBαI becomes immobilised on lipid droplets, which are composed of neutral lipids. T59A, which retained some PI transfer activity for PITPα (Tilley et al., 2004), was not observed on lipid droplets (Litvak et al., 2002).

PC choline head group-binding

Residues specific for PC binding and transfer are more difficult to predict from the crystal structures. C95 lies in the lipid-binding cavity and forms a hydrogen bond with PC indirectly via a water molecule (Figure 1.4, inset). Mutation of this residue to either threonine or alanine eliminates PC transfer, leaving PI transfer unaffected (Carvou et al., 2010). F225 has also been shown to be important for PC transfer: when the large aromatic residue, phenylalanine, is present in this position, PC transfer activity is high. However, when it is replaced with a leucine residue, as in rodent PITPβ, PC transfer is lower (Vordtriede et al., 2005). (In rat PITPα and human PITPβ this residue is a phenylalanine.) The authors of this study found that by mutating this residue alone, they could switch the PC transfer specificity of rat PITPα and PITPβ, so that PITPα F225L ≈ PITPβ and PITPβ L225F ≈ PITPα.

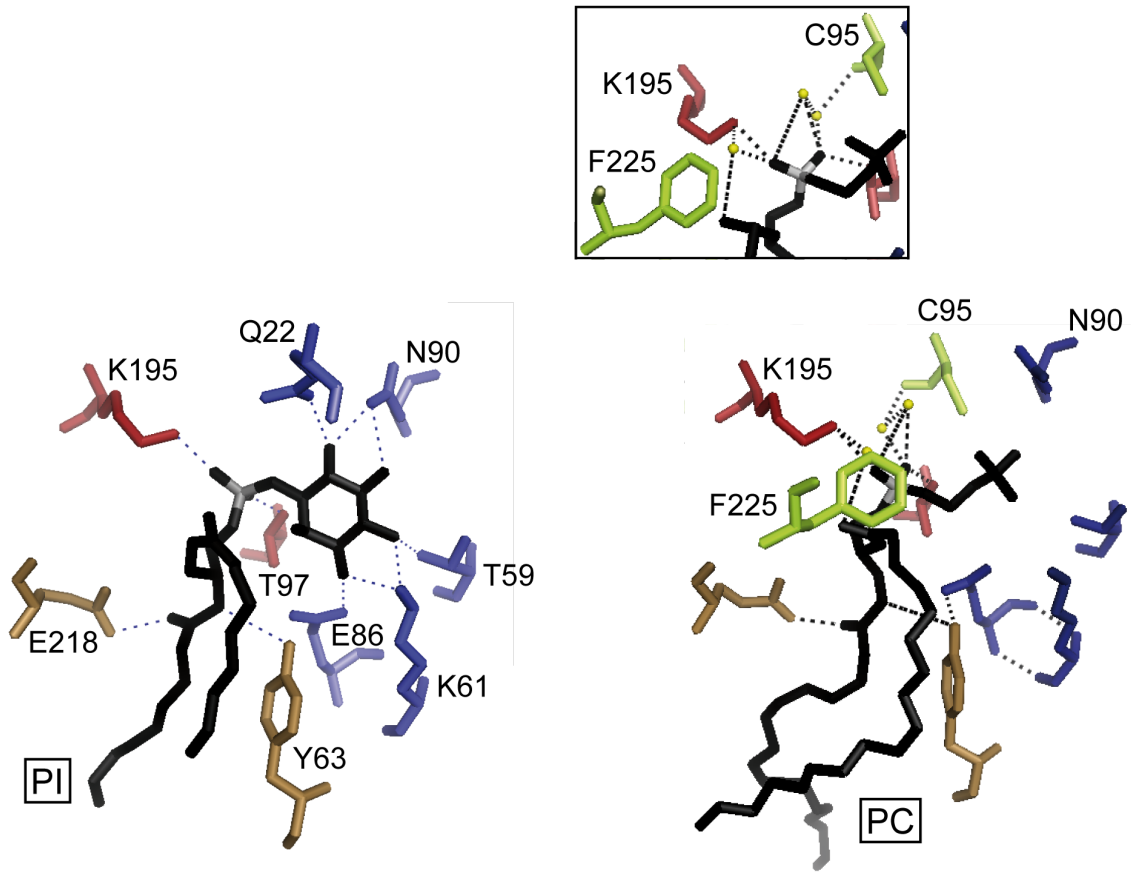

Figure 1.4: PI- and PC-binding residues in the PITPα lipid-binding cavity

Residues making hydrogen bond contact with the PI (left panel, PDB: 1uw5) and PC (right panel, PDB: 1t27) ligands in PITPα. Residues making hydrogen bond contacts with the lipid acyl chains, brown; the phospholipid phosphate group, red; inositol head group, blue. C95 and F225, lime green. Inset: PC head group and phosphate rotated to enable a clearer view of the C95 and F225 residues, and hydrogen bond network.

The finding that the inositol head group of PI is secured by direct hydrogen bonds with five residues in the PITP lipid-binding cavity, whereas choline makes none, gives a molecular grounding for the earlier report that PITP has a 16-fold-higher affinity for PI than for PC (van Paridon et al., 1987a).

Acyl chain selectivity

In the X-ray crystal structures of the PITP domain, clear channels for each of the *sn*1 and *sn*2 fatty acid tails of the bound phospholipid molecule can be observed. The PI and PC molecular species bound by PITPα have been examined using tandem electrospray ionisation mass spectrometry (ESI-MS/MS), and compared with the profile of PI and PC molecular species in HL60 cells (Hunt et al., 2004). PITPα showed a selectivity towards two mono-unsaturated PC species in particular, 16:0/16:1 and 16:1/18:1 (the first number is the number of carbon atoms in the acyl chain, and the second is the number of double bonds). The preference for cellular PC species was observed in the order, 16:1>16:0>18:1>18:0>20:4. The PI species bound by PITPα were also principally short-chain saturated and mono-unsaturated species, in particular 16:0/16:1, 16:1/18:1 and 16:0/18:1. The order of preference for PI molecular species exactly matched that seen for PC, 16:1>16:0>18:1>18:0>20:4>20:3, despite a much higher proportion of polyunsaturated PI species present in HL60 cells (Hunt et al., 2004).

The finding that PITP does not favour binding of long-chain PI or PC molecular species confirmed earlier experiments with prenylacyl-containing phospholipids, which also reported a preference in chain length in the order 16:1>16:0>18:0 (van Paridon et al., 1988).

1.2.4: Lipid presentation model and the PITP structure

The addition of PITP into permeabilised HL60 cells washed of cytosol increased the rate of lipid hydrolysis before the PI supply at the plasma membrane had been exhausted. This indicated to researchers that PLC and the lipid kinases preferred the substrate delivered by PITP to the PI already present in the signalling membrane (Cunningham et al., 1995). Indeed, the ability of PITP to stimulate lipid kinases was

also observed in other studies (Kauffmann-Zeh et al., 1995; Panaretou et al., 1997), and gave support to the lipid presentation model of PITP function (Figure 1.5 B) (Cunningham et al., 1995).

From the first reported X-ray crystal structure of PITPα, in its closed conformation with PC bound (Yoder et al., 2001), it was unclear how PITP would present PI to lipid kinases, since the inositol head group of PI appeared to be buried deep in the lipid-binding cavity, away from the cavity opening. Yoder and colleagues postulated interaction of lipid-modifying enzymes with the regulatory loop of the PITP domain. The structure of the PITP apo-conformation revealed that upon interaction with the membrane, a channel opened up in the structure, with a small opening between the N-terminus of αG helix and strands β2 and β3 (Schouten et al., 2002). This opening could expose the inositol head group of a PI molecule bound in the lipid-binding cavity to a lipid kinase docked on the regulatory loop, in support of the lipid presentation model, although it has been noted that this opening is very small (Wirtz et al., 2006). PITP has no affinity for transfer of PI(4)P (Schermoly and Helmkamp, 1983), promoting the deposition of this phosphoinositide to either a lipid kinase or into the membrane (Yoder et al., 2001). The evidence therefore supports the lipid presentation model up to PI(4)P. Subsequent phosphorylation of PI(4)P to $PI(4,5)P_2$ by PI4P-5-K could require a PITP co-factor, such as ARF (Fensome et al., 1996).

The notion that the PI, and subsequent PI(4)P, delivered by PITP is preferred by PLC may involve its membrane localisation. $PI(4,5)P_2$ is compartmentalised in mammalian cells into agonist-sensitive and -insensitive pools. Caveolae, which belong to the agonist-sensitive pool, are small invaginations in the plasma membrane rich in the protein, caveolin, and contain a variety of proteins involved in cell signalling, including small and heterotrimeric G proteins, Src family kinases, MAP kinase, the EGF receptor and the platelet-derived growth factor receptor. They are also enriched in glycosphinglipids and cholesterol, making them resistant to (0.5%) Triton X-100 (TX-100) extraction. It has been reported that both 50 nM EGF and 10 μM bradykinin (GPCR agonist) treatment (5 min) of A431 cells stimulates a reduction in the caveolar PIP_2, without any change in PIP_2 levels in the solubilised plasma membrane fraction (non-caveolar) (Pike and Casey, 1996). In this study, PIP_2 was evenly distributed

between the caveolar and non-caveolar, solubilised plasma membrane fractions under basal conditions. PITP-delivered PI might be favoured by PLC because it has been deposited into the agonist-sensitive pool. The targeting of PITP to the agonist-sensitive pool could be mediated by protein-protein interactions.

A reduced mobility of PITPα at the plasma membrane has been observed in response to EGF stimulation in COS-7 cells (15 min, 35 ng.mL^{-1}) (Larijani et al., 2003). PITP has been detected in an endogenous signalling complex with the EGF receptor, PI4K and PLCγ in A431 cells, and this association increased following stimulation with 100 nM EGF for 5 mins (Kauffmann-Zeh et al., 1995). In the developing nervous system, PITPα interacts with DCC/neogenin via its C-terminus, as removal of the C-terminal 20 aa of PITPα abolished the interaction, and this association is increased 4-fold by addition of the agonist, netrin-1 (Xie et al., 2005). This localisation at the plasma membrane might focus PITPα into the local presentation of PI to PI 4-kinase from agonist-insensitive to agonist-sensitive pools.

1.2.5: Regulation of Lipid Transfer: Serine 166

The Ser166 residue is conserved in almost all PITP sequences analysed and, like Thr59, is a consensus site for phosphorylation by PKC. PITPα can be phosphorylated *in vitro* by PKC (van Tiel et al., 2000; Morgan et al., 2004), and Ser166 is phosphorylated upon stimulation of HL60 cells with either FMetLeuPhe or PMA, and in rat brain cytosol (Morgan et al., 2004). When PITPα is phosphorylated at this residue, it is unable to exchange its bound PI for PC, yet retains the ability to exchange its bound PC for PI, thus providing a form of regulation of lipid transfer (Morgan et al., 2004). This implies that disassembly, but not re-assembly, of the hydrogen bond network securing the inositol head group of PI in place is permitted.

(Facing page) Figure 1.5: Mechanisms of PITP activity

(A) In its closed, compact form, PITP shields a single PI or PC molecule from the aqueous environment and transports it between membranes. Once docked onto the membranes, PITP undergoes a conformational change to a relaxed, apo-structure, permitting the exchange of its phospholipid cargo. Diagram adapted from (Schouten et al., 2002). (B) The lipid presentation model: PITP transports PI from the ER to PI4K and PI4P-5-K at the plasma membrane. PI remains bound to PITP in the lipid-binding cavity during sequential phosphorylation to PI(4)P, then PI(4,5)P_2, before finally being presented to PLC for hydrolysis. Diagram taken from (Cunningham et al., 1995). (C) (i) As shown in (A), the closed form of PITP mediates lipid transfer, and the relaxed, apo-form is only achieved at the membrane during lipid exchange. (ii) and (iii) demonstrate how PITP might present PI to a soluble PI3K and membrane-bound PI4K enzyme, respectively. Diagram taken from (Yoder et al., 2001).

A

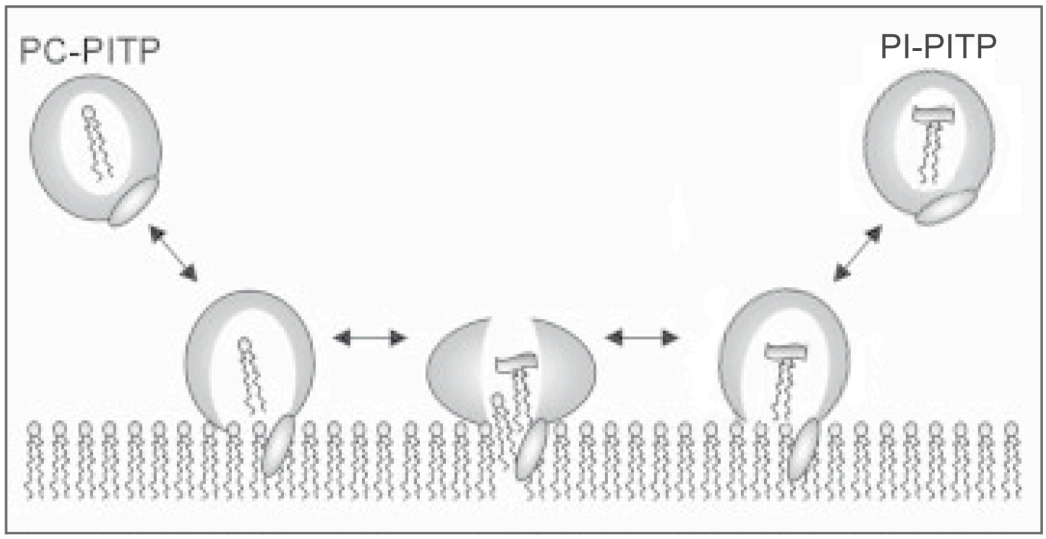
PC-PITP
PI-PITP

B

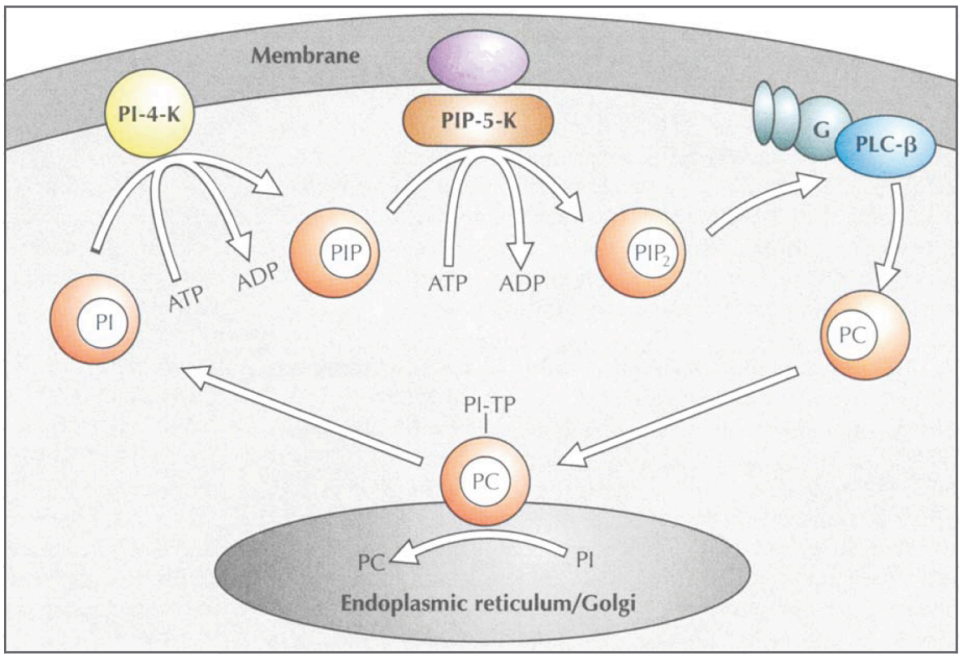
Membrane
PI-4-K
PIP-5-K
G
PLC-β
PIP
PIP2
PI
ATP
ADP
ATP
ADP
PC
PI-TP
PC
PC
PI
Endoplasmic reticulum/Golgi

C

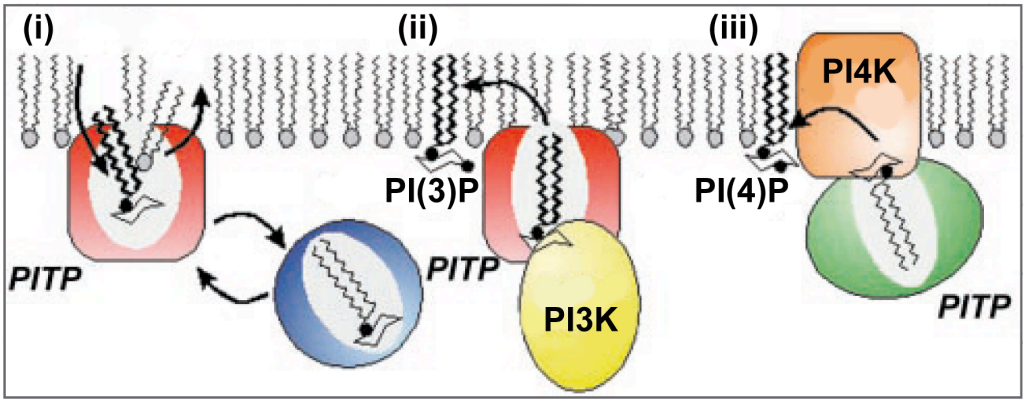
(i)
(ii)
(iii)
PI4K
PI(3)P
PI(4)P
PITP
PITP
PI3K
PITP

The phospho-mimetic mutant, S166E, was observed to be defective for both PI and PC binding and transfer, however (Morgan et al., 2004). The local concentration of negative charge and physical shape could act as a wedge to keep the lipid-binding cavity shut. The elution profile after size exclusion chromatography is distinct for phosphorylated vs non-phosphorylated PITPα, indicating that these two forms are structurally distinct (Morgan et al., 2004). If interaction with other proteins through the regulatory loop is required for *in vivo* function (particularly stimulated function), modification of Ser166 would interfere with these interactions. In support of this, EGFP-PITPα S166E was observed to have a similar pattern of localisation as the wild-type protein in COS-7 cells, but this was not observed to change upon EGF stimulation, unlike the wild-type protein (Larijani et al., 2003).

Ser166 lies in the regulatory loop, between the β7 and β8 strands (Figure 1.3 B). Ser166 is barely exposed in the apo-structure, and this is not different to the closed form (Figure 1.3 D). Nevertheless, X-ray crystal structures present a single fixed snapshot of the protein structure. It is possible that the PITP domain is more flexible in this region, or undergoes a more dramatic conformational change than that observed in the crystal structures to date to enable phosphorylation of Ser166 by PKC.

The PITP domain belongs to the large Bet v 1 superfamily of proteins, which have a common fold. Also a member of this superfamily, steroidogenic acute regulatory protein (StAR) facilitates the movement of cholesterol from the outer to the inner mitochondrial membrane, providing the substrate for steroid hormone biosynthesis. At low pH, 3.5-4.0, StAR partially unfolds to form a highly-helical 'molten globule' structure, facilitating its entry into mitochondria from the inter-membrane space, which has been made acidic by the action of the mitochondrial proton pump (Bose et al., 1999). Similarly, the Bet v 1 protein, the founding member of the Bet v 1 superfamily, undergoes a loss in tertiary structure upon interaction with membranes (Mogensen et al., 2007). A comparable conformational change might be possible for PITP, enabling access to the PI head group for phosphorylation by lipid kinases.

The PI transfer activity of lysates derived from rat cortical neurons stimulated with netrin-1 or BDNF has been assessed, and revealed that the activity was higher in lysates

derived from stimulated cells (Xie et al., 2005). The removal of PITPα from these lysates by immunoprecipitation abolished the transfer activity, indicating that PITPα is the dominant PITP in these cells. The ability of netrin-1 and BDNF to stimulate transfer activity could reflect dephosphorylation of PITPα at Ser166 in response to stimulation.

Cells under-expressing the 43 kDa inositol polyphosphate 5-phosphatase, which specifically removes the phosphate from the 5'-OH of IP_3, experience a 2.6-fold elevation in the basal level of IP_3 and a 4.1-fold increase in the concentration of intracellular Ca^{2+} (Speed et al., 1999). In these cells, a 32% decrease in $PI(4,5)P_2$ mass was observed, and PI transfer activity was found to be reduced by up to 70% compared to control cells, despite no difference in the amount of PITPα expressed (Speed and Mitchell, 2000). (The expression of other PITP family members was not assessed.) This may represent negative feedback, where high IP_3 and Ca^{2+} activates PKC to promote phosphorylation of PITP Ser166, to inhibit PI delivery and to switch off PLC activity. The significant depletion in $PI(4,5)P_2$ (and also PI and PI(4)P) was only observed in the caveolin-rich triton-insoluble fraction, not in the triton-soluble membrane fraction (Speed and Mitchell, 2000), again indicating that PITP delivers PI specifically to the agonist-specific pool.

1.3: The Class IIB soluble PITP, RdgBβ

In contrast to the other members of the PITP family, very little is known about the third soluble PITP, RdgBβ, and for this reason, RdgBβ will be the focus of this study going forward. RdgBβ was originally cloned in 1999 from a human infant brain cDNA library in a screen looking for novel human homologues of Dm-RdgBα (Fullwood et al., 1999). This protein is 332 amino acids long, with a calculated molecular mass of 38 kDa. Subsequently a second, shorter splice variant was identified in mouse (Takano et al., 2003), 269 amino acids in length, with a molecular mass of 31.7 kDa. For clarity I will refer to the long splice variant as RdgBβ-sp1, and the shorter variant as RdgBβ-sp2.

The gene encoding the RdgBβ protein, *PITPNC1*, lies on chromosome 11 in the human genome. The coding region for RdgBβ is made up of 10 exons and *PITPNC1* mRNA is

alternatively spliced to produce the two splice variants. RdgBβ-sp1 is encoded by exons 1-8 and 10, whereas RdgBβ-sp2 is encoded by exons 1-9. Therefore, RdgBβ-sp1 and -sp2 share an identical N-terminal region, but differ from one another in their C-terminal residues; the C-terminus of RdgBβ-sp1 is encoded by exon 10 and the C-terminal region of RdgBβ-sp2 is encoded by exon 9.

Northern analysis indicated that RdgBβ-sp1 is ubiquitously expressed in humans, with particularly strong expression in the heart, muscle, kidney, liver, and peripheral blood leukocytes (Fullwood et al., 1999). In the mouse, the use of RT-PCR indicated that RdgBβ-sp1 was expressed in the brain at E15, P0 and P49, and in the P49 heart, liver, kidney and testes (Takano et al., 2003). *In situ* hybridisation histochemistry was used to examine the localisation of mRNAs in the mouse brain: RdgBβ-sp1 was almost absent from the embryonic brain (E15), and increased after birth. At P7, RdgBβ-sp1 staining was detected weakly in all areas of the brain except the olfactory bulb, Purkinje cell layer and white matter. This is consistent into P49, with moderate RdgBβ-sp1 expression also detected in the Purkinje cell layer of the cerebellum by this time. By P49, RdgBβ-sp1 expression was intense in the dentate gyrus, with moderate expression in the thalamus (Takano et al., 2003).

By contrast, RdgBβ-sp2 expression in the brain was relatively higher in the embryonic stages, declining after birth. At E15, weak RdgBβ-sp2 transcript expression was observed in the ventricular and mantle zones of the cerebral cortex. By P7, RdgBβ-sp2 expression had gone from the cerebral cortex, and very weak staining was observed in the internal granule cell layer. At P49, weak RdgBβ-sp2 staining was observed in the granule cell layer of the cerebellum and in the ependyma (Takano et al., 2003). The use of RT-PCR confirmed RdgBβ-sp2 expression in the mouse brain at E15, P0 and P49, and in addition, expression in the P49 heart and small intestine (Takano et al., 2003).

Confocal laser scanning immunofluorescence microscopy of HEK-293 cells expressing FLAG-RdgBβ-sp1 showed diffuse staining throughout the cytoplasm (Fullwood et al., 1999). PC12 cells expressing GFP-RdgBβ-sp1 or GFP-RdgBβ-sp2 confirmed the RdgBβ-sp1 localisation to the cytoplasm, and revealed that RdgBβ-sp2 is weakly present in the nucleus, as well as in the cytoplasm (Takano et al., 2003).

RdgBβ-sp1 has been observed to exhibit robust PI transfer activity, comparable to that of PITPα, which is unaffected by removal of its C-terminal tail (Fullwood et al., 1999). In a protein-lipid overlay assay, the GST-tagged RdgBβ-sp2 bound to PI only, not to any of the other phospholipids, including PC, or phosphorylated PI derivatives (Takano et al., 2003).

1.4: An interaction between RdgBβ and ATRAP

A physical interaction between RdgBβ and the Angiotensin II receptor-associated protein, ATRAP, has been reported from a yeast two-hybrid screen (Rual et al., 2005). A later screen used RdgBβ as the bait, identified ATRAP as the target protein in the interaction, and reported the mRNA nucleotide accession numbers as BC007905 and BC017328, respectively (Venkatesan et al., 2009). This RdgBβ sequence is the short splice variant, RdgBβ-sp2.

1.4.1: ATRAP

ATRAP itself was identified in a yeast two-hybrid screen against a mouse kidney cDNA library looking for novel interacting partners of the murine Angiotensin II type 1 receptor (AT_1R) C-terminus (Daviet et al., 1999). Subsequently, the human homologue was cloned from a foetal brain cDNA library (Wang et al., 2002). ATRAP, encoded by the *AGTRAP* gene, is an integral membrane protein with three transmembrane domains at its N-terminus, and a hydrophilic C-terminal tail (Lopez-Ilasaca et al., 2003). The first transmembrane domain contains a signal peptide sequence which acts as a signal anchor domain to position the protein in the ER membrane. The N-terminus of ATRAP is oriented outside of the cell (or inside intracellular organelles) and its C-terminus projects into the cytosol (Lopez-Ilasaca et al., 2003). The mouse protein is small, comprising 161 aa with a molecular weight of 17.8 kDa.

ATRAP tissue expression

ATRAP is widely expressed in human, mouse and rat tissues. Assessment of ATRAP mRNA expression in the mouse by northern blot indicated relatively high levels in the kidney, testes and heart, but lower levels in the lung, liver, spleen and brain (Daviet et al., 1999). Using RT-PCR, ATRAP mRNA expression has been observed in all mouse tissues examined, with expression highest in the kidney and declining in the order: kidney > testes ≈ adrenal gland > heart > lung > liver ≈ brain ≈ spleen (Oppermann et al., 2010). RT-PCR also detected ATRAP transcripts in the mouse aortic tissue and vascular smooth muscle cells (VSMCs) (Daviet et al., 1999), and similarly in rat VSMCs in culture and *in situ* in the aortic wall (Azuma et al., 2007). RT-PCR confirmed the presence of ATRAP mRNA in mouse heart and in primary cultured mouse cardiomyocytes (Tanaka et al., 2005). In human tissues, northern blot analysis noted ATRAP expression in almost all of the tissues examined, with particularly abundant expression in the kidney, heart, pancreas and thyroid (Wang et al., 2002).

In the mouse, western blotting has detected high ATRAP protein expression in kidney, lung and testes. More moderate levels were observed in the spleen, and lower expression observed in the heart, brain, liver, skeletal muscle and aorta (Tsurumi et al., 2006). Another study observed ATRAP protein in mouse liver, spleen, heart, intestine and pancreas, and by immunohistochemistry noted ATRAP expression in the zona fasciculata of the adrenal cortex (Oppermann et al., 2010). Western blotting, immunofluorescence microscopy and immunohistochemical analyses all demonstrated that ATRAP protein is expressed in rat VSMCs in culture and *in situ* in the aortic wall (Azuma et al., 2007).

ATRAP protein expression has been reported to be regulated at the level of transcription. In mouse distal convoluted tubule cells of the renal cortex, serum starvation was shown to upregulate *AGTRAP* gene expression, in response to the runt-related transcription factor, Runx3 (Matsuda et al., 2011). Conversely, chronic Angiotensin II infusion (200, 1000 or 2500 $ng.kg^{-1}.min^{-1}$ for 14 days) significantly suppressed ATRAP expression in the outer medulla of the kidney, which could be blocked using the AT_1R antagonist, olmesartan (Wakui et al., 2010a). Similarly,

expression of ATRAP was reduced in mouse hearts from animals infused with 200 $ng.kg^{-1}.min^{-1}$ for 14 days (Wakui et al., 2010b). Lastly, basal expression of ATRAP was suppressed in a mouse brown adipocyte cell line in response to treatment with a β_3-adrenergic receptor agonist, mediated by the PKA and JAK/STAT signalling pathways (Westphal et al., 2008).

ATRAP subcellular localisation

Immunofluorescence microscopy has demonstrated that HA-tagged ATRAP expressed in COS-7 cells localises to intracellular cytoplasmic compartments as well as to the plasma membrane (Daviet et al., 1999), a distribution confirmed for the endogenous protein in HEK-293 cells (Lopez-Ilasaca et al., 2003). Specifically, ATRAP co-localises with a vesicle marker of the endocytic pathway, GFP-RhoB, and the *trans*-medial Golgi marker, ECFP-β-1,4-galactosyltransferase. It co-localises with structures stained by the fluorescent dye, 3,3'-dihexyloxacarbocyanine iodide ($DiOC_6$), which stains ER, vesicle membranes and mitochondria, and partially co-localises with the protein calreticulin, an ER marker (Lopez-Ilasaca et al., 2003). Markers of lysosomes and peroxisomes did not co-localise with ATRAP. ATRAP was also observed to co-localise with GFP-RhoB and ECFP-β-1,4-galactosyltransferase when over-expressed in the human cardiomyocyte cell line, H9c2, in neonatal mouse cardiomyocytes (Tanaka et al., 2005), and in cultured rat VSMCs (Azuma et al., 2007). A quantitative analysis suggested that 67% of total ATRAP was co-localised with endosomes (the GFP-RhoB marker) in unstimulated cells (Azuma et al., 2007), indicating that ATRAP constitutively localises to the endocytic pathway. Analysis of the distribution of ATRAP indicated that there is no significant change in the overall distribution of ATRAP upon stimulation of cells with Angiotensin II (Lopez-Ilasaca et al., 2003; Azuma et al., 2007). ATRAP was not observed to co-localise with caveolin-rich domains at the plasma membrane (Lopez-Ilasaca et al., 2003).

1.4.2: ATRAP and Angiotensin II signalling

The ATRAP-AT_1R interaction

ATRAP specifically interacts with the last 20 aa of the AT_1R (residues 339-359), but not with the C-termini of the AT_2R, the m_3 muscarinic, bradykinin B_2, or endothelin B receptors, nor did it associate with the G_s-coupled β_2-adrenergic receptor (Daviet et al., 1999). The ATRAP-AT_1R interaction has been confirmed for the human proteins (Wang et al., 2002), and the mouse proteins over-expressed in H9c2 cardiomyocytes (Tanaka et al., 2005), and in rat VSMCs by co-immunoprecipitation and bioluminescence resonance energy transfer (BRET) analysis (Azuma et al., 2007). Approximately 10% of ATRAP protein associated with the AT_1R in unstimulated cells (Daviet et al., 1999), and although this early study showed that stimulation of cells with Angiotensin II had no effect on the ATRAP-AT_1R interaction in immunoprecipitation experiments, later studies showed that the interaction was enhanced upon stimulation of the cells with Angiotensin II more than 2-fold (Tanaka et al., 2005; Azuma et al., 2007). Immunofluorescent microscopy has indicated that upon stimulation with Angiotensin II, the AT_1R and ATRAP are co-localised in intracellular compartments, rather than at the cell periphery (Daviet et al., 1999; Lopez-Ilasaca et al., 2003; Tanaka et al., 2005). Experiments using deletion mutants identified the AT_1R-binding site in the C-terminus of ATRAP, between 110 and 122 aa (Lopez-Ilasaca et al., 2003).

Angiotensin II signalling

Angiotensin II is an octapeptide hormone produced by the renin-angiotensin system in vertebrates. This hormone plays a central role in the regulation of blood pressure and maintenance of the water-electrolyte balance through a direct action on tubular re-absorption in the kidney, constriction of blood vessels and stimulation of the release of aldosterone from the adrenal cortex. Angiotensin II also plays a role in cardiovascular disease, including hypertension, cardiac hypertrophy, myocardial infarction and atherosclerosis.

At the cellular level, Angiotensin II has growth factor and cytokine-like properties: it modulates contraction and regulates cell growth, apoptosis and differentiation. It is pro-inflammatory, stimulates the production of other growth factors (e.g. platelet-derived growth factor) and vasoconstrictors (e.g. endothelin-1), and it trans-activates growth factor receptors (e.g. EGF receptor and insulin-like growth factor receptor) (Touyz and Berry, 2002).

There are two receptors for Angiotensin II in humans: AT_1R, of which there are two sub-types, $AT_{1a}R$ and $AT_{1b}R$, and the type 2 receptor (AT_2R). Both are GPCRs with seven transmembrane domains. The majority of the known actions of Angiotensin II are mediated by the AT_1R. The AT_1R, but not AT_2R, undergoes internalisation in response to agonist stimulation (Turu et al., 2006). Upon agonist binding, the AT_1R associates with heterotrimeric G proteins of the $G_{q/11}$ or $G_{12/13}$ class, stimulating PLCβ, promoting Ca^{2+} mobilisation and subsequent PKC activation. In addition, Angiotensin II promotes the activation of PLD, PLA_2, ERK1/2, NAD(P)H oxidase, and subsequently stimulates gene transcription (Touyz and Berry, 2002).

ATRAP has been reported to have a negative effect on Angiotensin II signalling and promote internalisation of the AT_1R. Over-expression of ATRAP suppresses inositol phosphate production by PLC in response to Angiotensin II stimulation (Daviet et al., 1999; Lopez-Ilasaca et al., 2003), without any change in PLCβ or PLCγ protein expression (Daviet et al., 1999). The use of ATRAP C-terminal deletion mutants indicated that the ATRAP-AT_1R interaction is necessary for the suppression of PLC activity (Lopez-Ilasaca et al., 2003). Membrane preparations from HEK-293 cells expressing AT_1R, with or without ATRAP co-expression, were assessed for GTP binding as a measure of G protein coupling: cells expressing ATRAP experienced a reduction in GTP binding following Angiotensin II stimulation (Lopez-Ilasaca et al., 2003).

Radioligand binding assays using membrane preparations indicated that ATRAP over-expression did not significantly affect the number of $AT_{1a}R$ receptors or their affinity for Angiotensin II (Daviet et al., 1999), but similar assays in intact adult VSMCs indicated that the Angiotensin II-induced down-regulation of surface receptors was exaggerated by ATRAP over-expression (Cui et al., 2000). This notion, that ATRAP increases AT_1R

internalisation in response to Angiotensin II stimulation, was confirmed using flow cytometry (Lopez-Ilasaca et al., 2003), and in VSMCs using quantitative fluorescence analysis and a surface AT_1R binding assay (Azuma et al., 2007). This latter study reported that ATRAP increased receptor internalisation, even under basal conditions. The removal of Angiotensin II indicated that ATRAP significantly inhibited the recovery of cell surface AT_1R, since the receptor was maintained in intracellular compartments (Tanaka et al., 2005; Azuma et al., 2007). These experiments indicate that ATRAP associates with the AT_1R under basal conditions, and that the interaction increases in response to Angiotensin II stimulation, promoting uncoupling of the receptor from G proteins and receptor internalisation. It seems plausible that it is the uncoupling from G_q that attenuates inositol phosphate production by PLC in response to Angiotensin II.

In addition to its effect on PLC signalling, the effect of ATRAP on other signalling pathways downstream of Angiotensin II has been assessed. In VSMCs, ATRAP suppressed the Angiotensin II-induced phosphorylation of PKB and STAT, as well as ERK phosphorylation after 60 min (but not 30 min) (Cui et al., 2000). In a different study, Angiotensin II-induced phosphorylation of ERK1/2 and JNK was not affected by ATRAP over-expression, however. Instead, activation of $p38^{MAPK}$ in response to Angiotensin II was significantly suppressed by over-expression of ATRAP (Tanaka et al., 2005).

Angiotensin II induces expression of the immediate early gene, *c-fos* (Sadoshima and Izumo, 1993). However, over-expression of ATRAP abolished the Angiotensin II-induced DNA synthesis, monitored by the incorporation of [^{3}H]-thymidine for 48 hrs (Cui et al., 2000). Another measure of DNA synthesis is by monitoring 5-bromodeoxyuridine (BrdUrd) incorporation. In control VSMCs, Angiotensin II treatment promoted an increase in BrdUrd incorporation of 1.4-fold at 48 hrs, yet ATRAP over-expression completely suppressed this activity (Azuma et al., 2007). Over-expression of ATRAP in CHO-K1 cells stably expressing the AT_1R led to a decrease in both the basal and Angiotensin II-stimulated transcriptional activity of the *c-fos* promoter luciferase reporter gene (Lopez-Ilasaca et al., 2003). Likewise, knock-down of ATRAP expression by transfecting ATRAP siRNA increased the basal level of *c-fos*

promoter activity 1.6-fold, and sensitised the effect of Angiotensin II on promoter activity, increasing it 2.1-fold (Azuma et al., 2007).

ATRAP-knockout mice ($ATRAP^{-/-}$) have been reported to be viable and grossly normal, yet have a significantly higher mean systolic and mean arterial blood pressure than wild-type mice (Oppermann et al., 2010). The plasma volume of the knockout mice was increased by over 20%, relative to the wild-type mice. A ligand binding assay using [^{125}I]-Angiotensin II indicated that $ATRAP^{-/-}$ mice had enhanced surface expression of AT_1R in the renal cortex (Oppermann et al., 2010).

Transgenic mice with cardiac-specific ATRAP over-expression (ATRAP-Tg52) are protected from Angiotensin II-mediated cardiac hypertrophy (Wakui et al., 2010b). In littermate control mice, Angiotensin II infusion significantly increased the diastolic intraventricular septum and diastolic left ventricle posterior wall thickness and heart/ body weight ratio, measures of cardiac hypertrophic responses, yet in the ATRAP-Tg52 mouse these responses to Angiotensin II infusion were completely suppressed. Likewise, upregulation of the cardiac hypertrophy-related genes, atrial natriuretic peptide and brain natriuretic peptide, by Angiotensin II infusion, was completely suppressed in ATRAP-Tg52 mice (Wakui et al., 2010b). Left ventricular $p38^{MAPK}$ was activated at 30 min and 14 days of Angiotensin II infusion in the littermate controls, yet in the ATRAP-Tg52 mice, $p38^{MAPK}$ was not at all activated. In this study, left ventricular JNK and ERK were not significantly activated by Angiotensin II infusion in either the littermate controls or the ATRAP-Tg52 mice (Wakui et al., 2010b).

Another transgenic mouse has been reported in which ATRAP mRNA was increased 3-4-fold in the heart, aorta and femoral artery (ATRAP-Tg) (Oshita et al., 2006). These mice showed no significant change in body weight, systolic blood pressure, heart rate or heart/body weight ratio. The placement of a polyethylene cuff around the femoral artery was used to induce inflammatory vascular injury and remodelling responses, and this has been shown to be accompanied by an increase in AT_1R and AT_2R expression. Proliferation of VSMCs and neointimal formation in the femoral artery was assessed 14 days after cuff placement and was found to be attenuated in the ATRAP-Tg mice. Superoxide production, NADPH oxidase activity and expression of $p22^{phox}$, a

membrane-associated NAD^+/NADPH oxidase subunit, were all attenuated in the injured artery of ATRAP-Tg compared with the wild-type mice (Oshita et al., 2006).

1.4.3: Other ATRAP-protein interactions

RACK1

Human ATRAP has been shown to interact with the receptor for activated C kinase, RACK1 (*GNB2L1*) (Wang et al., 2002). As its name suggests, RACK1 was originally identified as a scaffold protein for active PKC, directing its intracellular localisation (Mochly-Rosen et al., 1991), although many tens of binding partners of RACK1 have now been identified (McCahill et al., 2002). RACK1 binding partners can be divided into two groups, depending on whether stimulation is required for the interaction or not. The interaction between ATRAP and RACK1 is constitutive, occurring irrespective of phorbol ester stimulation (Wang et al., 2002).

The ATRAP-RACK1 association is interesting in light of the fact that the ATRAP domain is present in multi-domain proteins in lower organisms (ciliates and choanoflagellates[1]) alongside a C2 domain for Ca^{2+}-dependent phospholipid binding (similar to the C2 domain in mammalian PKC), a protein kinase catalytic domain and a Ser/Thr kinase catalytic domain. This may indicate a critical role for PKC in mediating the function of ATRAP.

---

[1] In the ciliate, *Paramecium tetraurelia strain d4-2*, the ATRAP domain is present in the following proteins alongside a C2 domain (*gene name*, accession no.): *GSPATT00019026001*, XP_001452241; *GSPATT00011180001*, XP_001442945; *GSPATT00004336001*, XP_001423640. In the choanoflagellate, *Monosiga brevicollis MX1*, the ATRAP domain is present alongside an ankyrin repeat domain, a protein kinase catalytic domain, an ADP ribosylation domain (which catalyses the transfer of ADP-ribose from NAD^+ to substrates), and a Ser/Thr kinase catalytic domain in the protein with gene name, *MONBRDRAFT_38704*, accession no., XP_001749410.

CAML

Due to the ability of ATRAP to suppress Angiotensin II signalling, a yeast two-hybrid screen was carried out to identify interacting partners of ATRAP. This study reported an interaction between ATRAP and the calcium-modulating cyclophilin ligand (CAML) (Guo et al., 2005). CAML activates the capacitative pathway of Ca^{2+} entry from the extracellular medium, which activates the phosphatase, calcineurin, which in turn dephosphorylates the nuclear factor of activated T cells (NFAT), permitting its entry into the nucleus to stimulate gene transcription. CAML is membrane-associated and interacts with ATRAP via its N-terminal, cytosolic domain (Guo et al., 2005). CAML and ATRAP were observed to co-localise at peri-nuclear ER structures, in a pattern similar to the distribution of endogenous ATRAP.

Treatment of HEK-293 cells expressing the AT_1R with 100 nM Angiotensin II for 18 hr, or CAML over-expression, increased transcription of the NFAT reporter gene 4-fold. Conversely, ATRAP over-expression reduced the basal NFAT reporter activity and reduced the Angiotensin II-induced activity (Guo et al., 2005).

Angiotensin II has also been shown to induce vascular senescence through stimulation of the AT_1R, and plays a critical role in vascular ageing and age-related vascular diseases. Senescence can be assessed by staining with senescence-associated β-galactosidase (SA-β-gal). Angiotensin II stimulation of mouse VSMCs was observed to significantly enhance SA-β-gal staining of control cells, starting 5 days after treatment, whereas cells prepared from transgenic mice with 3-4-fold more ATRAP protein expression in the heart, aorta and femoral artery (ATRAP-Tg mice) (Oshita et al., 2006), had markedly lower numbers of SA-β-gal-positive cells (Min et al., 2009). This effect of ATRAP over-expression was blocked by treatment with the AT_1R antagonist, valsartan. In contrast to control cells, which proliferated for 5 days before reaching a plateau, ATRAP-Tg VSMCs continued to proliferate until day 10 (Min et al., 2009).

Senescence in response to Angiotensin II is mediated by the NFAT pathway, and treatment of VSMCs with NFAT siRNA markedly attenuated the Angiotensin II-induced increase in SA-β-gal-positive cells, as well as the expression of p53 and p21, which are

important components in the induction of cellular senescence (Min et al., 2009). ATRAP-Tg mice showed marked attenuation of Angiotensin II-induced NFAT transcriptional activity by the tenth day of treatment.

Lastly, UV irradiation markedly enhanced NFAT transcriptional activity in wild-type VSMCs, whereas this UV-irradiation-induced NFAT transcription was reduced in ATRAP-Tg VSMCs. In contrast to stimulation of NFAT with Angiotensin II, treatment with the AT_1R antagonist, valsartan, did not alter NFAT transcriptional activity in either wild-type or ATRAP-Tg VSMCs (Min et al., 2009). This indicates an AT_1R-independent role for ATRAP in the NFAT pathway. Since ATRAP interacts with CAML (Guo et al., 2005), an upstream activator of NFAT, this likely indicates distinct roles for the ATRAP-protein interactions in the more general suppression of Angiotensin II signalling by ATRAP.

1.5: Thesis Aims

RdgBβ is a member of the PITP family, yet unlike the other PITPs, its biochemical properties have been scarcely characterised. This study aims to shed light on the role of this protein in mammalian cells through characterisation of its protein-protein interactions and lipid-binding properties.

- The PITPs differ mainly in their C-terminal residues. Most notably, RdgBβ-sp1 has a much longer C-terminal domain than either of the other two soluble PITPs, PITPα and PITPβ. The first aim is therefore the characterisation of the C-terminus of RdgBβ-sp1, using bioinformatic tools to assess whether this region contains any secondary structural elements, potential phosphorylation sites or other recognition motifs.

- An interaction between RdgBβ and ATRAP has been reported (Rual et al., 2005; Venkatesan et al., 2009). Both proteins are highly expressed in the heart and kidney (Daviet et al., 1999; Fullwood et al., 1999; Wang et al., 2002; Takano et al., 2003; Tanaka et al., 2005; Tsurumi et al., 2006; Oppermann et al., 2010). The second aim of this thesis will be to establish whether RdgBβ interacts with ATRAP in mammalian cells, using co-immunoprecipitation experiments. Whether RdgBβ is involved in Angiotensin II-stimulated PLC activity will also be examined.

- PITPα and PITPβ bind and transfer PI and PC between membranes. RdgBβ-sp1 transfers PI in a manner comparable to that of PITPα (Fullwood et al., 1999). The lipid binding properties of RdgBβ have been poorly characterised: RdgBβ-sp2 has been reported to bind PI in a lipid overlay assay, not to PC (Takano et al., 2003). The PITP domain of RdgBβ shares 41% sequence identity with the class I PITPs. The third aim will be to establish whether RdgBβ binds PI and PC, like PITPα and PITPβ, using a permeabilised HL60 cell assay.

CHAPTER 2: Materials and Methods

2.1: Bioinformatical sequence analysis and comparative modelling

Visualisation of protein structures was achieved using the PyMOL Molecular Graphics System, Version 0.99, Schrödinger, LLC.

2.1.1: Disorder prediction

The RdgBβ sequence Q9UKF7.2 (PITC1_HUMAN) was used as the target sequence for modelling of the RdgBβ PITP domain. The sequence was first uploaded to the DISOPRED2 Disorder Prediction Server (Ward et al., 2004) to predict the end of the compact PITP domain.

2.1.2: Template identification, structural alignment and comparative modelling

A PSI-BLAST search was performed using the RdgBβ PITP domain sequence as the query against the Protein Databank from the NCBI server (Altschul et al., 1997; Schäffer et al., 2001) to identify closely-related structures. The structure showing the highest sequence identity to the target was chosen to be the template: PDB: 1t27 (rat PITPα complexed with PC, (Yoder et al., 2001)). MODELLER was used for the template-target structure alignment (Figure 2.1 A) and comparative modelling (Eswar et al., 2006), largely using scripts based on the tutorials. The alignment was examined for insertions and deletions ('indels') and mapped onto the template structure visualised using PyMOL. If an indel occurred in a possible region of secondary structure, different positions of the indel were considered and several models made to compare the possible alignment options. Through comparison of the energy profiles for the variants I established that the original indels identified by the initial MODELLER structure alignment were best tolerated in the modelled structure. Five models were made from each alignment and the model performing best in terms of objective function (low), discrete optimised protein energy (DOPE) score (low) and GA341 score (high), were chosen for further analysis.

(Facing page) Figure 2.1: Comparative modelling of the RdgBβ PITP domain

(A) Template-target structure alignment of the 1t27 structure and human RdgBβ sequence (residues 1-251). The alignment was generated using MODELLER and used as the template for modelling the RdgBβ PITP domain. Void-contacting residues are surrounded by a small black box. Larger yellow boxes denote regions of secondary structure, α=helix, β=sheet. (B) PDB: 1t27 structure interpretation by LIGPLOT, obtained from PDBsum (Laskowski, 2009). Hydrogen bonds are indicated by a green dashed line labelled with the length of the bond in angstrom (Å); residues making non-bonded contacts with the ligand (i.e. contacts involving either a carbon or a sulphur atom, where the interaction distance is ≤3.9Å) are shown with red 'eyelashes', where the eyelashes point towards the contacted atom of the ligand. The appropriate atom has eyelashes pointing back. (C) RdgBβ PITP domain comparative model, with void in blue.

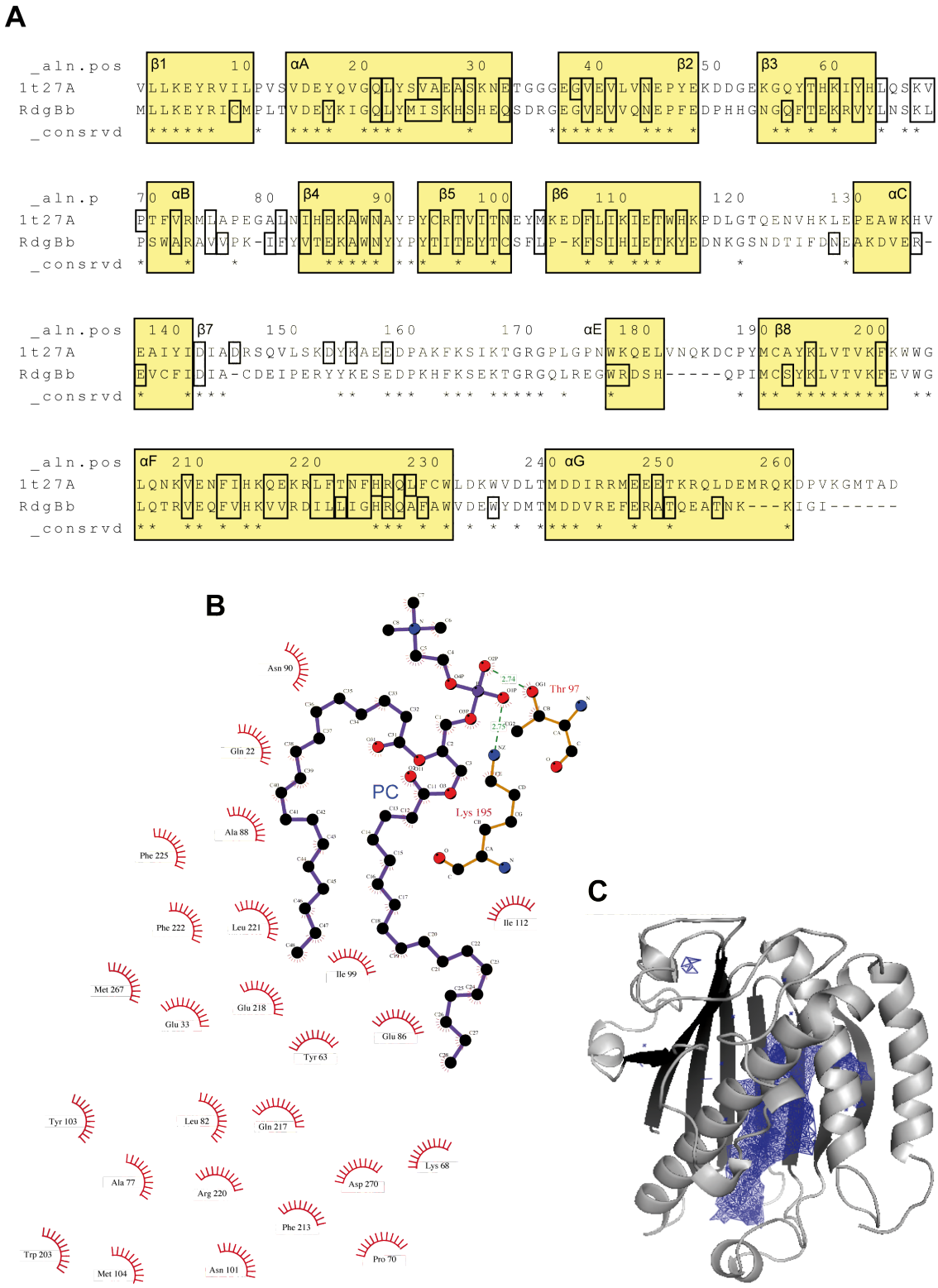
A
_aln.pos
1t27A
RdgBb
_consrvd
β1
αA
β2
β3
αB
β4
β5
β6
αC
αE
β7
β8
αF
αG
B
PC
Lys 195
Thr 97
Asn 90
Gln 22
Ala 88
Phe 225
Phe 222
Leu 221
Ile 99
Met 267
Glu 218
Glu 33
Tyr 63
Glu 86
Ile 112
Tyr 103
Leu 82
Gln 217
Ala 77
Arg 220
Asp 270
Lys 68
Phe 213
Trp 203
Met 104
Asn 101
Pro 70
C

Objective function or molecular probability distribution function (molpdf) is a relative score defined as the sum of all of the restrained terms that modeller is optimising when generating the final model; GA341 is a score indicating the reliability of the model, derived from statistical potentials. In cases where two different models satisfied these criteria, a DOPE score was generated for each residue and plotted on a graph. The model with the overall lowest profile at particular regions of interest in the protein was taken forward for further analysis.

2.1.3: Mapping of the lipid-binding cavity

Void determination was carried out using AVP (Another Void Program, (Cuff and Martin, 2004)). Unlike other void or cavity identification programs, AVP allows the user to define the radius of both the probe and solvent molecules. Initially an analysis of the 1t27 crystal structure was performed. It appeared necessary to delete both the ligand and the solvent co-ordinates from the PDB file to gain an accurate representation of the main cavity volume. Initially the program was run using a probe radius of 0.5Å and a solvent radius of 1.4Å, the standard radius of a water molecule. AVP operates by creating a box around the protein structure and then filling the space between the protein and the edges of the box with solvent molecules. Probe molecules are then placed where they will fit in the box that has not already been defined as either protein or solvent. Use of the solvent radius 1.4Å did not return any large cavities of the expected size in the PITPα structure 1t27, indicating that the inside of the cavity is exposed to the solvent, even when the protein adopts its 'closed' conformation. To identify the large lipid-binding cavity it was therefore necessary to increase the solvent radius to 5.0Å. The program outputs a list of residue atoms adjacent to the identified voids. This list was compared to the output of the LIGPLOT program (Wallace et al., 1995) for the 1t27 structure (Figure 2.1 B), which returned a list of all of the residues in the protein adjacent to the selected ligand. Many more residues were defined as touching a void by AVP than were identified by LIGPLOT as lining the PC-binding cavity. This is because a small probe size such as 0.5Å may also identify improper packing in a protein molecule, not just regions of the protein large enough to accommodate atoms or other molecules. A probe size of 1.2-1.4 Å was more appropriate (Cuff and Martin, 2004).

Probe sizes of 1.2 Å and 1.4 Å were tested sequentially. The 1.2 Å probe identified all of the residues identified by LIGPLOT as well as some additional residues, but not nearly as many as the 0.5 Å probe, which defined 48.0% of the total residues of PITPα as contacting a void (compared to 21.8% for the 1.2 Å probe, 18.5% for the 1.4 Å probe and 9.0% for the LIGPLOT output). At the 1.4 Å probe size, some of the LIGPLOT residues had been lost. 1.2 Å was therefore chosen as the probe size for the analysis of the RdgBβ model. The RdgBβ model in grey with determined void (blue) is shown in Figure 2.1 C. Residues contacting the void are indicated on the structural alignment (Figure 2.1 A).

2.1.4: Multiple sequence alignment

Multiple sequence alignments were carried out using Vector NTI (Invitrogen) or MATLAB student version R2011a, unless otherwise indicated. In MATLAB, the multialign command was used to align multiple sequences using a progressive method. The default scoring matrix was used: the 'BLOSUM80' to 'BLOSUM30' series.

2.1.5: Identification of trypsin cleavage sites

The PeptideCutter tool on the ExPASy proteomics server (Gasteiger, 2003) was used to predict trypsin cleavage sites in the RdgBβ-sp1 and -sp2 sequences, with a cleavage probability of <80% excluded (3 sites).

2.1.6: Identification of PEST sequences

The PEST sequences were identified using the pestfind algorithm on the Emboss server (http://emboss.bioinformatics.nl/) (Rogers et al., 1986). PEST motifs are defined as hydrophilic stretches of ≥12 aa with at least one proline, one glutamic acid or aspartic acid, and one serine or threonine residue. They are flanked by lysine, arginine or histidine residues; these positively charged residues are not allowed within the PEST sequence.

2.2: Molecular biology: engineering of expression vectors

2.2.1: Starting plasmids

RdgBβ

Double-stranded DNA plasmid pEFPLink2-FLAG-RdgBβ-sp1 (human RdgBβ-sp1 cDNA sequence with an N-terminal FLAG tag, under the control of the elongation factor 1a promoter) was a gift from Prof. Justin Hsuan (Dept. of Medicine, University College London) (Fullwood et al., 1999). This construct was used as the starting sequence by Dr. Roman Holic from which to clone RdgBβ-sp1 into pRSET-C-His vector (Invitrogen) for bacterial expression of the recombinant protein, using the *Xho*I/ *Eco*RI restriction sites (pRSET-C-His-RdgBβ-sp1) (Figure 2.2 A). The same sites were used by Roman Holic to clone RdgBβ-sp1 into the pIRES2-EGFP bis-cistronic vector (BD Bioscience) for mammalian expression of the untagged protein with EGFP co-expression.

The RdgBβ-sp1 truncated mutant (recombinant protein), pRSETc-RdgBβ-sp1 1-263, primer design was carried out by Roman Holic, with the substitution of a stop codon after residue 263; PCR, mini-preps and other later stages were carried out by myself.

The human RdgBβ-sp2 IMAGE clone cDNA (IMAGE: 4299595) was obtained from MRC Geneservice and cloned into the pRSET-C-His vector for bacterial expression using the *Xho*I/*Eco*RI restriction sites (pRSET-C-His-RdgBβ-sp2) (Figure 2.2 A) by Dr. Clive Morgan.

ATRAP

The double-stranded DNA plasmid pcDNA3-HA-ATRAP (mouse ATRAP sequence with an N-terminal HA tag, under the control of the CMV promoter) was a gift from Dr. Marco Lopez-Ilasaca (Brigham and Women's Hospital, Harvard Medical School, Boston, MA, U.S.A.) (Daviet et al., 1999) (Figure 2.2 B).

(Facing page) Figure 2.2: Plasmid maps

(A) Map of the pRSET-C plasmid showing the site of the ampicillin resistance gene (for selection in bacterial cells) and site of RdgBβ-sp1 or -sp2 inserted coding sequences. Expression in prokaryotes is driven by the strong bacteriophage T7 promoter ('P'). 'ATG' indicates the START codon (coding for a methionine), followed by the N-terminal polyhistidine sequence ('6x His'). *Xho*I, *Eco*RI and *Hind*III indicate the position of the restriction endonuclease recognition sequences discussed in the text. (B) Map of the pcDNA3-HA-ATRAP plasmid. Site of the ampicillin resistance gene is indicated, as well as the neomycin resistance gene (for selection in mammalian cells to create stable cell lines). Expression in mammalian cells is driven by the strong CMV promoter ('P') indicated. (C) Map of the pcDNA3.1(+/-) plasmid with the sites of the restriction endonuclease recognition sequences in the multiple cloning site ('MCS') indicated. (+) and (-) plasmids contain the MCS in different orientations.

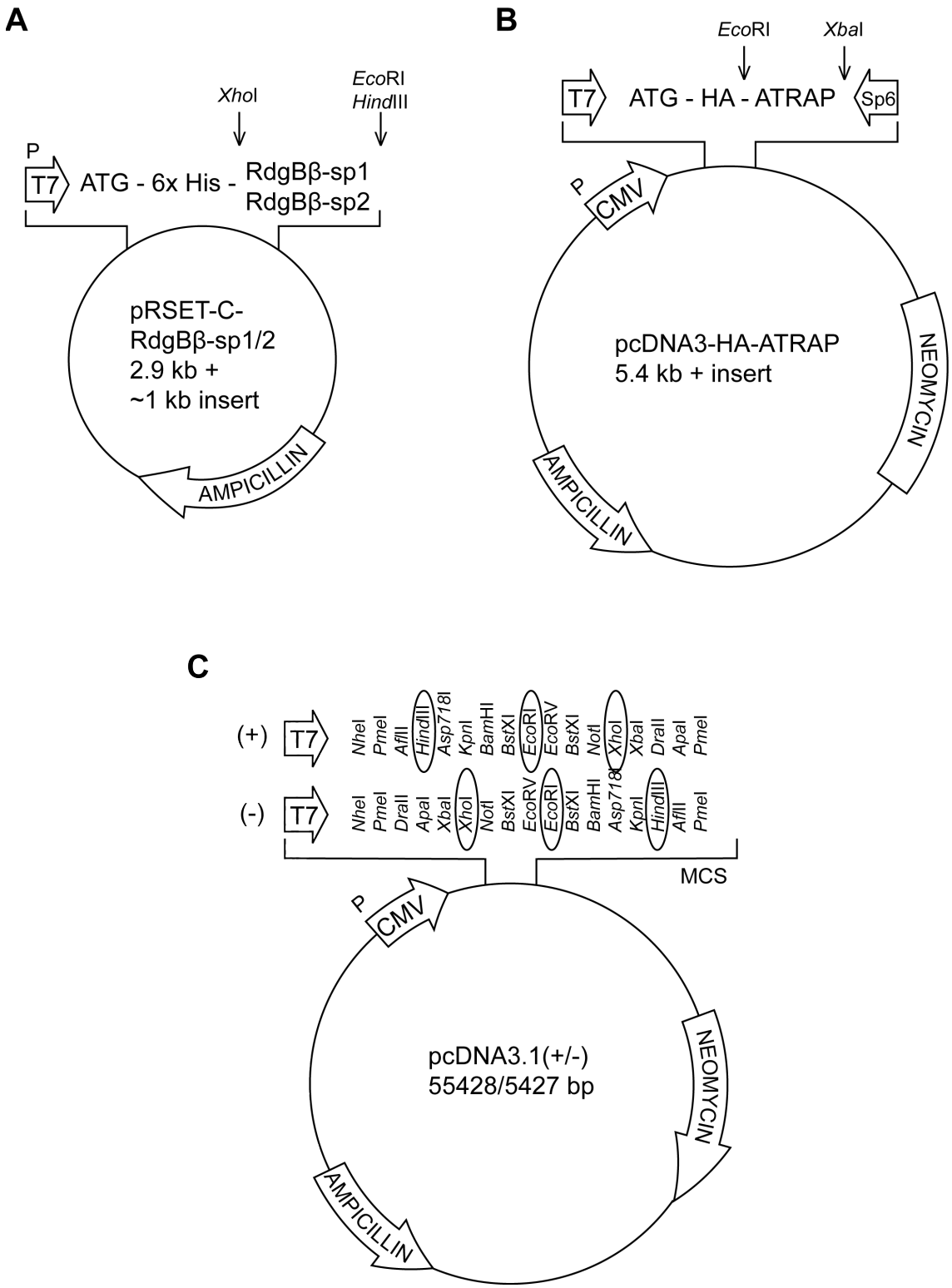
A
XhoI
EcoRI
HindIII
P
T7
ATG - 6x His -
RdgBβ-sp1
RdgBβ-sp2
pRSET-C-
RdgBβ-sp1/2
2.9 kb +
~1 kb insert
AMPICILLIN
B
EcoRI
XbaI
T7
ATG - HA - ATRAP
Sp6
P
CMV
pcDNA3-HA-ATRAP
5.4 kb + insert
NEOMYCIN
AMPICILLIN
C
(+)
T7
NheI PmeI AflII HindIII Asp718I KpnI BamHI BstXI EcoRI EcoRV BstXI NotI XhoI XbaI DraII ApaI PmeI
(-)
T7
NheI PmeI DraII ApaI XbaI XhoI NotI BstXI EcoRV EcoRI BstXI BamHI Asp718I KpnI HindIII AflII PmeI
MCS
P
CMV
pcDNA3.1(+/-)
55428/5427 bp
NEOMYCIN
AMPICILLIN

AT_1R

The rat $AT_{1a}R$ sequence with an N-terminal HA tag in the pcDNA3.1(+) expression vector, pcDNA3.1-HA-$AT_{1a}R$, was a gift from Dr. Kevin Catt, NICHD, NIH, Bethesda, MD, USA.

2.2.2: Gene cloning with the addition of a protein tag

Antibodies which recognise common protein tags have been well-characterised, are commercially available and cheap. Common protein tags used are FLAG (DYKDDDDK), HA (YPYDVPDYA) and Myc (EQKLISEEDL). The RdgBβ-sp1 and -sp2 sequences were amplified from the pRSET-C-His vectors by PCR, with the addition of the nucleotide sequence for one of the protein tags in the forward primer. The amplified sequences were then cloned into the pcDNA3.1(-) vector, rather than the (+) vector, due to the orientation of the multiple cloning site (Figure 2.2). In the pcDNA3.1 vector, strong protein expression is driven by the CMV promoter. By contrast, the elongation factor 1a promoter in the pEFPLink2 plasmid is a relatively weak promoter.

2.2.3: Primer design

Since both splice variants of RdgBβ share the same N-terminal sequence, the same forward primers could be used for each splice variant, one for each protein tag: FLAG, HA, Myc. Only a single reverse primer was required for each splice variant (Figure 2.3 A). The sequence for a restriction enzyme cleavage site was inserted into each primer: *Xho*I site into all of the forward primers, *Eco*RI into the RdgBβ-sp1 reverse primer, and *Hind*III into the RdgBβ-sp2 reverse primer.

The primers were designed following guidelines set out by Sambrook and Russell (Sambrook, 2001), together with protocol guides in the Fermentas and NEB product catalogues. To summarise, PCR primers were designed according to the following rules:

1. Primers should have 40-60% GC content (guanine and cytosine nucleotides), with an even distribution of all four bases along the length of the primer.
2. The region of the primer complementary to the template should be 18-25 nucleotides long, and members of a primer pair should not differ by >3 nucleotides.
3. No inverted repeat sequences or self-complementary sequences >3 nucleotides in length should be present, as these may form hairpin structures.
4. The calculated T_m (melting temperature) values of members of a primer pair should not differ by >5°c.
5. The 3' base of each primer should be a single G or C, not GC or CG, etc.

(Facing page) Figure 2.3: Cloning RdgBβ with the addition of an N-terminal tag

(A) Strategy for N-terminal protein sequence tagging, by the addition of the tag nucleotide sequence in the forward primer. (B) Agarose NA gel showing the first successful PCR of FLAG-RdgBβ-sp1 and -sp2 (5 µL PCR product per lane; 1 µL pRSET-C-RdgBβ-sp2 plasmid). (C) Agarose Prep gel of the FLAG-RdgBβ inserts after digestion. The exact insert size is 1037 nucleotides for sp1 and 845 nucleotides for sp2. The darker region indicates where the gel has broken, just above the insert bands. The inserts were isolated from this gel for ligation into the digested vector. (D) Ligated plasmids were used to transfect COS-7 cells. Cells were harvested 48 hrs after transfection, and 45 µg lysates were subjected to western blotting using anti-RdgBβ antibody #101 (left panels) or anti-FLAG antibody (right panels). FLAG-RdgBβ-sp2 is not detected by either antibody, despite a correct sequencing result.

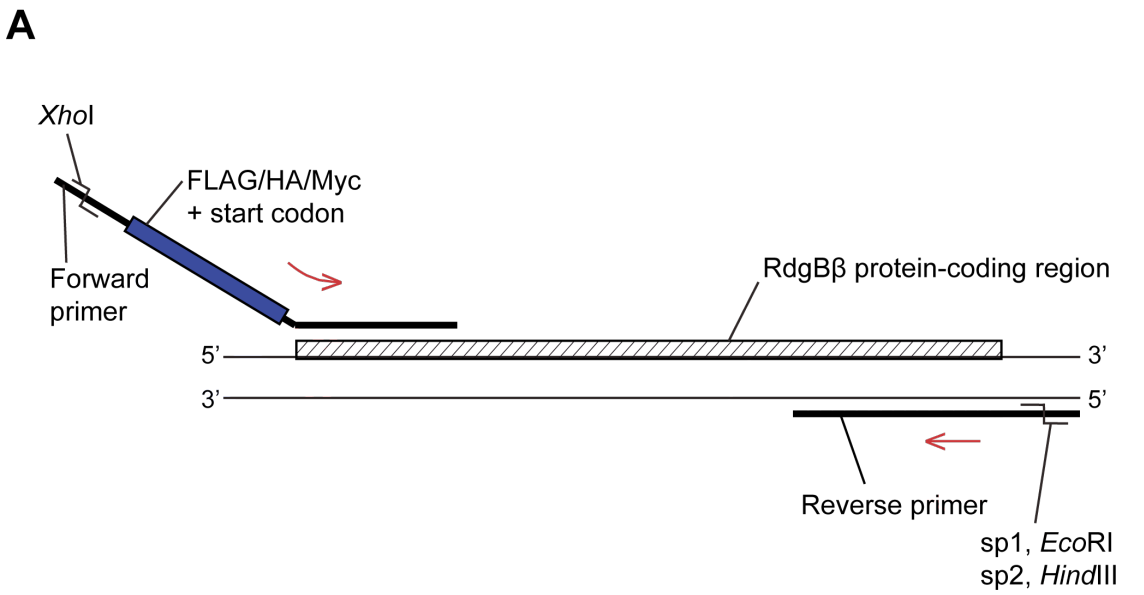
A
XhoI
FLAG/HA/Myc
+ start codon
Forward
primer
RdgBβ protein-coding region
5'
3'
3'
5'
Reverse primer
sp1, EcoRI
sp2, HindIII

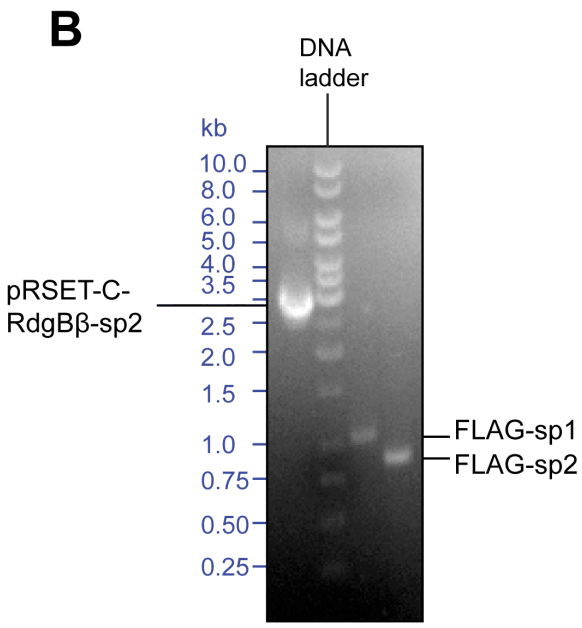
B
DNA
ladder
kb
10.0
8.0
6.0
5.0
4.0
3.5
2.5
2.0
1.5
1.0
0.75
0.50
0.25
pRSET-C-
RdgBβ-sp2
FLAG-sp1
FLAG-sp2

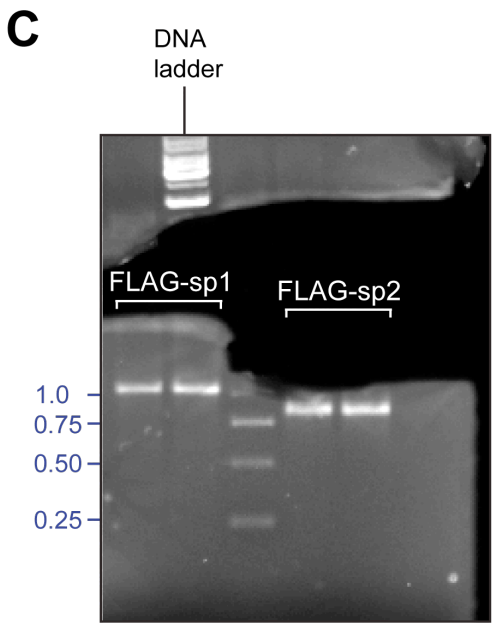
C
DNA
ladder
FLAG-sp1
FLAG-sp2
1.0
0.75
0.50
0.25

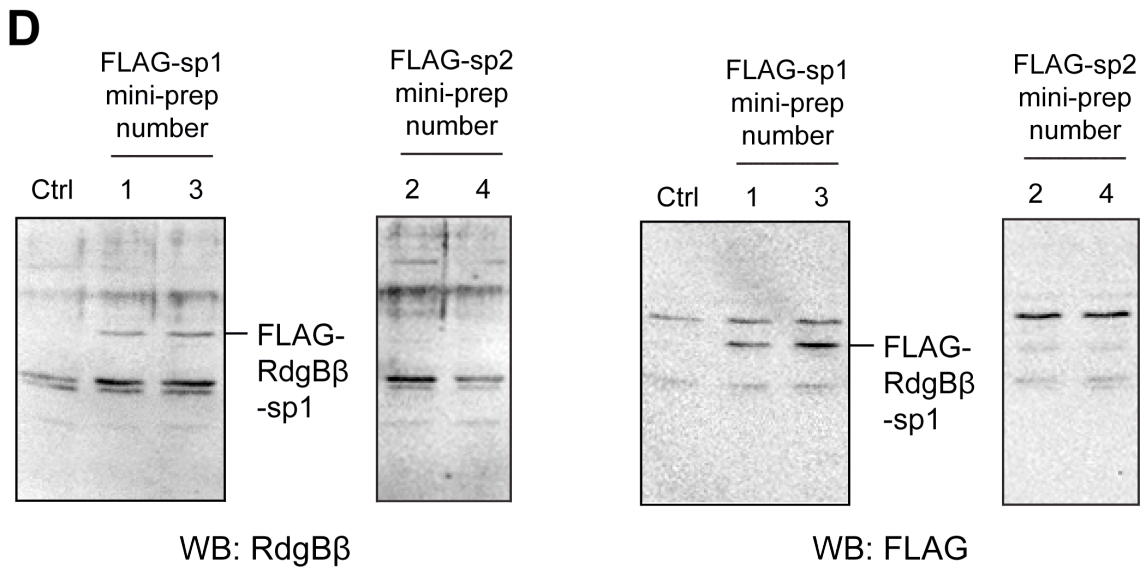
D
FLAG-sp1
mini-prep
number
FLAG-sp2
mini-prep
number
Ctrl
1
3
2
4
FLAG-
RdgBβ
-sp1
WB: RdgBβ
FLAG-sp1
mini-prep
number
FLAG-sp2
mini-prep
number
Ctrl
1
3
2
4
FLAG-
RdgBβ
-sp1
WB: FLAG

2.2.4: Primer sequences

^ Restriction endonuclease cleavage site.

Red Valine, start of protein coding sequence (mutated from methionine, ATG).

Blue Tag nucleotide sequence.

Green Alanine, inserted as a spacer.

FLAG-RdgBβ forward primer (65 nucleotides, 23 complementary).

(T_m = 89.9°c, GC = 50.7 %).

5’ - GACC^TCGAGCAATGGATTACAAGGATGACGACGATAAGGCAGTG

CTGCTGAAAGAGTACCGGATC – 3’

HA-RdgBβ forward primer (68 nucleotides, 23 complementary).

(T_m = 92.1°c, GC = 55.8 %).

5’ -GACC^TCGAGCAATGTACCCATACGACGTCCCAGACTACGCTGCAGTG

CTGCTGAAAGAGTACCGGATC – 3’

Myc-RdgBβ forward primer (71 nucleotides, 23 complementary).

(T_m = 90.6°c, GC = 49.2 %).

5’ - GACC^TCGAGCAATGGAACAAAAACTCATCTCAGAAGAGGATCTGGCA

GTGCTGCTGAAAGAGTACCGGATC – 3’

RdgBβ-sp1 reverse primer (68 nucleotides, 68 complementary).

(T_m = 88.9°c, GC = 45.5 %).

5’ -AAGCTTCG^AATTCTTACTCAGATTTGGGCCGACATGGCTTATCTG

AAGAGTGCATGCCGGGTAAATTC – 3’

RdgBβ-sp2 reverse primer (68 nucleotides, 68 complementary).

(T_m = 91.3°c, GC = 50.0 %).

5’ –GCAGCCGGATCA^AGCTTTCATGTACTTGTTTGGGCATGACTCTCT

ATGTCATCCACAGGGGAGGAATG – 3’

2.2.5: PCR

Primers were manufactured by Sigma-Aldrich custom oligos service. The primers were centrifuged prior to opening, then diluted to 100 μM with molecular grade water. The tubes were vortexed and then frozen at -20°c for 15 mins to help to dissolve the DNA. The RdgBβ-sp1 and -sp2 pRSET plasmids were diluted to 25 ng.μL^{-1}; the primers were further diluted to 125 ng.μL^{-1} (≈ 6.25 μM).

Six reaction mixtures (50 μL) were set up in coloured, thin-walled PCR tubes on ice:

- 5 μL 10X *Pfu* reaction buffer (Stratagene)
- 1 μL dNTP mix (Stratagene)
- 2 μL dsDNA template (50 ng; 125 nM) (pRSET-C-His-RdgBβ-sp1/sp2)
- 1 μL forward primer (FLAG/HA/Myc) (125ng)
- 1 μL reverse primer (sp1/sp2) (125ng)
- 39 μL molecular grade water
- 1 μL *Pfu* turbo DNA polymerase (Stratagene)

Pfu DNA polymerase has intrinsic 3'→5' exonuclease activity and therefore was added last to prevent the degradation of the primers. The elongation time of this enzyme is 2 min.kb^{-1}.

The PCR tubes were briefly vortexed and centrifuged, before being placed into the PCR machine (Techne GeneE Thermal Cycler). The PCR programme used is detailed in Table 2.1; the parameters were chosen according to Fermentas recommendations. The most sensitive parameter was the primer annealing temperature. This should be 5°c lower than the lowest primer T_m. Initially the T_m of the full primer length was considered: the lowest T_m was 88.9°c, and so 80°c was chosen for primer annealing.

After two failed attempts at the PCR I realised the T_m should refer only to the region of the primer complementary to the template sequence. At this point I also realised my primers were too long; although rule 2 from the primer design guidelines states that primer pair lengths should not differ by more than 3 nucleotides, it wasn't until after I had designed and ordered the primers that I realised this applied to the region of the

primer complementary to the plasmid sequence, i.e. 23 nucleotides. The T_m of the forward primers therefore decreases from 89.9-92.1°c to just 54°c, with a GC content of 52%. The reverse primer T_m is 88.9-91.3°c. The primer annealing temperature was dropped to 49°c and this time, the PCR was successful (Figure 2.3 B).

Programme	Segment	Temperature	Time	Activity
1	-	95°c	3 min	Initial denaturation
2 (25 cycles)	1	95°c	2 min	Denaturation
	2	49°c	2 min	Primer annealing
	3	72°c	4 min	Extension
3	-	72°c	10 min	Final extension

Table 2.1: Overview of PCR program for tagging RdgBβ

2.2.6: DNA gel electrophoresis

An agarose gel was run after the PCR to verify the presence of an amplified product. A 1% Agarose gel was made by dissolving 0.5 g Agarose NA (or Agarose Prep, if excision of the DNA from the gel was required), in 50 mL **Tris-acetate-EDTA buffer (TAE; 0.8 mM Tris-HCl pH 8.0, 0.4 mM acetic acid, 0.02 mM EDTA**; 1X TAE buffer was diluted from a laboratory stock solution of 50X, 40 mM Tris-HCl pH 8.0, 20 mM acetic acid, 1 mM EDTA), using a microwave at full power for 1 min. The agarose solution was then allowed to cool so that it was still warm but no longer burns to the touch. (Ethidium bromide is broken down at higher temperatures.)

2.5 µl ethidium bromide (of 10 $mg.mL^{-1}$ stock, for 50 mL agarose) was pipetted directly onto the gel tray, which was locked into the Bio-Rad gel caster. The agarose solution was then poured into the tray and mixed with the ethidium bromide using the comb. The

comb was placed into the designated comb slots at one end of the gel, and the gel left at room temperature for ~30mins to set.

Once the gel had set, the gel in its tray with the comb still in place was transferred to the Bio-Rad Mini-Sub Cell GT Cell (for submerged horizontal electrophoresis), with the comb end (sample wells) at the black (negative electrode) end. TAE buffer was poured into the apparatus, up to the line indicated on the side. The comb was then removed, allowing buffer to fill the wells.

Samples were loaded: 5 µL PCR product + 1 µL 6X DNA loading dye (Blue #R0611 or Orange #R0639, Fermentas), alongside 1 µg (10 µL) Fermentas GeneRuler 1 kb DNA ladder (0.1 $\mu g.\mu L^{-1}$, #SM0313, Fermentas) in narrow lanes (Figure 2.3 B). When purification of DNA was required, the whole DNA sample was loaded onto the Agarose Prep gel (in wide lanes), mixed with an appropriate quantity of loading dye. A single sample typically took up 2 wide lanes (Figure 2.3 C).

The safety lid was then placed onto the apparatus in the correct orientation, and electrical leads plugged into the Bio-Rad Power-Pac 3000. Agarose NA gels were run at 100 V for ~30 mins; Agarose Prep gels have a lower melting temperature, and were therefore run at 60 V until the dye front had travelled ⅔-¾ along the gel.

2.2.7: Digestion

The remainder of the PCR product (~45 µL) was purified using the GENECLEAN kit (MP Biochemicals). The purified DNA was eluted in 30 µL molecular grade water and digested in 50 µL:

30 µL PCR product
5 µL 10X BSA
5 µL 10X NEBuffer2* (New England Biolabs)
1 µL restriction enzyme 1 (*Xho*I for both sp1 and sp2)
1 µL restriction enzyme 2 (*Eco*RI for sp1; *Hind*III for sp2)
Molecular grade water to 50 µL.

*NEBuffers: *Xho*I and *Eco*RI have high activity in buffers 2, 3 or 4; *Hind*III only has a high rate of activity in buffer 2.

The mixture was briefly centrifuged, then placed at 37°c for 2 hrs. The entire digestion was then run on a 1% Agarose Prep gel for isolation of the digested inserts (e.g. FLAG-sp1 and FLAG-sp2, Figure 2.3 C). Digestion of the pcDNA3.1(-) plasmid with *Xho*I and *Eco*RI for sp1, or *Xho*I and *Hind*III for sp2, was carried out in 50 µL, as above, only with 7 µg plasmid (7 µL of 1 $\mu g.\mu L^{-1}$) instead of the PCR product. The digested plasmid was also run on an Agarose Prep gel.

For excision of the insert or digested plasmid, the gel was illuminated on a UV light box, briefly so as not to introduce mutations. The insert and cut plasmid were excised from the gel using a razor blade, and transferred into a pre-weighed 1.5 mL eppendorf tube. The tube with gel fragment was weighed again, and the DNA purified from the gel using the GENECLEAN Turbo kit. The purified DNA was eluted in molecular grade water.

2.2.8: Ligation

The ligation of the digested insert into the digested plasmid was carried out in 20 µL:

4 µL 5X ligase buffer (thawed slowly on ice)
0.5 µL T4 DNA ligase
1 µL digested pcDNA3.1(-) plasmid
4 µL digested insert
Molecular grade water to 20 µL

The ligation mixture was subjected to a brief vortex and incubated at room temperature for 1-2 hrs. For the HA- and Myc-tagged proteins, the first ligation was unsuccessful using the ratio of insert to digested plasmid above. Samples of the digested plasmid and insert were run side-by-side on an Agarose NA gel to estimate their relative concentrations. The insert band on the gel was very faint, so its quantity was maximised in the ligation mixture to 14.5 µL.

2.2.9: Transformation of XL1-blue competent cells

Pouring agar plates

Luria agar (25 $g.L^{-1}$) was autoclaved in Duran bottles and stored at room temperature until required. To make agar plates, the lid of the Duran bottle was loosened, and the bottle placed into the microwave on full power for ~1 min 10 sec to melt the agar. The bottle was then allowed to cool so that it was still warm but no longer burned to the touch (hand hot). (The ampicillin will be degraded if the agar is too hot.) 100 µL ampicillin solution (100 $mg.mL^{-1}$ stock) was added to the 100 mL Luria agar, giving a final ampicillin concentration of 100 $\mu g.mL^{-1}$. The addition of ampicillin permitted the selection of bacteria containing a plasmid carrying the ampicillin resistance gene.

With a bunsen flame close by to create aseptic conditions, 10 mL agar solution was poured into each of ten, 10 cm-diameter Petri dishes, which had been labelled on their bases. The plates were allowed to cool at room temperature until required.

Transformation of bacteria

The required number of agar plates were placed in the dry incubator at 37°c, upside down, propped at an angle on their lids to remove any moisture that had accumulated, for 1-2 hrs prior to use. Two plates were prepared per ligation.

For each ligation, 10 µL of ligation mixture was placed into a labelled eppendorf tube on ice, followed by 100-200 µL XL1-blue super-competent cells. The tubes were flicked briefly to ensure the contents were properly mixed, and incubated on ice for 20-30 mins. (For purified DNA, 1-2 µL DNA was used per transformation, where the concentration was 0.1-1.0 $\mu g.\mu L^{-1}$, as after a mini- or maxi-prep.)

The bacteria were then administered a ‘heat shock’ by placing the tubes into a water bath at 42°c for 45 sec (30 sec-1 min), before returning to ice for 2 mins.

500-800 μL Miller's Luria broth (LB) was added to each tube, the tubes inverted several times to ensure adequate mixing, and then placed at 37°c for 1 hr, either in a water bath or dry incubator. (200 mL LB (25 $g.L^{-1}$) was previously made up in a 250 mL Duran bottle and autoclaved. The bottle was stored at RT.)

With a bunsen flame close by, 300-500 μL transformed cells (i.e. half the combined volume of cells and added LB) were transferred onto each of two labelled agar plates and spread using a glass cell spreader, which had been sterilised with ethanol in the bunsen flame.

The agar plates were then returned to the dry incubator at 37°c, with the agar on the bottom for ~30 mins. Once the liquid had been absorbed by the agar, the plates were inverted and left in the incubator overnight. (Alternatively, plates were placed in the dark at RT over a weekend.)

2.2.10: Growth of bacterial culture, mini-prep and DNA sequencing

The next step was to get the plasmid sequenced. Four 'mini-prep' cultures per ligation were set up and grown for ~16 hrs in an incubator shaker at 37°c: 5 μL ampicillin (of 100 $mg.mL^{-1}$ stock, giving a final ampicillin concentration of 100 $\mu g.mL^{-1}$ in 5 mL culture) was added to 5 mL LB in a 15 mL falcon tube under aseptic conditions. A sterile pipette tip was then used to pick a single colony from the agar plate, which was then ejected directly into the tube. The falcon tubes were vortexed prior to overnight incubation.

The plasmid DNA was purified from the bacterial culture the following day using the QIAGEN QIAprep miniprep kit, following the manufacturer's instructions. The final elution was carried out in 50 μL molecular grade water.

The DNA concentration of the purified DNA was measured using a spectrophotometer at 260 nm absorbance. Of the four mini-preps carried out per ligation, the two with the highest DNA concentration were sent to Eurofins MG Operon for sequencing. 1.5 μg of each nucleic acid preparation was sent (at a concentration of 100 $ng.\mu L^{-1}$).

In addition, the purified plasmid was transfected into COS-7 cells, and the lysate subsequently subjected to SDS-PAGE and western blotting using a primary antibody directed against the added protein tag (Figure 2.3 D). (See method for transient transfection using FuGENE HD below.)

2.2.11: Site-directed mutagenesis

In order to assess the contribution of a single amino acid to protein function, site-directed mutagenesis can be used to substitute one or two nucleotides. The method used broadly followed that given in the Stratagene QuikChange kit. Short DNA primers were designed that complemented the parent plasmid exactly, barring for the one or two nucleotide alteration. PCR was then used to amplify the parent plasmid, incorporating the base change.

Primer design

Primers were designed using the online tool, PrimerX (http://www.bioinformatics.org/primerx/). For these primers, criteria given in the Stratagene QuikChange protocol was followed, which was more specific than that detailed in Section 2.2.3:

1. Primers should be 25-45 bases in length, with a $T_m \geq 78°c$.
2. The desired mutation should be in the middle of the primer with ~10-15 bases of correct sequence on both sides.
3. A GC content of >40% is recommended, and each primer should terminate in one or more C or G bases.

Site-directed mutagenesis was used to introduce the following mutations into pcDNA3.1-FLAG-RdgBβ-sp1: S274A, T278A, S299A, SS274/299AA, and the truncated mutant 1-250, where I251 was mutated into a stop codon (I251_STOP). The double mutant SS274/299AA was made by mutating S299A in the pcDNA3.1-FLAG-RdgBβ-sp1-S274A plasmid. The primer sequences and technical information are given

below. The star (*) above and below the primer sequence indicates the position of the substituted residue(s).

Primers were manufactured by Sigma-Aldrich custom oligos service or Eurofins MWG Operon. The websites automatically calculated the degree to which secondary structure formation within the primers was possible, or whether the uploaded sequences were susceptible to dimerisation. If strong secondary structure formation or dimerisation was predicted, I returned to the PrimerX list of designed primer options and chose a more appropriate sequence.

S274A

```
                          **
Forward: 5' CAGTGCGCCTTCTGCTGCTCCATCCAC 3'
Reverse: 5' GTGGATGGAGCAGCAGAAGGCGCACTG 3'
                        **
 GC content: 62.96%           Location: 807-833
 Melting temp: 75.3°C         Mismatched bases: 2
 Length: 27 bp                Mutation: Substitution
 5' flanking region: 13 bp    Forward primer MW: 8123.38 Da
 3' flanking region: 12 bp    Reverse primer MW: 8439.56 Da
```

T278A

```
                              *
Forward: 5' CTTCTAGTGCTCCATCCGCCCCTCTCTCCACAGAC 3'
Reverse: 5' GTCTGTGGAGAGAGGGGCGGATGGAGCACTAGAAG 3'
                             *
 GC content: 60.00%           Location: 815-849
 Melting temp: 83.8°C         Mismatched bases: 1
 Length: 35 bp                Mutation: Substitution
 5' flanking region: 17 bp    Forward primer MW: 10474.94 Da
 3' flanking region: 17 bp    Reverse primer MW: 11031.24 Da
```

S299A

```
                          *
Forward: 5' CCCCGGAAAAAGGCTGCCCCAGAAAC 3'
Reverse: 5' GTTTCTGGGGCAGCCTTTTTCCGGGG 3'
                          *
 GC content: 61.54%           Location: 883-908
 Melting temp: 77.0°C         Mismatched bases: 1
 Length: 26 bp                Mutation: Substitution
 5' flanking region: 12 bp    Forward primer MW: 7928.27 Da
 3' flanking region: 13 bp    Reverse primer MW: 8016.27 Da
```

I251_STOP

```
                                  ***
Forward: 5' CCACCAACAAGAAAATCGGCTAATTCCCACCTGCAATTTCTATC 3'
Reverse: 5' GATAGAAATTGCAGGTGGGAATTAGCCGATTTTCTTGTTGGTGG 3'
                                   ***
 GC content: 43.2%           Location: 731-774
 Melting temp: 76.8°C         Mismatched bases: 3
 Length: 44 bp                Mutation: Substitution
 5' flanking region: 20 bp    Forward primer MW: 13332.86 Da
 3' flanking region: 21 bp    Reverse primer MW: 13728.03 Da
```

PCR

Reaction mixtures were set up on ice, exactly as detailed in section 2.2.5. The PCR program used was a combination of that recommended by the Stratagene QuikChange protocol, and the program used for tagging of the RdgBβ sequences (Table 2.2). The pcDNA3.1(-) plasmid is 5.4 kb in length, and FLAG-RdgBβ-sp1 insert is approximately 1 kb in length, giving a total plasmid size of ~6.4 kb. An extension time of 13 min was therefore chosen to allow for the extension rate of 2 kb.min^{-1} by *Pfu* DNA polymerase.

Programme	Segment	Temperature	Time	Activity
1	-	95°c	2 min	Initial denaturation
2 (16 cycles)	1	95°c	2 min	Denaturation
	2	(5°c lower than lowest primer T_m)	1 min	Annealing
	3	68°c	13 min	Extension
3	-	68°c	10 min	Final extension

Table 2.2: Overview of PCR program for site-directed mutagenesis

Digestion of parental DNA

Once the PCR program had finished, the tubes were removed from the thermal cycler and placed on ice for 2 mins. 1 µL *Dpn*I restriction enzyme (10 $U.\mu L^{-1}$ stock) was added to each tube to digest the parental, non-mutated DNA. The tubes were then centrifuged briefly before being placed in either the water bath or dry incubator at 37°c for 1 hr. 2 µL DNA was then used to transform XL1-blue competent cells, mini-preps made and mutated DNA sent for sequencing as described above.

2.3: Production of Recombinant Proteins

2.3.1: Principle

Recombinant proteins can be produced by transforming bacteria, specifically the BL21 (DE3) pLysS competent *E. coli* strain (Stratagene), with a plasmid containing the gene of interest. This *E. coli* strain carries a chloramphenicol resistance gene, allowing for their selection in culture. IPTG (Isopropyl β-D-1-thiogalactopyranoside) is used to induce expression of the cloned gene. The bacteria are lysed and the recombinant protein purified using a His tag (short sequence at the protein N-terminus containing six histidine residues), which has been added to the nucleotide sequence. Recombinant proteins enable the analysis of protein function in *in vitro* assays.

2.3.2: Growth of bacterial cultures

Transformation of the BL21 (DE3) pLysS cells with the pRSET plasmid was carried out as detailed above for the XL1-blue cells (Section 2.2.9). The transformed cells were spread onto Luria agar plates containing both ampicillin and chloramphenicol, rather than ampicillin alone, however.

Four litres of bacterial culture were routinely grown for one recombinant protein preparation. Initially four 5 mL starter cultures were set up: 5 mL LB in a 15 mL falcon tube, with 100 $\mu g.mL^{-1}$ ampicillin (5 μL of 100 $mg.mL^{-1}$ stock made up in water, filter sterilised) and 40 $\mu g.mL^{-1}$ chloramphenicol (5 μL of 40 $mg.mL^{-1}$ stock made up in 100% ethanol). A single colony from the Luria agar plate was picked using a sterile pipette tip and used to inoculate one starter culture. The starter cultures were placed at 37°c in an incubator shaker for ~6 hrs.

One starter culture was then transferred into each of four 1L glass flasks containing 200 mL LB, 100 $\mu g.mL^{-1}$ ampicillin and 40 $\mu g.mL^{-1}$ chloramphenicol. The cultures were placed back into the incubator shaker for 16 hrs at 37°c.

Following this incubation, glycerol stocks were made if required: 1 mL of bacterial culture was added to 1 mL 30% glycerol in LB (autoclaved previously) in a sterile 2 mL screw-cap tube, and vortexed before long-term storage at -80°c.

The remainder of each of the bacterial cultures was then transferred to each of four flasks containing 900 mL LB with 100 $\mu g.mL^{-1}$ ampicillin and 40 $\mu g.mL^{-1}$ chloramphenicol, giving 1100 mL total in each 2 L flask. These large flasks were then placed into the incubator shaker at 37°c for 1½ hrs.

The bacteria were then induced to begin synthesis of the recombinant protein by the addition of 0.5 mM IPTG (1 mL of 500 mM stock) to each large flask. The flasks were returned to the incubator shaker, this time at the lower temperature of 27°c for 4-6 hrs.

The bacterial culture was next spun down in large beakers at 6000 rpm for 10 min, in a Sorvall RC 5B Plus ultracentrifuge using a GS-3 rotor. A total of three spins were required to clear the entire 4 L culture. The supernatant was discarded, and the cell pellets transferred into a single labelled 50 mL falcon tube. The pellet was re-suspended in 20 mL **Sonication buffer (50 mM phosphate buffer pH 8.0 [11.65 mL 1 M Na_2HPO_4, 0.85 mL 1M NaH_2PO_4], 300 mM NaCl, 1% Triton X-100)** with 20 µL DNase (Sigma-Aldrich). The tube was placed at -20°c for 16 hrs so that ice crystals formed rapidly to pierce the membranes and burst open the cells.

2.3.3: Purification of recombinant protein

The bacterial pellet was thawed at room temperature (2-3 hrs), divided equally between two 50 mL ultracentrifuge tubes and centrifuged at 37,000 rpm for 30 mins at 4°c in a Kontron ultracentrifuge.

The recombinant protein was captured using its His tag on a nickel column. The column was prepared at room temperature: 2 mL HIS-Select Nickel Affinity Gel (P6611, Sigma) was placed into a PD-10 column (Disposable Chromatography Column, Bio-Rad Laboratories). (2 mL is the bed volume, i.e. 0.5 mL per litre of culture.) The ethanol was first allowed to run off of the beads, then the beads washed in 25mL **Low Salt**

buffer (50 mM phosphate buffer pH 6.0 [23.3 mL 1 M Na_2HPO_4, 1.70 mL 1M NaH_2PO_4], 300 mM NaCl, 10% glycerol) to remove any residual ethanol. The bacterial cell supernatant was placed into the column. The nozzle cap was secured with parafilm, the lid replaced, and the column placed onto the rotating wheel for >30 min at 4°c for capturing of the recombinant protein.

After capturing, the nozzle cap and lid were removed from the column and excess liquid allowed to run off. The column was washed first in 25 mL low salt buffer, followed by 25 mL **High Salt buffer (50 mM phosphate buffer pH 6.0 [23.3 mL 1 M Na_2HPO_4, 1.70 mL 1 M NaH_2PO_4], 525 mM NaCl, 10% glycerol)**. 3 mL (1.5 X bed volume) 500 mM Imidazole in High Salt Buffer was applied to the column and the flow-through collected in a clean 15 mL falcon tube. The eluted 3 mL liquid was then pipetted onto a Buffer Exchange column, pre-equilibrated in **PIPES/salts pH 6.8 (20 mM PIPES, 137 mM NaCl, 2.7 mM KCl)**. (PIPES, 1,4-Piperazinediethanesulfonic acid, P6757, Sigma-Aldrich.) The excess liquid was allowed to run straight through as waste.

A clean 15 mL falcon tube was next placed underneath the Buffer Exchange column. 4 mL PIPES/salts was pipetted directly onto the column to elute the recombinant protein into the collection tube in PIPES/salts. Both the nickel column and buffer exchange column were washed and stored in PBS-azide for re-use.

The concentration of the purified recombinant protein was first assessed using the BCA assay (Section 2.3.4). 1.0, 2.0 and 5.0 μg of the freshly made protein were then run alongside 1.0, 2.0 and 5.0 μg recombinant PITPα on a SDS-PAGE gel stained with Coomassie dye, and the protein concentration of the new recombinant protein preparation adjusted accordingly, to account for impurities. The protein preparation was aliquoted into appropriate volumes (usually 100 μL) and stored at -80°c.

2.3.4: BCA assay for protein concentration

The Bicinchoninic Acid (BCA) kit (BCA1, Sigma-Aldrich), was used to assess protein concentration. Protein standard solutions were made up as indicated in Table 2.3, in distilled water, PBS or PIPES/salts, as appropriate, and stored at -20°c. The assay was

performed in a 96-well plate. 10 µL of each standard was pipetted into plate wells in duplicate. Purified protein or lysate of unknown concentration was diluted (usually three dilutions, 1:5, 1:10 and 1:20), and 10 µL of the diluted protein pipetted onto the plate alongside the standards, in duplicate.

A BCA/Copper (II) sulphate solution was made by mixing BCA solution and Copper (II) sulphate solution in a 50:1 ratio. 200 µL of this was pipetted into each well of the 96-well plate containing diluted protein or protein standard. The plate was then placed into the dry incubator for 30 min at 37°c whilst the colour developed. The relative intensity of the coloured liquids was read using a plate reader at λ=540nm.

Concentration ($mg.mL^{-1}$)	Dilution factor	Sigma standard (µL)	Diluent (µL)	Total (µL)
0.1	10	30	270	300
0.2	5	60	240	300
0.3	3.33	100	233	333
0.4	2.5	120	180	300
0.5	2	150	150	300
0.8	1.25	240	60	300
1.0	1	< 300	0	< 300

Table 2.3: BCA assay protein standards

2.4: Co-immunoprecipitation for analysis of protein-protein interactions

2.4.1: COS-7 cell culture

COS-7 cells (cell line originally derived from African green monkey kidney cells) were routinely grown in Dulbecco's Modified Eagle Medium (DMEM) cell culture medium supplemented with 10% heat-inactivated FCS [2] , 4 mM L-glutamine, 0.5 iu.mL^{-1} penicillin and 50 μg.mL^{-1} streptomycin, in a T75 cell culture flask. In general, cells were split 1:5 for 48 hrs growth or 1:10 for 72 hrs, in a class II laminar flow cabinet.

2.4.2: Transient transfection of DNA plasmids using FuGENE HD

For immunoprecipitation experiments, COS-7 cells were seeded onto 10 cm cell culture plates (one per condition, 10 mL media per plate), at a concentration of 1.0-2.0 x 10^5 cells.mL^{-1}, 6-16 hrs prior to transfection to allow the cells to adhere to the plastic.

Transfection was carried out using FuGENE HD (Roche Diagnostics). The ratio of plasmid DNA:transfection reagent required was determined empirically by western blotting of lysate derived from cells transfected with differing ratios of cDNA:FuGENE HD. For COS-7 cells this ratio was established to be 2:6 (Figure 2.4). For transfection of one well of a six-well plate, 2 μg DNA was used, along with 100 μL Opti-MEM and 6 μL FuGENE HD. These amounts were scaled up to 10 μg DNA, 500 μL Opti-MEM and 30 μL FuGENE HD for transfection of one 10 cm plate (containing 10 mL media). These quantities were used for each plate in an experiment, and the amount of a single plasmid was kept consistent throughout. An example is given in Table 2.4, for an experiment containing four conditions.

[2] Heat-inactivation was carried out by placing the unopened 500 mL bottle of FCS in a water bath at 56°c for 1 hr.

Condition	Empty control vector (pcDNA3.1) (μg)	pcDNA3.1-FLAG-RdgBβ-sp1 (μg)	pcDNA3-HA-ATRAP (μg)
Control	10	0	0
FLAG-RdgBβ-sp1	5	5	0
HA-ATRAP	5	0	5
FLAG-RdgBβ-sp1 + HA-ATRAP	0	5	5

Table 2.4: Example quantities of cDNA for transfection of two or more plasmids

In preparation for transfection, plasmid DNA and FuGENE HD were warmed to room temperature. FuGENE HD was subjected to 1 s vortex prior to use. Opti-MEM was warmed to 37°c in a water bath. Appropriate volumes of plasmid DNA were placed into labelled 1.5 mL eppendorf tubes. To this, the required volume of Opti-MEM was added. FuGENE HD was then added to each tube by pipetting directly into the Opti-MEM (the undiluted transfection reagent should not be allowed to touch the sides of the tube). The tubes were vortexed for 2 s before incubating at room temperature for 15 min to allow DNA-transfection complex formation to take place. Complexes were added dropwise to the cell culture dishes, and the dishes returned to the incubator.

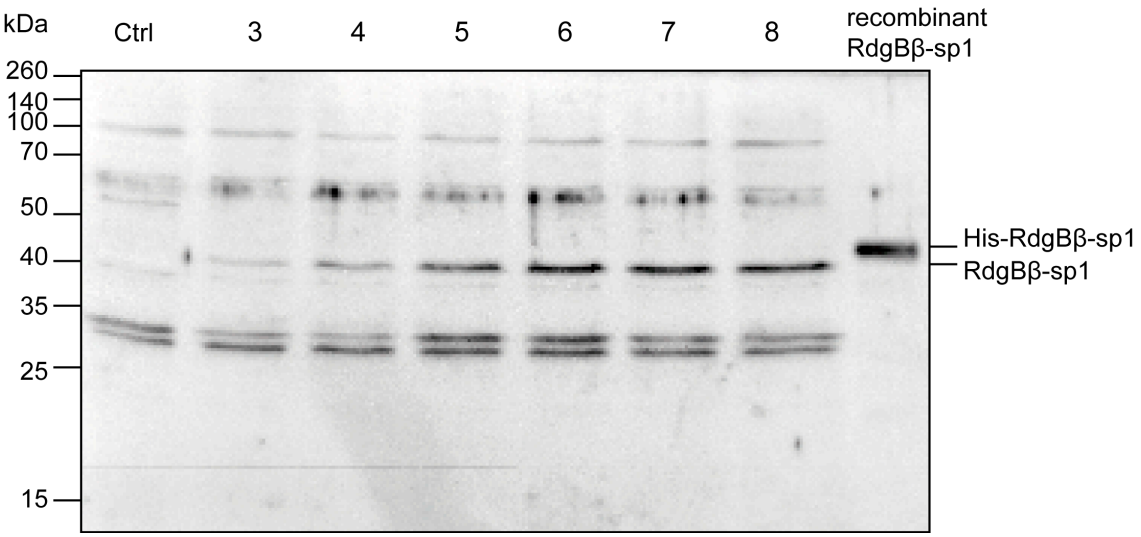

Figure 2.4: Identification of the optimum DNA: FuGENE HD ratio

COS-7 cells were seeded into wells of a six-well plate (2 mL per well) at a concentration of 1.0 x 10^5 cells.mL^{-1}. Transfection was carried out 6 hrs post-seeding, once the cells had adhered to the plastic. 2 µg pIRES2-RdgBβ-sp1 plasmid was transfected per well; complex formation was carried out for each with the volume of FuGENE HD transfection reagent indicated above the membrane (µL). One well of the six-well plate was transfected per condition. Control (Ctrl) are untransfected COS-7 cells. Cells were harvested 46 hrs post-transfection, in 100 µL RIPA buffer + protease inhibitors per well. 40 µg cell lysate was loaded per lane of a 12% resolving gel alongside 40 ng recombinant His-RdgBβ-sp1. Separated proteins were transferred to PVDF membrane and subjected to western blotting using the anti-RdgBβ antibody #101.

2.4.3: Treatment of cells with chemical compounds

Cells for immunoprecipitation experiments were harvested two days after transfection, i.e. 42-48 hrs, depending on the time of transfection. For treatment with chemical compounds, the cell culture media was aspirated and replaced with fresh media containing the compound at the appropriate time prior to cell harvest (Table 2.5).

Treatment name	Function	Concentration	Time	Manufacturer & Cat. No.
Angiotensin II	Hormone	100 nM - 1 µM	10 min-16 hrs	Sigma-Aldrich A9525
Bisindolylmaleimide I (BIM-I, GF 109203X)	Protein kinase C inhibitor	5 µM	4-16 hrs	Calbiochem #203290
EGF	Growth factor	50 ng.mL^{-1}	30 min	Calbiochem #324831
H-89	Protein kinase A inhibitor	10 µM	16 hrs	Calbiochem #371963
Insulin	Hormone	100 nM	30 min	Calbiochem #407709
Ionomycin	Calcium ionophore	5 µM	1-4 hrs	Calbiochem #407950
LY294002	PI 3-kinase inhibitor	10 µM	16 hrs	Calbiochem #440206
MG-132 (Z-leu-leu-leu-al)	Proteasome inhibitor	20 µM	4 hr	Sigma-Aldrich C2211
PMA	Phorbol ester	100 nM	1-16 hrs	Sigma-Aldrich P8139

Table 2.5: Chemical compounds.

2.4.4: Cell harvest

The cell culture plates were removed from the incubator and placed on ice. The media was aspirated from all plates, and the cells washed twice with cold PBS. The final wash was removed and the cell culture plates propped at 45° to enable residual liquid to collect and be removed from the plate. The plates were placed horizontal again, and 1 mL cold **Buffer B (50 mM Tris-HCl pH 7.4, 150 mM NaCl, 10 mM $MgCl_2$, 1% TX-100** plus protease inhibitors (Sigma-Aldrich, P8340)), was added to each plate. Phosphatase inhibitors were also added to the cell harvest buffer for experiments examining the RdgBβ-sp1-14-3-3 interaction, since phosphorylation is required for this interaction. (Phosphatase inhibitor cocktail 2 for tyrosine protein phosphatases, acid and alkaline phosphatases, Sigma-Aldrich, P5726; phosphatase inhibitor cocktail 3 for serine/threonine protein phosphatases and L-isozymes of alkaline phosphatase, Sigma-Aldrich, P0044.) The cells were scraped using a cell scraper. Again the plates were propped at 45° to allow the cells to collect in one place. The cells were next transferred to a labelled 1.5 mL eppendorf tube. The contents of the tubes were sonicated 1 x 15 s, then centrifuged at 10,000 $rev.min^{-1}$ for 10 min at 4°c. The cleared supernatant was transferred to a fresh eppendorf tube, and the protein concentration of the lysate assessed using the BCA assay (Section 2.3.4). Typical lysate concentrations were in the range 1.5-2.5 $mg.mL^{-1}$.

2.4.5: Treatment of cells with DSS cross-linkers prior to cell harvest

Disuccinimidyl suberate (DSS) is a chemical cross-linker. *N*-hydroxysuccinimide (NHS) ester groups at either end of a 8-carbon (11.4 Å) spacer arm react with amine groups (for example, on lysine residues) to form a non-cleavable bond between interacting proteins. DSS is membrane-permeable: cells do not have to be permeabilised for the compound to gain access to intracellular proteins.

Method

A 50 mM DSS solution was freshly made up in DMSO. While the compound was dissolving, the cell culture dishes were placed on ice and cells washed twice with ice-cold PBS. The final wash was replaced with 200 mM sodium phosphate, 150 mM NaCl pH 7.4 (10 mL per plate).

100 µL of the DSS solution was added to each plate to give a 0.5 mM final DSS concentration and 1% DMSO concentration. The cells were incubated in the DSS solution for 2 hrs on ice.

Excess DSS was quenched by the addition of 1.12 mL 1 M Tris-HCl pH 7.4, giving a final concentration of 100 mM Tris. The cells were incubated in this solution on ice for 15 mins.

The solution was then completely aspirated from the cell culture dishes and replaced with 1 mL cold Buffer B plus protease inhibitors per plate. The cells were harvested exactly as described in section 2.4.4.

2.4.6: Immunoprecipitation

For immunoprecipitation of HA-ATRAP via its HA tag, 300 µg lysate was added to 1.5 µg anti-HA monoclonal antibody (7.5 µL HA-probe (F-7) 200µg.mL^{-1} stock, Santa cruz (sc-7392) (mouse IgG2a)) in a 1.5 mL eppendorf tube, and the tubes placed on the rotating wheel at 4°c for 1 hr for protein capture by the antibody. Meanwhile, 20 µL Protein A/G PLUS-Agarose (Santa cruz, sc-2003) in a fresh tube was washed twice in 500 µL Buffer B (10,000 rev.min^{-1} for 2 min at 4°c). The supernatant was removed by aspiration following each centrifugation. The lysate/antibody tubes were removed from the rotating wheel and centrifuged, 10,000 rev.min^{-1} for 2 min at 4°c. The lysate/ antibody was then transferred to the prepared Protein A/G PLUS-Agarose tube. These tubes were then placed onto the rotating wheel for 1 hr at 4°c for capture of the antibody Fc region by the Protein A/G.

Alternatively, for immunoprecipitation of RdgBβ via its FLAG tag, anti-FLAG antibody was used, already conjugated to beads (ANTI-FLAG M2 Affinity Gel (Sigma A2220)). 40 µL ANTI-FLAG M2 Affinity Gel per immunoprecipitation was washed twice in 500 µL Buffer B (10,000 rev.min^{-1} for 2 min at 4°c), prior to the addition of 300 µg lysate to each tube. The tubes were then placed onto the rotating wheel for 2 hr at 4°c for capture of the FLAG-tagged protein by the ANTI-FLAG M2 affinity gel.

In both cases, if the volume of 300 µg lysate was less than 100 µL, 50-100 µL Buffer B was added to the tube to ensure the beads were able to move around adequately during the capturing step. Following the capturing step(s), the tubes were centrifuged at 10,000 rev.min^{-1} for 2 min at 4°c. The supernatant (unbound protein) was aspirated carefully. The beads were washed three times in 500 µL Buffer B, with the final wash transferred to a fresh eppendorf tube to eliminate any protein which may have adhered to the side of the tube. The final wash was aspirated, and the beads boiled at 95°c for 10 min in 20 µL 2X SDS-PAGE sample buffer. The immunoprecipitates were then loaded onto an SDS-PAGE gel for analysis of potential protein-protein interactions by western blotting.

2.5: SDS-PAGE Gel Electrophoresis and Western Blotting

2.5.1: Principle

Sodium dodecyl sulphate polyacrylamide gel electrophoresis (SDS-PAGE) is a technique used to separate proteins according to their mass. Protein samples are boiled in sample buffer containing SDS and β-mercaptoethanol to denature the proteins. SDS binds tightly and evenly to the uncoiled polypeptide chain so that the charge-density along its length is approximately equal. The reducing agent β-mercaptoethanol breaks disulphide bonds, disrupting protein tertiary structure. SDS is also present throughout the gel and running buffer, ensuring the proteins remain as denatured monomers.

The gel may be stained with a Coomassie stain for visualisation of all the proteins present on the gel (typically for µg purified protein), or the proteins may be transferred

to PVDF membrane to enable the detection of a single protein of interest using a primary antibody raised against that protein, in a process known as western blotting.

2.5.2: Pouring SDS-PAGE gels

For my experiments, the SDS-PAGE gels were cast in Bio-Rad mini-gel casting apparatuses. Glass plates (one small and one large piece of glass per gel) with minimal chips were placed on absorbent tissue paper and the side to be in contact with the gel wiped clean first with distilled water, and then with 70% ethanol. The comb and 1.5 mm spacers (for a gel 1.5 mm thick) were similarly cleaned before assembly of the gel cassette.

The resolving gel mixture was made up first. The percentage of acrylamide in the resolving gel dictates how fast the gel will run, and different acrylamide percentages may be chosen depending on the size of protein that needs to be resolved. The larger the protein of interest, the lower the percentage of acrylamide in the resolving gel. In this thesis I typically used an 8% gel to resolve ubiquitin, and 12% resolving gels mostly for all other proteins (RdgBβ, ATRAP, PITPα, PITPβ, ARF, 14-3-3) - occasionally 10% for resolution of RdgBβ. Table 2.6 details the volumes of stock solutions required to make 8, 10 or 12% resolving gels. The gel mixture was made up in a small glass flask. The APS and TEMED were added immediately prior to gel pouring since these are the ingredients that make the gel set. The gel mixture was applied between the two glass plates using a disposable plastic pasteur pipette, up to 1 cm below where the edge of the comb would reside. To this, 1 mL isobutanol saturated with water was added to exclude oxygen from the gel. The resolving gel was left on the bench at room temperature for ~30 mins to set.

Once the resolving gel had set, the isobutanol was tipped from the apparatus, and the top of the gel washed using a wash bottle containing distilled water. Residual water was removed using blotting paper. Next, the stacking gel mixture was made up (Table 2.7), and applied between the glass plates on top of the resolving gel, without delivery of any air bubbles. The 10- or 15-well comb was then positioned in the stacking gel, and the gel allowed to set for > 45 min at room temperature.

Once the gel had set, the gel cassette was removed from the casting apparatus and clipped into the electrode assembly, one gel on each side (or one gel and one empty cassette). The electrode assembly with gel cassettes was subsequently placed into the Bio-Rad mini-protean tank and the combs removed from the gels.

SDS-PAGE running buffer (25 mM Tris-HCl pH 8.3, 193 mM glycine, 0.1% SDS; typically 10X stock solution stored at RT) (800 mL per min-protean tank) was poured into the tank, filling the inner tank between the electrodes first, encouraging air bubbles to escape from the sample wells in the process. Running buffer was then poured into the lower tank, and the gels were now ready for loading of the protein samples.

	Acrylamide (%)		
	8	**10**	**12**
ddH_2O	8.0 mL	7.25 mL	6.50 mL
Acrylamide	3.0 mL	3.75 mL	4.50 mL
1.5 M Tris-HCl pH 8.8	3.75 mL	3.75 mL	3.75 mL
10% (*w*/*v*) SDS	150 µL	150 µL	150 µL
10% (*w*/*v*) APS	120 µL	120 µL	120 µL
TEMED	12 µL	12 µL	12 µL

Table 2.6: SDS-PAGE resolving gel recipe

Volume of solutions required for two mini-gels (15.0 mL) using 40% acrylamide solution (BP14021, Fisher Scientific). APS, ammonium persulphate; TEMED, *N,N,N′,N′*-tetramethylethylenediamine.

ddH_2O	3.80 mL
Acrylamide	0.60 mL
1.5 M Tris-HCl pH 8.8	1.50 mL
10% (*w*/*v*) SDS	60 µL
10% (*w*/*v*) APS	24 µL
TEMED	6 µL

Table 2.7: SDS-PAGE stacking gel recipe
Volume of solutions required for two mini-gels.

2.5.3: SDS-PAGE sample buffer

Prior to loading onto an SDS-PAGE gel, an appropriate volume of sample buffer was added to the protein sample to produce a final concentration (i.e. 1 X) of **10% (*v*/*v*) glycerol, 62.5 mM Tris-HCl pH 6.8, 2% SDS, 80 µg.mL^{-1} bromophenol blue, 5% β-mercaptoethanol**. SDS-PAGE sample buffer was typically made as 10 mL of 2X and 4X solution, which gives 20 x 500 µL aliquots. Aliquots were stored at -20°c. Tris-HCl pH 6.8 was kept at 4°c as a 1 M stock solution. Bromophenol blue stock was kept at room temperature as a 5 mg.mL^{-1} slurry in ddH_2O, and vortexed well before use.

The protein sample was boiled in sample buffer at 95°c for 10 min prior to loading onto the gel. Samples were loaded alongside 10 µL molecular weight markers to allow the determination of protein molecular weight, e.g. SeeBlue Plus2 Pre-Stained Standard (Invitrogen), Spectra^{TM} Multicolor Broad Range Protein Ladder (SM1841 or SM1842, Fermentas), or PageRuler^{TM} Plus Prestained Protein Ladder (SM1811 or SM1812, Fermentas). Samples, particularly for western blotting, were loaded in the reverse order, i.e. from right to left.

2.5.4: SDS-PAGE running conditions

Once the protein samples had been loaded, the gel was run at 130 V for 90-95 mins or until the dye front reached the desired point on the gel or fell off of the end of the gel. The apparatus was dismantled. The stacking gel was carefully cut from the rest of the gel using the edge of a spacer, then placed into either distilled water for Coomassie staining or blotting buffer for western blotting.

2.5.5: Gradient gels

For resolution of proteins of a range of molecular weights, NuPAGE Novex 4-12% Bis-Tris Gel 1.5mm, 10 well (Invitrogen, NP0335), were used in an XCell SureLock MiniCell. The apparatus was assembled following the manufacturer's instructions. The gel was run at 200 V for 35 mins, in NuPAGE MES SDS Running Buffer (Invitrogen, NP0002).

2.5.6: Coomassie staining of gels

Coomassie blue stain (0.1% (*w*/*v*) Coomassie blue R_{250}, 40% methanol, 10% acetic acid, 50% distilled water) and **destain (40% methanol, 10% acetic acid, 50% distilled water)** were made up in 2 L amber bottles and stored at room temperature. The SDS-PAGE gel was washed briefly in distilled water in a small plastic box prior to the addition of the Coomassie stain. Clingfilm was used to cover the box. The gel was then either: (a) incubated in stain overnight at room temperature on a rocker, followed by a brief wash in distilled water, then incubated in destain during the next day (with a small piece of sponge to aid in the removal of the stain); or (b) microwaved in stain for ~40 s to encourage the gel to take up the solution more easily, incubated in the stain at room temperature for 20 min, given a brief wash in distilled water, followed by incubation in destain at room temperature overnight without rocking.

Once the destaining was complete, by either method, the gel was re-hydrated in distilled water, the protein bands imaged using a Fujifilm LAS-3000 imaging device, and quantified using AIDA software. Where appropriate, an unpaired *t* test was carried out

as an assessment of statistical significance, using the GraphPad QuickCalcs tool (http://www.graphpad.com/quickcalcs/).

2.5.7: Protein transfer to PVDF membrane

Proteins separated by SDS-PAGE were transferred to PVDF membrane by the application of an electric field across the blotting sandwich. A piece of PVDF membrane was cut to an appropriate size (7 x 10 cm) and activated in methanol for 5 min before equilibration in **Blotting buffer (25 mM Tris-HCl pH 8.3, 192 mM, 10% methanol)**. Blotting buffer was typically stored as a 10X solution: 250 mM Tris-HCl pH 8.3, 1.92 M glycine, with 10% methanol added upon dilution to a 1X solution. 800 mL chilled Blotting buffer was required per mini-protean tank. The SDS-PAGE gel (home-made or pre-cast), blotting cassette, sponges and blotting paper were all equilibrated in Blotting buffer prior to assembly of the blotting sandwich.

The blotting sandwich was assembled in a large plastic box containing 1-2 cm blotting buffer. The plastic cassette was placed in the box first, with the outer side of the black leaflet face down. One sponge followed by one piece of blotting paper was placed onto the black leaflet. The gel was placed onto the blotting paper next with the 'front' of the gel (that which faced the inner chamber during SDS-PAGE) facing up so that the molecular weight markers were on the right. The PVDF membrane was placed on top of the gel and rolled over with a section of a 10 mL tube pipette to eliminate air bubbles. The second piece of blotting paper was placed on top of the membrane, rolled again, and then the second sponge completed the blotting sandwich. The sandwich was placed inside the blot transfer unit, with the black leaflet of the sandwich facing the black side of the blot transfer unit, alongside a second sandwich or blank plastic cassette, inside a Bio-Rad Mini Protean tank. A small magnetic stirrer was placed into the tank, and an ice block placed alongside the blot transfer unit in the tank. The tank was then placed onto a magnetic stirring device, which was turned on. Blotting buffer was poured into the tank, to the top. It was important that the membrane was not allowed to dry out at any point.

The lid was placed onto the tank, with the electrodes appropriately aligned and connected to the power pack. Blot transfer was carried out at 20 V for 16 hrs or 100 V for 60 min.

2.5.8: Western blotting

Blocking

Once blot transfer was complete, the blotting apparatus was dismantled. The membrane was cut at this point to the size of the gel while it was still in place, before being submerged in phosphate-buffered saline-0.02% tween (PBS-T) or Tris-buffered saline-0.02% tween (TBS-T) in a small plastic box. In general, cold PBS-T was used for the western blots in this thesis, whilst cold TBS-T was used for Far Western blotting (Section 2.5.11). (PBS: 20 mM phosphate buffer pH 7.0 [10 mM Na_2HPO_4, 2 mM KH_2PO_4], 300 mM NaCl or 1 tablet dissolved in 200 mL distilled water (P4417, Sigma-Aldrich) = 10 mM phosphate buffer pH 7.4, 2.7 mM KCl, 137 mM NaCl.)

The membrane was then stained in indian ink (1:1000 dilution in PBS-T) for 10 min or until the protein bands appeared. Excess ink was washed from the membrane by a brief wash in PBS-T. The membrane was then blocked in 5% milk-PBS-T for 1 hr RT on the platform rocker.

Primary antibody incubation

After blocking, the membrane was placed inside a 50 mL falcon tube (one membrane per tube) for subsequent antibody incubations. The appropriate primary antibody was diluted in PBS-T as indicated in Table 2.8 (5 mL per membrane), and the membrane incubated in antibody on a tube roller for 2 hrs at room temperature or 16 hrs at 4°c.

Antigen	Name	Manufacturer/ Cat. No. or ref.	Species	Dilution for WB	Typical quantity of lysate loaded onto gel (µg)
14-3-3	pan 14-3-3 (K-19)	Santa Cruz Biotech., sc-629	Rabbit	1:1000	3-5
ARF1	ARF, #678	Skippen et al., 2002	Rabbit	1:2000 (affinity purified)	10-12
FLAG	DDK	OriGene Technologies, TA50011	Mouse	1:2000 or 1:5000 for IP: FLAG re-probe	10-15 (FLAG-RdgBβ-sp1)
FLAG	OctA (D-8)	Santa Cruz Biotech., sc-807	Rabbit	1:500	10 (FLAG-RdgBβ-sp1)
HA	HA-probe (F-7)	Santa Cruz Biotech., sc-7392	Mouse	1:1000 or 1:5000 for IP: HA re-probe	3-5 (HA-ATRAP)
PITPα	674	Morgan et al., 2004	Rabbit	1:1000 (affinity purified)	15
PITPβ	1C1	Morgan et al., 2006	Mouse	1:1000 (affinity purified)	15
RdgBβ	101	Garner et al., 2011	Rabbit	1:1000 (serum)	(30-50 ng recombinant protein)
Ubiquitin	Ub	Sigma-Aldrich, U5379	Rabbit	1:100	(IP only)

Table 2.8: Primary antibodies used for western blotting

Antibodies raised in mouse are monoclonal; those raised in rabbit are polyclonal.

Primary antibody detection

After incubation with primary antibody, the membrane was washed with PBS-T three times for 5 mins each on the tube roller. Protein A conjugated to horseradish peroxidase (Protein A-HRP) (14-50-00, Kirkegaard & Perry Laboratories (KPL)) was used as the 'secondary antibody', at 1:2500 dilution in 5% milk-PBS-T. Protein A is a *Staphylococcus aureus* protein that recognises antibody in its native (tertiary) structure but not denatured antibody eluted from an IP (Lal et al., 2005). An immunoprecipitate run on a western blot displays characteristic heavy chain (~50 kDa) and light chain (~25 kDa) antibody bands, which can be a menace if the protein of interest is either of those sizes.

Blot exposure and imaging

Following secondary antibody incubation, the membrane was washed three times with PBS-T for 5 min each on the tube roller. For exposure, the membrane was placed into a plastic pocket cut to size with a single edge binding the two leaflets. 0.5 mL of each ECL or ECL Advance solution (ECL Western Blotting Detection Reagents, GE Healthcare) was mixed together and pipetted onto each membrane so that it was completely covered. The top leaflet of the plastic pocket was placed over the membrane (being careful not to trap any air bubbles against the membrane), and the membrane incubated in the solution for one minute. Excess liquid was then squeezed out from the pocket and from the membrane using absorbent paper. The chemoluminescence was measured using a LAS-3000 imaging system. Protein bands were quantified using AIDA software.

2.5.9: Stripping of western blots for re-probing

For re-probing, the western blot membrane was rinsed with PBS-T, then heat-sealed into a polythene bag along with 10 mL **Stripping buffer (0.2 M glycine-HCl pH 2.5, 0.05 % tween-20, 100 mM β-mercaptoethanol)**. The bag was immersed horizontally in a water bath pre-heated to 80°c for 20 mins. After incubation, the membrane was removed from the polythene bag into a small sandwich box containing PBS-T. The membrane was washed several times with PBS-T to remove the stripping buffer. The membrane was now ready for blocking in 5% milk-PBS-T and probing with primary, then secondary antibody, as described above.

2.5.10: Far western blotting

Far western blotting is an adaptation of western blotting, used for analysis of direct protein-protein interactions. The method used is as described by Moorhead and colleagues (Moorhead et al., 1999), and the reagents were a generous gift from Prof. Carol MacKintosh (MRC Protein Phosphorylation Unit, University of Dundee).

Immunoprecipitates (Section 2.4) were separated by SDS-PAGE as described above, and transferred to PVDF membrane. Longer blot transfer was preferred here (20 V, 16 hrs), to allow the proteins to renature and re-acquire their tertiary structure. The blot transfer apparatus was then dismantled, and the membrane transferred to a small plastic box containing TBS-T (20 mM Tris-HCl pH 7.4, 150 mM NaCl, 0.02% tween-20). The membrane was stained with indian ink (1:1000 dilution in TBS-T), and then blocked in 5% BSA-TBS-T for 1 hr RT.

The membrane was washed briefly in TBS-T before being transferred to a 50 mL falcon tube for all subsequent washes and incubations at room temperature on a tube roller. Here, the membrane was incubated with 1 $\mu g.mL^{-1}$ recombinant 14-3-3 with a digoxigenin (DIG) tag - BMH1 and BMH2 *Saccharomyces cerevisiae* 14-3-3 isoforms - in 5% BSA-TBS-T for 2 hrs.

The membrane was next washed in TBS-T three times for 5 min each time, before incubation with anti-DIG antibody Fab fragments conjugated to HRP (DIG-HRP) in TBS-T (1:2500 dilution), for 45 mins. Three 5 min washes followed this, and the protein bands exposed using ECL reagents as for western blotting.

2.5.11: Trypsin digestion of recombinant RdgBβ protein

100 µg recombinant RdgBβ-sp1 or -sp2 (in 500 µL) was incubated with 5 µL trypsin-EDTA solution (Sigma-Aldrich, T3924) at 37°c. 50 µL (10 µg) aliquots were removed directly into SDS-PAGE sample buffer at 0, 2, 5, 10 min. Trypsin digestion was carried out by Michelle Li.

2.5.12: Cycloheximide treatment of transiently-transfected cells

COS-7 cells grown on 16 x 3.5 cm cell culture dishes (2 mL media per dish) were transiently transfected. Two days later, the cell culture media was aspirated and replaced with fresh media containing 100 µg/ml cycloheximide (CHX). After 0, 2, 4 or 6 hrs the media was removed and the cells washed twice in PBS. The cells were harvested in 300 µL **RIPA buffer** per well **(50 mM Tris-HCl pH 7.5, 150 mM NaCl, 1% Triton X-100 (*v*/*v*), 0.5% sodium deoxycholate (*w*/*v*), 0.1% SDS (*w*/*v*)**, protease inhibitors) and incubated on ice for 30 min. The tubes were centrifuged 12,000 rev.min^{-1} for 15 mins at 4°c, and the supernatant transferred to a fresh tube. The BCA assay was used to assess the protein concentration of the lysates. 50 µg protein was boiled with SDS-PAGE sample buffer and loaded per lane of the gel. The cycloheximide experiments presented in this thesis were carried out by Michelle Li.

2.5.13: *In vitro* PKC phosphorylation assay

The method used was based on that described in Morgan et al., 2006. Reaction mixtures were prepared in 50 µL (in 1.5 mL eppendorf tubes) on ice:

20 µL RdgBβ-sp1 or -sp2 (10 µg, diluted in PIPES/salts, pH 6.8).

10 µL PKC* (350 ng) or 4 µL 2.5X buffer + 2 µL dH_20 for control.

20 µL 2.5X buffer, 100 $\mu g.mL^{-1}$ PS, 10 $\mu g.mL^{-1}$ DAG + 100 µM Mg-ATP.

* PKC purified from rat brain (Calbiochem #539494), predominantly the conventional isoforms, α, β1, β2 and γ. Concentration: 35 $\mu g.mL^{-1}$ in 20 mM Tris-HCl pH 7.5, 100 mM NaCl, 500 µM EDTA, 500 µM EGTA, 1 mM DTT, 10% glycerol. Stock activity: 1600 $U.mg^{-1}$ protein.

2.5X buffer: 50 mM Tris-HCl pH 7.5, 12.5 mM $MgCl_2$, 500 µM $CaCl_2$.

The following lipids were dried down under nitrogen gas and sonicated until dissolved in 1 mL 2.5X buffer:

250 µg PS (25 µL of 10 $mg.mL^{-1}$ stock).

25 µg DAG (2.5 µL of 10 $mg.mL^{-1}$ stock).

250 µM Mg-ATP was next added to the 1 mL sonicated lipids (2.5 µL of 0.1 M stock).

Final reaction conditions:

10 µg RdgBβ

350 ng rat brain PKC

20 mM Tris-HCl pH 7.5

5 mM $MgCl_2$

200 µM $CaCl_2$

100 µM Mg-ATP

100 $\mu g.mL^{-1}$ PS

10 $\mu g.mL^{-1}$ DAG

RdgBβ-sp1 or -sp2 was incubated -/+ rat brain PKC for 1 hr at 30°c in a water bath. The reaction was quenched by the addition of 16.67 µL of 4X SDS-PAGE sample buffer.

The tubes were vortexed, then boiled at 95°c for 10 mins. Following SDS-PAGE buffer addition, the concentration of RdgBβ was 150 μg.mL^{-1}.

2.5.14: Reconstitution of the RdgBβ-14-3-3 interaction *in vitro*

Assay conditions:

120 μg recombinant PITP protein (RdgBβ-sp1/PITPα) (200 μg.mL^{-1})

1 mM Mg-ATP

0.4 iu.mL^{-1} SLO

100 nM Ca^{2+} (pCa7) or 10 μM Ca^{2+} (pCa5)

+/- 100 nM PMA

The assay was prepared in 1.5 mL eppendorf tubes on ice, in a total volume of 600 μL. The components were added in the following order:

100 μL RdgBβ-sp1/PITPα

400 μL HL60 cells * + Mg-ATP

50 μL PMA or buffer for control

50 μL SLO + pCa7 or pCa5

* 60 mL HL60 cells (60 x 10^6 cells) were washed twice in 50 mL PIPES buffer and re-suspended in 2.4 mL PIPES.

The tubes were vortexed briefly, and then incubated in the waterbath at 37°c for 20 min. Immediately following the incubation, the assay tubes were centrifuged at 3000 rev.min^{-1} for 5 min at 4°c. 550 μL supernatant was then transferred to a fresh eppendorf tube and centrifuged again, at 12,000 rev.min^{-1} for 15 min at 4°c.

Of this >500 μL supernatant:

- 100 μL was transferred into a 1.5 mL eppendorf tube containing 40 μL nickel beads (HIS-select nickel affinity gel, Sigma-Aldrich, P6611) which had been washed twice in 500 μL PIPES/salts pH 6.8 buffer, at 10,000 rev.min^{-1} 2 min 4°c (i.e. as for Co-IPs).

- 400 µL was transferred to a mini-spin column containing 120 µL nickel beads that had been washed twice in 500 µL PIPES/salts pH 6.8 buffer, at 3,000 rev.min^{-1} 5 min 4°c (as for the Lipid Binding assay, Section 2.8.2).

In addition, 100 µL PIPES/salts pH 6.8 buffer was added to each tube or mini-spin column. The lids were then replaced and the eppendorf tubes and mini-spin columns placed onto the rotating wheel at 4°c for 1 hr re-capturing of the His-tagged recombinant proteins. After the 1 hr re-capturing, the nickel beads in the eppendorf tubes were washed three times in 500 µL PIPES/salts buffer, with the final wash transferred to a fresh eppendorf, exactly as for immunoprecipitation. The captured proteins were eluted in 20 µL 2X SDS-PAGE sample buffer. After boiling at 95°c for 10 min and a brief centrifuge (2 min 12,000 rev.min^{-1}), the full volume of supernatant was applied to an SDS-PAGE gel. Meanwhile, the nickel beads in the mini-spin columns were washed twice in 500 µL low salt buffer, followed by twice in 500 µL high salt buffer. The captured proteins were then eluted in 500 µL imadazole and buffer exchanged to 1 mL PIPES/salts pH 6.8 buffer. 45 µL of this purified protein was boiled with 15 µL 4X SDS-PAGE sample buffer, 50 µL of which was run on an SDS-PAGE gel.

2.6: PLC assay in intact cells

This assay was carried out in three different cell types/systems: HEK-293 cells (Human embryonic kidney cell line, ATCC No. CRL-1573) transiently transfected with pcDNA3.1-HA-AT_1R, COS-7 cells transiently transfected with pcDNA3.1-HA-AT_1R, and HEK-293 stably expressing the Angiotensin II type 1 receptor (AT_1R, FLAG-tagged) (HEK-293-AT_1 cells). The former two cell types were co-transfected with pcDNA3.1-FLAG-RdgBβ-sp1 and/or pcDNA3-HA-ATRAP alongside pcDNA3.1-HA-AT_1R. HEK-293 and HEK-293-AT_1 cells were seeded onto cell culture dishes pre-coated with poly-L-lysine solution and transfected using TurboFect reagent. COS-7 cells were seeded directly into the cell culture dishes and transfected with FuGENE HD as detailed in Section 2.4.2. COS-7, HEK-293 and HEK-293-AT_1 cells were all routinely grown in DMEM media supplemented with 10% HI FCS, 4 mM L-glutamine,

0.5 iu.mL^{-1} penicillin and 50 μg.mL^{-1} streptomycin, in a T75 cell culture flask. The HEK-293 cells had a doubling time of ~10 hrs, and therefore were split 1:3 for 24 hrs growth, 1:10 for 48 hrs or 1:15-1:20 for 72 hrs growth. By contrast, HEK-293-AT$_1$ cells grew much slower, with a doubling time of ~24 hrs, and so were split 1:2 for 24 hrs, 1:5 for 48 hrs or 1:10 for 72 hrs growth.

HEK-293-AT$_1$ cells were a generous gift from Dr. Tamas Balla, NIH, Bethesda, USA. In order to maintain the stable AT$_1$R expression, HEK-293-AT$_1$ cells were grown in DMEM supplemented with 10% heat-inactivated FCS, L-glutamine, penicillin, streptomycin and 500 μg.mL^{-1} G-418 (Geneticin) during routine culture but not when cells were set up for experiments.

2.6.1: Coating of cell culture plates with poly-L-lysine solution

200 μL 0.01% poly-L-lysine solution (P4832, Sigma-Aldrich) was placed into each well of a six-well plate. The plate was placed into the incubator at 37°c for a minimum of 1 hr for coating. When required, the plate was removed from the incubator and solution aspirated.

Cells of the appropriate type were trypsinised and counted, and seeded into the appropriate number of wells of a six-well plate, in triplicate, at 2.0 x 10^5 cells.mL^{-1}. Seeding of cells was carried out 6-16 hrs prior to transfection, to ensure the cells had adhered to the substratum prior to transfection.

2.6.2: Transfection of HEK-293 cells with TurboFect

As for FuGENE HD transfection, Opti-MEM was warmed to 37°c in a water bath, whilst the cDNA and TurboFect (Fermentas #R0531) were used at room temperature. The TurboFect reagent was vortexed for 2 s before use. The ratio of TurboFect to cDNA for use in HEK-293 cells was determined as for FuGENE HD, and like FuGENE HD, was determined as 2:6.

For each well of a six-well plate (35 mm diameter), 2 μg plasmid DNA was placed into a labelled 1.5 mL eppendorf. To this, 200 μL Opti-MEM was added, followed by 6 μL TurboFect, which was pipetted directly into the Opti-MEM to prevent it from touching the plastic of the eppendorf tube. The tube was vortexed immediately, and then incubated at room temperature for 15-20 mins to enable complex formation to take place. The cDNA-transfection reagent was then added drop-wise to the appropriate well of the cell culture plate. The plate was returned to the incubator, 42-48 hrs prior to the experiment.

2.6.3: Labelling the cells with [^{3}H]-inositol

The next day, the media were aspirated from the wells and replaced with M199 medium supplemented with 1% HI dialysed FCS, 4 mM L-glutamine, 0.5 iu.mL^{-1} penicillin, 50 μg.mL^{-1} streptomycin and 2-5 μCi.mL^{-1} [^{3}H]-inositol (ART 0116A, American Radiolabeled Chemicals, Inc.). The amount of radioactivity added was dependent on the age of the radioactive stock, since the inositol itself had been observed to degrade over time. M199 medium contains low inositol, and dialysis removes small molecules, including inositol, from the FCS. The cell culture plates were returned to the incubator for 24 hrs labelling.

For cells pre-treated with PMA, the time for labelling with [^{3}H]-inositol was reduced to 16 hrs and was carried out in conjunction with 100 nM treatment, in M199 medium supplemented with 1% HI dialysed FCS, 4 mM L-glutamine, 0.5 iu.mL^{-1} penicillin, 50 μg.mL^{-1} streptomycin. For the PMA-pre-treated cells, PMA was maintained in the HEPES buffer throughout the experiment: in the washes and in the buffer containing Angiotensin II for stimulation.

2.6.4: PLC assay

HEPES buffer (also known as Tyrodes buffer; 20 mM HEPES pH 7.2 (H9136, Sigma-Aldrich), 137 mM NaCl, 2.7 mM KCl, 2 mM $MgCl_2$, 1 mM $CaCl_2$, 5.6 mM glucose, 1 mg.mL^{-1} BSA), was made fresh on the day of the experiment and warmed to

37°c in a dry incubator; methanol was chilled in a Duran bottle on ice. For the PLC assay, HEPES buffer was supplemented with 10 mM LiCl throughout the experiment.

The cell plates were removed from the incubator, briefly viewed under the microscope to gauge health, and then washed twice in HEPES/LiCl buffer. The final wash was replaced with 1.5 mL buffer per well, and the plate placed at 37°c for 20 min to equilibrate. Meanwhile, the stimulant was prepared at room temperature at 4X concentrated, in a volume of 500 μL per well.

Once equilibrated, the 500 μL stimulant was added to the 1.5 mL buffer already present in each well of the six-well plate, as appropriate, and the plates returned to the incubator for the required amount of time.

A number of 15 mL solvent tubes were labelled, one for each well. Immediately after the stimulation step, the cell culture plates were removed from the incubator and placed on ice. The solution was completely aspirated from each of the wells and replaced with 500 μL cold methanol to quench the cells.

The cells were then scraped from each well using a cell scraper. An additional 500 μL methanol was added following scraping, rinsing the cell scraper in the process. The 1 mL methanol/cells was transferred to the appropriate solvent tube. The cell scraper was wiped on absorbent tissue between wells.

900 μL distilled water, followed by 1 mL chloroform, was added to the methanol/cells in each of the solvent tubes, and the tubes vortexed for 5 s. The tubes were next centrifuged at room temperature, 2,000 rev.min^{-1} for 10 mins to separate the aqueous and lipid phases. The top, aqueous phase was clear by completion of the centrifugation.

Isolation of the inositol phosphates using Dowex columns

Dowex columns constituted Dowex 1 x 8 anion exchange resin in a glass Pasteur pipette. These short columns were regenerated at the beginning of each experiment by

washing three times with 2 mL 2 M ammonium formate/0.1M formic acid, followed by 3-5 washes with 2 mL distilled water.

1 mL of the aqueous layer from each solvent tube was loaded onto a prepared Dowex column, and the liquid allowed to run through. This 1 mL was of a possible 2 mL, and was taken into account in the data analysis.

The columns were then washed with 6 mL distilled water (3 x 2 mL) to elute unbound [^{3}H]-inositol, followed by 6 mL 5 mM sodium tetraborate/60 mM sodium formate to elute glycerophosphoinositol.

The columns were now transferred to large scintillation vials, and the total inositol phosphates eluted by the application of 3 mL 1 M ammonium formate/0.1 M formic acid to each column, 1 mL at a time. When the elution was complete, 5 mL UltimaFLO scintillation fluid was added to each vial, and the radioactivity contained within the vials counted using the liquid scintillation counter.

The entire lower chloroform layer from each solvent tube (~900 µL) was removed to a small scintillation vial, and the lipids dried using the Savant SpeedVac (~30 min). 100 µL methanol was placed into each of these vials to re-solubilise the lipids, followed by 3 mL Ultima GOLD scintillation fluid. The vials were vortexed and the radioactivity contained within them counted using the liquid scintillation counter.

Data analysis

A mean of the triplicate inositol phosphate values was calculated (dpm) and expressed as a proportion of the inositol phosphates produced in control-transfected cells treated with the same stimulation. This enabled multiple experiments to be combined. Where a single experiment was carried out (n=1), error bars are not shown; for n=2, error bars are standard deviation; and for $n \geq 3$, standard errors are given.

2.7: Lipid binding assay

2.7.1: Principle

In order to monitor the binding of lipids by PITPs, HL60 cells were metabolically labelled with [^{14}C]-acetic acid to label all lipids. The cells were permeabilised with SLO, which binds to cholesterol. SLO monomers diffuse laterally in the membrane and oligomerise with one another to form large transmembrane pores that can reach up to 35 nm in diameter. These pores allow the passage of proteins up to 100 kDa in size (Walev et al., 2001), including PITPs, without affecting the structural integrity of the cell. This assay required that the recombinant PITPs carried out a single round of membrane docking and lipid exchange to pick up a radioactive lipid. The proteins were then re-captured using their His-tag, lipids extracted using Chloroform-Methanol, and the lipids resolved using thin layer chromatography (TLC).

2.7.2: HL60 cell culture

HL-60 cells (ATCC No. CCL-240) were routinely grown in suspension in 40 mL RPMI-1640 medium (Sigma-Aldrich, R0883), supplemented with 11.5% HI FCS, 4 mM L-glutamine, 0.5 iu.mL^{-1} penicillin and 50 µg.mL^{-1} streptomycin in a T75 cell culture flask. Cells were re-suspended before splitting by gently pipetting up and down. Confluent cells are 1 x 10^6 cells.mL^{-1}, and were not diluted beyond 1 x 10^5 cells.mL^{-1}. The doubling time of HL60 cells is ~24 hrs, and so they were split 1:4 for 48 hrs growth, to 0.25 x 10^6 cells.mL^{-1} (i.e. 10 mL confluent cells added to 30 mL fresh media), or 1:8 for 72 hrs growth, to 0.125 x 10^6 cells.mL^{-1}. All cell culture was carried out under aseptic conditions in a class II laminar flow cabinet.

2.7.3: Radionucleotide labelling of HL60 cells

[^{14}C]-acetic acid, [^{3}H]-choline and [^{3}H]-ethanolamine

Unless otherwise indicated, 10 mL confluent HL60 cells (10^7 cells) were required per assay volume on the day of the experiment. For [^{14}C]-acetic acid or [^{3}H]-choline ([methyl-^{3}H]-choline chloride) labelling, the required volume of cells in normal growth media (RPMI-1640, 11.5% HI FCS, 4 mM L-glutamine, 0.5 iu.mL^{-1} penicillin and 50 μg.mL^{-1} streptomycin) was supplemented with 1 μCi.mL^{-1} (37 kBq.mL^{-1}) radioactivity for 48-72 hrs growth prior to the experiment. For [^{3}H]-ethanolamine-labelling, the concentration of radioactivity was increased to 10 μCi.mL^{-1}, for 72 hrs growth.

[^{3}H]-sphingosine

40 x 10^6 HL60 cells were centrifuged at 1,300 rev.min^{-1} 5 min RT. The cell pellet was washed once in 40 mL PBS before resuspension in 40 mL unsupplemented RPMI-1640 media, 2% BSA (from a 30% sterile fatty acid-free stock solution) and 0.1 μCi.mL^{-1} (3.7 kBq.mL^{-1}) sphingosine, D-erythro [3-^{3}H] (ARC (UK)). The cells were returned to the incubator for 24 hrs labelling prior to the lipid binding experiment.

For the experiment in which HL60 cells were labelled with different radionucleotides, and the extracted lipids run alongside one another on a TLC plate, 20 mL HL60 cells were labelled with [^{3}H]-sphingosine in supplemented RPMI-1640 growth media.

[^{3}H]-palmitic acid

[^{3}H]-palmitic acid is stored in toluene (methyl benzene), which must be removed prior to addition to the cells. The required volume of radioactivity was placed into a 50 mL falcon tube and dried under nitrogen gas to remove the toluene. 3 mL fresh HEPES buffer was added to the dried lipids and sonicated for 3 x 15 s to re-suspend the palmitic acid. Meanwhile, 20 mL unlabelled, confluent HL60 cells were centrifuged at 1,300 rev.min^{-1} for 5 min RT to remove the growth medium, washed once with 20 mL PBS, and then re-suspended in 17 mL HEPES buffer. The re-suspended cells were added to

the [^{3}H]-palmitic acid tube, the contents mixed by inverting, and the tube placed in the dry incubator at 37°c for 3 hrs.

[^{3}H]-inositol

For labelling with [^{3}H]-inositol, the required number of cells were first transferred into a 50 mL falcon tube and centrifuged at 1,300 rev.min^{-1} to pellet the cells. The supernatant was discarded and cell pellet re-suspended in the appropriate volume of M199 supplemented with 10% HI dialysed FCS, 4 mM L-glutamine, 0.5 iu.mL^{-1} penicillin and 50 μg.mL^{-1} streptomycin, together with 1-4 μCi.mL^{-1} (37-148 kBq.mL^{-1}) *myo*-[2-^{3}H]-inositol for 48-72 hrs labelling. The HL60 cells did not tend to grow as fast in M199 as they did in RPMI, and so the cells were seeded at twice the usual concentration.

2.7.4: Lipid binding assay

Permeabilisation of HL60 cells with SLO

Labelled HL60 cells were washed twice in **PIPES buffer (20 mM PIPES pH 6.8, 137 mM NaCl, 2.7 mM KCl, 2 mM $MgCl_2$, 5.6 mM glucose, 1 mg.mL^{-1} BSA)**, with centrifugation at 1200 rev.min^{-1} for 5 mins, and then resuspended in 5 mL Permeabilisation Cocktail (0.6 iu.mL^{-1} SLO, 2 mM Mg-ATP). Cells were permeabilised in a water bath at 37°c for a maximum of 10 min.

Chilled PIPES buffer was added to ~45 mL, and the tube centrifuged at 3000 rev.min^{-1} for 5 mins at 4°c. The permeabilised cells were washed twice in 30 mL PIPES, and then re-suspended in an appropriate volume of PIPES buffer for the experiment, supplemented with 1 mM Mg-ATP. A small volume of permeabilised cells was also taken into account for extraction of the total HL60 cellular lipids (‘total lipids’).

Lipid binding by recombinant PITP

The assay volume was 600 μL, of which the following was added in the order given, to labelled 1.5 mL eppendorf tubes on ice:

100 μL PITP protein (200 $\mu g.mL^{-1}$; 120 μg protein per assay tube).

500 μL permeabilised cells.

In some experiments these volumes were adjusted, for example for more dilute recombinant protein preparations, but the total assay volume was maintained at 600 μL. The recombinant protein was diluted in **PIPES/salts buffer (20 mM PIPES pH 6.8, 137 mM NaCl, 2.7 mM KCl)**. This enabled the removal of 2.4 μg of the diluted protein (2% protein present in one assay volume) to run on an SDS-PAGE gel for Coomassie staining, without BSA contamination. This was further diluted with PIPES/salts buffer and 2X SDS-PAGE sample buffer to a final volume of 20 μL, and boiled for 10 min at 95°c.

PITP protein was incubated with permeabilised HL60 cells in a water bath pre-heated to 37°c for 20 mins. Immediately following this incubation, the assay tubes were centrifuged at 3,000 $rev.min^{-1}$ for 5 min at 4°c. 550 μL of the supernatant was transferred to a fresh eppendorf tube and centrifuged again, this time at 11,500 x *g* for 10 min at 4°c to remove any remaining debris.

Recapturing of the His-tagged PITP

120 μL HIS-select nickel affinity gel (Sigma-Aldrich, P6611) ('nickel beads') was placed into the required number of mini-spin columns (one per assay tube). The nickel beads were washed twice in 500 μL PIPES/salts by centrifugation at 3,000 $rev.min^{-1}$ for 5 min at 4°c. 500 μL cleared supernatant was then placed onto the mini-spin column. This supernatant contained cytosolic proteins, and, more importantly, the recombinant PITP with bound radiolabelled lipid. With the lids replaced, the columns were placed onto the rotating wheel for 30 mins at 4°c for capturing.

Washing of the nickel beads, elution of protein and buffer exchange

Following the re-capturing step, the mini-spin columns were centrifuged at 3,000 rev.min^{-1} for 5 min at 4°c, to elute unbound material. The nickel beads were washed twice with 500 µL **Low Salt buffer (50 mM phosphate buffer pH 6.0 [23.3 mL 1 M Na_2HPO_4, 1.70 mL 1 M NaH_2PO_4], 300 mM NaCl, 10% glycerol)**, followed by twice with **High Salt buffer (50 mM phosphate buffer pH 6.0 [23.3 mL 1 M Na_2HPO_4, 1.70 mL 1 M NaH_2PO_4], 525 mM NaCl, 10% glycerol)**. Finally, the recombinant proteins were eluted into fresh 2 mL eppendorf tubes by the addition of 500 µL of 500 mM imidazole (in high salt buffer) to each column with centrifugation 3,000 rev.min^{-1} for 5 min at 4°c.

Buffer exchange columns were prepared by washing twice with PIPES/salts buffer. These columns were re-used between experiments and were stored in PBS-0.05% sodium azide (*w*/*v*). 500 µL eluted protein was loaded onto a prepared buffer exchange column. The displaced liquid was allowed to run through; the recombinant protein was captured by the resin. The column was then placed into a 15 mL solvent tube, and 1 mL PIPES/salts applied to the column to elute the protein into the solvent tube.

20 µL of the eluted protein was transferred to a 1.5 mL eppendorf tube containing 6.67 µL 4X SDS-PAGE sample buffer, which was then vortexed briefly and boiled at 95°c for 10 min before running on an SDS-PAGE gel alongside the input sample. The gel was stained with Coomassie and protein bands quantified to assess protein recovery.

2.7.5: Lipid extraction and analysis of phospholipids by TLC

The ‘total lipids’ sample retained from the beginning of the experiment was diluted to 1 mL with buffer and transferred to a labelled 15 mL solvent tube alongside the eluted proteins. To each solvent tube, the following was added:

3.75 mL Chloroform: Methanol (1:2 (*v*/*v*)).

1.25 mL chloroform.

1.25 mL water.

The mixture was vortexed for 5 s, and a separation of lower organic and upper aqueous phases was observed. The tubes were then centrifuged at 2,000 rev.min^{-1} for 10 min RT to ensure clean separation of the phases.

Two 1.5 mL eppendorfs were labelled per 15 mL solvent tube. The lower organic layer was removed from the solvent tubes and divided between the two eppendorf tubes. The eppendorfs were then placed into the Savant SpeedVac (pre-cooled for >30 min prior to use), without lids attached for ~1.5 hrs, until the lipids (and the tubes) were completely dry.

50 µL fresh chloroform was placed into each of the dried lipid tubes, the lids rapidly closed, and the tubes vortexed to re-suspend the lipids.

10 µL of the re-suspended 'total lipids' was placed into a small liquid scintillation vial. The chloroform rapidly evaporated. 100 µL methanol was added to re-suspend the lipids. 3 mL UltimaGOLD scintillation fluid was then placed into the vial, the vial vortexed, and the sample counted using a liquid scintillation counter.

The lipid samples were then spotted onto a Whatman silica gel 60 TLC plate which had been desiccated in an oven at 100°c for >1 hr previously to remove any moisture on the plate. The lipids were each spotted in a distinct narrow line, 2 cm from the bottom of the plate. Alongside, 50,000-100,00 dpm of the total HL60 lipids were spotted and/or 12-24 µg unlabelled lipid standard for identification of phospholipids bound, as required.

Once the lipid spots were dry, the TLC plate was placed into a solvent tank containing Chloroform: Methanol: Acetic acid: Water (75: 45: 3: 1 *v*/*v*) . This solvent system was prepared and placed into the tank several hours before the tank was required to allow the solvent to equilibrate throughout the tank and chromatography paper. The solvent front was allowed to migrate to approximately 5 mm from the top of the plate (~1.5 hr) before the plate was removed from the tank and allowed to dry in a fume hood. The plate was then incubated with a clean white Fuji phosphor imager screen for approximately 5 days before imaging using a Fuji BAS1000 phosphor imager. SDS-

PAGE gels and TLC plate images were quantified by 2D densitometry using AIDA software. Data analysis was carried out as described in the text and/or figure legends.

2.7.6: Identification of bound lipids

For the experiment in which HL60 cells were labelled with different radionucleotides and the extracted lipids run alongside one another on a TLC plate, six cultures of 20 mL HL60 cells were set up with the radionucleotides indicated in Table 2.9. Labelling was carried out as described in Section 2.7.3: [^{3}H]-inositol in M199 medium, [^{3}H]-palmitic acid in HEPES, and all others in supplemented RPMI-1640 medium.

After labelling, the cells were transferred to 50 mL falcon tubes and washed once in 20 mL PBS. The cell pellet was re-suspended in 1 mL and transferred to a 15 mL solvent tube for lipid extraction. 3.75 mL Chloroform: Methanol (1:2 *v*/*v*) was added, followed by 1.25 mL chloroform and 1.25 mL water. The tubes were vortexed for 5 s, then centrifuged to separate the lower organic and upper aqueous phases. The lower, chloroform-soluble phase was carefully removed to 2 x 1.5 mL eppendorf tubes per label, and the lipids dried using the Savant SpeedVac. The dried lipids were re-suspended in 50 μL fresh chloroform, and 10 μL of each was transferred into a small liquid scintillation vial for counting using the liquid scintillation counter. Radioactivity incorporation is recorded in Table 2.9.

Approximately 100,000 dpm of each sample was spotted onto a TLC plate, which was then placed into a solvent tank containing the solvent system Chloroform: Methanol: Acetic acid: Water (75: 45: 3: 1 *v*/*v*). As before, the TLC plate was removed from the tank once the solvent tank had migrated to ~5 mm from the top of the plate. The plate was allowed to dry before being incubated with a blue phosphor imager screen for approximately one week before being imaged using a BAS-1000 phosphor imager.

No.	Radionucleotide	Labelling concen-tration (µCi/ml)	Labelling time (hrs)	Radioactivity in 10 µL extracted lipid (dpm)	Amount of lipid spotted onto TLC plate (dpm)
1	Sphingosine, D-erythro-[3-^{3}H]	0.5	48	800,182	150,000
2	Choline chloride methyl-[^{3}H]	1	48	327,926	100,000
3	[^{3}H]-inositol	2	48	135,300	100,000
4	[^{3}H]-ethanolamine hydrochloride	10	24	3,239,743	200,000
5	[^{3}H]-palmitic acid (C16:0)	2	3	303,687	175,000
6	[^{14}C]-acetic acid	1	48	197,824	75,000

Table 2.9: Radionucleotide labelling of HL60 cells

2.7.7: Purification of RdgBβ-bound lipids by two-dimensional TLC

The binding assay was scaled up, such that 50 x 10^{6} (50 mL) [^{14}C]-acetate-labelled HL60 cells and 300 µg recombinant RdgBβ-sp1 protein was used for a single incubation. The assay was otherwise carried out as described above. In addition, lipids were extracted from 10 mL unlabelled HL60 cells, and 40 mL permeabilised [^{14}C]-HL60 cells.

The extracted lipids were dried and re-suspended in 2 x 50 µL chloroform per sample. 10 µL of the total labelled lipids, counted using the liquid scintillation counter, contained 2,384,908 (~2,400,000) dpm. Two 2D TLC plates were run, one with total [^{14}C]-HL60 lipids and the other with RdgBβ-bound [^{14}C]-lipids. 10 µL of the total [^{14}C]-HL60 lipids (240,000 dpm), was spotted into one corner (2 cm from each edge) of one 20 x 20 cm TLC plate. This was 1/10th of the total volume, therefore equivalent to 4 mL cells. The dried unlabelled lipids were also re-suspended in 2 x 50 µL chloroform.

So that both TLC plates ran the same, approximately the same mass of material needed to be run on both plates. Therefore, 40 μL of the unlabelled lipids, corresponding to 4 mL cells, was added to the lipids extracted from RdgBβ, and spotted onto the corner of the second TLC plate.

Both TLC plates were placed facing one another into the first tank, with the spotted lipids at the bottom-left of each plate. This first tank had been prepared with the solvent system, Chloroform: Methanol: 28% Ammonia (65: 35: 5 *v*/*v*). The solvent was allowed to migrate to within ~5 mm of the top of the plates, and then the plates were removed and allowed to dry in the fume hood.

Both plates were then placed into the second tank, again facing one another, but rotated 90° counter-clockwise so that the origin was now on the bottom right of each of the plates. This second tank had been prepared with the solvent system, Chloroform: Methanol: Acetic acid: Water (75: 45: 3: 1 *v*/*v*). As before, the solvent was allowed to migrate to within ~5 mm of the top of the plates, the plates were removed, allowed to dry, and then placed with a white phosphor imager screen for 5 days prior to imaging.

2.7.8: Phospholipid deacylation: treatment with a primary amine

The PI and mystery lipid radioactive spots derived from the lipids bound by RdgBβ-sp1 were excised from the 2D TLC plate: the silica was moistened using a fine water spray, scraped, and the scrapings transferred to a 15 mL solvent tube. 1 mL distilled water was added and the tube vortexed to break up the silica. 3.75 mL Chloroform: Methanol (1:2 *v*/*v*) was added to the tube, followed by 1.25 mL chloroform and 1.25 mL distilled water. The tube was vortexed (>5 s), then centrifuged at 2,000 rev.min^{-1} 10 min RT to separate the organic and aqueous phases. The lower organic phase was removed and separated equally between two 1.5 mL eppendorf tubes. The lipid were then dried using the Savant SpeedVac.

The air was evacuated from one each of the lipid tubes using nitrogen gas, and these ‘untreated’ tubes were placed at -20°c during monomethylamine treatment of the other lipid tubes.

Monomethylamine reagent was made previously by Dr. Alison Skippen, using the method introduced by Clarke and Dawson (Clarke and Dawson, 1981), and stored at -20°c. Monomethylamine gas was passed into a 40 mL mixture of Methanol: Water: *n*-Butanol (4: 3: 1 *v*/*v*) contained in a graduated container in an ice bath, until the volume in the flask had increased to 65 mL.

200 µL monomethylamine reagent was placed into each of the two remaining tubes containing dried lipid, and the tubes incubated at 53°c for 30 mins. The tubes were then returned to the SpeedVac to remove the monomethylamine reagent, which is volatile, and to dry the treated lipids. The 'untreated' lipid tubes were now removed from the freezer. 100 µL dH_2O was added to each of the four lipid tubes, followed by 375 µL Chloroform: Methanol (1:2 *v*/*v*). The tubes were vortexed, and then 125 µL chloroform, followed by 125 µL water, was added. The tubes were vortexed, centrifuged, and each of the lower organic layers removed to fresh eppendorf tubes and dried once more in the SpeedVac. The dried lipids were next re-suspended in 50 µL fresh chloroform and spotted onto a TLC plate. The solvent-soluble lipids were resolved in the solvent system, Chloroform: Methanol: Acetic acid: Water (75: 45: 3: 1 *v*/*v*).

2.7.9: PLA_2 treatment of [^{3}H]-ethanolamine liposomes

Total HL60 cell lipids labelled with [^{3}H]-ethanolamine, which had been left over from previous experiments and stored at -20°c, were combined into a single 1.5 mL eppendorf tube and dried using the Savant SpeedVac. The dried lipids were then re-suspended in 1 mL PIPES/salts pH 6.8 buffer with the aid of 3 x 15 s sonication bursts. 10 µL liposomes contained 369,840 dpm (~370,000 dpm) radioactivity.

100 µL [^{3}H]-ethanolamine liposomes was placed into each of four labelled eppendorf tubes on ice, and incubated with 1 U phospholipase A2 (from bee venom, P-9279, Sigma-Aldrich), for 0, 1, 2 or 4 min in a water bath at 25°c. The hydrolysis reaction was terminated by the addition of 375 µL Chloroform: Methanol (1:2 *v*/*v*), the tube vortexed and returned to ice. Once all of the incubations had finished, 125 µL chloroform and 125 µL water were added to each tube, the tubes vortexed and then centrifuged in a

table-top centrifuge at 10,000 rev.min^{-1} 2 min RT. The lower, organic phase was then removed to a fresh eppendorf tube, and the lipids dried using the Savant SpeedVac. The dried lipids were re-suspended in 50 μL fresh chloroform, 10 μL counted using the liquid scintillation counter, and 100,000 dpm spotted onto a TLC plate alongside unlabelled phospholipid standards, PE, PMME and PI.

2.7.10: Preparation of samples for mass spectrometry

For analysis of bound lipids by mass spectrometry, the experiment was carried out as described above (Sections 2.7.4), with minor modifications. The amount of recombinant protein was increased to 600 μg in each assay volume, and the amount of cells for each assay was increased to 50 mL confluent cells. HL60 cells were unlabelled for mass spectrometry. All chloroform extractions were performed in borosilicate glass screw-capped tubes to prevent polymer contamination of the samples. The organic phase was carefully transferred into glass amber vials using a glass pasteur pipette and the lipids dried using the Savant SpeedVac. The air was evacuated from the glass vial and replaced by nitrogen gas to prevent oxidation of the lipids. Samples were transported to Southampton at 4°c within 24 hrs of completion of the experiment. All mass spectrometry and subsequent data analysis was carried out by our collaborators, Dr. Alan Hunt and Grielof Koster (University of Southampton).

The phospholipids were analysed by electrospray ionisation mass spectrometry (ESI-MS) using a Quatro Ultima triple quadrupole mass spectrometer (Micromass, Wythenshaw, UK) equipped with direct infusion or nanoflow interfaces, depending on the sample size (Hunt et al., 2004). A full screening of glycerophospholipid species was carried out under both positive and negative ionisation with selective precursor of all phospholipids of potential interest, including PA, PC, PE, PI, PS and related lysophospholipids. Bacterial lipids including PG were absent from all samples. The PA species were identified from scanning for the precursors of the glycerophospholipid fragment (*m*/*z* -153) and their identities and dominant acyl compositions confirmed by specific peak fragmentations, while the PI species were detected by scanning for the precursor of inositol phosphate (*m*/*z* -241).

2.7.11: Treatment of [^{14}C]-PI and [^{14}C]-PC with PLD

Total HL60 [^{14}C]-lipids from previous experiments were removed from the freezer, where they had been stored at -20°c, and the chloroform replenished where required. The lipids were spotted in 4 cm-wide bands, 2 cm from the bottom of two TLC plates. The lipids were migrated in the usual solvent system, Chloroform: Methanol: Acetic acid: Water (75: 45: 3: 1 *v*/*v*), and the plates placed with a white phosphor imager screen for 24 hrs prior to imaging. The [^{14}C]-PI and [^{14}C]-PC lipids were identified and the silica scraped into 50 mL falcon tubes, one for each lipid. The lipids were extracted in 2.5 mL: first, 2.5 mL water was placed into the falcon tubes with the scraped silica, and the tubes vortexed for >5 s. Next, 7.5 mL chloroform: methanol (1:2 *v*/*v*) was added, followed by a further 2.5 mL chloroform and 2.5 mL water. The tubes were again vortexed for >5 s, and centrifuged, 2,000 rev.min^{-1} 10 min RT. The lower, solvent phase was removed to a single 1.5 mL eppendorf for each lipid. The lipids were dried using the Savant SpeedVac, and more lipid was added to each tube every 30 min-1 hr.

The dried lipid was re-suspended in 400 µL 0.2 M sodium acetate pH 5.6, by 2 x 15 s sonication bursts, until no lipid could be seen sticking to the inside of the tubes.

Phospholipase D (EC 3.1.4.4), Type III from Peanut (209 units.mg^{-1} solid, P-0640, Sigma-Aldrich): 10.2 mg PLD was dissolved in 850 µL acetate buffer, to give a solution of 12 mg.mL^{-1} or 2,500 units.mL^{-1}.

The total assay volume was 1.3 mL, of which:

400 µL lipid (PI or PC)
400 µL PLD (1000 units)
100 µL $CaCl_2$ (1 M stock)
400 µL ether (diethyl ether)

The tubes were mixed well, then incubated at RT for 16 hrs. The following day, the caps were removed from the eppendorf tubes and the tubes placed into a fume cabinet to allow the ether to evaporate (~10 min). The contents of each eppendorf tube was transferred to a 15 mL solvent tube for lipid extraction by the addition of 3.75 mL

chloroform: methanol (1:2 *v/v)*, 1.25 mL chloroform and 1.25 mL water. The tubes were vortexed 5 s and centrifuged 2,000 rev.min^{-1} 10 min RT. The lower, organic phase was removed to 2 x 1.5 mL eppendorf per lipid, labelled PI-PA and PC-PA, and the lipids dried using the Savant SpeedVac. 100 µL fresh chloroform was then added to each eppendorf tube, and the tubes vortexed to re-suspend the lipids. 10 µL of each lipid was counted using the liquid scintillation counter: PI-PA, 26,480.7 dpm; PC-PA, 25,916.7 dpm. 100,000 dpm of each lipid was spotted onto a TLC plate alongside 20 µg each of PI and PC unlabelled phospholipid standards. The lipids were migrated in the usual solvent system, Chloroform: Methanol: Acetic acid: Water (75: 45: 3: 1 *v/v*).

2.7.12: Permeabilised HL60 cell assay for [^{14}C]-lipid transfer

The lipid binding assay described above monitors a single round of docking and lipid exchange by the PITPs. To establish whether the bound lipid was transferred and deposited in an acceptor membrane, the permeabilised HL60 cell assay was adapted to include unlabelled acceptor liposomes. At the end of the incubation, 0.2 M sodium acetate/0.25 M sucrose pH 5.0 was added to pellet the HL60 cell membranes. The transferred [^{14}C]-acetic acid lipids were extracted from the liposomes (supernatant), and analysed by TLC.

50 mL labelled HL60 cells were washed twice in PIPES buffer, then permeabilised with 0.6 iu.mL^{-1} SLO in 5 mL PIPES with 2 mM Mg-ATP at 37°c for 10 min. The permeabilised cells were then washed once in PIPES, and re-suspended in 1 mL PIPES with 1 mM Mg-ATP.

6 mL PC:PI liposomes (98:2, molar ratio) were prepared in PIPES buffer: 4.7 mg PC (47 µL of 100 mg.mL^{-1} Egg PC stock) and 100 µg PI (4µL of 50 mg.mL^{-1} stock (50% pure, Sigma-Aldrich, P6636, L-α-Phosphatidylinositol from soybean)), were placed into a 15 mL falcon tube. The chloroform was evaporated under nitrogen gas. The lipids were then re-suspended in 6 mL PIPES buffer using 3 x 15 s sonication bursts. This gave 784 µg PC and 16 µg PI per mL assay volume.

The assay volume was 400 µL, prepared on ice:

100 µL permeabilised cells.

200 µL liposomes.

100 µL recombinant PITP protein (80 µg, 200 µg.mL^{-1}).

The assay was incubated in a water bath at 37°c for 20 min. The tube rack was then returned to ice, and the experiment quenched by the addition of 100 µL ice-cold 0.2 M sodium acetate/0.25 M sucrose pH 5.0 (total volume now 500 µL). The tubes were vortexed and incubated on ice for >10 min. The tubes were then centrifuged at 12,000 rev.min^{-1} for 15 min at 4°c to pellet the cell membranes.

400 µL of the supernatant was transferred to a labelled 15 mL solvent tube for lipid extraction by the addition of 1.5 mL chloroform: methanol (1:2, *v*/*v*), followed by 500 µL chloroform and 500 µL water. The solvent tubes were vortexed for 5 s, and then centrifuged at 2,000 rev.min^{-1} for separation of the lipid and aqueous phases. The lower, solvent phase was removed to a labelled 1.5 mL eppendorf tube, and the lipids dried using the Savant SpeedVac.

The dried lipids were re-suspended in 50 µL chloroform per tube, spotted onto two TLC plates (one per replicate) and migrated in the solvent system, Chloroform: Methanol: Acetic acid: Water (75: 45: 3: 1 *v*/*v*).

2.7.13: Lipid binding assay with stimulation of cells by GTPγS or PMA

In order to assess the effect of stimulation of the HL60 cells on lipid binding, the lipid binding assay described in Section 2.7.4 was modified. Instead of permeabilising the HL60 cells and washing them of cytosol before use in the binding assay, SLO was added to the cells at the same time as recombinant PITP, thus combining the permeabilisation and lipid-binding incubations.

10 mL confluent HL60 cells labelled with [^{14}C]-acetate were required per assay volume. Instead of permeabilisation, labelled cells were washed twice in fresh PIPES buffer, and then re-suspended in PIPES buffer with 1 mM Mg-ATP.

The assay volume was 600 μL, of which the following were added in the order given:

100 μL recombinant RdgBβ/PITPα (200 μg.mL^{-1}; 120 μg protein per assay vol.).

400 μL washed HL60 cells + 1 mM Mg-ATP.

50 μL stimulation: 100 nM PMA or 100 μM GTPγS or buffer for control.

50 μL 0.4 iu.mL^{-1} SLO, + 3 mM pCa7 or 3 mM pCa5.

The experiment was otherwise carried out exactly as described above.

CHAPTER 3: The RdgBβ-sp1 C-terminus and an interaction with 14-3-3

3.1: Introduction

Members of the PITP family all carry the defining PITP domain at their N-terminus, yet differ in their C-terminal sequences. For some PITPs, it has been reported that this region mediates protein-protein interactions and is therefore important in localisation, and potentially function. PITPα interacts with the netrin-1 receptors, DCC and neogenin, via its C-terminus (Xie et al., 2005). This association increases 4-fold upon netrin-1 stimulation, and likely functions to localise PITPα at the plasma membrane to present PI to PI4K. The RdgBα proteins have an FFAT motif which binds VAP proteins, targeting RdgBαI to the ER membrane (Amarilio et al., 2005).

The two splice variants of RdgBβ, RdgBβ-sp1 and -sp2, share the same PITP domain, yet differ in their C-termini. The RdgBβ PITP domain is encoded by exons 1-8 of the *PITPNC1* gene; the RdgBβ-sp1 C-terminus is encoded by exon 10, and the RdgBβ-sp2 C-terminus is encoded by exon 9. I therefore begin my study of RdgBβ by analysing its C-terminus. Bioinformatics tools are used to identify that this region of RdgBβ-sp1 is disordered, a finding that is confirmed by trypsin digestion of the recombinant protein. Furthermore, RdgBβ-sp1 is ubiquitinated and undergoes a moderate rate of turnover. A database search indicates that the C-terminus is phosphorylated, and that two of the phosphorylation sites lie in consensus sites for 14-3-3 binding. I show that RdgBβ-sp1 binds 14-3-3 via phosphorylated Ser274 and Ser299 in its C-terminus, and that phosphorylation is in part mediated by PKC.

3.2: The C-terminal region of RdgBβ-sp1 lacks secondary structure

The PITPs differ mainly in their C-termini. RdgBβ-sp1 is ~60 aa longer in sequence than PITPα and PITPβ, and I therefore began my study of RdgBβ with the C-terminal domain. These regions of RdgBβ-sp1 and -sp2 were analysed using bioinformatics tools to establish whether they have any discernible secondary structure or significant homology to other protein domains. The DISOPRED2 server was used to predict regions of disorder (lacking secondary structure) within a protein (Ward et al., 2004). Analysis of the human sequences, RdgBβ-sp1 (Accession no.: Q9UKF7) and RdgBβ-sp2 (NP_858057.1), identified several regions of disorder (Figure 3.1 A).

In both splice variants a region of disorder (27-39 aa) is present in the PITP domain, which lies in a region of the domain near to the opening of the lipid binding cavity between the αA helix and β2 strand. In addition, the C-termini of both splice variants are disordered: the disorder for RdgBβ-sp1 begins at residue 251, whereas for RdgBβ-sp2 it begins at residue 246. For RdgBβ-sp1 this means a long disordered region composed of 82 amino acids, broken only by a short α-helix. The helix lies either at 300-305 (gap predicted by DISOPRED) or 309-313 (α-helix predicted by PSIPRED, the secondary structure prediction arm of DISOPRED (Bryson et al., 2005)).

To investigate this prediction experimentally I reasoned that the unstructured or disordered regions of the protein would be more susceptible to digestion with a protease than a compact domain. Analysis of the RdgBβ-sp1 and -sp2 sequences revealed 30 potential trypsin cleavage sites in their common PITP domain sequence, 9 additional cleavage sites in the C-terminus of RdgBβ-sp1, but only 2 sites in the C-terminus of RdgBβ-sp2 (Figure 3.1 B). In agreement with this, treatment of the recombinant proteins with trypsin for 10 minutes saw a prominent size shift for RdgBβ-sp1, but no discernible shift in size for RdgBβ-sp2 (Figure 3.1 C). This indicates that the stable protein band reached by 10 minutes is the stable PITP domain. The stable protein unit is ~37 kDa for RdgBβ-sp1 and 38 kDa for RdgBβ-sp2.

(Facing page) Figure 3.1: The C-terminus of RdgBβ-sp1 is disordered and contains two PEST sequences

(A) DISOPRED2 disordered profile plots for, *left panel*: RdgBβ-sp1, and, *right panel*: RdgBβ-sp2. (B) Multiple sequence alignment of the human sequences of RdgBβ-sp1 (Accession no.: Q9UKF7.2) and RdgBβ-sp2 (Accession no.: NP_858057.1). The yellow region indicates the sequence identical between the two splice variants, i.e. the region encoded by exons 1-8. The predicted trypsin cleavage sites and PEST sequences are also indicated. (C) Trypsin digestion of recombinant RdgBβ-sp1 and -sp2 (0-10 min). *Left panel*: Coomassie-stained SDS-PAGE gel; 2 μg protein loaded per lane. *Right panel*: western blot using anti-RdgBβ antibody, #101; 30 ng loaded per lane. (Experiment carried out by Michelle Li.)

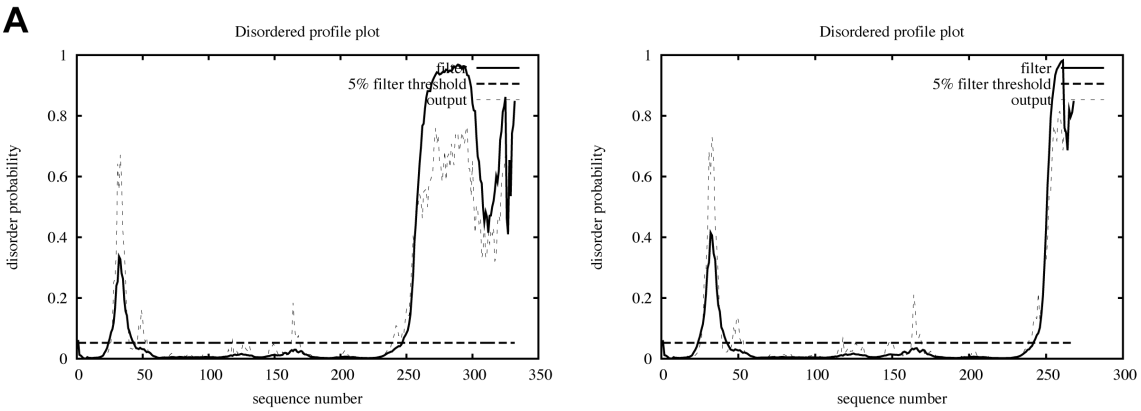
A
Disordered profile plot
filter
5% filter threshold
output
disorder probability
sequence number
Disordered profile plot
filter
5% filter threshold
output
disorder probability
sequence number

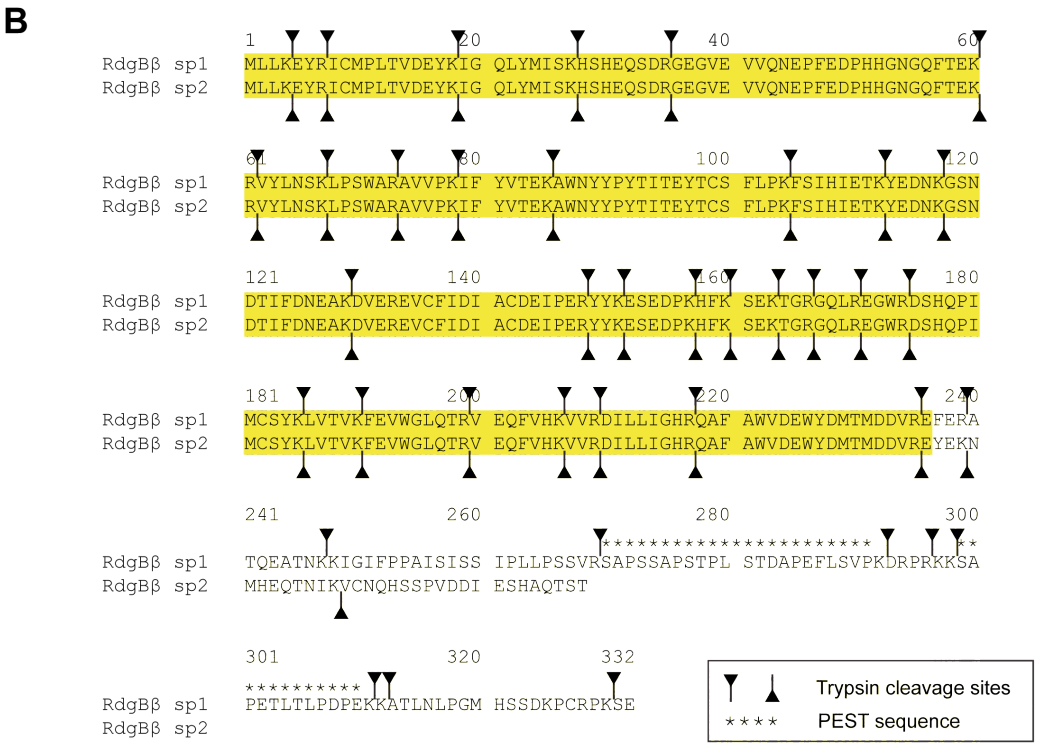
B
RdgBβ sp1
RdgBβ sp2
MLLKEYRICMPLTVDEYKIG QLYMISKHSHEQSDRGEGVE VVQNEPFEDPHHGNGQFTEK
RVYLNSKLPSWARAVVPKIF YVTEKAWNYYPYTITEYTCS FLPKFSIHIETKYEDNKGSN
DTIFDNEAKDVEREVCFIDI ACDEIPERYYKESEDPKHFK SEKTGRGQLREGWRDSHQPI
MCSYKLVTVKFEVWGLQTRV EQFVHKVVRDILLIGHRQAF AWVDEWYDMTMDDVREFERA
MCSYKLVTVKFEVWGLQTRV EQFVHKVVRDILLIGHRQAF AWVDEWYDMTMDDVREYEKN
TQEATNKKIGIFPPAISISS IPLLPSSVRSAPSSAPSTPL STDAPEFLSVPKDRPRKKSA
MHEQTNIKVCNQHSSPVDDI ESHAQTST
PETLTLPDPEKKATLNLPGM HSSDKPCRPKSE
Trypsin cleavage sites
PEST sequence

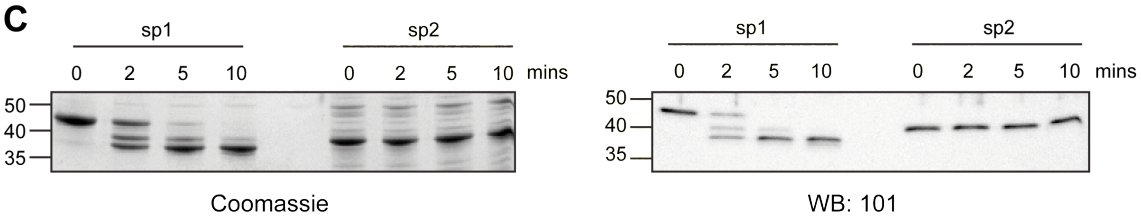
C
sp1
sp2
0 2 5 10 0 2 5 10 mins
50
40
35
Coomassie
sp1
sp2
0 2 5 10 0 2 5 10 mins
50
40
35
WB: 101

3.3: RdgBβ-sp1 is subject to turnover in mammalian cells

The trypsin protease has been used as a tool here to examine the structure of RdgBβ, but this property may also be relevant *in vivo*. Disordered regions, especially at the N- or C-terminus of a protein, may spell a more rapid degradation and turnover of a protein in cells. The sequence is more accessible to proteases and could permit the protein to literally be unravelled from this polypeptide chain. Further analysis of the RdgBβ-sp1 C-terminus uncovers two PEST sequences (Figure 3.1 B), rich in Proline, glutamate (E), Serine and Threonine residues. The PEST sequence was originally identified as being common to proteins with a high rate of turnover in cells - the protein concentration is reduced by half within 2 hrs (Rogers et al., 1986; Rechsteiner and Rogers, 1996). To test whether RdgBβ-sp1 is undergoing rapid turnover, COS-7 cells were transfected with a pcDNA3.1 plasmid containing the wild-type RdgBβ-sp1 sequence tagged with a FLAG tag. 48 hrs later, the cells were treated with the protein synthesis inhibitor, cycloheximide, and the relative quantity of FLAG fusion protein was monitored at specific time points by western blotting (Figure 3.2 A). The wild-type FLAG-RdgBβ-sp1 is reduced by half by 5 hrs cycloheximide treatment (Figure 3.2 B). This is compared to another soluble PITP, PITPβ, which is not seen to degrade at all in the 6 hr experiment time.

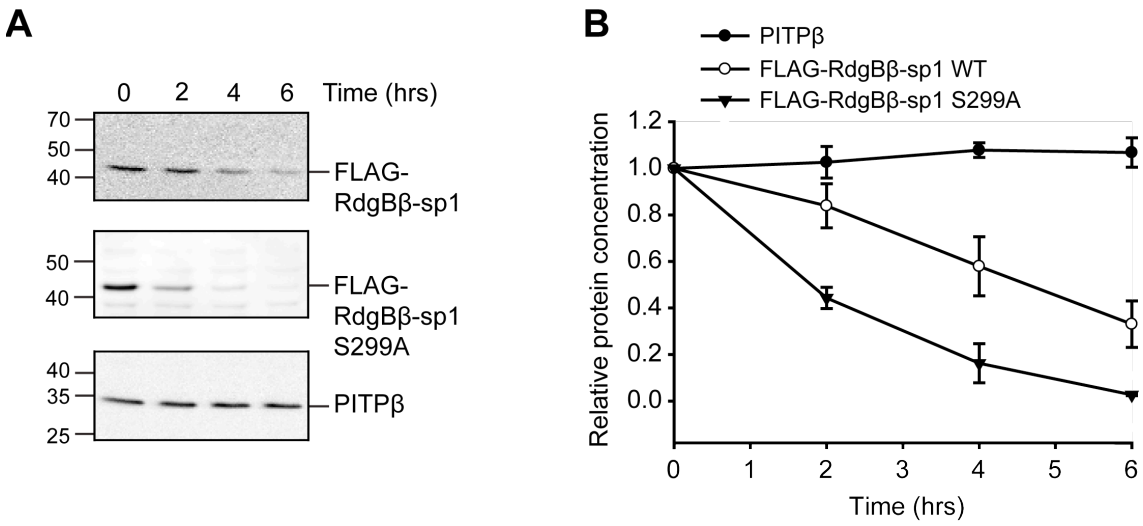

Figure 3.2: RdgBβ-sp1 is subject to turnover in mammalian cells

(A) COS-7 cells were transfected with pcDNA3.1-FLAG-RdgBβ-sp1 WT or S299A mutant. On the morning of the experiment, the culture media was removed and replaced with fresh media containing 100 μg.mL^{-1} cycloheximide. Cells were harvested at 0, 2, 4 and 6 hrs and subjected to western blotting using anti-FLAG antibodies (DDK). Membranes were stripped and re-probed for endogenous PITPβ #1C1 (single membrane shown). (Experiment carried out by Michelle Li.) (B) Protein bands were quantified using densitometry, background intensity subtracted and protein concentration calculated relative to expression at zero time. Error bars are SEM; FLAG-RdgBβ-sp1 WT, *n*=5; PITPβ and FLAG-RdgBβ-sp1 S299A, *n*=2.

3.4: RdgBβ-sp1 is ubiquitinated and phosphorylated

The most common signal for intracellular protein degradation is the addition of a ubiquitin tag by an E3 ubiquitin ligase. Probing a FLAG-RdgBβ-sp1 immunoprecipitate with anti-Ubiquitin antibodies indicated that RdgBβ is ubiquitinated. Cells were harvested after treatment with the 26S proteasome inhibitor, MG-132. Without treatment, ubiquitin is barely detectable in the FLAG-immunoprecipitate, and increases noticeably upon 26S proteasome inhibition (Figure 3.3). A ubiquitin tag is most commonly conjugated to an ε-NH_2 group of an internal lysine residue. Studies aimed at identifying a consensus sequence surrounding the ubiquitinated lysine have reported no common sequence (Glickman and Ciechanover, 2002). Since the RdgBβ-sp1 sequence contains 27 lysines, it is difficult to narrow down the precise location of the ubiquitin signal on RdgBβ.

Alternatively, other post-translational modifications, such as phosphorylation, can regulate the recruitment of E3 ubiquitin ligases, or of other proteins that hide or expose recognition sequences. High-throughput proteomics screens are increasingly being used to identify phosphorylation sites on proteins using mass spectrometry. Such screens often have the aim of identifying proteins involved in the progression of a particular disease state by looking at its changing regulation. Multiple sites have been identified in RdgBβ as being phosphorylated in the human and mouse sequences. Figure 3.4 maps the position of these sites and indicates the number of reports concerning each phosphorylation. Three sites are associated with >5 reports: Ser274, Thr278 and Ser299. The most thorough screen carried out to date is by Huttlin and colleagues, who identified phosphorylated peptides from nine organs (brain, brown fat, heart, liver, lung, kidney, pancreas, spleen, testis), harvested from 3-week-old Swiss-Webster mice (Huttlin et al., 2010). The Ser166 residue, phosphorylated in PITPα (van Tiel et al., 2000; Morgan et al., 2004), and conserved in almost all PITPs identified, including RdgBβ (equivalent residue Ser161), has not been reported as phosphorylated in RdgBβ to date.

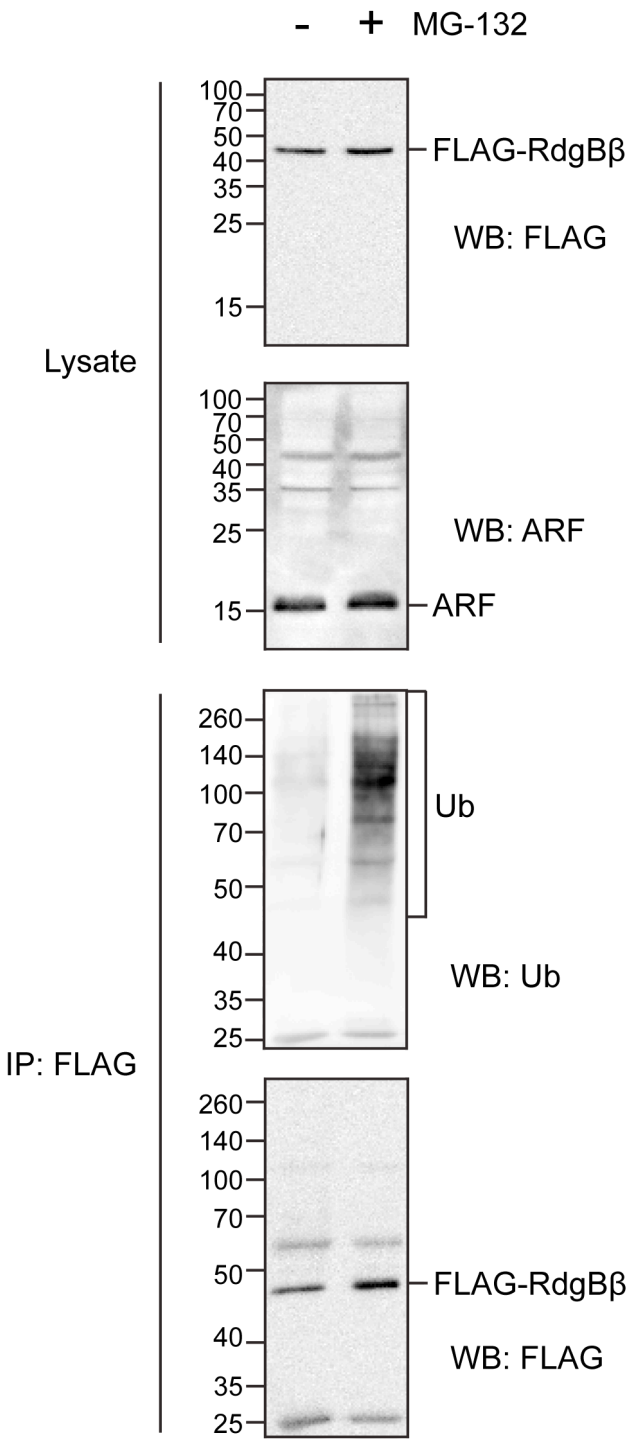

Figure 3.3: RdgBβ-sp1 is ubiquitinated

COS-7 cells expressing FLAG-RdgBβ-sp1 fusion protein were treated without or with 20 μM MG-132 proteasome inhibitor for 4 hrs prior to cell harvest. RdgBβ was immunoprecipitated using its FLAG tag and subjected to western blotting with anti-Ubiquitin (Ub) antibody (*third panel*). The PVDF membrane was re-probed to confirm presence of FLAG-RdgBβ in the immunoprecipitate (DDK) (*fourth panel*). 12 μg lysate was probed for FLAG-RdgBβ expression on a separate membrane (*first panel*); this membrane was stripped and re-probed for ARF1 loading control (*second panel*).

(Facing page) Figure 3.4: Reported mouse and human RdgBβ phosphorylation sites

CLUSTAL O (1.0.3) multiple sequence alignment of the human (*Hs*) RdgBβ-sp1 (NP_036549) and -sp2 (NP_858057) sequences with mouse (*Mm*) RdgBβ sequences (Q8BTD8 and NP_665822). Residue numbering begins at the human methionine start codon. Residues reported as being phosphorylated are indicated on either the human or mouse sequence, as appropriate. The frequency of reports is indicated in brackets after the residue name. Residues Ser274, Thr278 and Ser299 have over 5 observations of being phosphorylated, and are coloured dark orange.

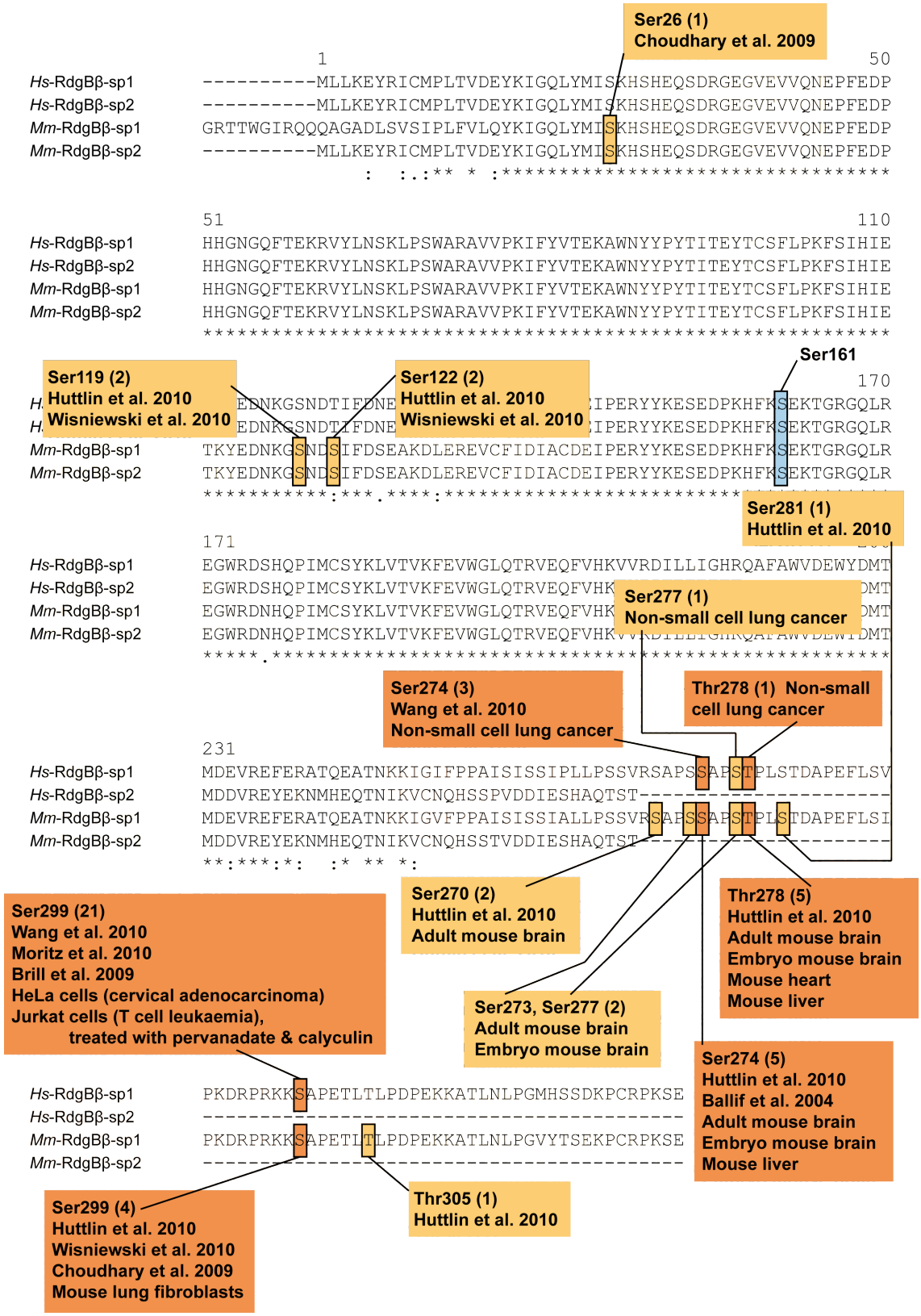
Ser26 (1)
Choudhary et al. 2009
Hs-RdgBβ-sp1
Hs-RdgBβ-sp2
Mm-RdgBβ-sp1
Mm-RdgBβ-sp2
Ser119 (2)
Huttlin et al. 2010
Wisniewski et al. 2010
Ser122 (2)
Huttlin et al. 2010
Wisniewski et al. 2010
Ser161
Ser281 (1)
Huttlin et al. 2010
Ser277 (1)
Non-small cell lung cancer
Ser274 (3)
Wang et al. 2010
Non-small cell lung cancer
Thr278 (1) Non-small
cell lung cancer
Ser270 (2)
Huttlin et al. 2010
Adult mouse brain
Thr278 (5)
Huttlin et al. 2010
Adult mouse brain
Embryo mouse brain
Mouse heart
Mouse liver
Ser299 (21)
Wang et al. 2010
Moritz et al. 2010
Brill et al. 2009
HeLa cells (cervical adenocarcinoma)
Jurkat cells (T cell leukaemia),
treated with pervanadate & calyculin
Ser273, Ser277 (2)
Adult mouse brain
Embryo mouse brain
Ser274 (5)
Huttlin et al. 2010
Ballif et al. 2004
Adult mouse brain
Embryo mouse brain
Mouse liver
Thr305 (1)
Huttlin et al. 2010
Ser299 (4)
Huttlin et al. 2010
Wisniewski et al. 2010
Choudhary et al. 2009
Mouse lung fibroblasts

RdgBβ-sp1 Ser274 was found to be phosphorylated most prominently in mouse brain and heart, with low levels in brown fat, lung, liver and spleen (Huttlin et al., 2010). This phosphorylation has also been identified in the developing mouse brain (fore-brain and mid-brain from E16.5) by another group (Ballif et al., 2004), and in adult and embryo mouse brains, as well as the mouse liver (2008, PhosphoSitePlus database, Cell Signalling Technology, (Hornbeck et al., 2004)). In the human sequence this phosphorylation has been identified in non-small cell lung carcinoma (H1703 cell line, 2006, PhosphoSitePlus database, Cell Signalling Technology, (Hornbeck et al., 2004)) and in a study that looked at metastasis-associated phosphoproteomic alterations in non-small cell lung cancer (Wang et al., 2010).

Phosphorylated RdgBβ-sp1 Thr278 was found primarily in mouse heart and brain, with low levels in kidney and liver (Huttlin et al., 2010). In separate experiments, this site has been identified as being phosphorylated in untreated mouse organs: adult and embryo brain, heart and liver (2008, PhosphoSitePlus database, Cell Signalling Technology, (Hornbeck et al., 2004)). In the human sequence this phosphorylation has been identified in non-small cell lung carcinoma (H1703 cell line, 2006, PhosphoSitePlus database, Cell Signalling Technology, (Hornbeck et al., 2004)).

RdgBβ-sp1 Ser299 has been identified as a phosphorylated site following receptor tyrosine kinase stimulation of human cancer cell lines (H1703, H3255 and MKN45 cells) by EGF, PDGF and c-Met (Moritz et al., 2010), in embryonic stem cells (Brill et al., 2009), in a metastasising non-small cell lung cancer (Wang et al., 2010), in HeLa (cervical adenocarcinoma) cells and in Jurkat (T cell leukaemia) treated with the phosphatase inhibitors, pervanadate and calyculin (2009, PhosphoSitePlus database, Cell Signalling Technology, (Hornbeck et al., 2004)). In the mouse, RdgBβ-sp1 S299A has been found to be phosphorylated in the brain (Huttlin et al., 2010; Wiśniewski et al., 2010), after stimulation of signalling by the oncogenic mutant of Flt3 in mouse 32Dcl3 cells (IL-3-dependent myeloid cell line) (Choudhary et al., 2009), and melanomas from TG3 mutant mice (ectopic Grm1 (a glutamate receptor) expression, leading to constitutive activation of the Erk signalling pathway) (Zanivan et al., 2008). In addition, the Ser299 residue has been identified as a phosphorylated residue in mouse lung

fibroblasts (2009, PhosphoSitePlus database, Cell Signalling Technology, (Hornbeck et al., 2004)).

To investigate the role of each of these C-terminal phosphorylations on ubiquitination of RdgBβ-sp1, I constructed point mutations of each residue (Ser/Thr to Ala) in the FLAG-tagged protein, using site-directed mutagenesis. The mutant proteins were each immunoprecipitated using their FLAG tags and the immunoprecipitate probed by western blotting with anti-Ubiquitin antibodies. No significant difference in the amount of ubiquitin detected for the mutants was observed (Figure 3.5). However, protein expression did vary significantly between the wild-type protein and the mutants (Figure 3.5 B). The FLAG-RdgBβ-sp1 S299A mutant was therefore assessed for protein stability, inhibiting protein synthesis using cycloheximide (Figure 3.2). The RdgBβ-sp1 S299A mutant was more rapidly degraded than the wild-type protein: the quantity of the wild-type protein was reduced by half within 5 hrs cycloheximide treatment; for the S299A mutant the quantity of protein in the cell lysate was reduced by half within 2 hrs treatment.

(Facing page) Figure 3.5: Mutation of C-terminal Ser/Thr phosphorylation sites has no effect on RdgBβ-sp1 ubiquitination

COS-7 cells transfected with pcDNA3.1 empty vector control, FLAG-RdgBβ-sp1 WT, S274A, S299A, SS274/299AA or T278A, were treated with 20 μM MG-132 for 4 hrs prior to cell harvest. (A) Fusion proteins were immunoprecipitated using their FLAG tag and subjected to western blotting with the anti-Ubiquitin antibody (Ub). The PVDF membrane was stripped and re-probed to confirm the presence of the FLAG fusion proteins (DDK). 10 μg lysates were also subjected to western blotting with the anti-FLAG antibody (DDK). This membrane was stripped and re-probed for ARF1 loading control. The western blot protein bands were quantified using AIDA software. (B) Quantity of FLAG-RdgBβ-sp1 fusion proteins present in the lysate have first been adjusted for ARF1 loading control, and then are expressed relative to WT protein to allow multiple experiments to be combined. Error bars are SEM, n=5. * p<0.05, ** p<0.01, *** p<0.001. (C) Quantity of Ubiquitin present in the immunoprecipitate adjusted for quantity of FLAG fusion protein present, relative to WT protein. Error bars are SEM, n=2.

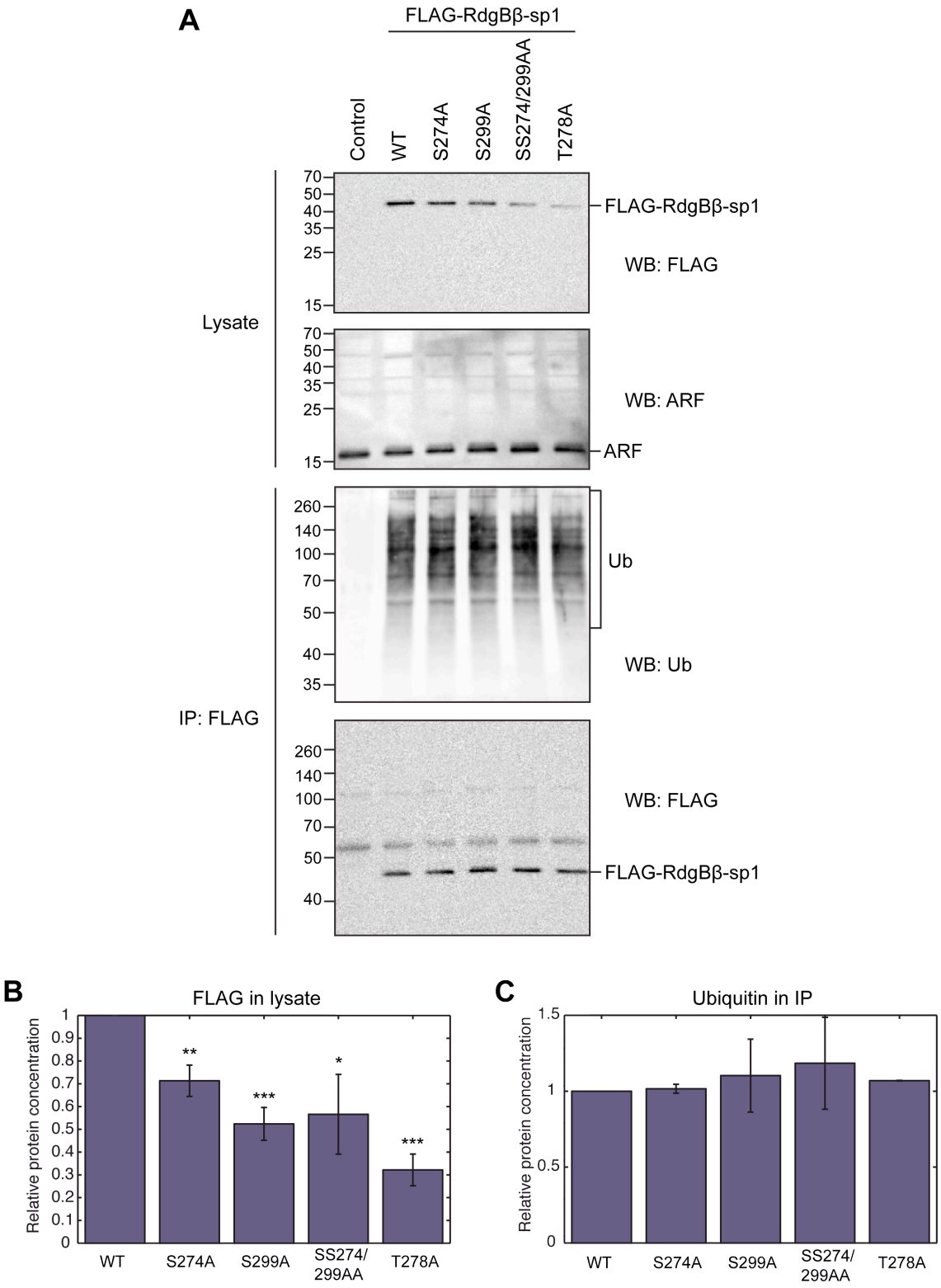
A
FLAG-RdgBβ-sp1
Control
WT
S274A
S299A
SS274/299AA
T278A
Lysate
IP: FLAG
FLAG-RdgBβ-sp1
WB: FLAG
WB: ARF
ARF
Ub
WB: Ub
WB: FLAG
FLAG-RdgBβ-sp1
B
FLAG in lysate
Relative protein concentration
C
Ubiquitin in IP
Relative protein concentration
WT
S274A
S299A
SS274/
299AA
T278A

3.5: A search for RdgBβ-sp1-interacting partners uncovers 14-3-3

Although mutation of the C-terminal phosphorylation sites to alanine did not affect the ubiquitination of RdgBβ-sp1, mutation of Ser299 did reduce the stability of the protein and increase turnover rate. This indicates that the ability for this residue to be phosphorylated is required for protection of RdgBβ-sp1 from degradation. Phosphorylation commonly regulates protein function by altering protein-protein interactions. Furthermore, knowledge of a protein's interaction partners could provide an indication of the protein's function.

I first determined that RdgBβ-sp1 binds neither to itself to form homo-oligomers (Figure 3.6), nor to PITPα nor PITPβ (Figure 3.7). The sequence of human RdgBβ-sp1 (Accession no.: Q9UKF7), was scanned using the cell signalling interaction prediction program, Scansite (Obenauer et al., 2003), at high stringency, and was also uploaded to the PhosphoMotif Finder tool at the Human Protein Reference database (Amanchy et al., 2007). Both indicated that the region surrounding the phosphorylated Ser299 is a consensus site for binding of 14-3-3 proteins, specifically the mode I consensus 14-3-3 binding sequence, RSXpSXP (where pS is the phosphorylated serine residue) (Yaffe et al., 1997); the Ser299 sequence is RKKpSAP (see Figure 3.4). Although not identified by either program, the sequence surrounding the phosphorylated Ser274 is RSAPSpSAP, also remarkably similar to the mode I consensus sequence for 14-3-3 binding. 14-3-3 proteins have been shown to bind two tandem sites on a single target protein resulting in strong 'bidentate' binding (Yaffe et al., 1997; Kostelecky et al., 2009). Ser274 and Ser299 could therefore form two such 14-3-3-binding sites on RdgBβ-sp1.

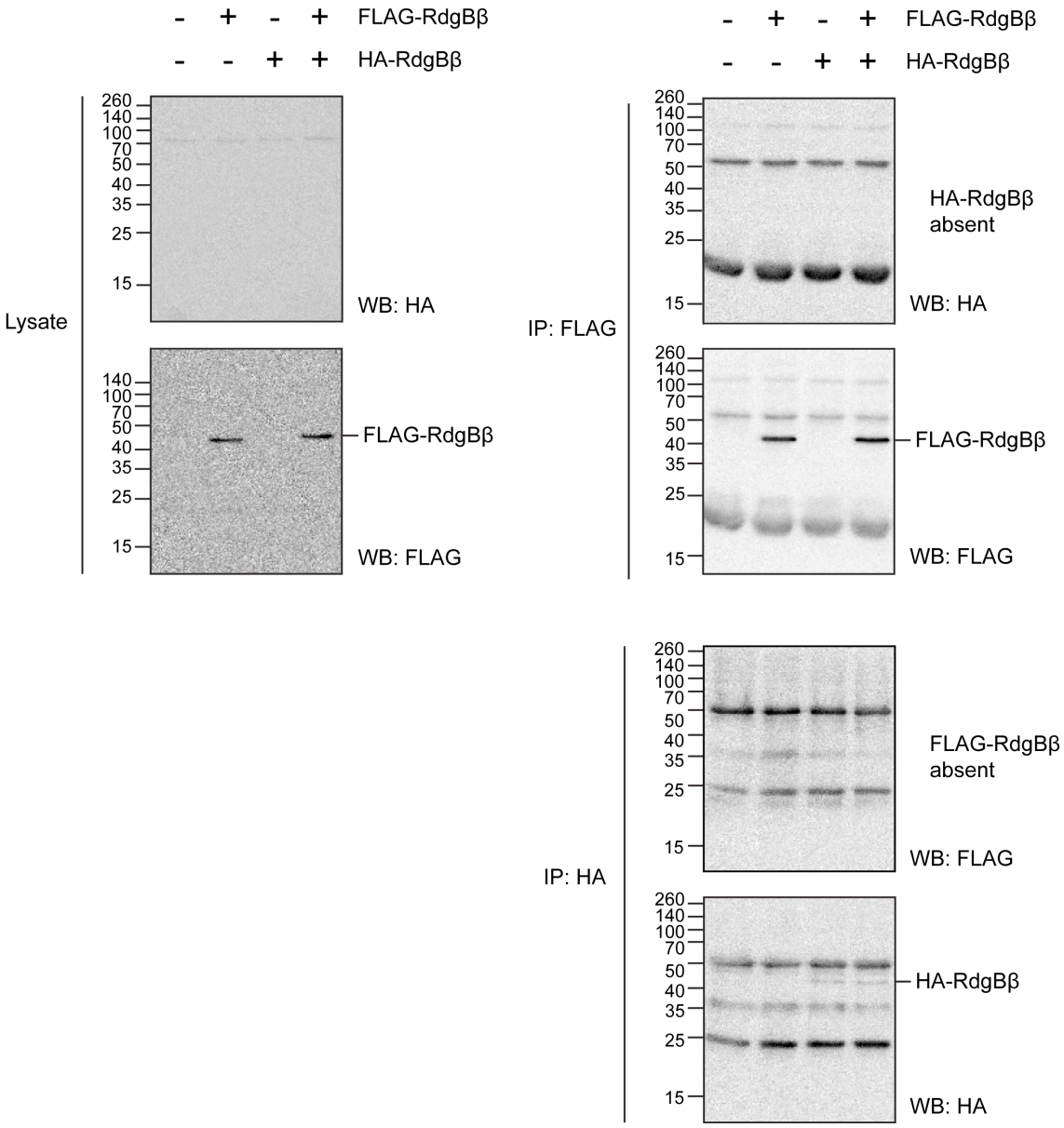

Figure 3.6: RdgBβ-sp1 does not form homo-oligomers

COS-7 cells were transfected with a plasmid containing FLAG-RdgBβ-sp1, HA-RdgBβ-sp1 or both constructs. The fusion proteins were immunoprecipitated using their FLAG- or HA-tag, and subjected to western blotting against the other tag (anti-HA or anti-FLAG (DDK) antibodies, respectively). Despite low HA-RdgBβ-sp1 expression, this fusion protein can be seen in the HA-immunoprecipitate. Membranes were re-probed for the immunoprecipitated protein. The HA-RdgBβ-sp1 fusion protein was not present in the FLAG-RdgBβ-sp1 immunoprecipitate, and vice versa. The experiment was repeated with RdgBβ-sp2 fusion proteins but the protein expression was too low even to be seen in the immunoprecipitate.

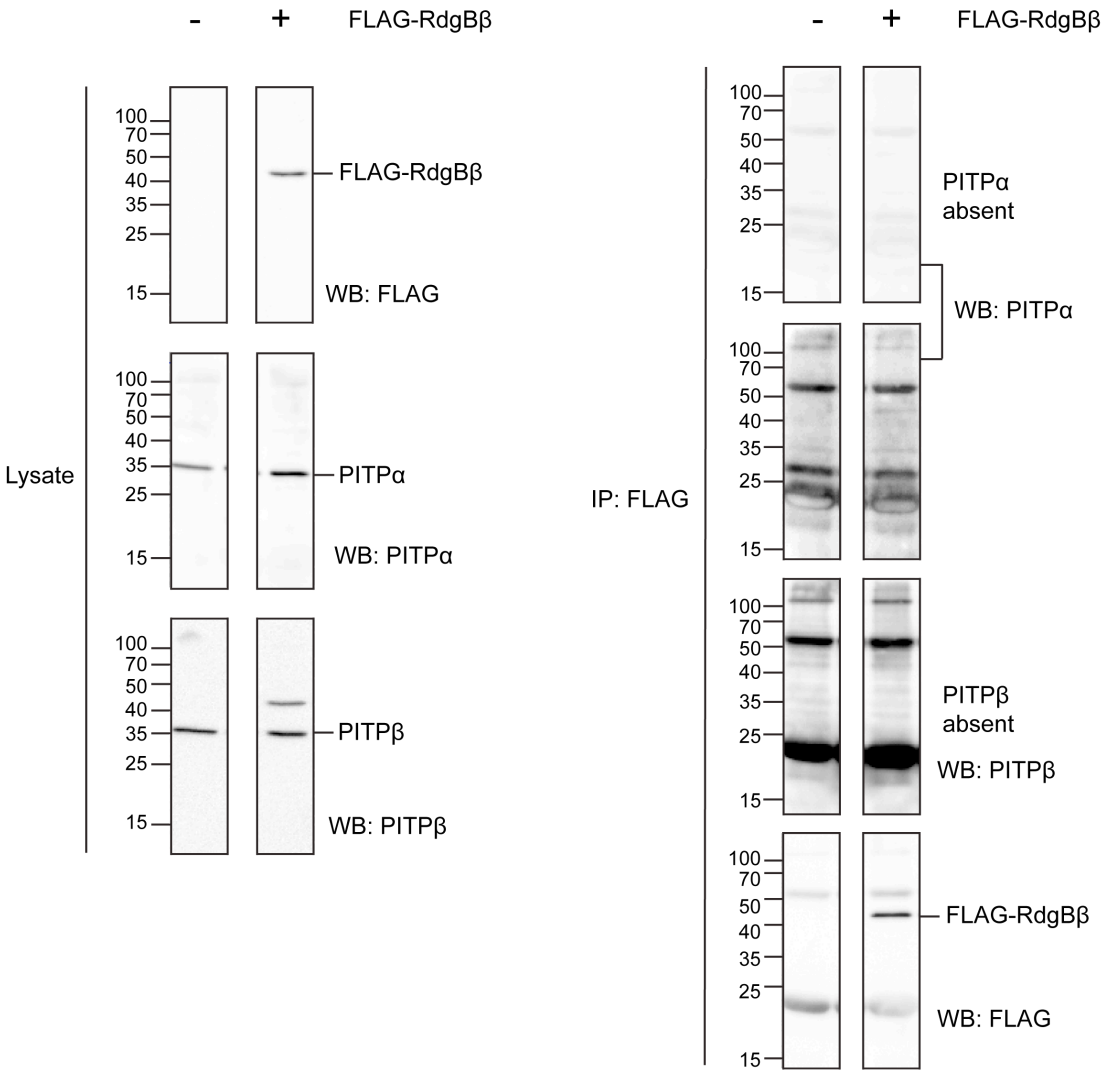

Figure 3.7: RdgBβ interacts with neither PITPα nor PITPβ

COS-7 cells were transfected with a plasmid containing FLAG-RdgBβ-sp1 or empty control plasmid. FLAG-RdgBβ-sp1 was immunoprecipitated using its FLAG-tag. The immunoprecipitate was run on an SDS-PAGE gel and subjected to western blotting using anti-PITPα antibody #674 or anti-PITPβ antibody #1C1. The membranes were stripped and re-probed using anti-FLAG antibody DDK to confirm the presence of FLAG-RdgBβ in the immunoprecipitate. (Only one re-probed membrane shown.)

To examine whether RdgBβ-sp1 binds endogenous 14-3-3 proteins, COS-7 cells were transfected with the pcDNA3.1 empty control vector or pcDNA3.1-FLAG-RdgBβ-sp1 (Figure 3.8). RdgBβ was immunoprecipitated using its FLAG tag, and the immunoprecipitate separated by SDS-PAGE. The proteins were transferred to PVDF membrane and subjected to western blotting using the pan 14-3-3 antibody, which recognises all isoforms of 14-3-3 (Figure 3.8, fifth panel). Endogenous 14-3-3 is clearly present in the FLAG-RdgBβ-immunoprecipitate. An identical membrane was subjected to far western blotting by incubating the membrane with recombinant 14-3-3 protein to look for a direct interaction between RdgBβ-sp1 and 14-3-3 (Figure 3.8, fourth panel). Recombinant 14-3-3 proteins bound to RdgBβ-sp1 in the far western blot. Both membranes were stripped and re-probed to confirm the presence of FLAG-RdgBβ in the immunoprecipitate (Figure 3.8, sixth panel). Taken together, this indicates that RdgBβ-sp1 interacts with 14-3-3, and that this interaction is direct. In this experiment, the amount of serum in the growth media was 0%, 1.5% or 10% FCS, as indicated; 14-3-3 associated with RdgBβ irrespective of this variation.

Since 14-3-3 ordinarily binds phosphorylated serine or threonine motifs, I reasoned that 14-3-3 would be unable to bind to recombinant RdgBβ-sp1, expressed in *E. coli*. The recombinant proteins RdgBβ-sp1, -sp2 and truncated sp1 (1-263 aa), when separated by SDS-PAGE and transferred to PVDF membrane, were not found to bind to the recombinant 14-3-3 in the far western blot (Figure 3.9). The recombinant 14-3-3 clearly only binds the RdgBβ-sp1 expressed in COS-7 cells which has had the opportunity to be phosphorylated, not to recombinant RdgBβ-sp1 lacking the phosphorylation nor RdgBβ-sp2 or -sp1 (1-263) which lack the consensus 14-3-3 binding sites.

(Facing page) Figure 3.8: RdgBβ-sp1 interacts with 14-3-3

COS-7 cells were transfected with empty vector or a plasmid containing the FLAG-RdgBβ-sp1 sequence, 42 hrs prior to the experiment. 18 hrs later, the media were aspirated from all plates and replaced with fresh DMEM containing 0%, 1.5% or 10% FCS (with L-glutamine, penicillin and streptomycin) for 24 hrs as indicated. On the day of the experiment the cells were harvested, FLAG-RdgBβ was immunoprecipitated using its FLAG tag, and the immunoprecipitates subjected to SDS-PAGE and western blotting (*fifth panel*) and far western blotting using 14-3-3-DIG recombinant proteins (*fourth panel*). Membranes were stripped and re-probed using anti-FLAG antibody (DDK) (only one shown) (*sixth panel*). 12 µg of each lysate was run together on separate western blots (*upper three panels*); 3 µg lysate run alongside immunoprecipitates (*lower three panels*).

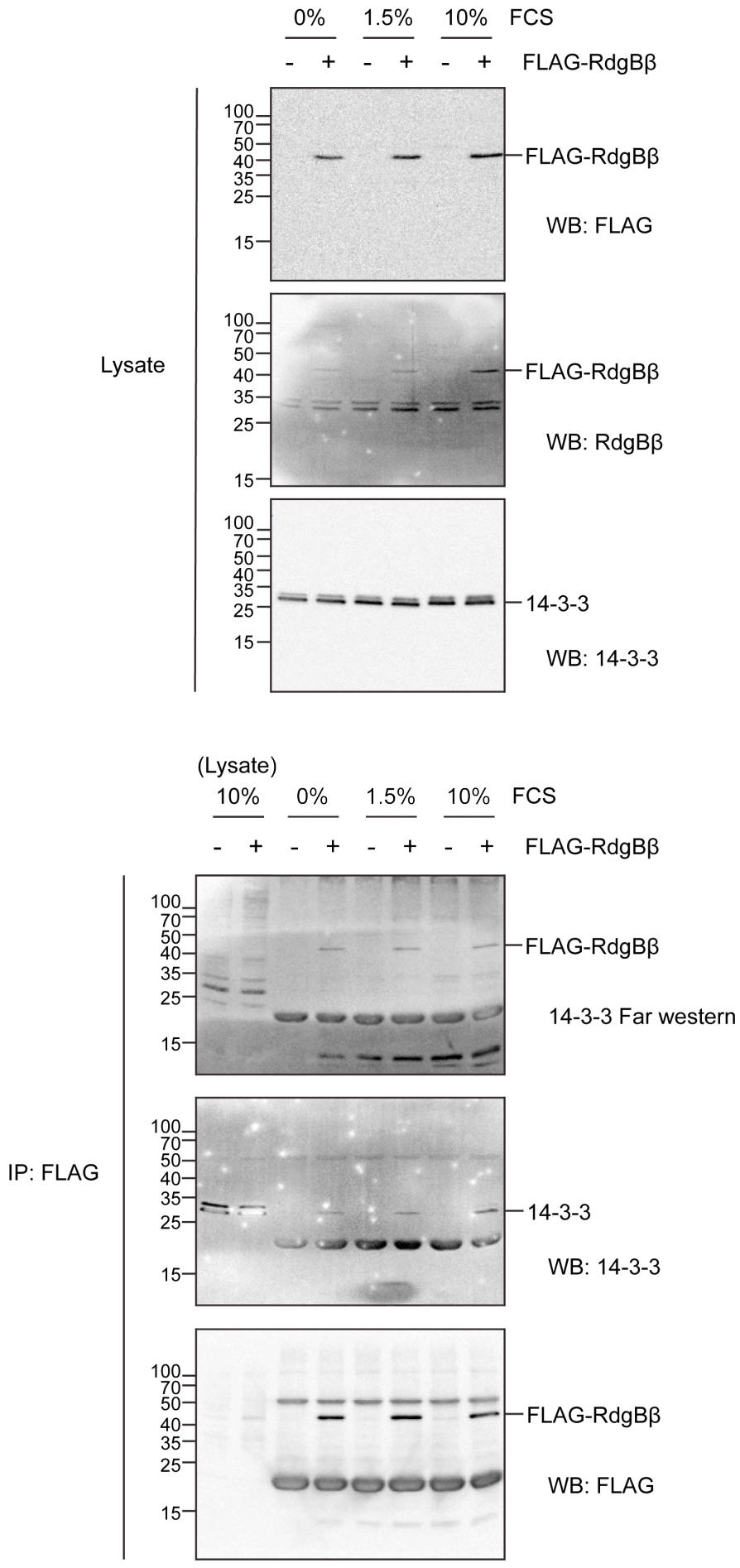
0%
1.5%
10%
FCS
- + - + - +
FLAG-RdgBβ
Lysate
100
70
50
40
35
25
15
FLAG-RdgBβ
WB: FLAG
FLAG-RdgBβ
WB: RdgBβ
14-3-3
WB: 14-3-3
(Lysate)
10%
0%
1.5%
10%
FCS
- + - + - + - +
FLAG-RdgBβ
IP: FLAG
FLAG-RdgBβ
14-3-3 Far western
14-3-3
WB: 14-3-3
FLAG-RdgBβ
WB: FLAG

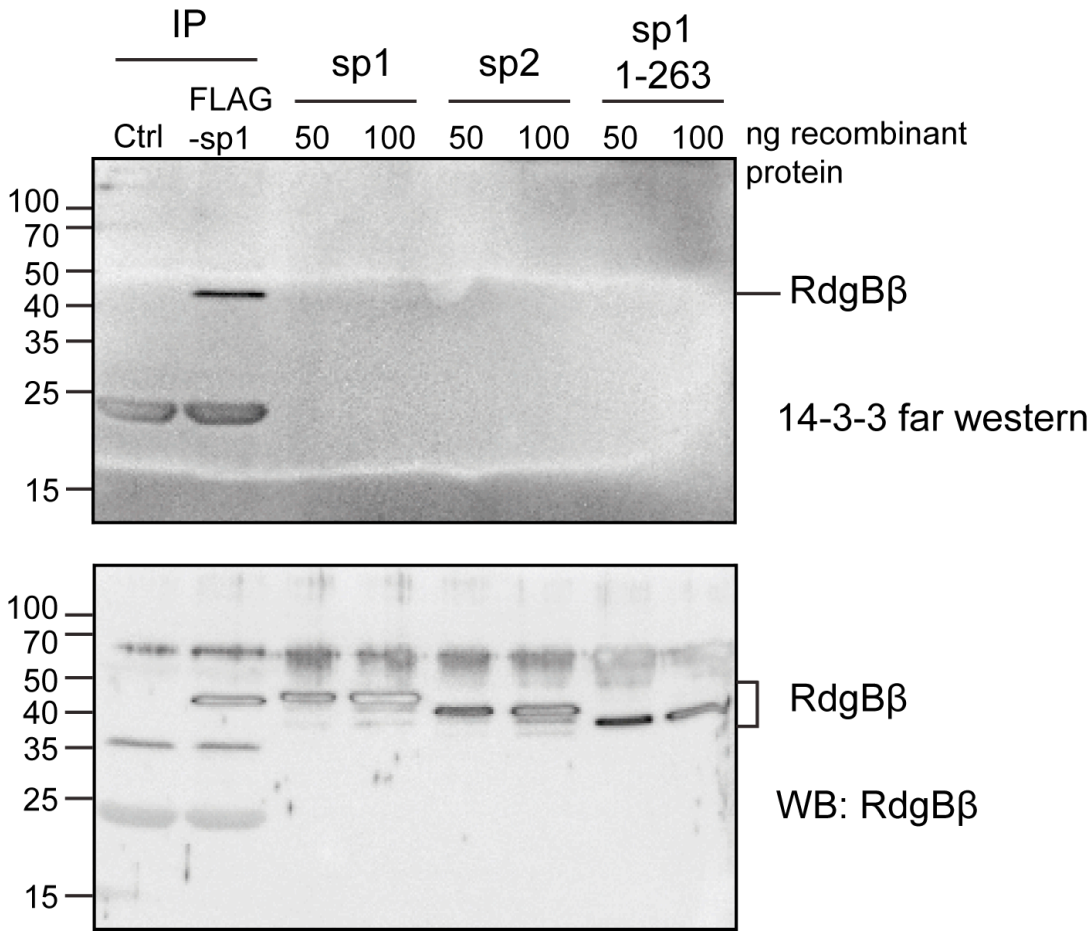

Figure 3.9: Unmodified recombinant RdgBβ does not interact with 14-3-3

FLAG-RdgBβ-sp1 was immunoprecipitated from cells expressing the FLAG-fusion protein, and loaded onto an SDS-PAGE gel alongside recombinant RdgBβ-sp1, -sp2, and truncated sp1 (1-263) (50 and 100 ng). The separated proteins were transferred to PVDF membrane and subjected to far western blotting using 14-3-3-DIG recombinant proteins (*upper panel*), stripped and re-probed by western blotting technique using the anti-RdgBβ antibody #101 (*lower panel*) .

3.6: C-terminal phosphorylation mutants are defective in 14-3-3 binding

Since phosphorylated Ser299 lies in a consensus site for binding to 14-3-3, and since phosphorylated Ser274 might lie in a degenerate 14-3-3-binding motif, the FLAG-RdgBβ-sp1 point mutants S274A, T278A, and S299A, together with the double mutant, SS274/299AA, were examined for binding to 14-3-3. Mutation of either Ser274 or Ser299 abolished binding to 14-3-3 (Figure 3.10). Although Thr278 is not predicted to bind 14-3-3, a considerable loss of 14-3-3-binding is observed for the T278A mutant (~90%).

(Facing page) Figure 3.10: RdgBβ-sp1 C-terminal phosphorylation mutants are defective in 14-3-3 binding

(A) COS-7 cells were transfected with pcDNA3.1 empty vector control, FLAG-RdgBβ-sp1 WT, S274A, S299A, SS274/299AA or T278A. Two days later, the lysates were harvested, FLAG fusion proteins immunoprecipitated via their FLAG tag and subjected to western blotting for 14-3-3. The membrane was stripped and re-probed for FLAG-RdgBβ in the immunoprecipitate (DDK). (B) Quantification of the amount of 14-3-3 present in the immunoprecipitate adjusted for the amount of FLAG-RdgBβ immunoprecipitated (*n*=1).

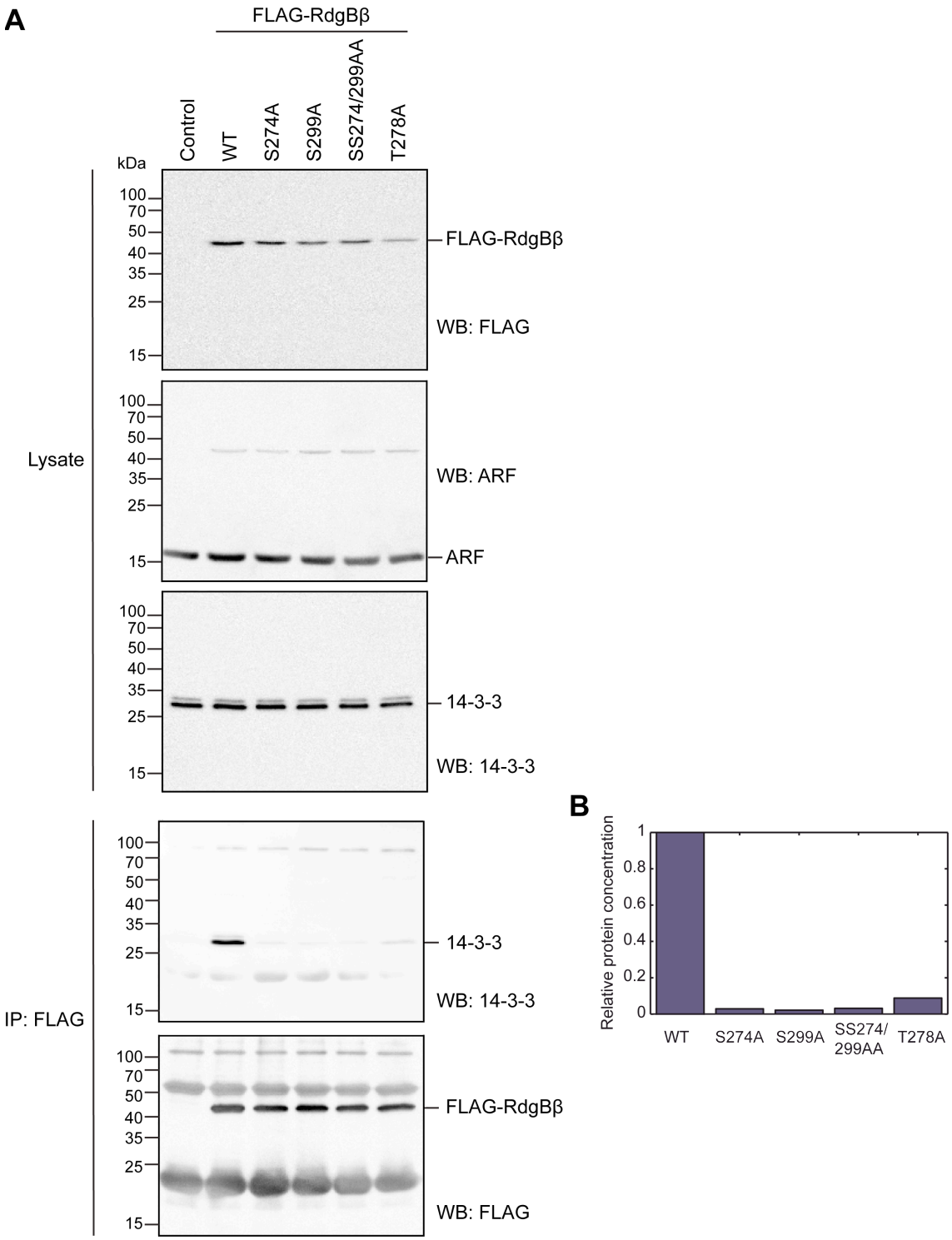
A
FLAG-RdgBβ
Control
WT
S274A
S299A
SS274/299AA
T278A
kDa
100
70
50
40
35
25
15
FLAG-RdgBβ
WB: FLAG
Lysate
WB: ARF
ARF
14-3-3
WB: 14-3-3
IP: FLAG
14-3-3
WB: 14-3-3
FLAG-RdgBβ
WB: FLAG
B
Relative protein concentration
1
0.8
0.6
0.4
0.2
0
WT
S274A
S299A
SS274/
299AA
T278A

3.7: The RdgBβ-sp1-14-3-3 interaction is reduced upon PKC inhibition

Since serine phosphorylation of the RdgBβ-sp1 C-terminus is essential for 14-3-3 binding, the human RdgBβ-sp1 sequence (Q9UKF7) was scanned for kinase recognition sequences using the Scansite program (Obenauer et al., 2003). At high stringency the program indicated that Ser299 lies in a consensus sequence for phosphorylation by PKB, a basophilic Ser/Thr protein kinase. At medium stringency this residue may also lie in a consensus sequence for phosphorylation by PKA. At this stringency, the sequence surrounding Thr278 conforms to the glycogen synthase kinase-3 (GSK-3) recognition sequence. This kinase is a Ser/Thr protein kinase and likely requires prior phosphorylation of Ser274. Thr278 also lies in an ERK1 recognition sequence (a proline-dependent Ser/Thr kinase). Running the program at low stringency indicates Ser274 may be phosphorylated by PKB, GSK-3 or ERK-1; Thr278 may be phosphorylated by p38 MAPK, Cdk5 or Cdc2 (all proline-dependent Ser/Thr kinases); and Ser299 may be phosphorylated by Clk2 kinase (a basophilic Ser/Thr kinase). Indeed, when Huttlin and colleagues analysed and displayed their data online they have accompanied it with broad predictions for the kinases that may be responsible for the particular phosphorylations; they reported Ser274 would be phosphorylated by a kinase of category 'other' (does not fit comfortably as basophilic, acidophilic, nor proline-dependent Ser/Thr kinase), Thr278 would be phosphorylated by a proline-directed kinase, and Ser299 would be phosphorylated by a basophilic kinase (Huttlin et al., 2010). Another group noted that 14-3-3 consensus binding sites show high similarity to the consensus sequences for phosphorylation by the basophilic kinases PKA, PKB and PKC (Yaffe et al., 1997), and I therefore began by looking at the effect of different basophilic kinase inhibitors on 14-3-3 binding by FLAG-RdgBβ-sp1.

PKC was not identified as a potential kinase for Ser274, Thr278, nor Ser299, yet only treatment with the inhibitor of PKC, BIM-I, caused a reduction in 14-3-3 binding (Figure 3.11). The amount of 14-3-3 present in the immunoprecipitate was adjusted for the amount of FLAG-RdgBβ present, therefore the same amount of FLAG-RdgBβ binds half the amount of 14-3-3 in the presence of BIM-I, compared with the untreated cells (0.55 ±0.11 SEM (n=3) p<0.05). In addition, cells treated with BIM-I exhibited a

significantly lower expression of FLAG-RdgBβ-sp1 in the lysates (0.49 ±0.06 SEM (n=4) p<0.001) (Figure 3.11 B, left panel).

PKB is activated by PI(3,4,5)P_3 produced by PI3K, and therefore the activity of PKB can be blocked by the PI3K inhibitor, LY294002. The use of this compound, however, did not have a significant effect on FLAG-RdgBβ-sp1 protein expression or 14-3-3 binding (Figure 3.11 B). Inhibition of PKA with H89 resulted in an increase in both FLAG-RdgBβ-sp1 expression (1.48 ±0.16 SEM (n=4) p<0.05) and 14-3-3 binding (1.60 ±0.17 SEM (n=3) p<0.05) (Figure 3.11 B).

Phorbol esters, such as phorbol 12-myristate 13-acetate (PMA), are analogues of DAG and potent activators of PKC. PMA and DAG stimulate PKC activity by increasing the affinity of the enzyme for Ca^{2+} and phospholipids, promoting translocation of the enzyme to the membrane. Ultimately, PKC activity is terminated by dephosphorylation, which the active conformation is more sensitive to than the inactive form, and degradation ('down-regulation'). Different PKC isozymes appear to be subject to different rates of down-regulation: >90% of the type II conventional PKC isozyme (PKCβ) was found to be lost from RBL-2H3 cells after only 5 min treatment with 20 nM PMA, whereas degradation of the type III isozyme (PKCα) is slower - a significant degradation was only observed after 10-30 min PMA treatment (Huang et al., 1989). PKC activity was reduced by >96% in neonatal rat cardiac ventricular myocytes which had been treated with 1 μM PMA (Rogers et al., 1990). I therefore reasoned that 16 hrs 100 nM PMA treatment would remove PKC isozymes and mimic the effect of PKC inhibition on 14-3-3 binding by RdgBβ.

However, PMA more than doubled the expression of FLAG-RdgBβ in the lysate (2.27 ±0.40 SEM (n=4) p<0.05), and mildly increased binding to 14-3-3 (1.30 ± 0.03 SEM (n=3) p<0.001) (Figure 3.11). A time course of the effect of PMA treatment on FLAG-RdgBβ-sp1 protein expression indicates that maximal protein expression is reached by 4 hrs PMA treatment (Figure 3.12).

(Facing page) Figure 3.11: PKC inhibition suppresses the RdgBβ-14-3-3 interaction

(A) COS-7 cells transfected with pcDNA3.1-FLAG-RdgBβ-sp1 were treated with 10 μM H89, 10 μM LY294002 (LY), 5 μM BIM-I or 100 nM PMA, for 16 hrs prior to cell harvest. FLAG-RdgBβ was immunoprecipitated via its FLAG tag and subjected to western blotting for 14-3-3. The membrane was then stripped and re-probed using anti-FLAG antibody (DDK). Similarly, lysate was subjected to western blotting for FLAG, and the membrane stripped and re-probed for ARF1 loading control. (B) Protein bands were quantified using densitometry. Error bars are SEM. *P* values are calculated relative to unstimulated FLAG-RdgBβ-sp1: * $p<0.05$, *** $p<0.001$. *Left panel*: Amount of FLAG-RdgBβ present in the lysate adjusted for ARF1 loading control, $n=4$. *Right panel*: Amount of 14-3-3 present in the immunoprecipitate adjusted for the amount of FLAG-RdgBβ immunoprecipitated, $n=3$.

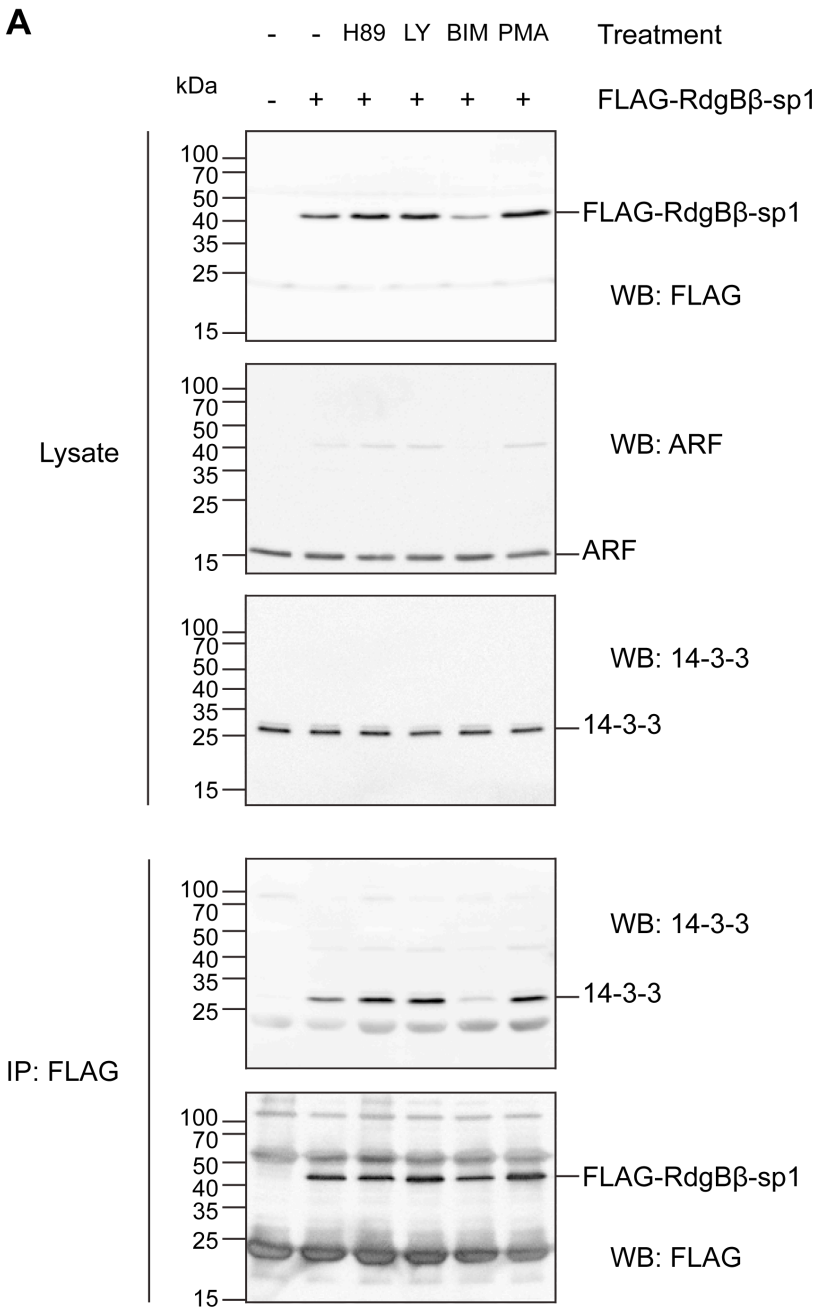
A
- - H89 LY BIM PMA Treatment
kDa
- + + + + + FLAG-RdgBβ-sp1
100
70
50
40
35
25
15
FLAG-RdgBβ-sp1
WB: FLAG
Lysate
WB: ARF
ARF
WB: 14-3-3
14-3-3
IP: FLAG
WB: 14-3-3
14-3-3
FLAG-RdgBβ-sp1
WB: FLAG

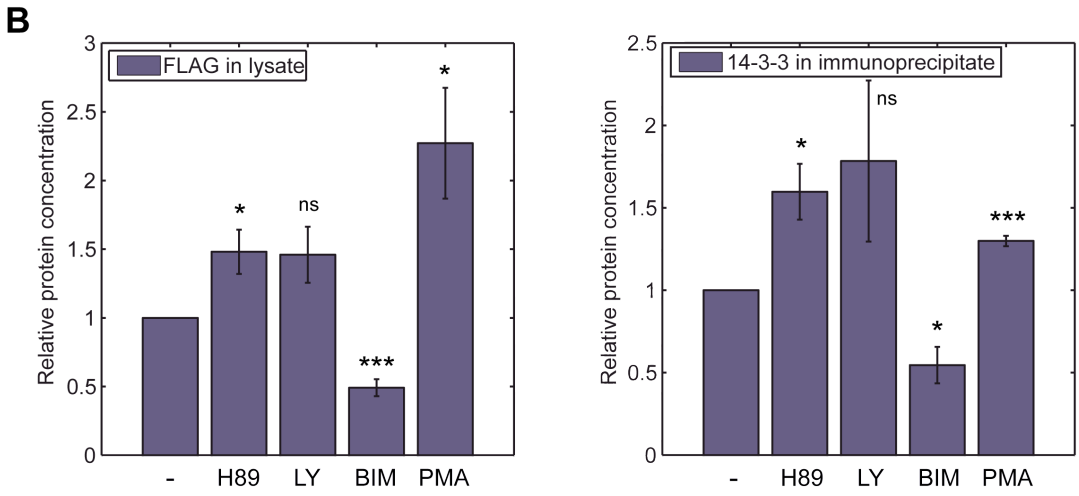
B
FLAG in lysate
Relative protein concentration
3
2.5
2
1.5
1
0.5
0
*
ns
***
*
- H89 LY BIM PMA
14-3-3 in immunoprecipitate
Relative protein concentration
2.5
2
1.5
1
0.5
0
*
ns
*
***
- H89 LY BIM PMA

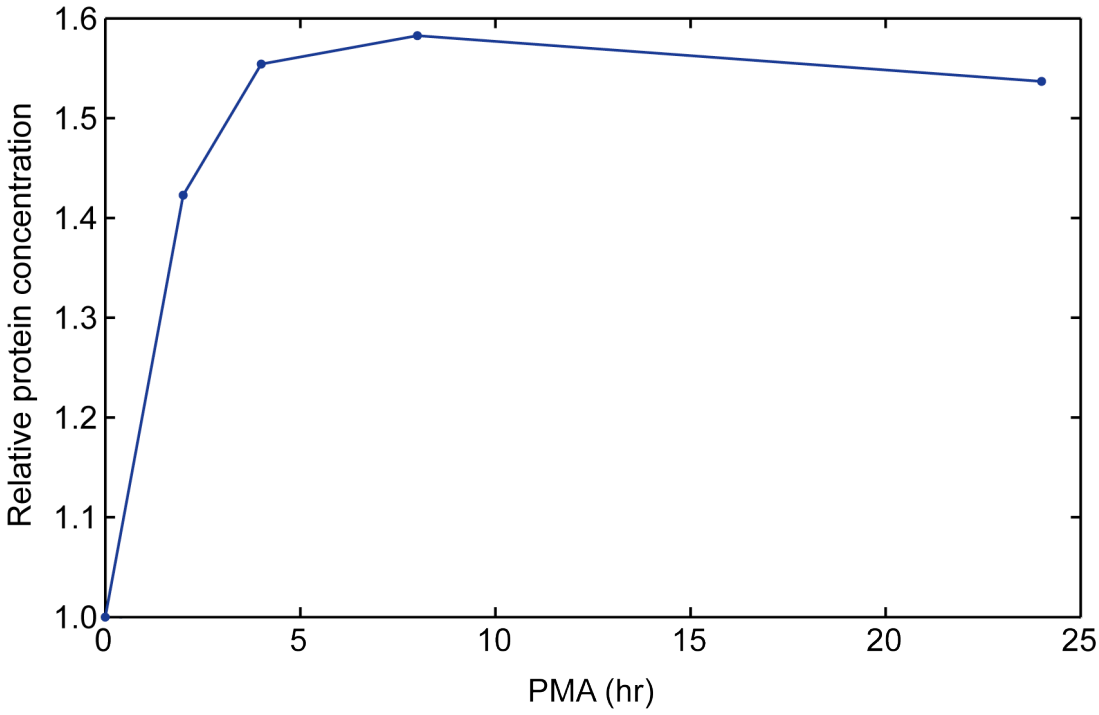

Figure 3.12: Time course of FLAG-RdgBβ stabilisation by PMA

COS-7 cells were seeded into 35 mm cell culture dishes at a concentration of 2.0 x 10^5 cells.mL^{-1}, and transfected with control empty vector or pcDNA3.1-FLAG-RdgBβ-sp1 6 hrs later. 40 hrs after transfection, cells were treated with or without 100 nM PMA and harvested in RIPA buffer on ice at the end of the appropriate time period. 50 µg of each lysate was subjected to western blotting using anti-FLAG antibody (DDK) for FLAG-RdgBβ-sp1 expression. Western blot protein bands were quantified using AIDA software. A single background value for each blot was subtracted from the intensity value for each band, and the protein concentration at each time point expressed relative to its zero time control. The data depicted in the graph are concentration of FLAG-RdgBβ-sp1 expression treated with PMA minus untreated control samples at each time point.

3.8: Towards reconstitution of the RdgBβ-14-3-3 interaction *in vitro*

To begin to understand the significance of the RdgBβ-14-3-3 interaction, reconstitution of the complex was attempted *in vitro*. Firstly, recombinant RdgBβ-sp1 required phosphorylation. Since PKC is the only kinase that I have identified as being required for the serine phosphorylation and 14-3-3 interaction, I set up an *in vitro* assay for phosphorylation of RdgBβ-sp1 by PKC. Since RdgBβ-sp2 doesn't contain the Ser274 and Ser299 sites, I used this protein as a negative control. Recombinant proteins were incubated without or with PKC purified from rat brain (predominantly the conventional PKC isoforms, α, β1, β2 and γ), alongside PS, DAG (for full activation of PKC) and Mg-ATP (phosphate donor). I used a 14-3-3 far western blot as a read-out for phosphorylation of RdgBβ-sp1. However, no 14-3-3 binding to RdgBβ-sp1 (or -sp2) was observed after incubation of RdgBβ with PKC (Figure 3.13, top panel). RdgBβ-sp1 and -sp2 appeared no different in terms of molecular weight when the far western blot was re-probed using the anti-RdgBβ antibody #101 (Figure 3.13, middle panel), or on a Coomassie-stained gel (Figure 3.13, bottom panel).

Since phosphorylation by PKC was insufficient to promote 14-3-3-binding, I exposed the RdgBβ-sp1 recombinant protein to HL60 cells with their full complement of Ser/Thr protein kinases to see whether this would promote phosphorylation of RdgBβ. I incubated 120 μg His-RdgBβ-sp1 or His-PITPα as a negative control, with washed HL60 cells and 0.4 iu.mL^{-1} SLO to acutely permeabilise the cells and allow entry of the recombinant PITPs. I buffered the calcium in the experiment at either physiological Ca^{2+} (100 nM, pCa7) or high (10 μM, pCa5), and added 100 nM PMA to one each of the pCa5 tubes. The assay was incubated at 37°c for 20 min prior to incubation with nickel beads for re-capture of the recombinant proteins via their His tags. The nickel beads were next either crudely washed and proteins eluted in SDS-PAGE sample buffer (Figure 3.14 A), or washed in increasing concentrations of salt to purify the re-captured proteins, before elution from the beads in imidazole and buffer exchange to PIPES/salts buffer (Figure 3.14 B).

Both sets of samples were subjected to western blotting using the pan 14-3-3 antibody. In the unpurified samples, a clear band is seen in both the RdgBβ and PITPα lanes at 28

kDa, likely to be binding of non-specific proteins. Above this, at ~30 kDa, is a band faintly present in the pCa7 RdgBβ lane and stronger in both pCa5 RdgBβ lanes, likely to correspond to 14-3-3 (Figure 3.14 A). This 30 kDa band is absent from the PITPα lanes and is no longer detectable after protein purification (Figure 3.14 B), whereas the 28 kDa nonspecific protein band is. The pan 14-3-3 antibody detects a protein at 48 kDa in all three RdgBβ lanes, which survives purification but is absent from the PITPα lanes. Crude staining of the membrane with indian ink is shown in the lower panels of Figure 3.14: RdgBβ and PITPα can clearly be identified and the bands indicate approximately equal loading.

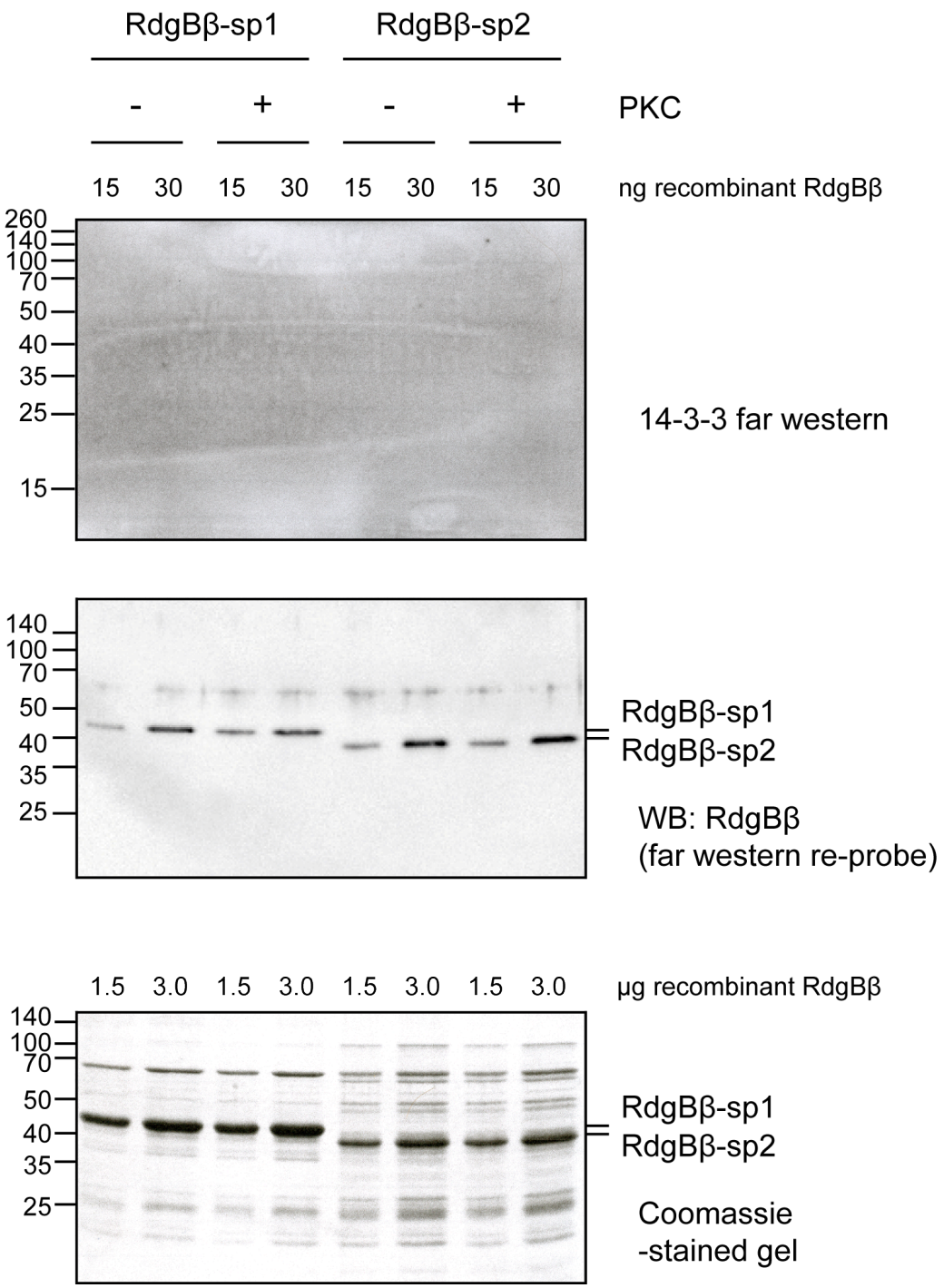

Figure 3.13: Phosphorylation of RdgBβ by PKC *in vitro*

Recombinant RdgBβ-sp1 or -sp2 (10 µg per reaction) was incubated -/+ rat brain PKC for 1 hr at 30°c. The reaction was quenched with SDS-PAGE sample buffer, and 15 & 30 ng or 1.5 & 3.0 µg protein were subjected to SDS-PAGE for far western blotting with recombinant 14-3-3 proteins (*top panel*) or Coomassie-staining (*bottom panel*), respectively. The far western blot was stripped and re-probed using the anti-RdgBβ antibody #101 by western blotting (*middle panel*).

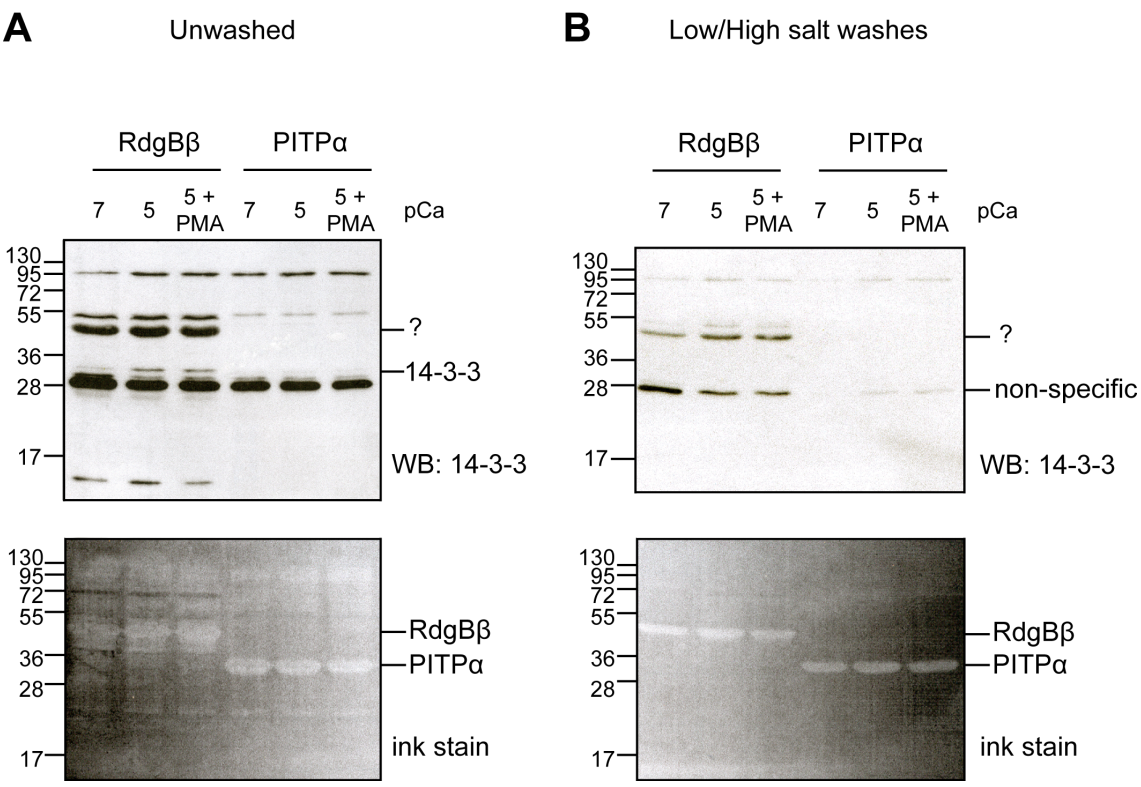

Figure 3.14: Reconstitution of the RdgBβ-14-3-3 complex *in vitro*

Unlabelled HL60 cells were incubated for 20 min at 37°c with recombinant His-RdgBβ-sp1 or His-PITPα, at pCa7 (100 nM Ca^{2+}) or pCa5 (10 µM Ca^{2+}), with 100 nM PMA, where indicated, and 0.4 iu.mL^{-1} SLO to permeabilise the cells and allow PITP entry. Supernatants were then incubated with nickel beads for re-capture of the His-tagged proteins. (A) Captured proteins eluted directly from the nickel beads in SDS-PAGE sample buffer. (B) Nickel beads (in mini-spin columns) washed twice in low, then high, salt buffer, prior to elution of captured proteins in imidazole. The buffer was exchanged to PIPES/salts pH 6.8 before SDS-PAGE sample buffer addition. All samples (A & B) were boiled 10 min at 95°c before SDS-PAGE and transfer to PVDF membrane. *Top panels*: membranes subjected to western blotting using the pan 14-3-3 antibody. *Bottom panels*: membranes stained with indian ink.

3.9: Discussion

I have demonstrated that the long, unique C-terminus of RdgBβ-sp1 is disordered and contains two PEST sequences, often found in proteins subject to rapid turnover in cells. RdgBβ is ubiquitinated, phosphorylated and directly interacts with 14-3-3 via two phosphorylated serine residues in its C-terminus. I have shown that RdgBβ-sp1 is rapidly degraded in cells, more so when the protein is mutated at Ser299. Lastly, I have presented evidence suggesting that protein kinase C phosphorylates RdgBβ-sp1 at one or both of the serine residues to facilitate 14-3-3 binding: PKC is necessary but not sufficient to promote 14-3-3 binding.

3.9.1: Phosphorylation of RdgBβ-sp1 by PKC

Two phosphorylated residues in the RdgBβ-sp1 C-terminus, Ser274 and Ser299, mediate the interaction between RdgBβ and 14-3-3. Treatment of COS-7 cells expressing FLAG-RdgBβ-sp1 with the PKC inhibitor, BIM-I, resulted in reduced 14-3-3 binding: the amount of 14-3-3 found in the FLAG-RdgBβ-immunoprecipitate from cells treated with BIM-I was approximately half that seen in untreated cells, relative to the same amount of FLAG-RdgBβ-sp1 immunoprecipitated. This implies that PKC is responsible for one or both of the phosphorylations enabling 14-3-3-binding. The fact that some 14-3-3-binding remains implicates at least one other kinase in facilitating 14-3-3-binding; indeed, in the *in vitro* assay, phosphorylation of RdgBβ-sp1 by PKC alone failed to promote an interaction between RdgBβ and 14-3-3.

In addition to reduced 14-3-3 binding, the amount of FLAG-RdgBβ-sp1 present in the COS-7 lysate is reduced by half upon PKC inhibition, compared to the untreated control. As the C-terminus of RdgBβ-sp1 is disordered and susceptible to protease digestion, binding of 14-3-3 to the C-terminus could protect the protein from degradation. This is supported by the observation that the RdgBβ-sp1 S299A mutant, unable to bind 14-3-3, is degraded more rapidly than the wild-type protein: the concentration of the wild-type protein was observed to half within 5 hrs, whereas for the S299A mutant, this time was reduced to 2 hrs. The reduced FLAG-RdgBβ-sp1

expression upon PKC inhibition therefore reflects a reduced protein stability in the absence of 14-3-3-binding.

There are ten PKC isozymes, which can be grouped into the categories, conventional, novel and atypical, based on their sequence and activation profile. BIM-I has been reported to inhibit the conventional isozymes, α and β1 (but not β2 or γ), the novel isozymes, δ and ε (but not η or θ), and the atypical isozyme, ζ (but not ι (human) or λ (mouse) (Martiny-Baron et al., 1993). By contrast, rat brain PKC, which failed to promote an interaction between RdgBβ-sp1 and 14-3-3, is predominantly the conventional isoforms, α, β1, β2, and γ. This could imply that the 14-3-3-binding site is alone mediated by either of the novel isozymes, δ or ε, or the atypical isozyme, ζ.

The use of a single inhibitor for PKC makes it difficult to draw conclusions. In addition to using several different inhibitors for each kinase, it would have been more appropriate to use each inhibitor at multiple concentrations. Chemical inhibitors are rarely specific for one target protein and instead may inhibit other proteins at different concentrations. For example, BIM-I has many reported off-target effects: the manufacturer's documentation warns that it will also inhibit GSK-3 in primary adipocyte lysates (IC_{50}=360 nM) and GSK-3β in immunoprecipitates (IC_{50}=170 nM). In addition it may inhibit PKA at high concentrations (K_i=2 μM), although in my experiments the potential for PKA to be the kinase responsible for facilitating the RdgBβ-sp1-14-3-3 interaction can be excluded due to the use of the PKA inhibitor, H89. BIM-I could also inhibit MAPKAP kinase 1β (IC_{50}=50 nM) and p70 S6 kinase (IC_{50}=100nM) (Alessi, 1997).

3.9.2: The effect of PKA on FLAG-RdgBβ-sp1 expression and the RdgBβ-14-3-3 interaction

Whereas indirect inhibition of PKB had no significant effect on FLAG-RdgBβ-sp1 expression or 14-3-3-binding, use of the PKA inhibitor, H89, increased both FLAG-RdgBβ-sp1 and 14-3-3 presence in the FLAG-RdgBβ-sp1-immunoprecipitate by 48% and 60%, respectively. It would have been interesting to assess the effect of forskolin, which activates adenylyl cyclase to produce cAMP and so activate PKA, on FLAG-

RdgBβ-sp1 expression and the RdgBβ-sp1-14-3-3 - likely it would have reduced both FLAG-RdgBβ-sp1 expression and the interaction between RdgBβ-sp1 and 14-3-3. One explanation for the effect of PKA on FLAG-RdgBβ-sp1 and RdgBβ-sp1-14-3-3 is that PKA phosphorylates 14-3-3 proteins, inhibiting their ability to dimerise and interact with target proteins (Gu et al., 2006). Inhibition of PKA would then provide more 14-3-3 for binding to RdgBβ-sp1, stabilising more of the protein against degradation. The fact that binding to 14-3-3 can be increased by this treatment indicates that not all RdgBβ-sp1 protein molecules are bound to 14-3-3 under basal conditions.

3.9.3: The effect of PMA on FLAG-RdgBβ-sp1 expression and the RdgBβ-14-3-3 interaction

Inhibition of PKC reduces FLAG-RdgBβ-sp1 expression by half, and this reduced amount of RdgBβ protein binds half of the amount of 14-3-3 as the untreated FLAG-RdgBβ-sp1 population. This indicates that PKC activity is required for formation of the RdgBβ-14-3-3 complex, and that binding of 14-3-3 stabilises expression of the RdgBβ-sp1 protein. Prolonged treatment with phorbol esters, such as PMA, promotes PKC down-regulation, and therefore chronic treatment with PMA would be expected to mimic the effect of PKC inhibition. However, the reverse effect was observed: the expression of FLAG-RdgBβ in the lysate more than doubled after 100 nM PMA treatment for 16 hrs, yet the amount of 14-3-3 in the FLAG-RdgBβ-sp1-immunoprecipitate was mildly increased (1.3-fold). As discussed for PKA above, this latter result, though only a small increase, indicates that not all of the RdgBβ-sp1 molecules are bound to 14-3-3.

Whereas BIM-I inhibits PKC consistently throughout the 16 hrs treatment, PMA strongly activates PKC at first and only down-regulates it later. Early in the treatment, PKC might phosphorylate RdgBβ-sp1 in its C-terminus, promoting 14-3-3 binding and stabilisation of the protein. At later time points, the down-regulation of PKC is irrelevant, since a large pool of stable RdgBβ-sp1 bound to 14-3-3 has accumulated. Only new RdgBβ-sp1 made at the later time points will be affected, as this protein will not be phosphorylated by PKC, and therefore not bound to 14-3-3 and stabilised.

Consistent with this hypothesis, FLAG-RdgBβ-sp1 protein expression reaches a maximal concentration by 4 hrs PMA treatment.

3.9.4: The RdgBβ-sp1 Thr278 residue

The Thr278 residue does not lie in a consensus site for 14-3-3-binding, yet mutation of Thr278 to an alanine residue reduced 14-3-3 binding to RdgBβ-sp1 by ~90%. It may be that phosphorylation of either Ser274 or Ser299 is dependent on prior phosphorylation of Thr278. Alternatively, removal of the Thr278 phosphorylation could affect the local protein structure, making it unfavourable for binding of 14-3-3. Phosphorylated Thr278 might make additional contacts with 14-3-3, or permit the binding of other protein partners, required for the full, stable binding of 14-3-3. Thr278 lies adjacent to a proline residue, a common recognition motif in protein-protein interactions, and phospho-T278 lies in a consensus site for binding the BRCT domain (Rodriguez et al., 2003), PBD domain (Elia et al., 2003a; 2003b), and WW domain (Lu et al., 1999b). It is notable that expression of RdgBβ-sp1 T278A was lower than that observed for S299A, indicative of its instability.

3.9.5: Reconstitution of the RdgBβ-14-3-3 complex *in vitro*

Experiments using recombinant proteins could aid in our understanding of the significance of the RdgBβ-14-3-3 complex *in vivo*. Phosphorylation of recombinant RdgBβ-sp1 by rat brain PKC failed to promote 14-3-3 binding to RdgBβ in a 14-3-3 far western blot. However, exposure of recombinant RdgBβ-sp1 to the intracellular environment of HL60 cells led to endogenous 14-3-3-binding, which was most notable at high Ca^{2+} (10 μM). The addition of PMA to the assay had no effect on 14-3-3-binding. The RdgBβ-14-3-3 association was disrupted by washing with a high salt buffer (525 mM NaCl). High salt disrupts electrostatic, and therefore protein-protein, interactions. Since purified, phosphorylated RdgBβ would be required for analysis of the RdgBβ-14-3-3 complex *in vitro*, recombinant (GST-tagged) 14-3-3 needs to be used along with the HL60 cell-phosphorylated RdgBβ. This will also give a much higher yield of 14-3-3 than would be possible in mammalian cells.

The presence of a 48 kDa band in the pan 14-3-3 blots is peculiar (Figure 3.14, upper panels). Since this band is not observed in FLAG-RdgBβ-sp1-immunoprecipitates from COS-7 cells, and since the band is not present in the PITPα lanes, this protein must be contamination derived from the recombinant His-RdgBβ-sp1 protein preparation.

CHAPTER 4: An interaction between RdgBβ and ATRAP

4.1: Introduction

Two yeast two-hybrid screens have reported an interaction between RdgBβ and the Angiotensin II receptor-associated protein, ATRAP (Rual et al., 2005; Venkatesan et al., 2009). ATRAP interacts with the AT_1R (Daviet et al., 1999; Wang et al., 2002; Lopez-Ilasaca et al., 2003), an association that increases more than 2-fold upon Angiotensin II stimulation (Tanaka et al., 2005; Azuma et al., 2007). Over-expression of ATRAP suppresses inositol phosphate production by PLC in response to Angiotensin II stimulation (Daviet et al., 1999; Lopez-Ilasaca et al., 2003), likely by promoting uncoupling from G_q protein and receptor internalisation (Lopez-Ilasaca et al., 2003; Tanaka et al., 2005; Azuma et al., 2007). CAML has also been identified as a binding partner of ATRAP (Guo et al., 2005), and it appears that this interaction has a distinct, yet related, function to the ability of ATRAP to down-regulate Angiotensin II signalling (Min et al., 2009).

The biochemical property uniting PITPs is their ability to bind and transfer PI, and a role for these proteins in PLC activity has been established (Thomas et al., 1993; Xie et al., 2005; Adachi et al., 2010). PITPs deliver PI to the agonist-sensitive pool at the plasma membrane, making the PI delivered by this protein a more favourable substrate for PI kinases and subsequently PLC (Cunningham et al., 1995). Furthermore, PITPs have also been shown to exert a stimulatory activity on PI kinases (Kauffmann-Zeh et al., 1995; Kular et al., 1997; Panaretou et al., 1997).

Both RdgBβ and ATRAP are highly expressed in the heart and kidney (Daviet et al., 1999; Fullwood et al., 1999; Wang et al., 2002; Takano et al., 2003; Tanaka et al., 2005; Tsurumi et al., 2006; Oppermann et al., 2010). Since ATRAP reduces Angiotensin II-stimulated inositol phosphate production by PLC, and other PITPs have a role in providing the substrate for PLC activity, it seems possible that an interaction between RdgBβ and ATRAP is functionally significant. I therefore begin this part of my study by assessing whether an interaction can be observed between RdgBβ and ATRAP using co-immunoprecipitation experiments. I find that an RdgBβ-ATRAP association is only

observed after stimulation of cells with PMA for 4-16 hrs and can be blocked by inhibition of PKC or protein synthesis. I deduce that RdgBβ interacts with ATRAP via its PITP domain, and despite sharing ~40% identity with the class I PITPs, PITPα and PITPβ, the interaction between ATRAP and the PITP domain is specific to RdgBβ. Candidate ATRAP-binding residues on the RdgBβ PITP domain are proposed. The relationship between Angiotensin II, PLC activity and the RdgBβ-ATRAP interaction is explored.

4.2: RdgBβ does not interact with ATRAP under basal conditions

I first sought to demonstrate an interaction between FLAG-RdgBβ and HA-ATRAP proteins expressed in COS-7 cells. However, initial co-immunoprecipitation experiments failed to confirm an interaction between the two proteins. Some protein-protein interactions are very transient and as a consequence the interacting partners may dissociate during immunoprecipitation. One method that may be used to stabilise protein-protein interactions is to treat cells with cell-permeable cross-linkers prior to cell harvest. In the experiment shown in Figure 4.1 A I have treated the cells with 0.5 mM disuccinimidyl suberate (DSS) before harvesting and immunoprecipitation of HA-ATRAP. HA-ATRAP is clearly seen in the immunoprecipitate, yet no additional protein bands are present in the far right-hand lane of the anti-FLAG blot, indicating an absence of FLAG-RdgBβ-sp1.

The second yeast-two hybrid screen that reported an interaction between RdgBβ and ATRAP, recorded the RdgBβ nucleotide (mRNA) accession number as BC007905 (Venkatesan et al., 2009), which translates to protein AAH07905 and is the sequence of the short splice variant, RdgBβ-sp2. Both splice variants receive coding sequence from exons 1-8 of the *PITPNC1* gene. In addition, a short C-terminus for sp2 is encoded by exon 9. RdgBβ-sp1 receives the sequence for its long C-terminus from exon 10. It is therefore possible that ATRAP interacts with RdgBβ-sp2, not sp1, via the 32 residues coded for by exon 9. To test this hypothesis I used COS-7 cells transiently transfected with empty control vector or pcDNA3-HA-ATRAP, immunoprecipitated HA-ATRAP from the cell lysates using its HA tag and subjected the immunoprecipitate to western

blotting using the anti-RdgBβ polyclonal antibody, #101, which recognises both RdgBβ-sp1 and sp2 (Garner et al., 2011). Neither RdgBβ-sp1 nor -sp2 were found to be present in the HA-ATRAP immunoprecipitate (Figure 4.1 B). However, although the 101 antibody clearly detects the recombinant RdgBβ-sp1 (10-30 ng), endogenous RdgBβ is not detected in the lysates.

4.3: RdgBβ interacts with ATRAP when cells are stimulated with PMA

The 101 antibody recognises the recombinant RdgBβ proteins at quantities of >5 ng (Garner et al., 2011) but not the endogenous proteins in COS-7 cells (Figure 2.3, p. 87; Figure 2.4, p. 105), implies that the protein is expressed at very low amounts. This can be compared to another PITP, PITPβ: the 1C1 antibody used in Figure 3.2 clearly detects the endogenous PITPβ, and detects recombinant protein above 6.2 ng (Morgan et al., 2006). I have demonstrated that FLAG-RdgBβ-sp1 is subject to rapid turnover in COS-7 cells (Figure 3.2), and therefore hypothesised that there may simply not be enough RdgBβ protein present, even with over-expression, to enable an interaction between RdgBβ and ATRAP to be seen. I observed that 16 hr treatment with the phorbol ester PMA more than doubled the expression of FLAG-RdgBβ-sp1 (Figure 3.11) and I therefore questioned whether an interaction between RdgBβ and ATRAP could be observed under these conditions. COS-7 cells were transfected with plasmids encoding FLAG-RdgBβ-sp1 and HA-ATRAP, and half of the plates were treated with 100 nM PMA for 16 hrs prior to cell harvest. HA-ATRAP co-immunoprecipitated with FLAG-RdgBβ-sp1, and vice versa, when cells were treated with PMA (Figure 4.2).

The PMA treatment was performed in normal COS-7 cell culture medium (DMEM containing 10% FCS). Since FCS contains growth factors and is used to promote cell division in culture, I assessed whether the presence of serum affected the RdgBβ-ATRAP interaction. The presence or absence of FCS had no effect: the RdgBβ-ATRAP interaction was still only observed when cells were treated with PMA (Figure 4.3).

(Facing page) Figure 4.1: An RdgBβ-ATRAP interaction is not observed under basal conditions

(A) COS-7 cells were transfected with pcDNA3 empty control vector, pEFPLink-FLAG-RdgBβ-sp1 or pcDNA3-HA-ATRAP plasmids as indicated. Two days after transfection the cells were treated with DSS cross-linker prior to harvest. HA-ATRAP was immunoprecipitated using its HA tag. Eluted proteins were run alongside 9 µg whole cell lysate on an SDS-PAGE gel. Separated proteins were transferred to PVDF membrane and probed with anti-FLAG (polyclonal, OctA) antibody, and re-probed with anti-HA (HA-probe) antibody. The position of the antibody heavy (Ab HC) and light (Ab LC) chains in the immunoprecipitate are indicated. (B) COS-7 cells were transfected with either pcDNA3 empty control vector or pcDNA3-HA-ATRAP plasmid, as indicated. HA-ATRAP was immunoprecipitated using its HA tag, and the eluted proteins run alongside 10 µg whole cell lysate and His-RdgBβ-sp1 recombinant proteins (quantities indicated) on an SDS-PAGE gel. The separated proteins were transferred to PVDF membrane and probed with anti-RdgBβ polyclonal antibody #101, then re-probed with HA-probe antibody.

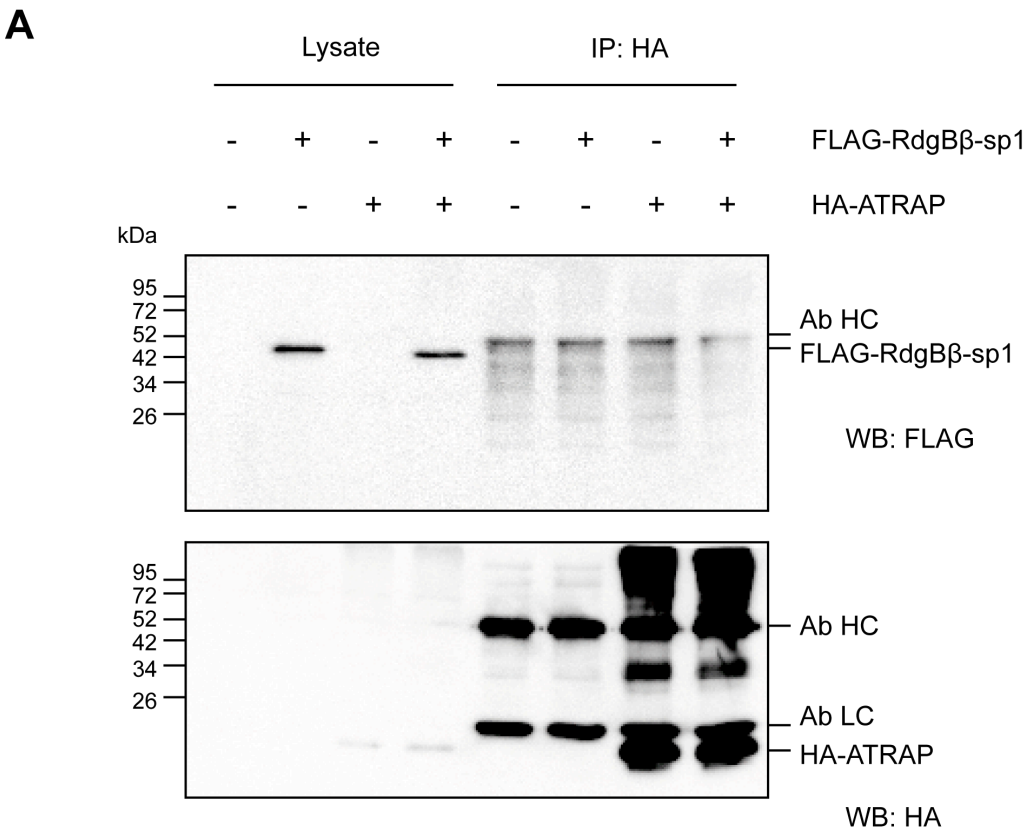
A
Lysate
IP: HA
- + - + - + - +
FLAG-RdgBβ-sp1
- - + + - - + +
HA-ATRAP
kDa
95
72
52
42
34
26
Ab HC
FLAG-RdgBβ-sp1
WB: FLAG
95
72
52
42
34
26
Ab HC
Ab LC
HA-ATRAP
WB: HA

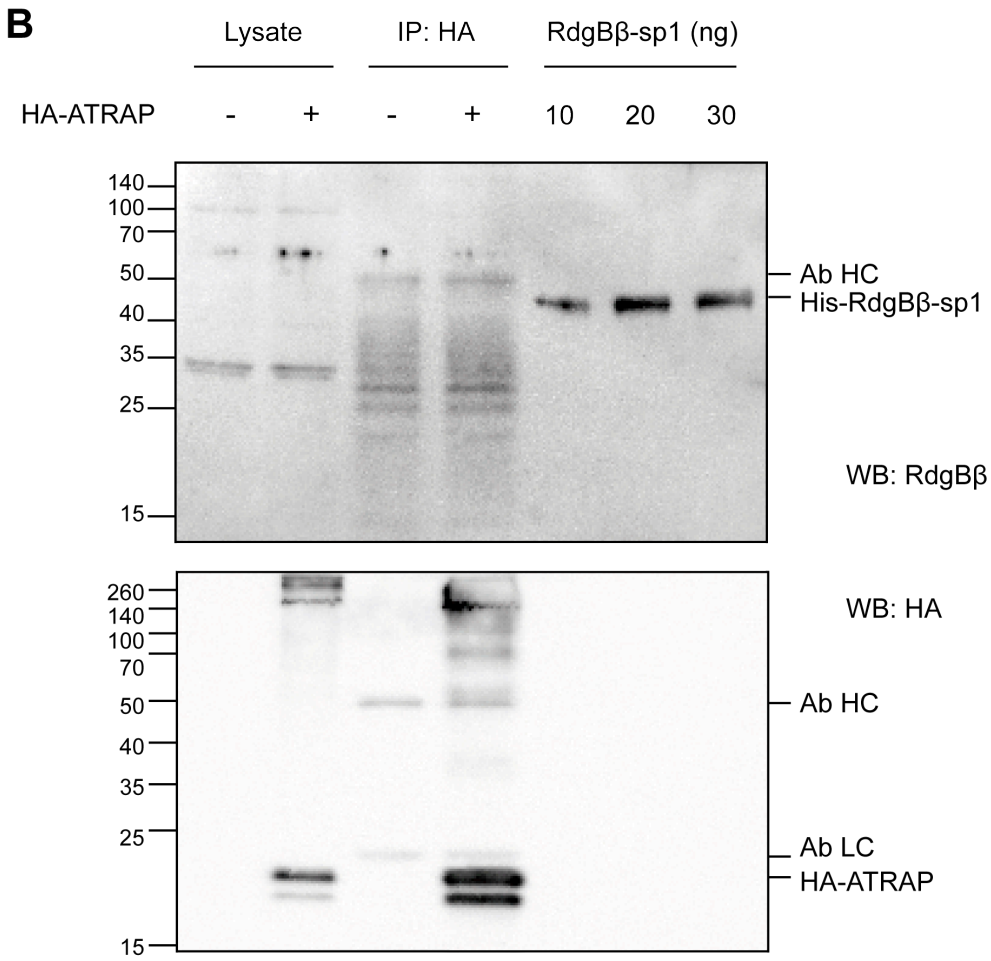
B
Lysate
IP: HA
RdgBβ-sp1 (ng)
HA-ATRAP
- + - +
10 20 30
140
100
70
50
40
35
25
15
Ab HC
His-RdgBβ-sp1
WB: RdgBβ
260
140
100
70
50
40
35
25
15
WB: HA
Ab HC
Ab LC
HA-ATRAP

(Facing page) Figure 4.2: RdgBβ interacts with ATRAP when cells are stimulated with PMA

COS-7 cells were transfected with pcDNA3.1-FLAG-RdgBβ-sp1 with or without pcDNA3-HA-ATRAP co-transfection. Cells were then unstimulated or stimulated with 100 nM PMA for 16 hrs prior to cell harvest and FLAG-immunoprecipitation. Lysates were run on SDS-PAGE gels for western blotting with anti-FLAG (DDK) and anti-HA antibodies (18 µg and 3 µg, respectively). FLAG- and HA-immunoprecipitates were separated by SDS-PAGE and subjected to western blotting using anti-HA and anti-FLAG (DDK) antibodies, respectively. The IP: FLAG membrane was stripped and re-probed for the presence of FLAG in the IP.

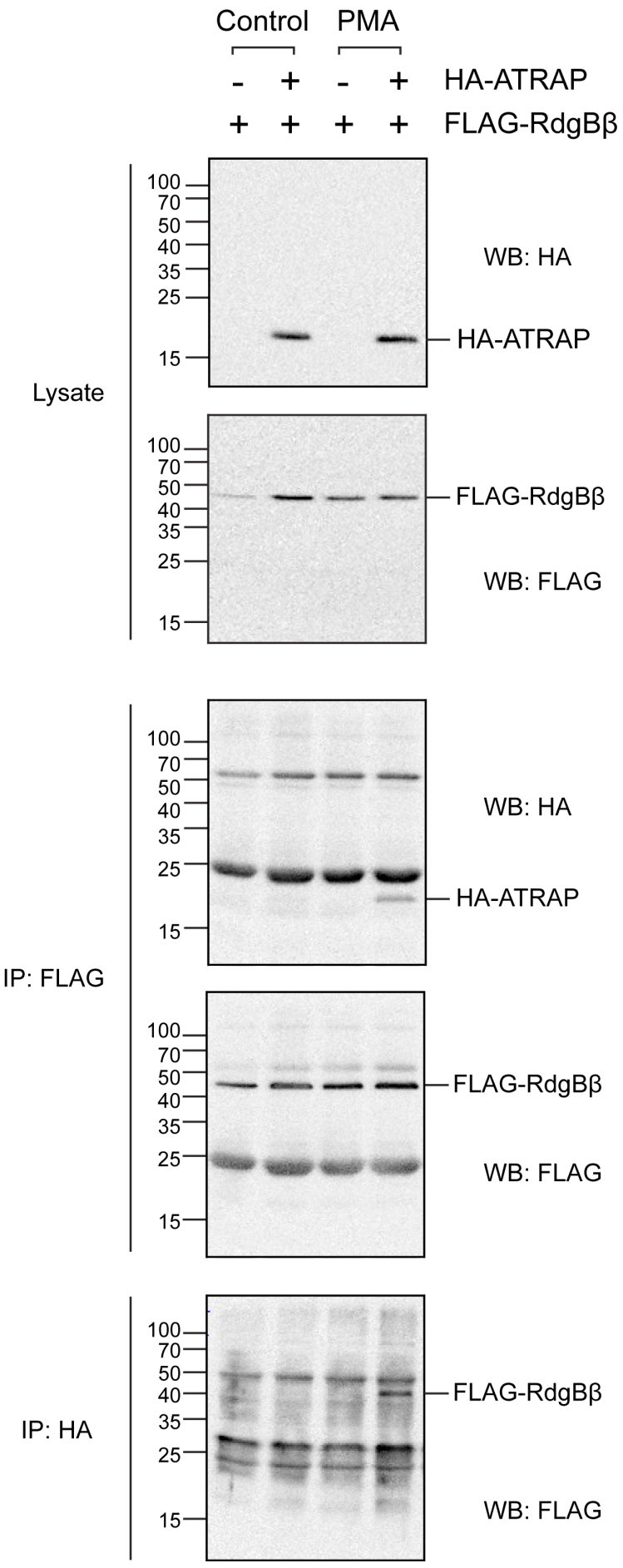
Control
PMA
- + - + HA-ATRAP
+ + + + FLAG-RdgBβ
Lysate
100
70
50
40
35
25
15
WB: HA
HA-ATRAP
FLAG-RdgBβ
WB: FLAG
IP: FLAG
IP: HA

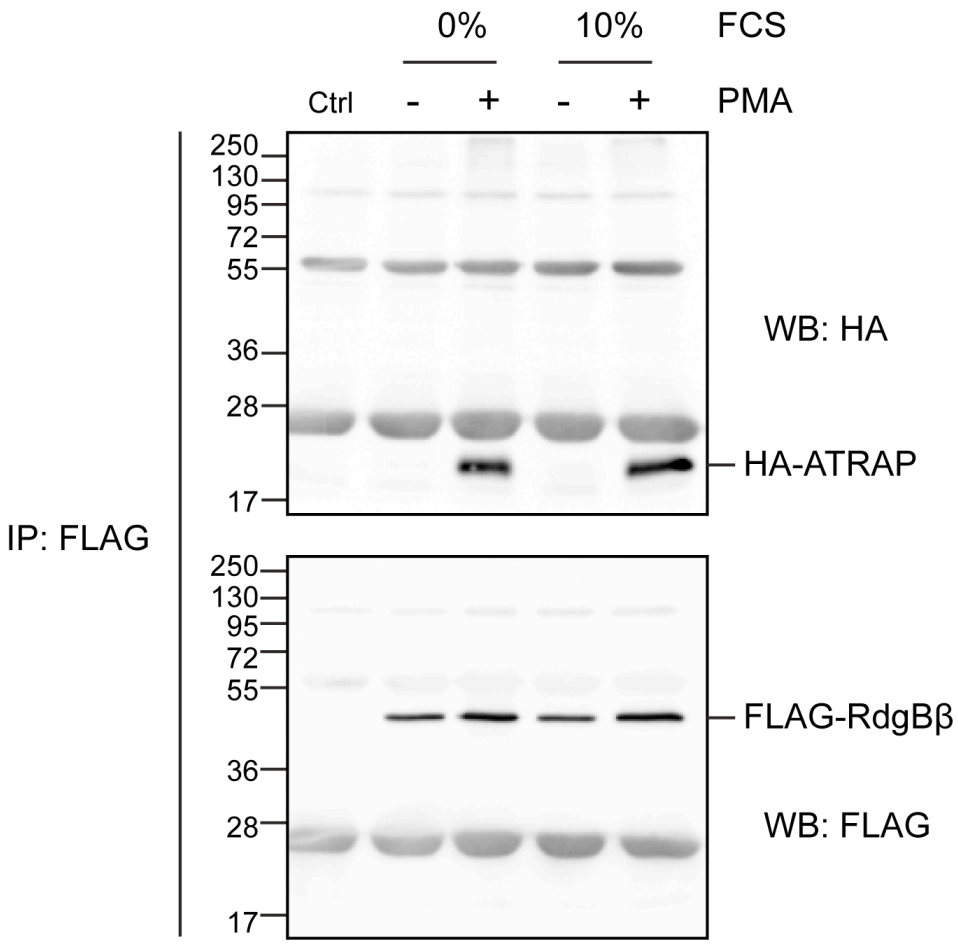

Figure 4.3: The RdgBβ-ATRAP interaction is unaffected by serum in the cell culture medium

COS-7 cells were transfected with pcDNA3.1-FLAG-RdgBβ-sp1 and pcDNA3-HA-ATRAP, or pcDNA3.1 empty control vector. Cells then were treated with or without 100 nM PMA and 10% FCS in the cell culture medium, for 16 hrs prior to cell harvest. RdgBβ was immunoprecipitated using its FLAG tag, and the immunoprecipitates probed by western blotting using anti-HA antibodies. The membrane was stripped and re-probed for the presence of FLAG-RdgBβ in the immunoprecipitate.

4.4: PKC activity and protein synthesis are required for the PMA-induced RdgBβ-ATRAP interaction

Since PMA is an analogue of DAG, PKC is a direct target of PMA. I therefore wanted to find out whether the interaction between RdgBβ and ATRAP was mediated by this kinase by using an inhibitor of PKC, BIM-I. I also reasoned that since maximal FLAG-RdgBβ-sp1 expression is reached by 4 hrs PMA treatment (Figure 3.12), the RdgBβ-ATRAP interaction would also be observed at 4 hrs. Only trace amounts of HA-ATRAP were present in the FLAG-RdgBβ-sp1 immunoprecipitate when cells were treated with both 100 nM PMA and 5 μM BIM-I for 4 hrs prior to harvest, in contrast to 4 hr PMA treatment alone, at which time the interaction between RdgBβ and ATRAP was very clear (Figure 4.4).

I have demonstrated that FLAG-RdgBβ-sp1 expression is reduced by half within 5 hrs of inhibition of protein synthesis using cycloheximide (Figure 3.2). To determine whether the stabilisation of nascent RdgBβ is required before the RdgBβ-ATRAP interaction is observed, I treated cells with 100 $\mu g.mL^{-1}$ cyclohexmide in combination with 100 nM PMA for 4 hrs prior to cell harvest. CHX abolished the PMA-induced RdgBβ-ATRAP interaction, despite the presence of FLAG-RdgBβ in the FLAG-immunoprecipitate (Figure 4.4).

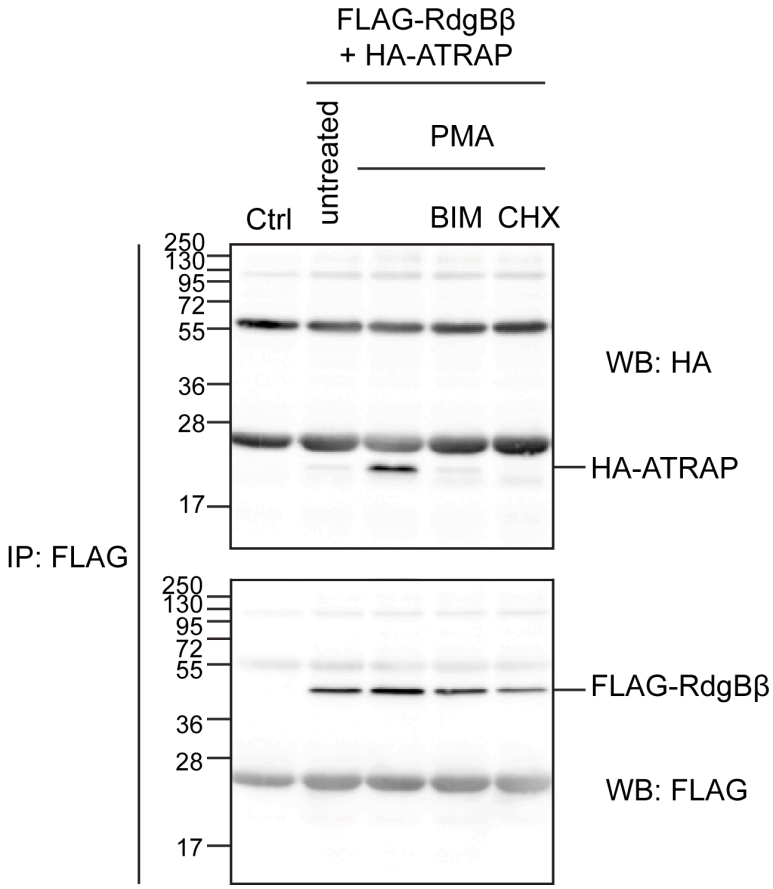

Figure 4.4: PKC and protein synthesis inhibition block the RdgBβ-ATRAP interaction

COS-7 cells were transfected with pcDNA3.1-FLAG-RdgBβ-sp1 and pcDNA3-HA-ATRAP, or pcDNA3.1 empty control vector. Cells were then either untreated, or treated with 100 nM PMA, with or without 5μM BIM-I or 100 μg.mL^{-1} CHX for 4 hr prior to cell harvest as indicated. FLAG-immunoprecipitates were subjected to western blotting using anti-HA antibodies, and the membrane was re-probed to confirm the presence of FLAG-RdgBβ-sp1.

4.5: The PMA-induced RdgBβ-ATRAP interaction and a calcium ionophore

PMA is an analogue of DAG, yet for full activity PKC requires the presence of phosphatidylserine (PS), DAG and Ca^{2+}. High intracellular Ca^{2+} can be recapitulated in a number of ways, one of which is by treatment of cells with a calcium ionophore, such as ionomycin. Ionomycin raises the intracellular Ca^{2+} level by transporting it across the plasma membrane of the cell from the extracellular medium. Although treatment of cells expressing FLAG-RdgBβ-sp1 and HA-ATRAP with ionomycin alone did not induce an interaction between RdgBβ-sp1 and ATRAP, dual treatment with both PMA and ionomycin doubled the amount of HA-ATRAP observed in the FLAG-immunoprecipitate (Figure 4.5). PMA and ionomycin, neither alone nor in conjunction, induced an interaction between RdgBβ-sp1 and ATRAP at 1 hr treatment.

(Facing page) Figure 4.5: The PMA-induced RdgBβ-ATRAP interaction and a Ca^{2+} ionophore

(A) COS-7 cells were transfected with pcDNA3.1-FLAG-RdgBβ-sp1 and pcDNA3-HA-ATRAP, or pcDNA3.1 empty control vector. Cells were treated with 100 nM PMA and/or 5 µM ionomycin ('iono') for 1 or 4 hrs prior to cell harvest. 20µg lysate was loaded in each well of the lysate gels. FLAG-immunoprecipitates were separated by SDS-PAGE and subjected to western blotting using anti-HA antibodies. The membrane was stripped and re-probed using anti-FLAG (DDK) antibodies to confirm the presence of FLAG-RdgBβ in the immunoprecipitate. (B) Protein bands were quantified using AIDA software. The amount of HA-ATRAP in the immunoprecipitate was adjusted for the amount of FLAG-RdgBβ present for each data point. Across each experiment, values were adjusted relative to HA-ATRAP present at 4 hr PMA treatment to enable independent experiments to be combined. Error bars are SEM; n=2. Significance values are calculated relative to untreated control using an unpaired t test: * p<0.05, *** p<0.001.

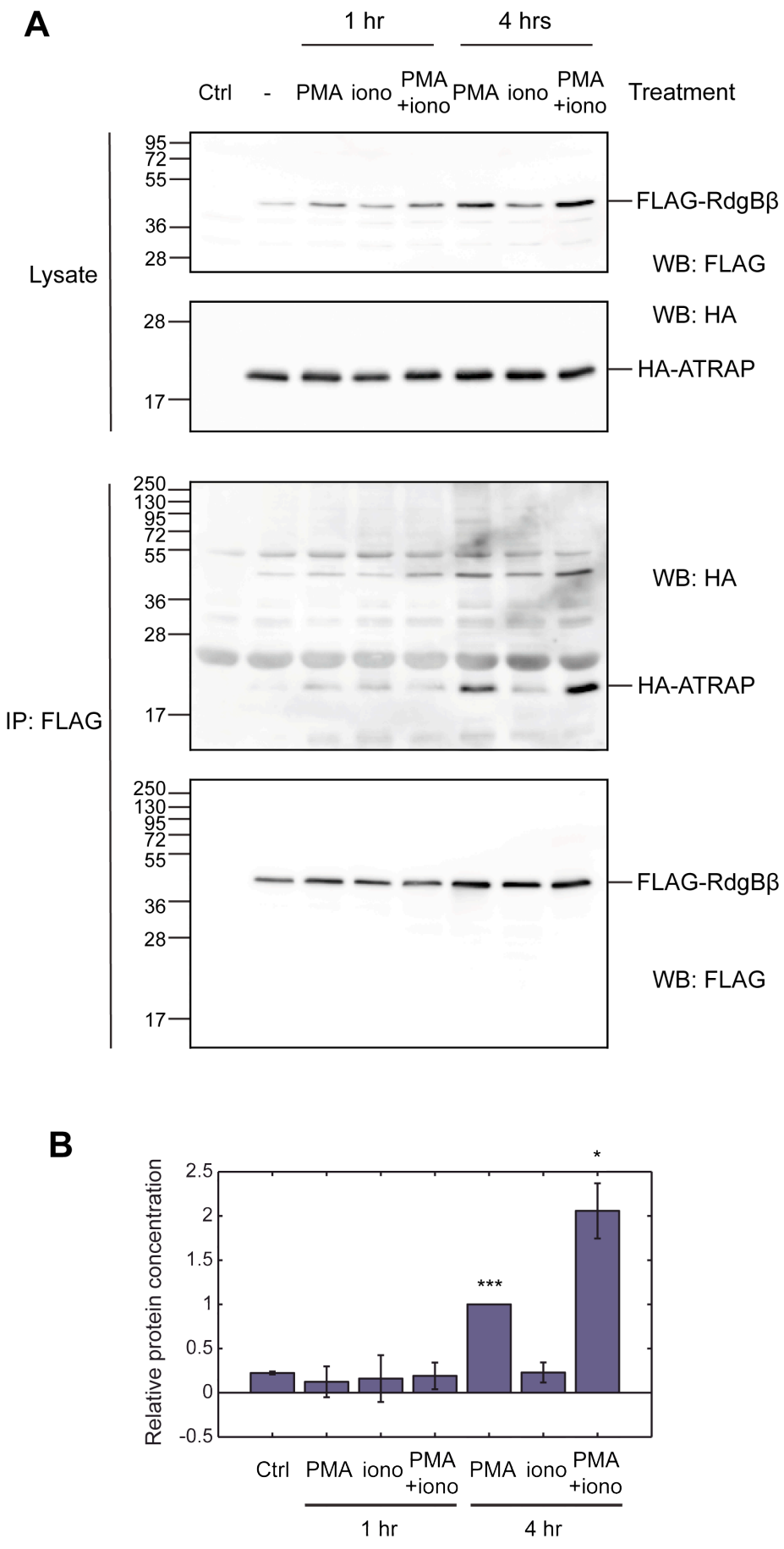
A
1 hr
4 hrs
Ctrl
-
PMA
iono
PMA +iono
PMA
iono
PMA +iono
Treatment
Lysate
95
72
55
36
28
FLAG-RdgBβ
WB: FLAG
28
17
WB: HA
HA-ATRAP
IP: FLAG
250
130
95
72
55
36
28
17
WB: HA
HA-ATRAP
FLAG-RdgBβ
WB: FLAG
B
Relative protein concentration
2.5
2
1.5
1
0.5
0
-0.5
*
***
Ctrl
PMA
iono
PMA +iono
PMA
iono
PMA +iono
1 hr
4 hr

4.6: ATRAP interacts with the PITP domain of RdgBβ-sp1, a domain distinct from the 14-3-3-binding site

Whereas ATRAP only binds to RdgBβ-sp1 when cells are stimulated with PMA for 4-16 hrs, 14-3-3 interacts with RdgBβ-sp1 under both basal and PMA-stimulated conditions. The C-terminus of RdgBβ-sp1 is the region of the protein most likely to serve as a protein-protein interaction domain, since it lacks secondary structure and is therefore flexible. To assess whether ATRAP also binds to the C-terminus of RdgBβ-sp1, a mutation was made in the pcDNA3.1-FLAG-RdgBβ-sp1 plasmid to convert Ile251 into a stop codon so that only residues 1-250 of RdgBβ-sp1 would be translated - in essence completely removing the disordered C-terminus. This mutant was investigated for binding to ATRAP alongside the RdgBβ-sp1 S299A mutant, which is unable to bind 14-3-3.

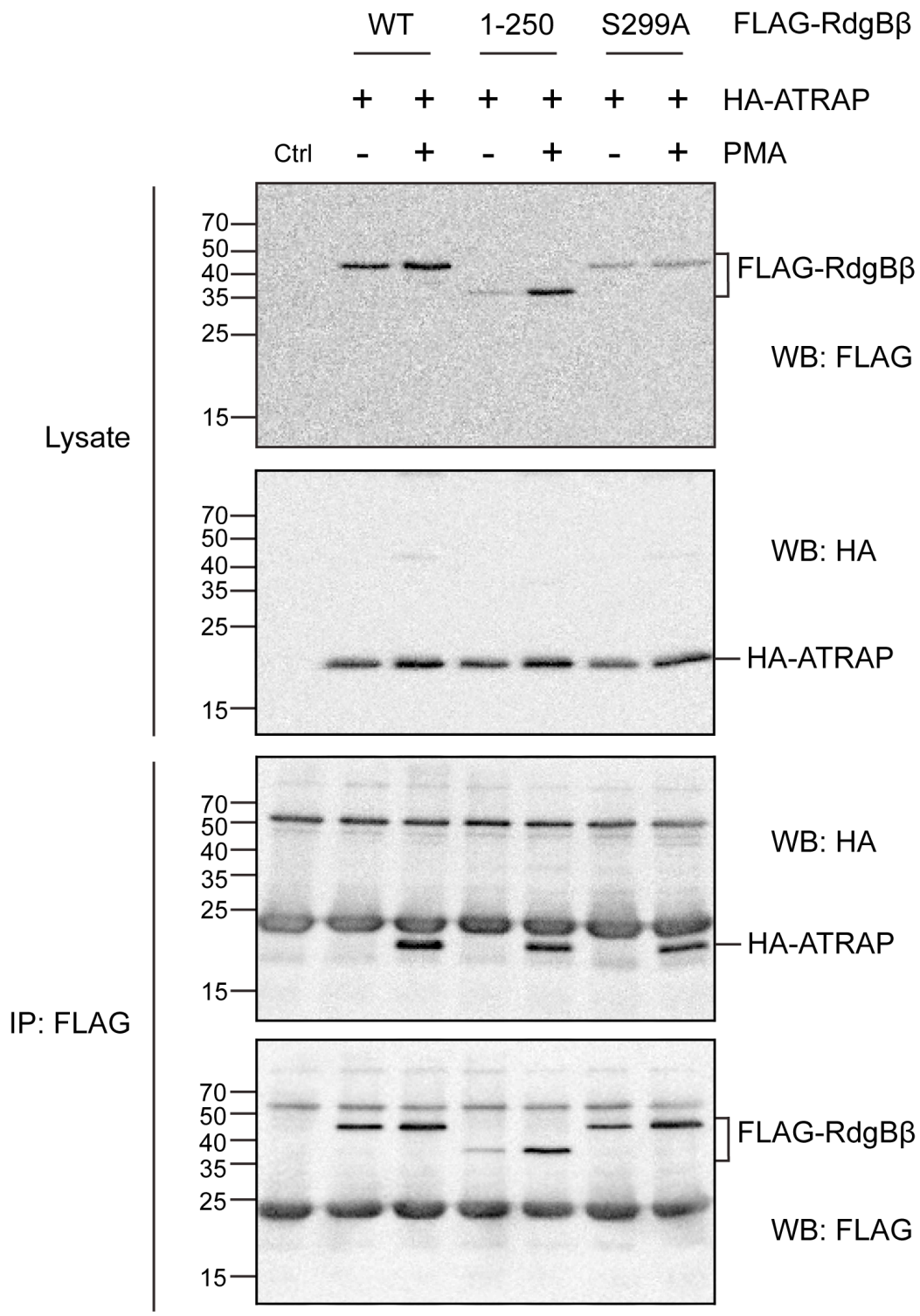

Figure 4.6: ATRAP interacts with the PITP domain of RdgBβ

COS-7 cells were transfected with pcDNA3-HA-ATRAP and either pcDNA3.1-FLAG-RdgBβ-sp1 WT, the truncated 1-250 or S299A mutants. Cells were then treated with or without 100 nM PMA in the cell culture medium for 16 hrs prior to cell harvest. FLAG-immunoprecipitates were subjected to western blotting using anti-HA antibodies alongside cell lysates, and re-probed for FLAG (DDK).

Surprisingly, HA-ATRAP was found in the FLAG-immunoprecipitates of both RdgBβ-sp1 1-251 and S299A mutants (Figure 4.6), indicating that ATRAP binds to the PITP domain of RdgBβ-sp1 rather than to its C-terminus. Like the wild-type protein, the expression of both FLAG-RdgBβ-sp1 1-250 and the S299A mutant appears to increase upon treatment with PMA.

Since ATRAP binds to the PITP domain of RdgBβ-sp1 and 14-3-3 binds to the extended C-terminus, it is possible that both proteins bind simultaneously upon PMA treatment. To investigate this possibility, COS-7 cells were transfected with both pcDNA3.1-FLAG-RdgBβ-sp1 and pcDNA3-HA-ATRAP plasmids and stimulated with PMA prior to cell harvest. HA-ATRAP was immunoprecipitated using its HA tag, and the immunoprecipitate probed using the pan 14-3-3 antibody by western blotting to see whether the FLAG-RdgBβ-sp1 bound to HA-ATRAP came along with 14-3-3. FLAG-RdgBβ-sp1 and HA-ATRAP are clearly present in the right-hand lane of the western blot, where both proteins together with PMA stimulation are present (Figure 4.7 A). The 30 kDa 14-3-3 band is not present, however, but there does seem to be a particularly large quantity of non-specific proteins in the immunoprecipitate. This can be seen more clearly when FLAG-RdgBβ-sp1-immunoprecipitates are run alongside HA-ATRAP immunoprecipitates on a gradient gel and subjected to western blotting using pan 14-3-3 antibody (Figure 4.7 B). The HA-immunoprecipitates have very dark non-specific bands where 14-3-3 would ordinarily be seen in the FLAG-RdgBβ-sp1-immunoprecipitate.

(Facing page) Figure 4.7: Investigating the relationship between RdgBβ-ATRAP and RdgBβ-14-3-3

(A) COS-7 cells expressing either FLAG-RdgBβ-sp1 alone or with HA-ATRAP were treated with 5 μM BIM-I or 100 nM PMA, as indicated, for 16 hrs prior to cell harvest. HA-ATRAP was immunoprecipitated using its HA tag (1.5 μg HA-probe, 20 μL Protein A/G PLUS Agarose), the eluted proteins separated by SDS-PAGE and transferred to PVDF membrane. The HA-immunoprecipitate was probed by western blotting using anti-FLAG monoclonal antibody (DDK), pan 14-3-3 and re-probed with anti-HA monoclonal antibody. (B) FLAG-RdgBβ-sp1-immunoprecipitate (FL) and HA-ATRAP-immunoprecipitate (using one third the amount of antibody for IP, 0.5 μg) from control COS-7 cells (left two lanes) and cells expressing both FLAG-RdgBβ-sp1 and HA-ATRAP, treated with 100 nM PMA prior to cell harvest (right two lanes), have been run alongside one another on a NuPAGE 4-12% gradient gel. The separated proteins were transferred to PVDF membrane and probed by western blotting using the pan 14-3-3 antibody.

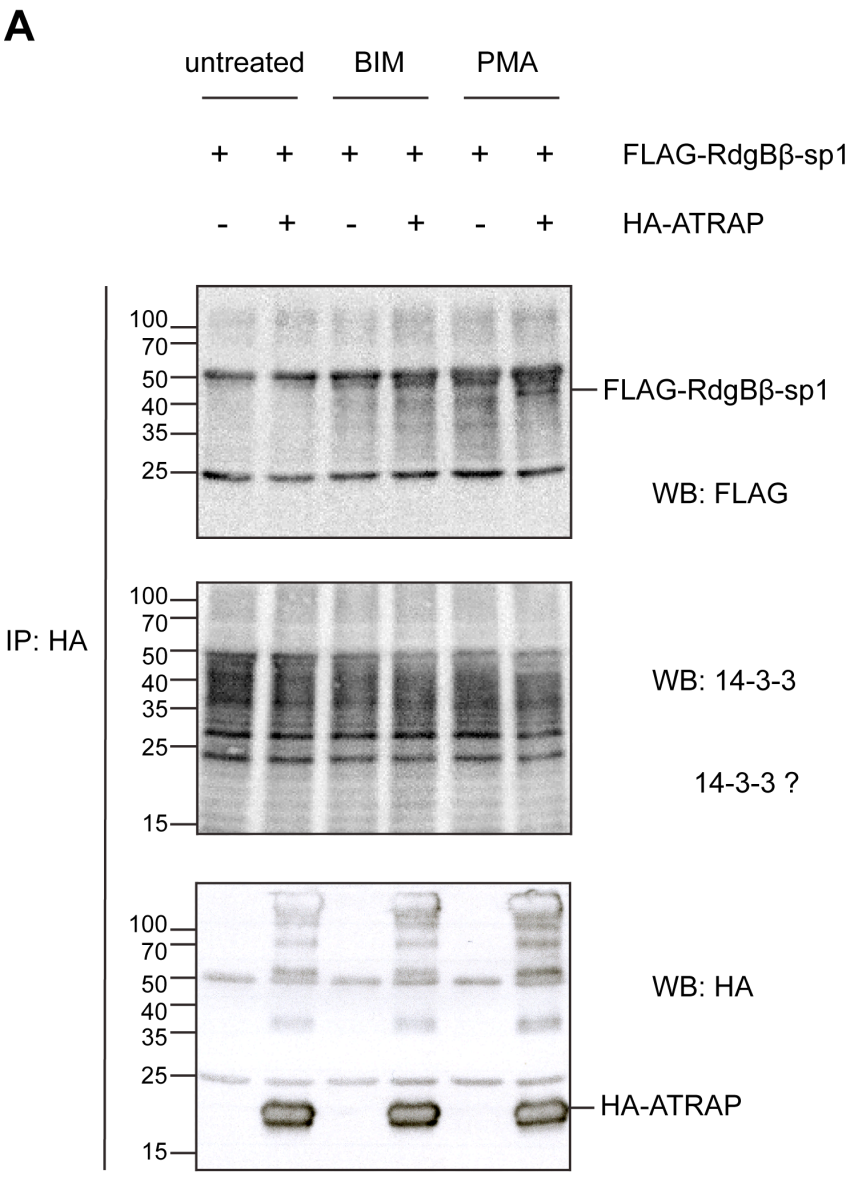
A
untreated
BIM
PMA
+ + + + + +
FLAG-RdgBβ-sp1
- + - + - +
HA-ATRAP
IP: HA
100
70
50
40
35
25
15
FLAG-RdgBβ-sp1
WB: FLAG
WB: 14-3-3
14-3-3 ?
WB: HA
HA-ATRAP

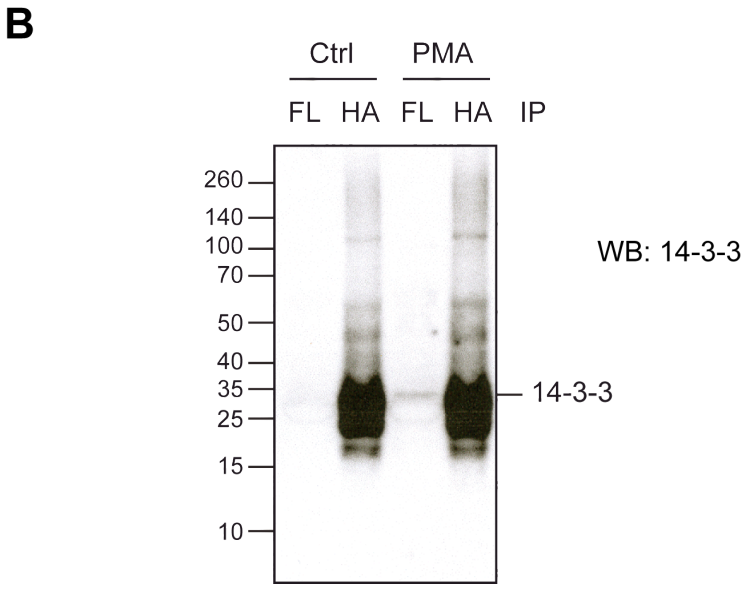
B
Ctrl
PMA
FL HA FL HA IP
260
140
100
70
50
40
35
25
15
10
WB: 14-3-3
14-3-3

4.7: Binding of ATRAP to the PITP domain is specific to RdgBβ

Since the human RdgBβ sequence is ~40% identical to PITPα and PITPβ in its PITP domain, and ATRAP binds to the PITP domain of RdgBβ, it is important to question whether ATRAP binds to either PITPα or PITPβ. The available PITPα and PITPβ antibodies exhibit good recognition of the endogenous proteins, and so HA-ATRAP alone was expressed in COS-7 cells and immunoprecipitated using its HA tag following 16 hrs PMA treatment. The HA-immunoprecipitates were separated using SDS-PAGE, transferred to PVDF membrane and probed using anti-PITPα or anti-PITPβ antibodies (Figure 4.8). Neither PITPα nor PITPβ was present in the HA-ATRAP-immunoprecipitate.

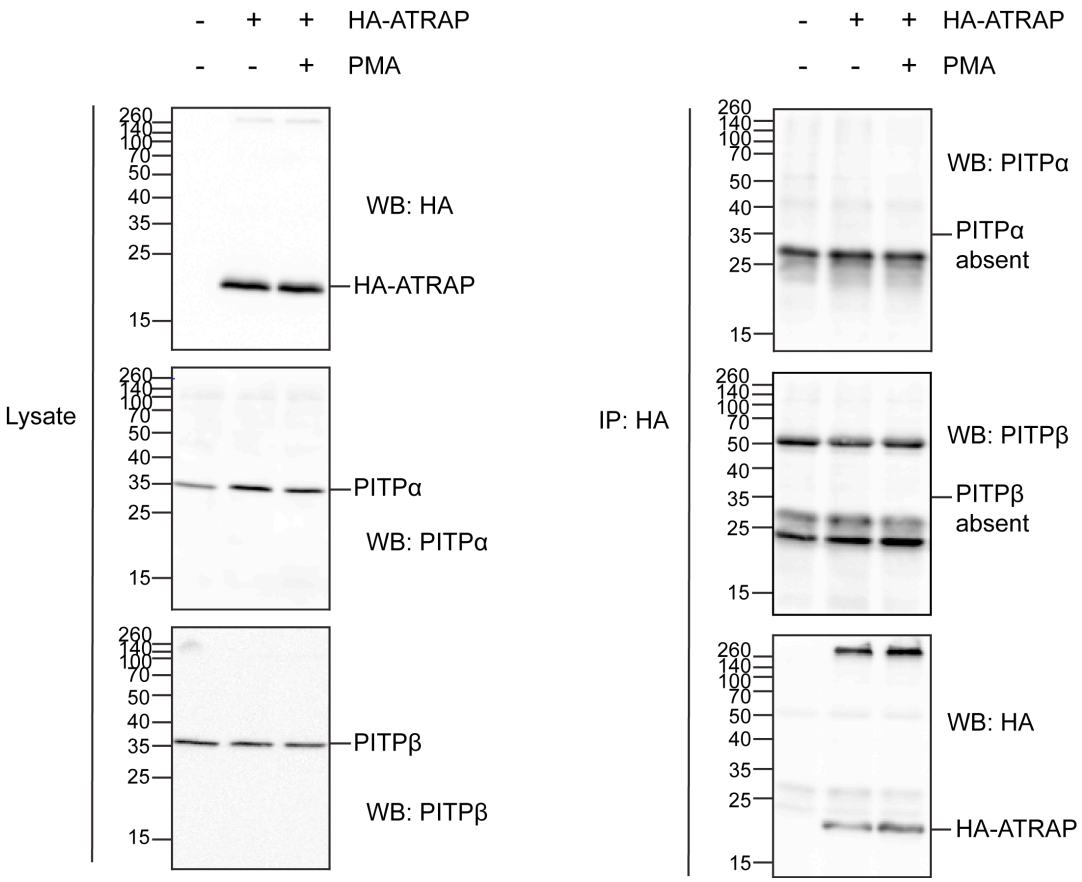

Figure 4.8: Binding of ATRAP to the PITP domain is specific to RdgBβ

HA-ATRAP was expressed in COS-7 cells and immunoprecipitated using its HA tag from lysates following 16 hrs 100 nM PMA treatment. HA-immunoprecipitates were separated by SDS-PAGE, the proteins transferred to PVDF membrane and subject to western blotting using anti-PITPα antibody #674 or anti-PITPβ antibody #1C1.

4.8: Determination of candidate RdgBβ ATRAP-binding residues

ATRAP binds to the PITP domain of human RdgBβ (1-250 aa), and binding is specific to RdgBβ despite ~40% identity shared between RdgBβ and the class I PITPs. This information can be used to determine candidate residues for binding of ATRAP. A multiple sequence alignment of the human PITPα, PITPβ and RdgBβ (1-250) indicated that 91 residues in the RdgBβ sequence are identical to those in PITPα and PITPβ (red amino acids; highly conserved residues), 102 residues have similar physicochemical properties (magenta amino acids; conserved residues), and 57 residues differ from the PITPα and PITPβ sequences (black residues; unconserved) (Figure 4.9 A). As ATRAP binds to RdgBβ but not to PITPα or PITPβ, the identical and conserved residues were excluded as candidate ATRAP-binding residues, leaving 57 potential ATRAP-binding residues.

An X-ray crystal structure of the RdgBβ protein has not been reported. The MODELLER program (Eswar et al., 2006), was therefore used to produce a comparative model of the RdgBβ PITP domain based on the structure of rat PITPα (PDB: 1t27; (Yoder et al., 2001)), which shares the highest number of identical residues with human RdgBβ of all of the class I PITP structures reported. The location of the lipid-binding cavity (‘void’) was determined using AVP (Cuff and Martin, 2004), and a list of the residues lining the cavity generated (Figure 2.1). These too were excluded as candidate ATRAP-binding residues, as the ATRAP-binding site most likely lies on the surface of the RdgBβ PITP domain. This removed 17 potential ATRAP-binding residues, leaving 40 candidates remaining.

The candidate ATRAP-binding residues were then mapped onto the RdgBβ model, grouping them into patches of residues. A further 3 residues were excluded as candidate ATRAP-binding residues as they are not, or are only barely, exposed on the surface of the protein (L12, I138, A221). Remaining candidate residues were grouped into 10 patches (Figure 4.9 B). One residue, Q43, is largely exposed on the surface of the protein, but does not appear to form part of a cluster of residues. Notably, 19 out of the 37 remaining residues lie in the regulatory loop: 8 residues lie in the β6-αC loop, and 11 residues lie in the β7-β8 loop.

(Facing page) Figure 4.9: Candidate ATRAP-binding residues on the RdgBβ PITP domain

(A) Multiple sequence alignment of the human sequences RdgBβ-sp1 1-250 aa (NP_036549.2), PITPα (NP_006215.1) and PITPβ (NP_036531.1), using the MATLAB multialign function. Red=highly conserved (identical) residues, magenta=conserved (similar) residues, black=non-conserved residues. x=non-conserved residues previously identified as cavity-lining residues, o=candidate ATRAP-binding residues in the RdgBβ sequence. (B) Candidate ATRAP-binding residues were mapped onto the comparative model of the RdgBβ PITP domain. For each patch of amino acids, their location is first given in terms of secondary structure, followed by the residues making up the patch using single letter amino acid code. (For naming of α-helices or β-strands, see Figure 1.3 C for the tertiary structure, and Figure 2.1 A for the primary sequence.) For patches comprised of residues from more than one location, details are as follows: D115/H177/Q178/I180 patch: D115 lies in the β6-αC loop, whereas the other residues lie in the β7-αE loop. H51/G53/Y89 patch: H51 and G53 lie in the β2-β3 loop, whereas Y89 is contributed from the β4-β5 loop. Hydrophobic patch: W71 lies on αB helix, V193 lies in the β8-αF loop. Cysteine patch: C136 is located on the β7 strand, whereas C142 lies in the β7-αE loop. E162/Y227 patch: E162 lies in the β7-αE loop, whereas Y227 is located in the αF helix.

A

```
PITPa_NP_006215.1| phosphatidylinositol transfer protein alpha i
PITPb_NP_036531.1| phosphatidylinositol transfer protein beta is
RdgBb_NP_036549.2| cytoplasmic phosphatidylinositol transfer pro

soform [Homo sapiens]          MVLLKEYRVILPVSVDEYQVGQLYSVAEASKN
oform [Homo sapiens]           MVLIKEFRVVLPCSVQEYQVGQLYSVAEASKN
tein 1 isoform a [Homo sapiens] M-LLKEYRICMPLTVDEYKIGQLYMISKHSHE
                                          x  o          x   x

ETGGGEGVEVLVNEPYEKDGE-KGQYTHKIYHLQSKVPTFVRMLAPEGALNIHEKAWNAYPYCR
ETGGGEGIEVLKNEPYEKDGE-KGQYTHKIYHLKSKVPAFVRMIAPEGSLVFHEKAWNAYPYCR
QSDRGEGVEVVQNEPFEDPHHGNGQFTEKRVYLNSKLPSWARAVVPK-IFYVTEKAWNYYPYTI
   o        o        o o       ox        o         x o o      o   xo

TVITNEYMKEDFLIKIETWHKPDLGTQENVHKLEPEAWKHVEAVYIDIADRSQVLSKDYKAEED
TIVTNEYMKDDFFIKIETWHKPDLGTLENVHGLDPNTWKTVEIVHIDIADRSQVEPADYKADED
TEYTCSFLPK---FSIHIETKYEDNKGSNDTIFDNEAKDVEREVCFIDIACDEIPERYYKESED
 ox x             ox x o  o  ooo  x  o oo x o ox  o   oo o

PAKFKSIKTGRGPLGPNWKQELVNQKDCPYMCAYKLVTVKFKWWGLQNKVENFIHKQERRLFTN
PALFQSVKTKRGPLGPNWKKELANSPDCPQMCAYKLVTIKFKWWGLQSKVENFIQKQEKRIFTN
PKHFKSEKTGRGQLREGWRDSHQ-----PIMCSYKLVTVKFEVWGLQTRVEQFVHKVVRDILLI
  o   o      o o       oo       o            o              xx     x

FHRQLFCWLDKWVDLTMDDIRRMEEETKRQLDEMRQKDPVKGMTADD-
FHRQLFCWIDKWIDLTMEDIRRMEDETQKELETMRKRGSVRGTSAADV
GHRQAFAWVDEWYDMTMDEVREFERATQEATNKKIG----------
x     o     o                    ooo
```

B

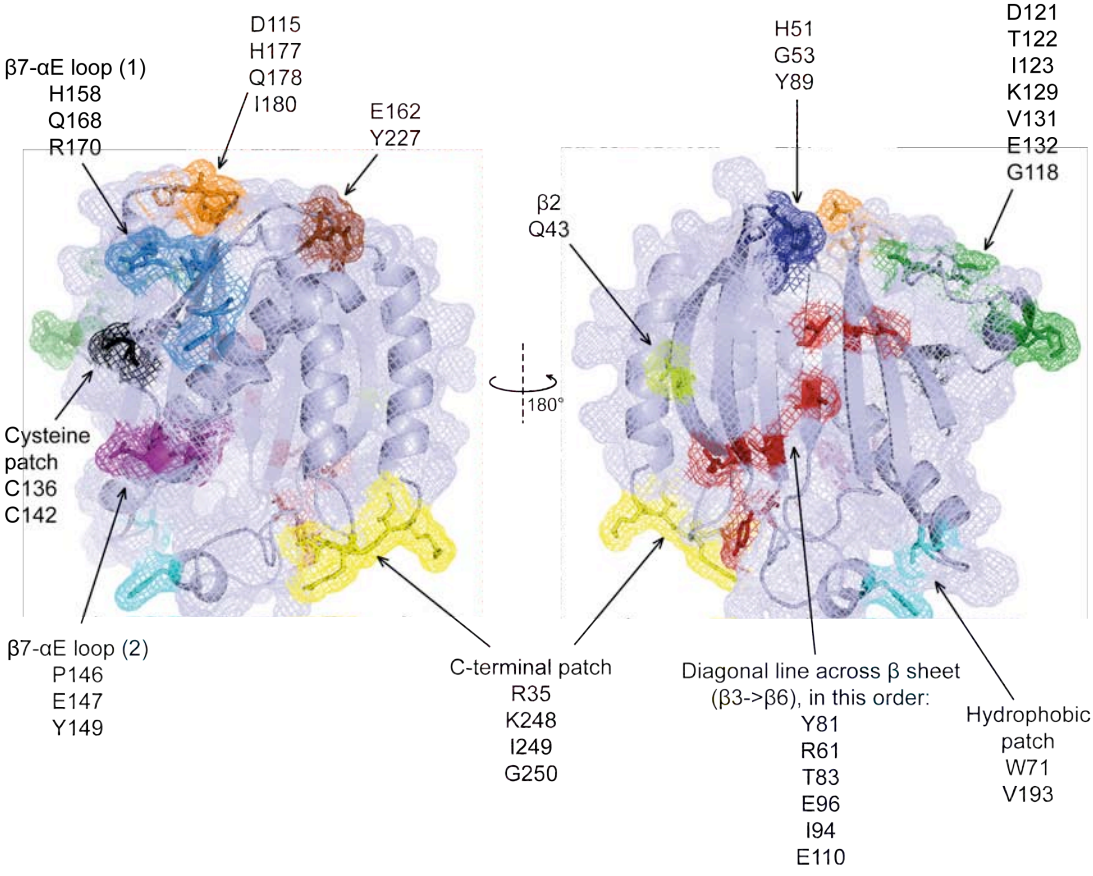

4.9: Determination of a potential ATRAP RdgBβ-binding site

Lopez-Ilasaca and colleagues reported that ATRAP has three transmembrane domains and that the protein is oriented with its N-terminus outside of the cell (Lopez-Ilasaca et al., 2003). The class I PITPs, PITPα and PITPβ, are cytosolic proteins, and fluorescence microscopy has been used to show that the same is true for RdgBβ (Fullwood et al., 1999; Takano et al., 2003). In addition, the RdgBβ protein sequence does not contain any organelle import sequences; the default address for proteins leaving the Golgi apparatus is the cytosol. Therefore, RdgBβ would be expected to interact with ATRAP through its cytosolic domains, the intracellular loop and protein C-terminus. The ATRAP protein sequence I have used in my immunoprecipitation experiments is the mouse sequence, and the yeast two-hybrid screens from which the interaction was first identified was with human proteins (Rual et al., 2005; Venkatesan et al., 2009). Therefore, candidate RdgBβ-binding residues on the ATRAP protein are residues common to both the human and mouse sequences in the intracellular loop and C-terminal residues. The human and mouse sequences share 76% identity, however, making it difficult to narrow down the binding site further without further experiments.

4.10: The RdgBβ-ATRAP interaction and Angiotensin II

Thus far, the interaction between RdgBβ and ATRAP has only been observed when cells are stimulated with PMA. Unlike DAG, the phorbol ester PMA is not metabolised by mammalian cells and so promotes a much more potent, sustained activation of PKC than would be instigated in a physiological setting. The interaction between RdgBβ and ATRAP is also not seen at short periods of PMA, only at >4 hrs, making the conditions under which the RdgBβ-ATRAP interaction might occur *in vivo* difficult to predict. ATRAP interacts with the AT_1R, and binding is increased upon Angiotensin II stimulation. Angiotensin II was therefore tested for its ability to stimulate the RdgBβ-ATRAP interaction. COS-7 cells were co-transfected with FLAG-RdgBβ-sp1, HA-ATRAP and HA-AT_1R plasmids and stimulated with Angiotensin II for differing time periods (Figure 4.10).

In Figure 4.10 A, COS-7 cells transfected with the HA-AT_1R have been stimulated with 100 nM Angiotensin II for 10 mins following 16 hrs serum starvation. In the FLAG-immunoprecipitate, FLAG-RdgBβ-sp1 is clearly seen in all but the first, control-transfected lane. In the lysate, HA-ATRAP is well-expressed in the final two lanes. However, when the FLAG-immunoprecipitate is probed with the anti-HA antibody, no clear HA-ATRAP band is seen. In this experiment, as in the next three, Figure 4.10 B-D, HA-AT_1R is not seen when the lysate is probed with anti-HA antibody.

The experiment shown in Figure 4.10 B is slightly more complex. The third lane from the left is intended to be the positive control: cells expressing FLAG-RdgBβ-sp1 and HA-ATRAP have been treated for 16 hrs with 100 nM PMA (in DMEM containing 0% FCS, as in Figure 4.3), yet the band corresponding in size to HA-ATRAP in the FLAG-RdgBβ-immunoprecipitate is faint compared to other experiments. Lanes 6, 7, 8 have been treated for 30 min (following 16 hr serum starvation) with EGF, insulin and 100 nM Angiotensin II, respectively, with only the cells in the final lane co-transfected with HA-AT_1R. The cells in lanes 4 and 5 have been transfected with the plasmid encoding FLAG-RdgBβ-sp2 rather than -sp1, together with HA-ATRAP, and treated either without (lane 4) or with (lane 5) 100 nM PMA for 16 hr. Despite FLAG-RdgBβ-sp2 expression being almost completely absent, it is enriched in the FLAG-immunoprecipitate. In both the lysate and FLAG-immunoprecipitate, more FLAG-RdgBβ-sp2 is observed in the cells treated with PMA than those without, indicating a similar stabilising effect of PMA on RdgBβ-sp2. Unusual in this experiment is the variability in HA-ATRAP expression in the lysate - HA-ATRAP is normally expressed at a similar level throughout. If RdgBβ expression must be stabilised so that the protein is allowed to accumulate before ATRAP-binding is observed, then it is important also to quantify FLAG-RdgBβ in the lysate, re-probed and adjusted for ARF loading control. Compared to untreated control (lane 2) (1.0), the quantity of FLAG-RdgBβ-sp1 in PMA-treated cells was 1.66, in EGF-treated cells it was 1.33, following insulin treatment it was 1.04, and in Angiotensin II-treated cells it was 1.37.

Plasmids encoding FLAG-RdgBβ-sp1 and HA-AT_1R were transfected into all cells in the experiment shown in Figure 4.10 C; the HA-ATRAP plasmid was transfected into cells in lanes 2, 4 and 6. Cells with and without HA-ATRAP expression were then either

untreated, or treated with 1 μM PMA or 1 μM Angiotensin II for 90 mins, without prior serum starvation. Again, no clear HA-ATRAP bands are observed in the FLAG-immunoprecipitate, and the ARF bands in the re-probe of the lysate membrane and surprisingly variable in this experiment, making any comment about stabilisation of FLAG-RdgBβ difficult to substantiate. Looking at the FLAG-immunoprecipitate alone, the most believable HA-ATRAP band is in the lane treated with 1 μM Angiotensin II, with the second most likely being in the final lane, the cells treated with 1 μM PMA. Similarly, the FLAG-RdgBβ-sp1 in the immunoprecipitate appears to be higher in the Angiotensin II-treated lane, although one could argue that all of the (non-specific) protein bands in that lane are darker, which would indicate a higher amount of total protein loaded onto the gel.

In Figure 4.10 D, 16 hr treatment of Angiotensin II (1 μM) and PMA (1, 10, 100 nM) have been administered prior to cell harvest and immunoprecipitation. The positive control band for HA-ATRAP in the immunoprecipitate is clearly seen for 100 nM PMA, and also for 10 nM PMA. The band may also be present, although very faint, for 1 nM PMA, and by extension a band of the same molecular weight might be present in the immunoprecipitate of the Angiotensin II-treated cells, but even fainter. As in the previous experiment (Figure 4.10 C), the FLAG-RdgBβ-sp1 expression in the whole cell lysates seems misleading - the protein bands have an increased intensity towards the centre of the western blot as though there was inadequate mixing during antibody incubation, development with ECL or imaging.

(Facing page, and subsequent three pages) Figure 4.10: The RdgBβ-ATRAP interaction and Angiotensin II stimulation

All experiments were carried out in COS-7 cells transiently transfected with HA-AT_1R and with FLAG-RdgBβ-sp1 and HA-ATRAP, as indicated. RdgBβ was immunoprecipitated using its FLAG tag, the immunoprecipitate subjected to western blotting using the anti-HA antibody, HA-probe, followed by re-probing of the membrane to confirm the presence of FLAG-RdgBβ-sp1 in the immunoprecipitate. Whole cell lysates were also probed to confirm protein expression: HA-AT_1R was not seen in any of the HA lysate blots. (A) Cell culture medium containing 10% FCS was removed and replaced with fresh DMEM containing 0% FCS for serum starvation of the cells, 16hrs prior to 100 nM Angiotensin II treatment for 10 mins in HEPES buffer. (B) Serum-starved cells were treated with 100 nM Angiotensin II, 50 $ng.mL^{-1}$ EGF or 100 nM insulin for 30 mins prior to harvest. In addition, cells transiently expressing FLAG-RdgBβ-sp1 or -sp2 and HA-ATRAP were treated with 100 nM PMA prior to harvest. (C) Cells in this experiment were not serum-starved prior to treatment; cells were treated with 1 μM PMA or angiotensin II in HEPES buffer prior to cell harvest and immunoprecipitation of FLAG-RdgBβ. (D) Cells were treated with 1 μM angiotensin II in DMEM + 10% FCS for 16 hrs prior to cell harvest, alongside 1, 10 and 100 nM PMA.

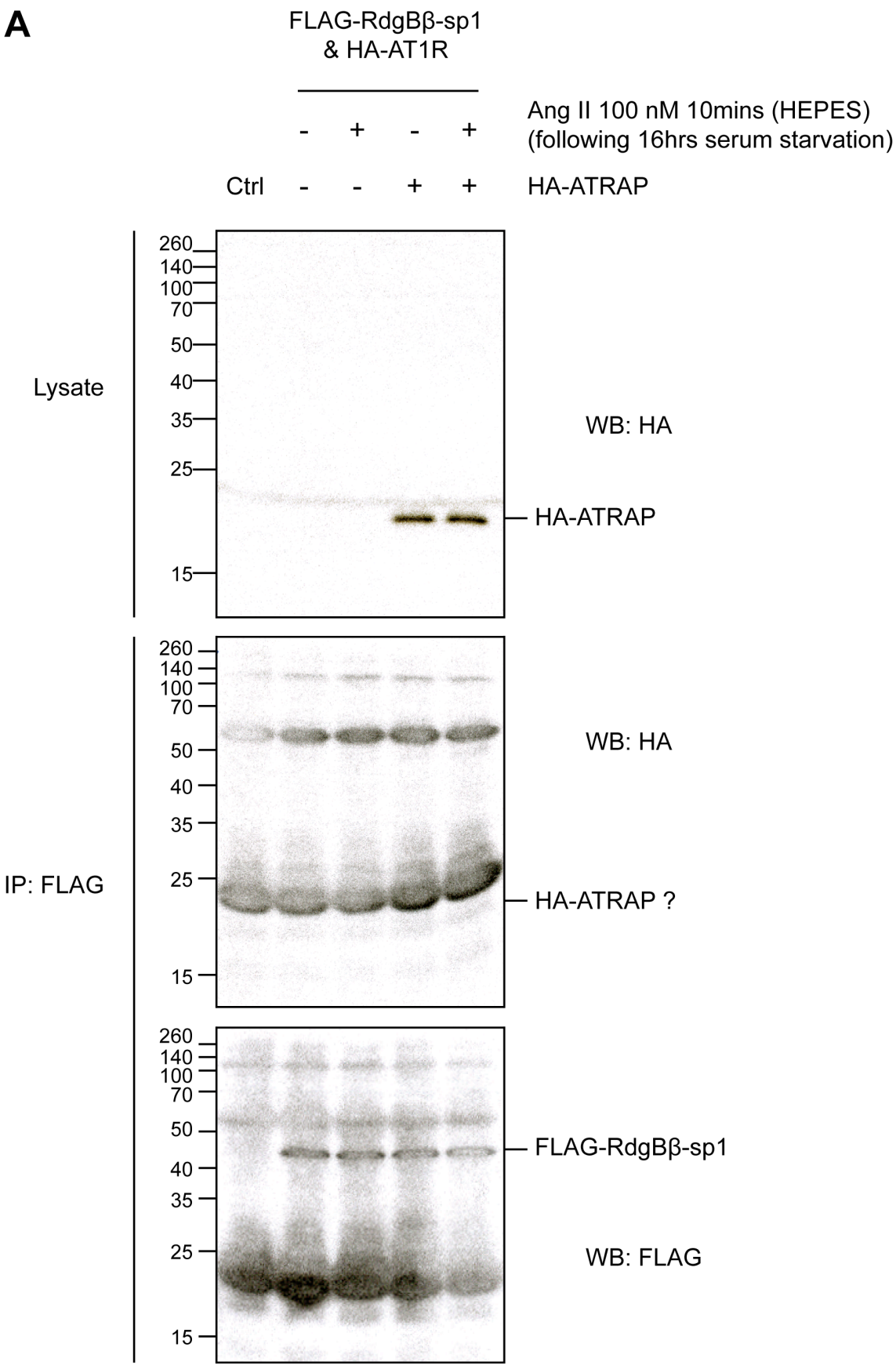
A
FLAG-RdgBβ-sp1
& HA-AT1R
Ang II 100 nM 10mins (HEPES)
(following 16hrs serum starvation)
- + - +
Ctrl - - + +
HA-ATRAP
Lysate
260
140
100
70
50
40
35
25
15
WB: HA
HA-ATRAP
IP: FLAG
WB: HA
HA-ATRAP ?
FLAG-RdgBβ-sp1
WB: FLAG

B

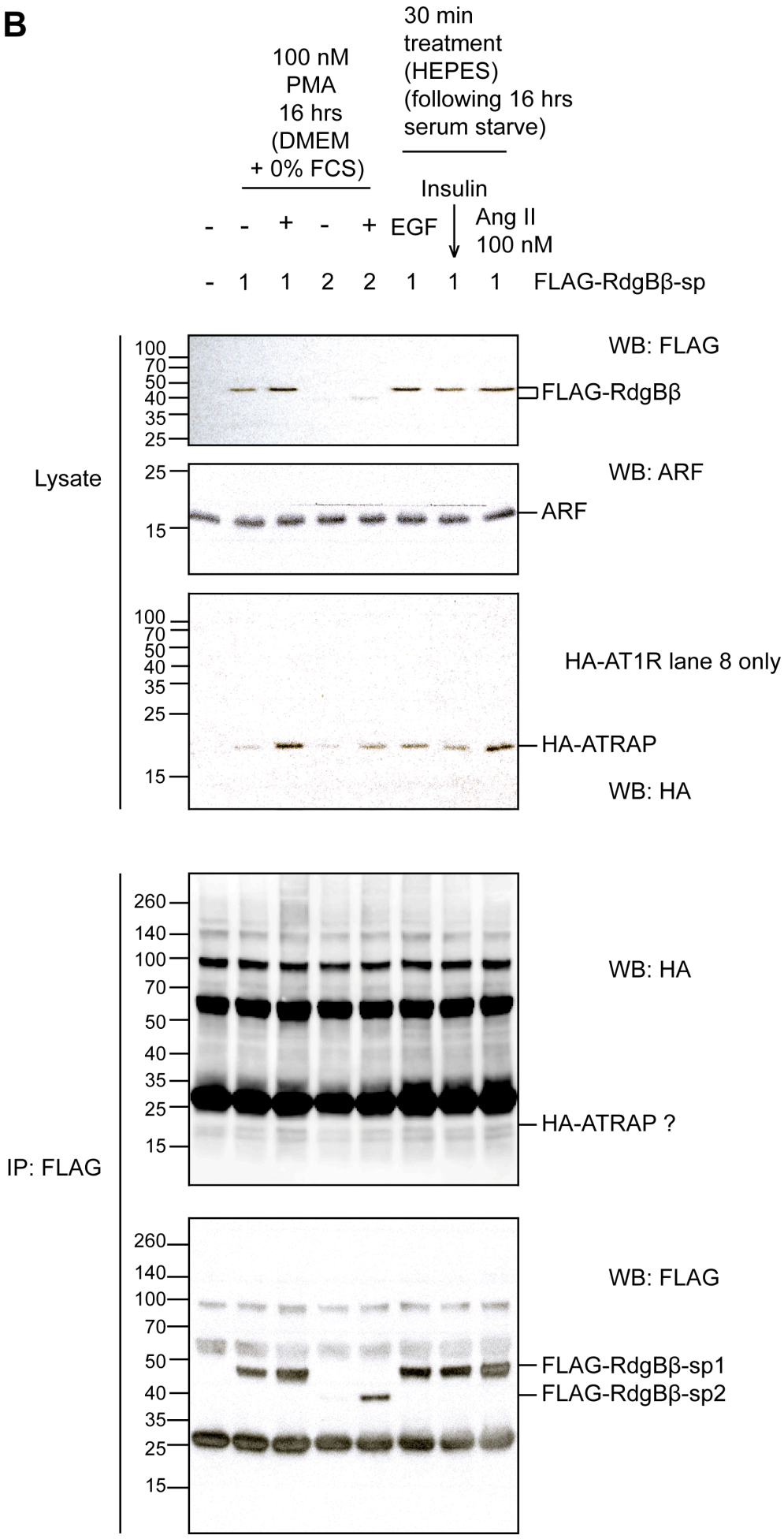
100 nM
PMA
16 hrs
(DMEM
+ 0% FCS)
30 min
treatment
(HEPES)
(following 16 hrs
serum starve)
Insulin
- - + - + EGF
Ang II
100 nM
- 1 1 2 2 1 1 1 FLAG-RdgBβ-sp
Lysate
100
70
50
40
35
25
WB: FLAG
FLAG-RdgBβ
25
15
WB: ARF
ARF
HA-AT1R lane 8 only
HA-ATRAP
WB: HA
IP: FLAG
260
140
100
70
50
40
35
25
15
WB: HA
HA-ATRAP ?
WB: FLAG
FLAG-RdgBβ-sp1
FLAG-RdgBβ-sp2

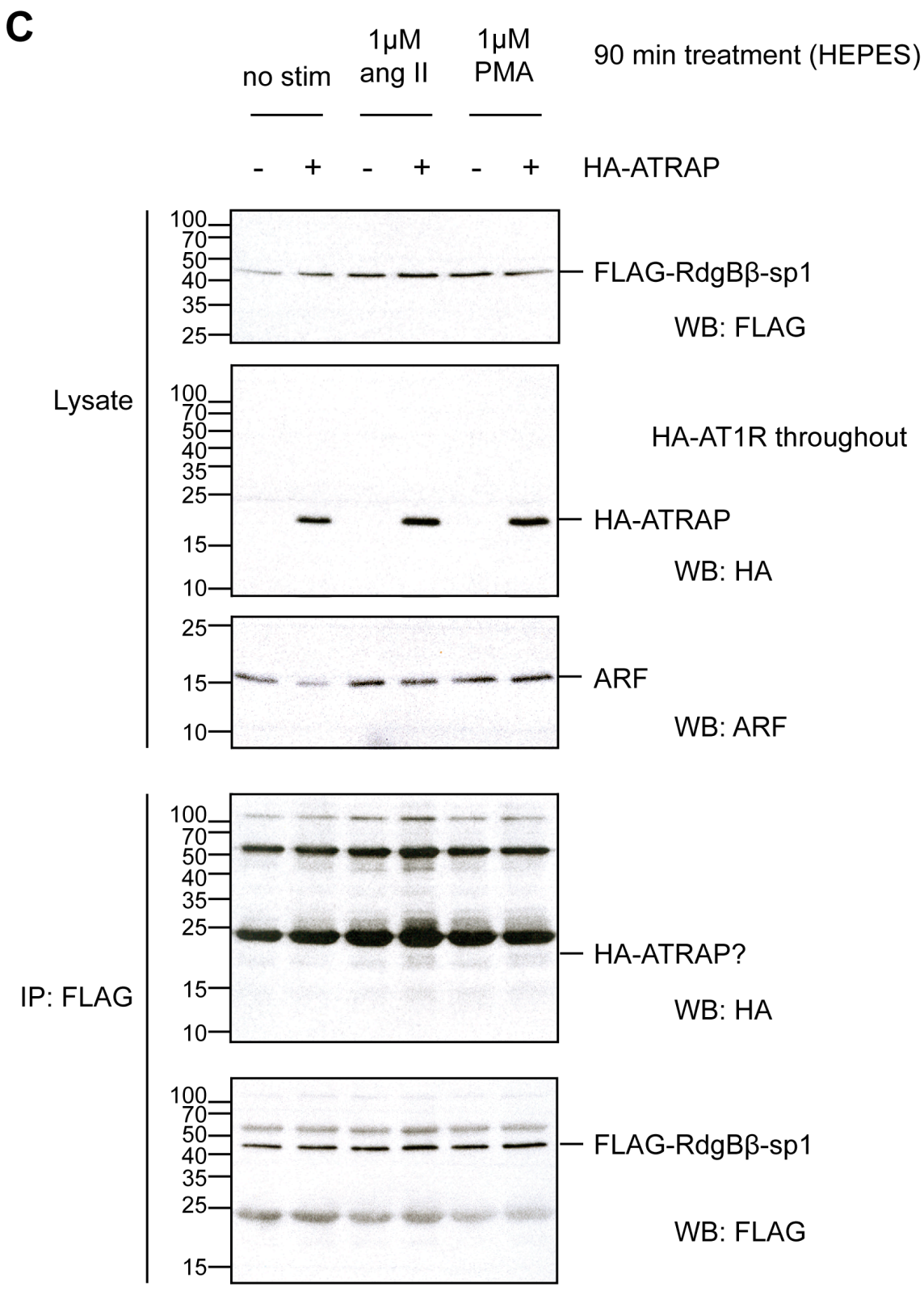
C
no stim
1μM ang II
1μM PMA
90 min treatment (HEPES)
- + - + - +
HA-ATRAP
Lysate
100
70
50
40
35
25
15
10
FLAG-RdgBβ-sp1
WB: FLAG
HA-AT1R throughout
HA-ATRAP
WB: HA
ARF
WB: ARF
IP: FLAG
HA-ATRAP?
WB: HA
FLAG-RdgBβ-sp1
WB: FLAG

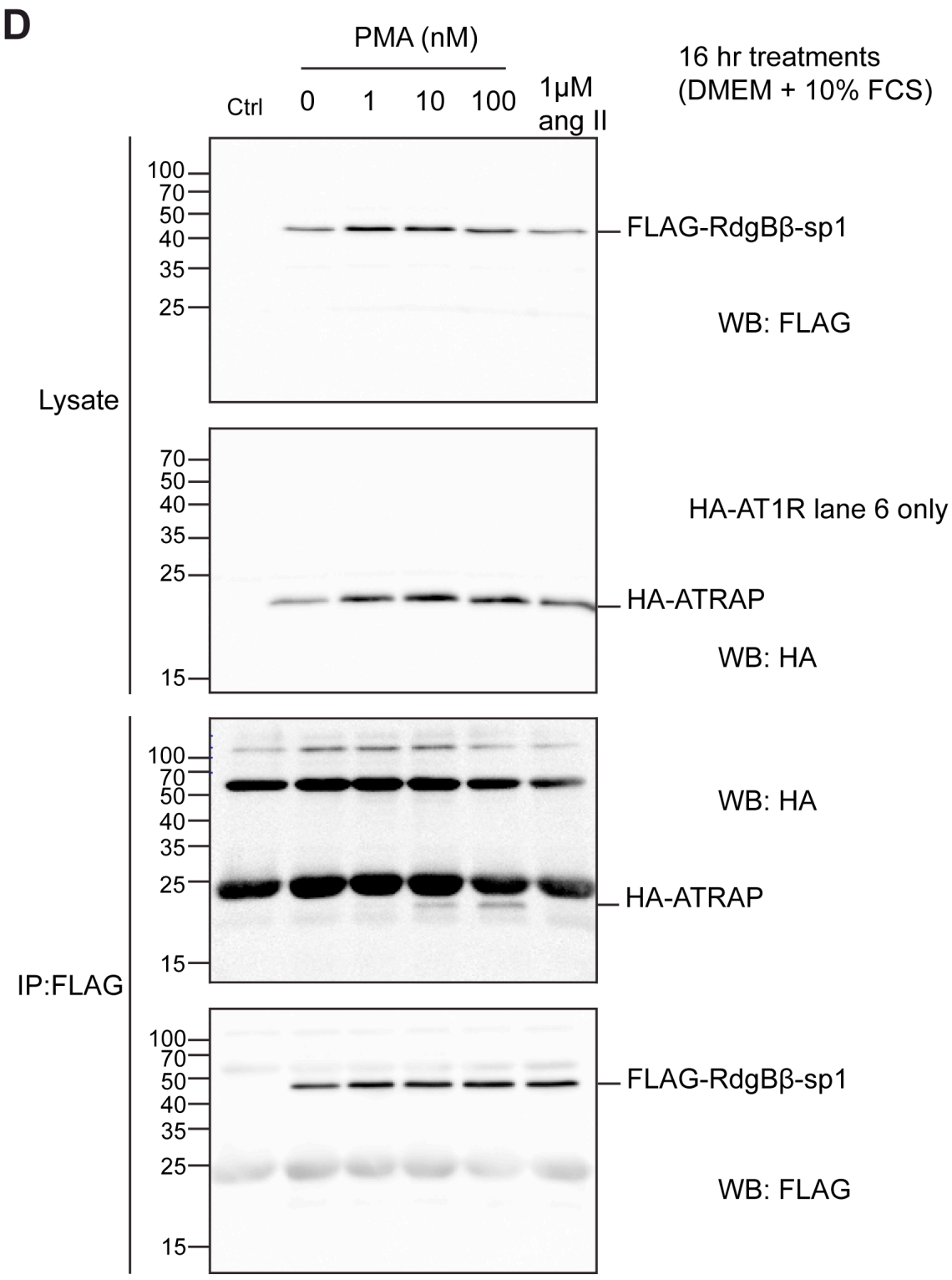
D
PMA (nM)
16 hr treatments
(DMEM + 10% FCS)
Ctrl
0
1
10
100
1μM
ang II
100
70
50
40
35
25
FLAG-RdgBβ-sp1
WB: FLAG
Lysate
70
50
40
35
25
15
HA-AT1R lane 6 only
HA-ATRAP
WB: HA
100
70
50
40
35
25
15
WB: HA
HA-ATRAP
IP:FLAG
100
70
50
40
35
25
15
FLAG-RdgBβ-sp1
WB: FLAG

4.11: RdgBβ and the stimulation of PLC activity

PITP is required for the reconstitution of PLC activity (Thomas et al., 1993; Kauffmann-Zeh et al., 1995; Cunningham et al., 1996), and ATRAP suppresses Angiotensin II-stimulated inositol phosphate production (Daviet et al., 1999; Lopez-Ilasaca et al., 2003). I therefore wondered whether there was a function for the RdgBβ-ATRAP interaction in PLC signalling.

I first tested whether RdgBβ is involved in Angiotensin II-stimulated PLC activity. HEK-293 cells were transfected with a plasmid encoding HA-AT_1R, with or without RdgBβ-sp1 co-transfection. Cells were labelled for 24 hrs with [^{3}H]-inositol prior to Angiotensin II stimulation. The [^{3}H]-inositol phosphates were separated from the [^{3}H]-inositol lipids by Chloroform-Methanol extraction, and from other water soluble components by isolation using Dowex columns. RdgBβ over-expression was observed to increase inositol phosphate production by PLC (Figure 4.11 A).

By contrast, the reverse was seen upon ATRAP co-expression with the AT_1R (Figure 4.11 A). Inositol phosphate production was reduced to ~40% of that observed upon AT_1R expression alone (0.41 ±0.02 SD, *n*=2, mean fold difference across both Angiotensin II concentrations). With ATRAP over-expression, inositol phosphates are produced in an Angiotensin II dose-dependent manner. This is in contrast with the results for RdgBβ over-expression: for RdgBβ, no significant difference is observed between 10 nM and 1 μM Angiotensin II.

Since an interaction is only observed between RdgBβ and ATRAP following 4-16 hrs PMA treatment, I assessed the effect of this treatment on PLC activity. For this experiment I used COS-7 cells transiently transfected with the HA-AT_1R plasmid and a HEK-293 cell line stably expressing AT_1R (HEK-293-AT_1R). Angiotensin II treatment time was reduced to 5 min, at 100 nM.

Notably, RdgBβ and ATRAP over-expression do not produce the same response in the absence of PMA as seen in the previous graph. Here, RdgBβ has no effect on Angiotensin II-stimulated inositol phosphate production, and the effect of ATRAP is to

increase inositol phosphates rather than reduce them, although the error bars are very large (Figure 4.11 B & C). The over-expression of RdgBβ and ATRAP together reduces Angiotensin II-stimulated inositol phosphate production in COS-7 cells.

In general, PMA pre-treatment caused a reduction in inositol phosphate production in response to Angiotensin II. An exception is seen for control HEK-293-AT_1, where the reverse is observed (Figure 4.11 C).

(Facing page) Figure 4.11: PLC activity in intact cells with RdgBβ and ATRAP over-expression

(A) [^{3}H]-inositol-labelled HEK-293 cells transiently expressing HA-AT_1R, and co-expressing RdgBβ-sp1 and/or HA-ATRAP, were treated with Angiotensin II (AngII) at the concentrations indicated for 20 min prior to quenching and isolation of inositol phosphates. [^{3}H]-Inositol phosphates produced are expressed relative to unstimulated cells. nd, not done. Error bars are absent where *n*=1, SD where *n*=2 or SEM where *n*≥3. 10 nM AngII, Control *n*=2, RdgBβ *n*=2; 100 nM AngII, Control *n*=6, RdgBβ *n*=4, ATRAP *n*=2; 1 μM AngII, Control *n*=3, RdgBβ *n*=2, ATRAP *n*=1. (B) [^{3}H]-inositol-labelled COS-7 cells transiently expressing HA-AT_1R, and co-expressing RdgBβ-sp1 and/or HA-ATRAP, were treated with 100 nM Angiotensin II for 5 mins, following 16 hrs pre-treatment with 100 nM PMA, where indicated. [^{3}H]-Inositol phosphates produced are expressed relative to unstimulated cells. AngII - PMA, *n*=2; AngII + PMA, *n*=1. (C) [^{3}H]-inositol-labelled HEK-293 cells stably expressing AT_1R (HEK-293-AT_1 cells), and transiently expressing RdgBβ-sp1 and/or HA-ATRAP, were pre-treated 100 nM PMA for 16 hr as indicated prior to stimulation with 100 nM Angiotensin II for 5 mins. nd, not done. Data expressed as in (B). Control, *n*=3; RdgBβ, *n*=1; ATRAP, *n*=1; RdgBβ + ATRAP, *n*=1.

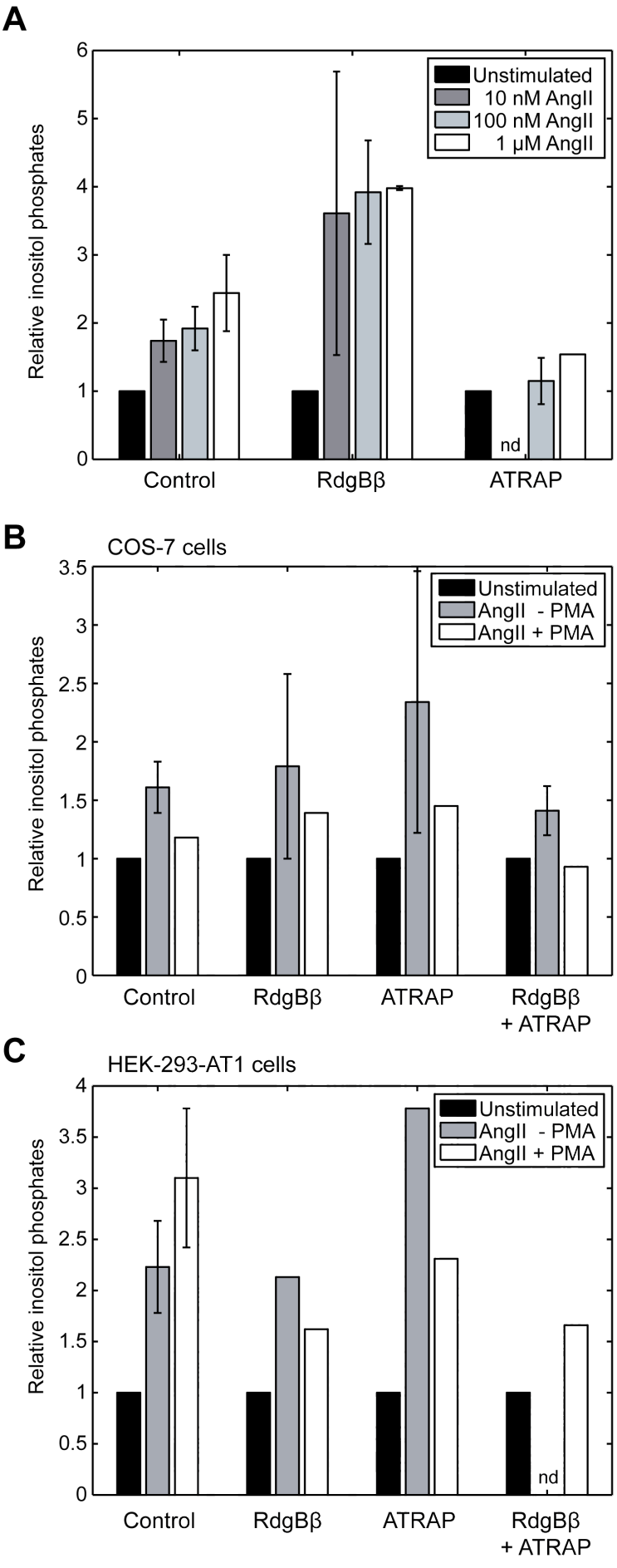
A
Relative inositol phosphates
Unstimulated
10 nM AngII
100 nM AngII
1 μM AngII
nd
Control
RdgBβ
ATRAP
B
COS-7 cells
Relative inositol phosphates
Unstimulated
AngII - PMA
AngII + PMA
Control
RdgBβ
ATRAP
RdgBβ
+ ATRAP
C
HEK-293-AT1 cells
Relative inositol phosphates
Unstimulated
AngII - PMA
AngII + PMA
nd
Control
RdgBβ
ATRAP
RdgBβ
+ ATRAP

4.12: Discussion

I have demonstrated that RdgBβ binds to the Angiotensin II receptor-associated protein, ATRAP, when cells are stimulated for 4-16 hr with PMA. This interaction was blocked by inhibition of PKC or protein synthesis. ATRAP interacts with the PITP domain of RdgBβ, a region distinct from the 14-3-3-binding site.

4.12.1: Conditions of the RdgBβ-ATRAP interaction

RdgBβ and ATRAP are not observed to interact with one another in unstimulated cells in co-immunoprecipitation experiments. However, an RdgBβ-ATRAP interaction is observed following stimulation of cells with PMA for 4-16 hrs, conditions which increase FLAG-RdgBβ expression. The PMA-induced interaction is blocked by 4 hrs treatment with the protein synthesis inhibitor, cycloheximide, indicating that a certain threshold concentration of RdgBβ must be reached before the RdgBβ-ATRAP interaction is observed.

The RdgBβ-ATRAP association is not seen when cells are co-transfected with the AT_1R and stimulated with Angiotensin II. This is either a result of PMA and Angiotensin II not activating the same downstream effectors, or because Angiotensin II is not as potent at increasing FLAG-RdgBβ concentration as PMA, at the Angiotensin II doses tested.

The PMA-induced RdgBβ-ATRAP interaction was also blocked by inhibition of PKC with BIM-I, indicating that the direct target of PMA in this instance might be PKC. Activation of PKC also requires Ca^{2+}, and treatment of cells with the Ca^{2+} ionophore, ionomycin, increased the PMA-induced RdgBβ-ATRAP interaction two-fold. The effect of PKC on FLAG-RdgBβ-sp1 stability is distinct from its ability to promote the interaction between RdgBβ and 14-3-3, since both the RdgBβ-sp1 1-250 mutant, lacking the disordered C-terminus, the RdgBβ-sp1 S299A mutant, unable to bind 14-3-3, and RdgBβ-sp2, with its distinct C-terminus, all experience a PMA-induced increase in protein expression. It is likely that PMA acts on the cell's protein synthesis machinery to effect a global upregulation of protein synthesis, and here this effect is indistinguishable from the targeted stabilisation of protein expression by PMA.

The observation that RdgBβ-sp2 expression is increased in response to PMA, and that ATRAP interacts with RdgBβ-sp1 via its PITP domain, indicates that RdgBβ-sp2 will also participate in an interaction with ATRAP. Indeed, the second yeast two-hybrid study to identify the RdgBβ-ATRAP interaction reported the nucleotide sequence for RdgBβ as BC007905 (Venkatesan et al., 2009), which corresponds to the RdgBβ-sp2 sequence, rather than RdgBβ-sp1.

4.12.2: The relationship between RdgBβ-14-3-3 and RdgBβ-ATRAP

14-3-3 interacts with RdgBβ-sp1 via its long, disordered C-terminus, yet ATRAP interacts with RdgBβ via its PITP domain. Both proteins interact with RdgBβ when cells are stimulated with PMA, but whether both proteins bind to the same RdgBβ molecule simultaneously has not been clear from my experiments.

FLAG-(RdgBβ)-immunoprecipitates and HA-(ATRAP)-immunoprecipitates were prepared from the COS-7 cells using two distinct methods, which may explain why blotting the HA-immunoprecipitate with anti-14-3-3 antibody produced such a large amount of non-specific protein bands. Immunoprecipitation of FLAG-RdgBβ used anti-FLAG M2 antibody covalently attached to agarose beads, enabling a single capturing step consisting of 2 hr incubation of 300 μg lysate with anti-FLAG M2 affinity gel on the rotating wheel. HA-immunoprecipitation, by contrast, utilised a two-step method: firstly 300 μg lysate was incubated with 1.5 μg anti-HA monoclonal antibody for 1 hr, to enable the antibody to bind the HA tag of ATRAP, and secondly this mixture was incubated with 20 μL Protein A/G PLUS Agarose to enable capture of the Fc region of the HA antibody by Protein A/G. Perhaps an anti-HA antibody conjugated to agarose beads for a one-step capture would have yielded cleaner 14-3-3 western blots. An alternative would have been to change the HA tag on ATRAP to a FLAG tag, transfect this alongside HA- or Myc-RdgBβ-sp1, and use the anti-FLAG M2 affinity gel, as for immunoprecipitation of FLAG-RdgBβ.

4.12.3: RdgBβ candidate ATRAP-binding residues

RdgBβ interacts with ATRAP via its PITP domain. The ATRAP interaction is specific to RdgBβ: neither PITPα nor PITPβ bind to ATRAP upon PMA stimulation. These observations led to the identification of 37 residues organised into 10 patches on the RdgBβ PITP domain surface as potential ATRAP-binding residues. Of the 37 residues, 19 lie in the regulatory loop, proposed as a site of protein interactions (Yoder et al., 2001). Specifically, 8 residues lie in the β6-αC loop and 11 residues lie in the β7-β8 loop. Notably, the loop β6-αC also contains the Ser119 and Thr122 residues, which have been reported to be phosphorylated in the mouse brain (Huttlin et al., 2010; Wiśniewski et al., 2010), imparting on this loop a means by which to regulate protein-protein interactions. A scan of the human RdgBβ sequence (Q9UKF7), with the PhosphoMotif Finder tool at the Human Protein Reference Database (http://www.hprd.org/PhosphoMotif_finder/) indicates that Ser119 lies in a consensus site for phosphorylation by PKA, PKC, and Casein kinase I and II, whereas Thr122 could be phosphorylated by Casein kinase II.

4.12.4: RdgBβ and Angiotensin II signalling

An obvious concern for the experiments to assess whether Angiotensin II could promote the RdgBβ-ATRAP interaction in transiently transfected COS-7 cells was that the HA-AT_1R was not observed in any of the anti-HA western blots of the whole cell lysates. This was not properly explored. It is possible that not enough lysate was loaded onto the gel, since a clear HA-ATRAP band was consistently observed in merely 3-5 μg lysate. Other researchers have found the AT_1R difficult to resolve through western blotting of whole cell lysates due to the presence of post-translational modifications including phosphorylation and glycosylation. AT_1R has a typical molecular weight of 41-58 kDa (although a value as high as 75 kDa has been recorded) (Cook et al., 2006), due to these modifications. Others see several diffuse bands over the range 70-200 kDa, representing extensive glycosylation of the receptor. These can be reduced to ~40 kDa upon treatment with peptide *N*-glycosidase F (PNGase F) to deglycosylate the AT_1R (Hunyady et al., 2002). Several studies immunoprecipitate the receptor from membrane fractions before western blotting (Smith et al., 1998; Tanaka et al., 2005; Azuma et al.,

2007). It seems unlikely, therefore, that I would have seen HA-AT_1R in whole cell lysates in my experiments. COS-7 cells transiently transfected with the pcDNA3.1-HA-AT_1R plasmid using the same transfection protocol as used prior to co-immunoprecipitation (Figure 4.10), did respond to Angiotensin II in the form of PIP_2 hydrolysis by PLC (Figure 4.11), indicating the presence of a functional AT_1R in the co-immunoprecipitation experiments.

RdgBβ over-expression increases inositol phosphate production by PLC when cells are stimulated by Angiotensin II for 20 mins. 10 nM, 100 nM and 1 μM Angiotensin II all produce ~3.8 times the amount of inositol phosphates compared to unstimulated cells expressing both the AT_1R and RdgBβ-sp1. Inositol phosphate production appears relatively unaffected by Angiotensin II dose, indicating that PIP_2 hydrolysis has reached near-maximum by 20 min treatment with either of the three Angiotensin II concentrations. The Angiotensin II dose response curve has shifted to the left with respect to cells transfected with the receptor only; a larger inositol phosphate response is produced by a reduced Angiotensin II dose. This could reflect either an increase in PIP_2 substrate availability or an increase in the rate of PIP_2 hydrolysis by PLC.

In contrast, over-expression of ATRAP was observed to reduce inositol phosphate production in response to Angiotensin II stimulation. This trend is in agreement with a previous study, in which a significant reduction ($p<0.05$) in inositol phosphate production was observed upon ATRAP over-expression following treatment with 10 nM, 100 nM and 1 μM Angiotensin II for 60 mins (Daviet et al., 1999) (transient transfection of COS-7 cells with HA-ATRAP and FLAG-AT_1R plasmids). In a different study, CHO-K1 cells stably expressing the AT_1R were transiently transfected with an ATRAP expression plasmid. Maximal suppression of inositol phosphate production in response to 1 μM Angiotensin II was observed at 5 min, and the difference between ATRAP-expressing cells and control cells was indistinguishable by 20 min Angiotensin II treatment (Lopez-Ilasaca et al., 2003). These differences clearly reflect differences in the concentrations of receptor, PLC enzyme and PIP_2 substrate in different cell types. The latter study indicates that ATRAP has no effect on substrate availability, since inositol phosphate production 'caught up' by 20 min, rather it either tempers substrate

availability or has a direct effect on PLC activity by reducing the rate of PIP_2 hydrolysis by PLC.

In COS-7 cells transiently transfected with the AT_1R and HEK-293-AT_1 cells, ATRAP over-expression was observed to increase inositol phosphate production in response to 5 min 100 nM Angiotensin II stimulation, rather than decrease it. There were few replicates carried out, but this variation could reflect a difference in ATRAP function depending on cell type. Perhaps a different complement of ATRAP-interacting proteins are present here, tipping the effect of ATRAP over-expression towards a stimulatory, rather than a suppressor, function.

Li^+ in the HEPES buffer used for the PLC assays inhibits inositol monophosphatase, promoting inositol phosphate accumulation and preventing PI re-synthesis. Li^+ is present throughout the experiment, and therefore longer stimulation time points would be expected to produce a more accurate picture of the effect of over-expression of particular proteins on PLC activity, and likely explains the variability of the results gained after 5 min stimulation. However, if the effect of a particular protein is to reduce or increase the rate of PLC activity, this may not be observed at longer time points since maximal inositol phosphate production may have been reached.

In general, PMA pre-treatment reduced Angiotensin II-stimulated inositol phosphate production. This is in accordance with previous studies which have shown that PKC phosphorylates the AT_1R to promote heterologous desensitisation, uncoupling it from G_q protein and attenuating PLC activity (Tang et al., 1998). In this way, PKC provides negative feedback to limit the magnitude and duration of Angiotensin II signalling.

CHAPTER 5: RdgBβ binds PI and PA

5.1: Introduction

Resolution of X-ray crystal structures of PI- and PC-bound class I PITPs has revealed that the PITP domain is composed of eight β-strands that form a large, concave sheet, together with seven α-helices. The PI or PC cargo occupies the same space in the ligand-binding cavity, formed between the β-sheet and two of the long α-helices, αA and αF. PITPα has a 16-fold higher affinity for PI than it does for PC (van Paridon et al., 1987a): the inositol head group of PI is secured by direct hydrogen bonds with residues Q22, T59, K61, E86 and N90, whereas the choline head group of PC is not observed to form any direct bonds. C95 forms a hydrogen bond with PC indirectly via a water molecule, and the presence of F225 has also been reported to be important for PC transfer (Vordtriede et al., 2005). In contrast to binding of the lipid head group, the phosphate group of either PI or PC is secured by hydrogen bonds to T97 and K195, and the acyl chains form bonds with Y63 and E218.

The structure of the PITP domain of RdgBβ has not been reported, however. RdgBβ-sp1 has been observed to exhibit robust PI transfer activity, comparable to that of PITPα, and this activity was unaffected by removal of its C-terminal tail (Fullwood et al., 1999). RdgBβ shares ~40% sequence identity with PITPα and PITPβ, yet a protein-lipid overlay assay indicated that RdgBβ-sp2 binds only PI, not to any of the other phospholipids, including PC and phosphorylated PI derivatives (Takano et al., 2003). Whether RdgBβ actually differs from the class I PITPs in its lipid binding properties is of significance.

I therefore begin this part of my study by establishing whether the residues shown to be important for PI- or PC-binding in the class I PITPs are also present in RdgBβ. Using a permeabilised HL60 cell assay for lipid binding, I observe that PC binding by RdgBβ is negligible. RdgBβ binds PI, together with a mystery lipid, in approximately equal proportions. The mystery lipid is not labelled with [^{3}H]-sphingosine, and monomethylamine treatment of the isolated lipid indicates that the mystery lipid is a glycerol phospholipid, with ester linkages connecting the fatty acids to the backbone.

[^{3}H]-ethanolamine appears to label the mystery lipid, yet I rule out its identity as either PMME or lyso-PE. Finally, the mystery lipid is identified as PA by mass spectrometry. RdgBβ selects for short-chain monounsaturated or saturated PA species, yet is non-selective in its preference of PI species. The addition of GTPγS to the lipid binding assay at high calcium increases PA binding by RdgBβ.

5.2: The RdgBβ lipid-binding cavity: sequence and structural analysis

A sequence alignment of both splice variants of RdgBβ (sp1 and sp2) with PITPα and PITPβ, indicates that the residues responsible for binding the inositol head group of PI (Q22, T59, K61, E86, N90) and the phosphate group (T97 and K195) are all conserved in human RdgBβ (Figure 5.1 A). However, the residues co-ordinating the phospholipid acyl chains are not conserved: Y63 and E218 in PITPα and PITPβ are present as valine residues in RdgBβ.

Since an X-ray crystal structure of RdgBβ has not been reported, modelling of the RdgBβ PITP domain was undertaken. The PDB: 1t27 structure was used as the template since it shares the highest sequence identity with the RdgBβ sequence. Pairwise comparisons were made between the RdgBβ model and each reported PITP crystal structure in turn using the 'Align' command in Pymol. This allowed the PI and PC ligands from the published PDB files to be modelled in the RdgBβ structure, and the proximity of particular residues to the ligand to be analysed. The consequences of the Y63V and E218V substitutions in the RdgBβ sequence are visualised in Figure 5.1 B, and clearly indicate that a phospholipid in the RdgBβ lipid-binding cavity is unlikely to be positioned as securely or tightly as it would in the class I structures.

In the PC-bound PITPα and PITPβ structures, no residues in the lipid-binding cavity directly contact the choline head group. C95 contacts the PC (not PI) phosphate group indirectly via a molecule of water, yet the residue at position 95 in RdgBβ is a threonine residue (Figure 5.1 A). F225, also relevant for PC transfer, is present in RdgBβ as a glycine residue. The two tryptophan residues, W203 and W204, important for membrane interaction in the class I PITPs, are V203 and W204 in the RdgBβ sequence.

(Facing page) Figure 5.1: Bioinformatic analysis of the RdgBβ lipid-binding cavity

(A) Sequence alignment of human sequences: PITPα Q00169.2, PITPβ P48739.2, RdgBβ-sp1 Q9UKF7.2, RdgBβ-sp2 NP_858057.1. Residues that contact the inositol head-group of PI in PITPα and PITPβ (Q22, T59, K61, E86, N90) are indicated in blue; those that make hydrogen bonds with the phosphate group of PI (T97 and K195) are indicated in red; and those that contact the acyl chains (Y63 and E218) are indicated in brown. C95/T95 are indicated in lime green, and the WW residues (W203 and W204) are indicated in green. The F225/G225 residue is also indicated. (B) RdgBβ lacks two residues that make stabilising hydrogen bond contacts to the PC (or PI) acyl chains. *Left and middle panels*: PC acyl chains are stabilised by hydrogen contacts with E218 and Y63 residues in PITPβ (and PITPα; PITPβ (PDB: 2a1l) shown here). *Right panel*: RdgBβ lacks these stabilising hydrogen bonds; in RdgBβ, these residues are valine residues (RdgBβ comparative model with PC ligand from 2a1l overlay).

A

```
                                  Q22                                                                  T59
                          1                                                                            60
PITPα             (1)     MVLLKEYRVILPVSVDEYQVGQLYSVAEASKNETGGGEGVEVLVNEPYEKDGE-KGQYTH
PITPβ             (1)     MVLIKEFRVVLPCSVQEYQVGQLYSVAEASKNETGGGEGIEVLKNEPYEKDGE-KGQYTH
RdgBβ-sp2         (1)     -MLLKEYRICMPLTVDEYKIGQLYMISKHSHEQSDRGEGVEVVQNEPFEDPHHGNGQFTE
RdgBβ-sp1         (1)     -MLLKEYRICMPLTVDEYKIGQLYMISKHSHEQSDRGEGVEVVQNEPFEDPHHGNGQFTE
Consensus         (1)     MMLLKEYRICLPLSVDEYQIGQLYSIAKHSKNQSGRGEGVEVLQNEPFEKPHHGNGQFTH

                  K61  Y63/V63                  E86  N90   C95
                                                          /T95 T97
                          61                                                                           120
PITPα             (60)    KIYHLQSKVPTFVRMLAPEGALNIHEKAWNAYPYCRTVITNEYMKEDFLIKIETWHKPDL
PITPβ             (60)    KIYHLKSKVPAFVRMIAPEGSLVFHEKAWNAYPYCRTIVTNEYMKDDFFIKIETWHKPDL
RdgBβ-sp2         (60)    KRVYLNSKLPSWARAVVPK-IFYVTEKAWNYYPYTITEYTCSFLPK-FSIHIETKYEDNK
RdgBβ-sp1         (60)    KRVYLNSKLPSWARAVVPK-IFYVTEKAWNYYPYTITEYTCSFLPK-FSIHIETKYEDNK
Consensus         (61)    KRYHLNSKLPSFVRMVVPKGILYVTEKAWNYYPYTRTEYTNSFLPKDFSIKIETWHKPNL

                          121                                                                          180
PITPα             (120)   GTQENVHKLEPEAWKHVEAVYIDIADRSQVLSKDYKAEEDPAKFKSIKTGRGPLGPNWKQ
PITPβ             (120)   GTLENVHGLDPNTWKTVEIVHIDIADRSQVEPADYKADEDPALFQSVKTKRGPLGPNWKK
RdgBβ-sp2         (118)   GSNDTIFDNEAKDVER-EVCFIDIAC-DEIPERYYKESEDPKHFKSEKTGRGQLREGWR-
RdgBβ-sp1         (118)   GSNDTIFDNEAKDVER-EVCFIDIAC-DEIPERYYKESEDPKHFKSEKTGRGQLREGWR-
Consensus         (121)   GSNDTIHDNEPKDWKRVEVVFIDIADRSQIPERYYKESEDPKHFKSEKTGRGQLRPNWK

                  K195   WW203/204          E218/V218  F225/G225
                          181                                                                          240
PITPα             (180)   ELVNQKDCPYMCAYKLVTVKFKWWGLQNKVENFIHKQERRLFTNFHRQLFCWLDKWVDLT
PITPβ             (180)   ELANSPDCPQMCAYKLVTIKFKWWGLQSKVENFIQKQEKRIFTNFHRQLFCWIDKWIDLT
RdgBβ-sp2         (175)   ----DSHQPIMCSYKLVTVKFEVWGLQTRVEQFVHKVVRDILLIGHRQAFAWVDEWYDMT
RdgBβ-sp1         (175)   ----DSHQPIMCSYKLVTVKFEVWGLQTRVEQFVHKVVRDILLIGHRQAFAWVDEWYDMT
Consensus         (181)   EL NDSHQPIMCAYKLVTVKFKWWGLQTKVENFIHKVVRRILTNGHRQLFCWVDKWYDLT

                          241                                                                          300
PITPα             (240)   MDDIRRMEEETKRQLDEMR----------------QKDPVKGMTADD-------------
PITPβ             (240)   MEDIRRMEDETQKELETMR----------------KRGSVRGTSAADV------------
RdgBβ-sp2         (231)   MDDVREYEKNMHEQTNIKV----------------CNQHSSPVDDIESHAQTST------
RdgBβ-sp1         (231)   MDDVREFERATQEATNKKIGIFPPAISISSIPLLPSSVRSAPSSAPSTPLSTDAPEFLSV
Consensus         (241)   MDDIRRMEKETQEQTN MR                K  VRPTSA DS   T

                          301                                  342
PITPα             (271)   ------------------------------------
PITPβ             (272)   ------------------------------------
RdgBβ-sp2         (269)   ------------------------------------
RdgBβ-sp1         (291)   PKDRPRKKSAPETLTLPDPEKKATLNLPGMHSSDKPCRPKSE
Consensus         (301)
```

B

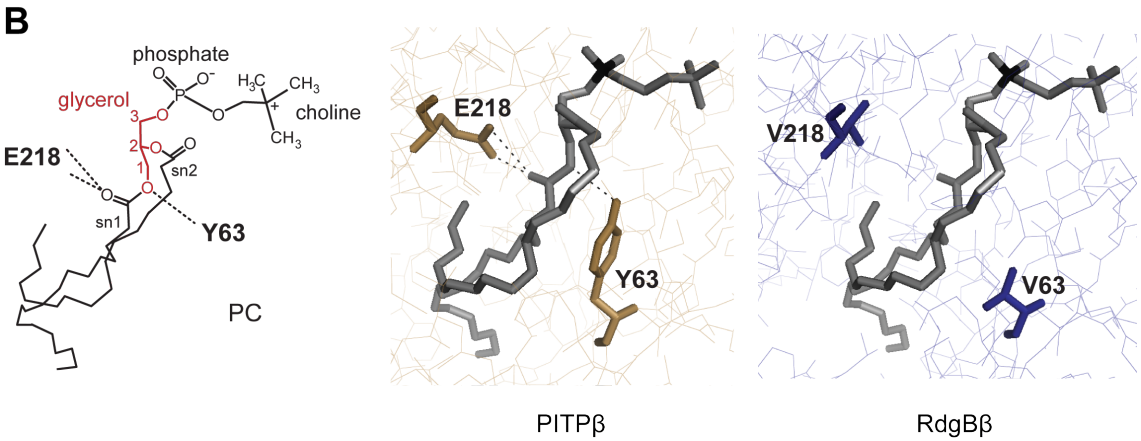

5.3: RdgBβ binds PI and a mystery lipid, rather than PI and PC

The lipid binding properties of RdgBβ-sp1 were assessed by exposing the recombinant protein to HL60 cells which had been metabolically labelled with [^{14}C]-acetic acid and permeabilised with SLO to allow PITP entry. Lipid binding by PITPα was assessed alongside RdgBβ as a positive control.

As previously reported, it is clear that PITPα binds PI and PC in approximately equal quantities (Figure 5.2 A, B). RdgBβ, by contrast, binds only trace amounts of PC, and in addition to PI, binds another lipid, which runs faster than PI on the TLC plate (Figure 5.2 A). RdgBβ binds PI and the mystery lipid in equal amounts (Figure 5.2 B). When the values are adjusted to account for the relative amount of PITP protein recovered, it is clear that RdgBβ binds only one tenth of the amount of phospholipid that PITPα does under these conditions (PITPα, 100 ± 0; RdgBβ 9.9 ± 3.4 SEM, *n*=3).

(Facing page) Figure 5.2: RdgBβ binds PI and a mystery lipid

(A) Assessment of the lipids bound by RdgBβ-sp1 and PITPα after exposure to permeabilised [^{14}C]-HL60 cell membranes. *Left*: TLC plate phosphor image. 'Total' indicates total [^{14}C]-acetic acid-labelled HL60 lipids, 50,000 dpm. *Right*: Coomassie-stained SDS-PAGE gel showing input and output protein quantity. 1, Control (No PITP); 2, PITPα; 3, RdgBβ. (B) Phospholipids bound are expressed as a percentage of the total PC+PI+mystery lipid. Error bars are SEM (PITPα (*n*=6), RdgBβ (*n*=5)). (C) Phospholipids bound are adjusted for the amount of protein recovered, where PI bound by PITPα is set at 100 to enable comparison of multiple datasets. Error bars are SEM; PITPα, *n*=5, RdgBβ, *n*=3.

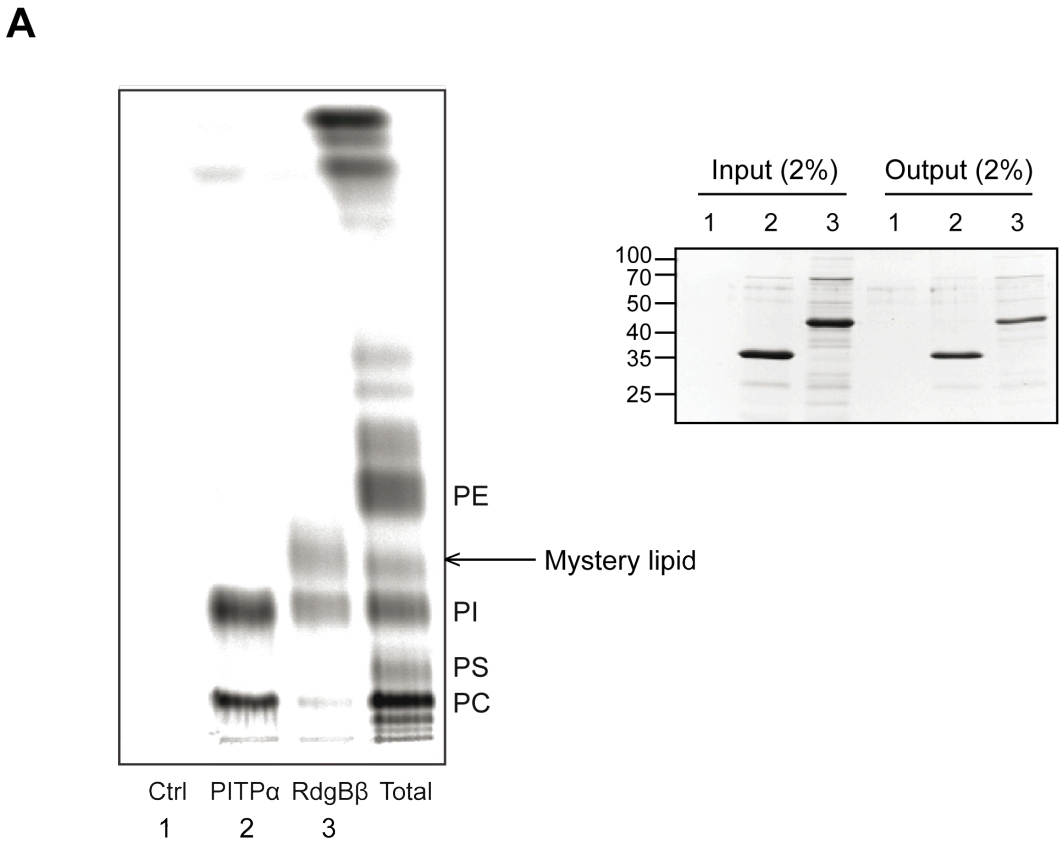
A
Input (2%)
Output (2%)
1 2 3 1 2 3
100
70
50
40
35
25
PE
Mystery lipid
PI
PS
PC
Ctrl PITPα RdgBβ Total
1 2 3
B
PC
PI
Unknown
Lipid binding (%)
60
50
40
30
20
10
0
PITPα
RdgBβ
C
PC
PI
Unknown
Relative lipid binding per µg protein
140
120
100
80
60
40
20
0
PITPα
RdgBβ

5.4: The hunt for the identity of the mystery lipid

RdgBβ binds PI and the mystery lipid in comparable amounts, yet binds little PC. I therefore sought to determine the identity of this mystery lipid.

Figure 5.3 A shows a tracing of unlabelled phospholipid standards which have been run on a TLC plate and stained with iodine. The mystery lipid runs between PI and phosphatidylethanolamine (PE); only a trace contaminant of cardiolipin (CL) is present at this position on the standard phospholipids plate. CL itself is almost exclusively found in mammalian cells in the inner mitochondrial membrane and, since it is composed of two phosphatidic acid (PA) molecules (i.e. a total of four fatty acid chains) connected by a glycerol molecule (Figure 5.3 B), CL would be too large to fit into the lipid-binding cavity of RdgBβ. PA and phosphatidylglycerol (PG) are intermediates in CL synthesis: PA runs to the same place as PE, or slightly higher (Figure 5.3 A), and PG runs between PE and CL (Figure 5.3 C).

(Facing page) Figure 5.3: TLC analysis of unlabelled phospholipids

(A, C) Unlabelled lipids were spotted onto a TLC plate (20µg, as indicated), which was migrated in the solvent system, Chloroform: Methanol: Acetic acid: Water (75: 45: 3: 1). Once dry, the plate was stained with iodine to visualise the lipids. The lipid spots were traced in pencil and the image scanned using a flatbed scanner. The darkest spots have been shaded. CL, cardiolipin; PA, phosphatidic acid (Sigma-Aldrich, P9511); PE, phosphatidylethanolamine; PG, phosphatidylglycerol; PS, phosphatidylserine; PI, phosphatidylinositol (~50% purity reported - contains PE and possibly PA contamination; Sigma-Aldrich, P6636); PC, phosphatidylcholine; SM, sphingomyelin. (B) The molecular structure of CL.

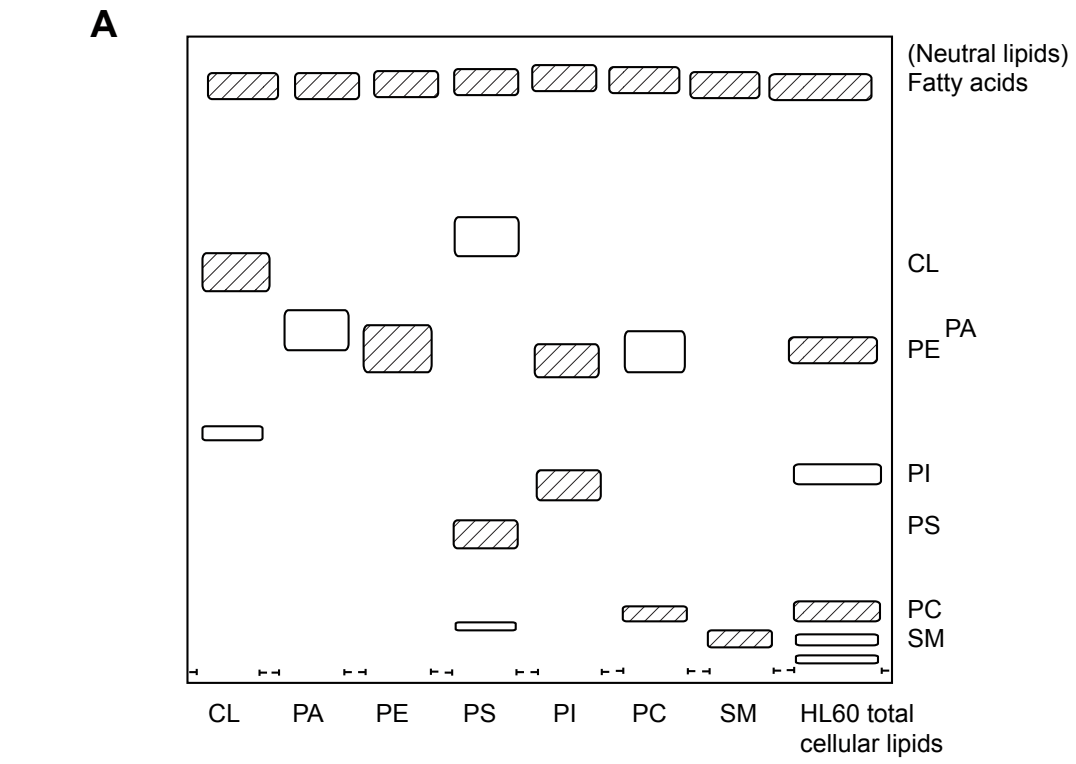
A
(Neutral lipids)
Fatty acids
CL
PA
PE
PI
PS
PC
SM
CL
PA
PE
PS
PI
PC
SM
HL60 total
cellular lipids

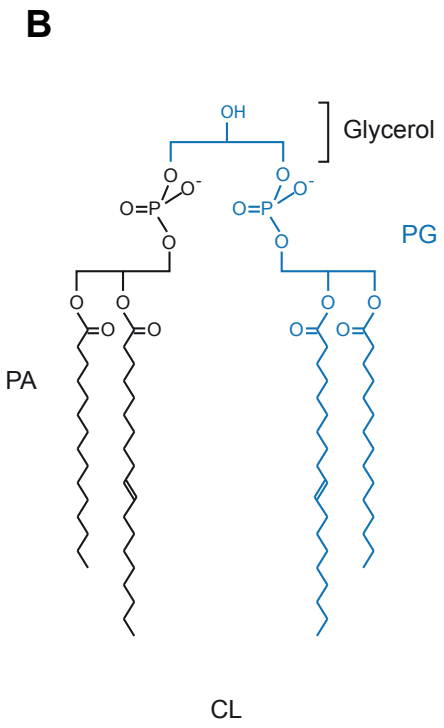
B
OH
Glycerol
PG
PA
CL

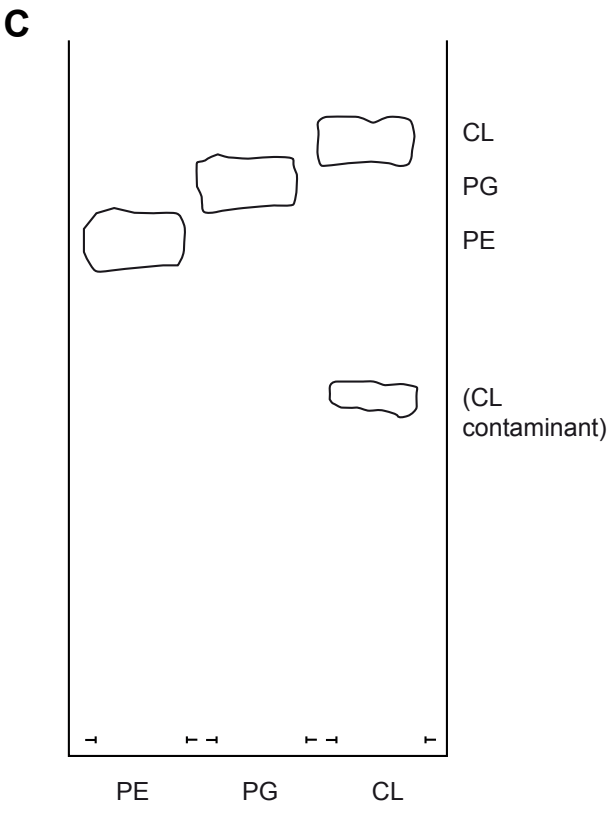
C
CL
PG
PE
(CL
contaminant)
PE
PG
CL

To further advance the search for the mystery lipid, 20 mL volumes of HL60 cells were labelled with different radionucleotides: [^{3}H]-sphingosine, [^{3}H]-choline chloride, [^{3}H]-inositol, [^{3}H]-ethanolamine, [^{3}H]-palmitate, [^{14}C]-acetic acid. The lipids were extracted and appropriate quantities run side-by-side on a TLC plate (Figure 5.4). Some [^{3}H]-sphingosine-labelled lipids appear to run between PI and PE. I therefore carried out a lipid binding assay exactly as for [^{14}C]-acetate labelling, only labelling cells with [^{3}H]-sphingosine for 24 hrs prior to the experiment. No [^{3}H]-sphingosine-labelled lipids were enriched in the RdgBβ-bound material (Figure 5.5). Only sphingomyelin (SM) and sphingosine were observed in the 'Total' lipids lane.

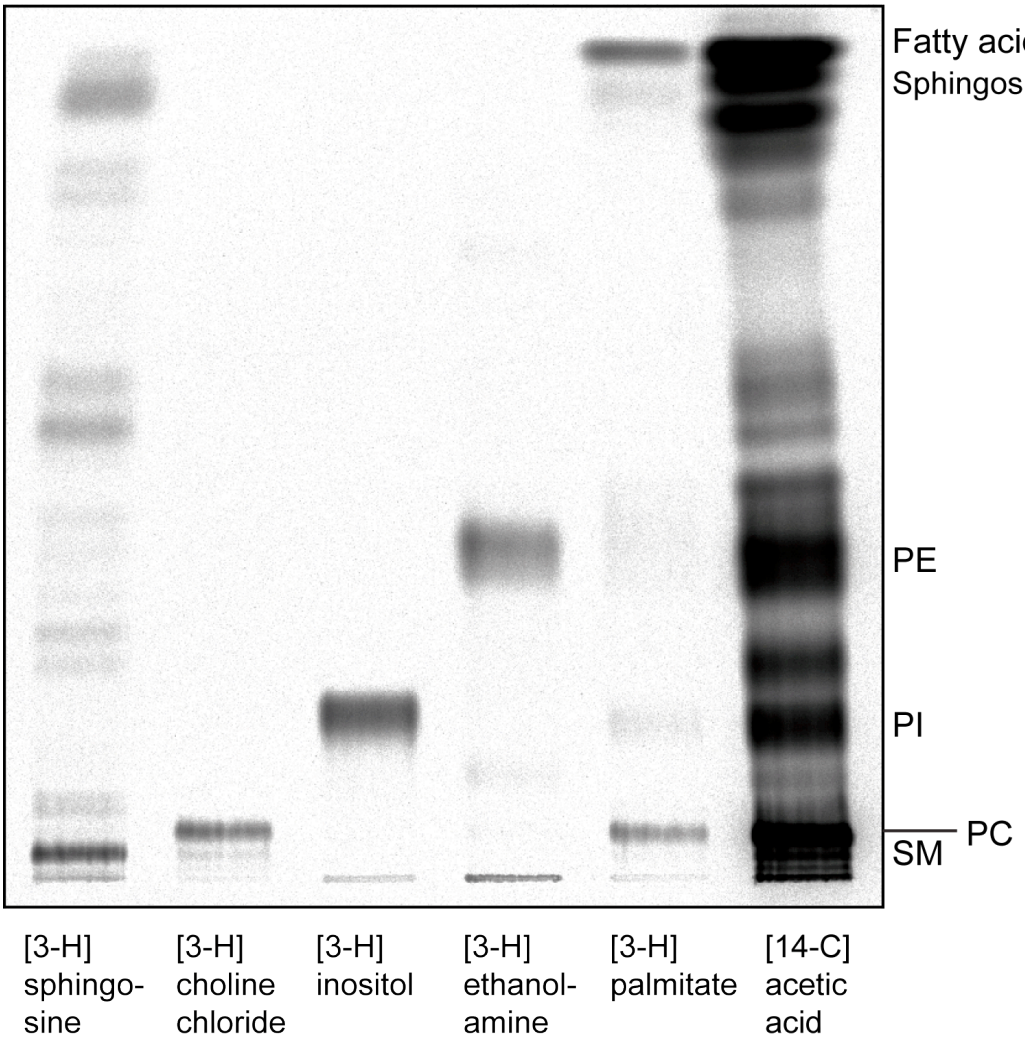

Figure 5.4: Labelling HL60 cells with different radionucleotides

HL60 cells were labelled with different radionucleotides and the lipids extracted. 75,000-200,000 dpm of each lipid was spotted per lane of the TLC plate (detailed in Table 2.9).

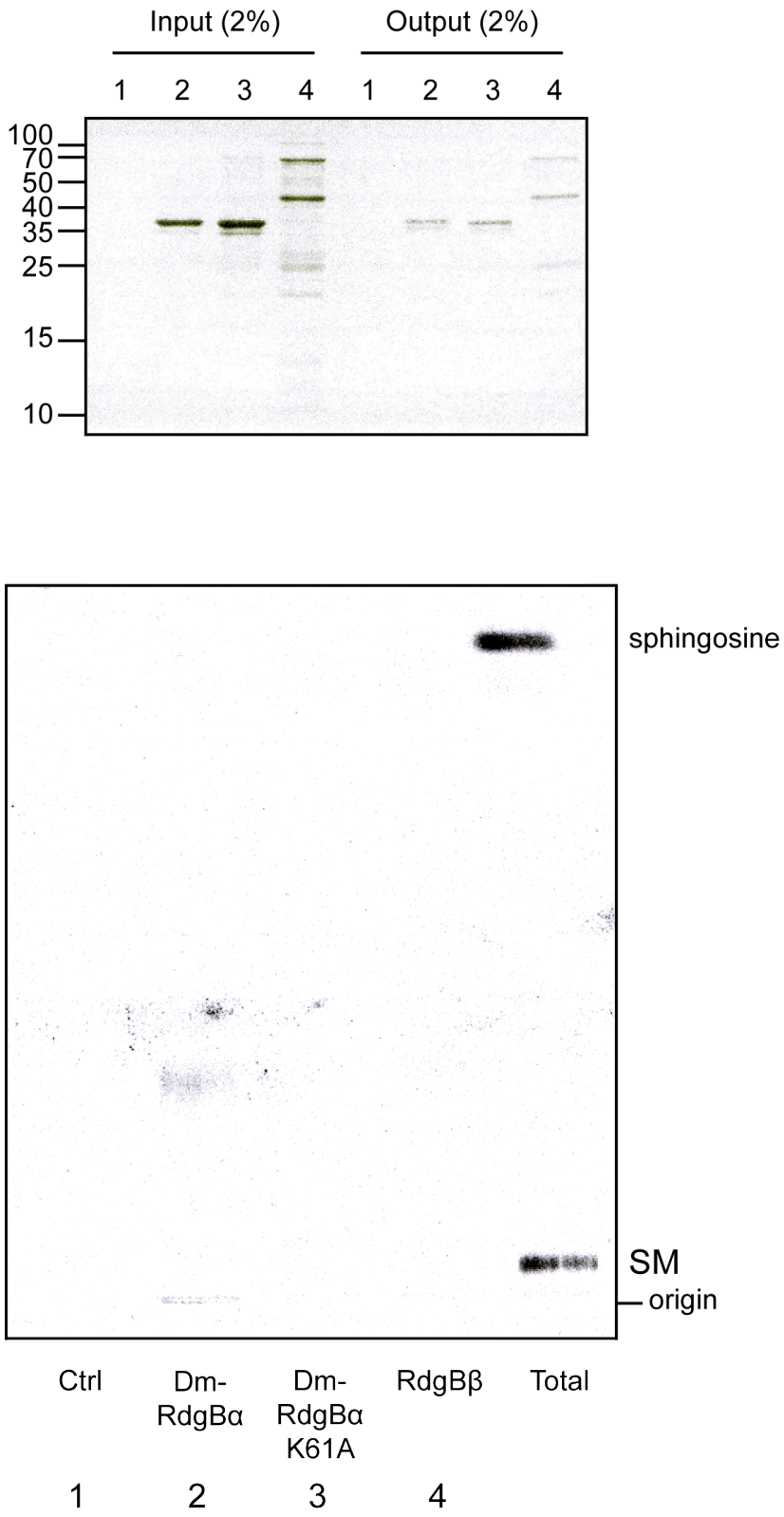

Figure 5.5: RdgBβ does not bind [^{3}H] sphingosine-labelled lipids

120 µg recombinant RdgB proteins were exposed to permeabilised [^{3}H]-sphingosine HL60 cells prior to re-capture and lipid extraction. *Upper panel*: Coomassie-stained SDS-PAGE gel showing input and output proteins. *Lower panel*: TLC plate. 50,000 dpm [^{3}H]-sphingosine-labelled HL60 cell lipids were spotted into the 'Total' lipid lane.

Sphingolipids are built from sphingosine, an amino alcohol with a long, unsaturated hydrocarbon chain, rather than glycerol. To this, a single fatty acid is attached by an amide bond; in glycerol phospholipids two fatty acids are attached to the glycerol backbone using ester bonds (Figure 5.6). This property can be used to deduce whether a given lipid is a sphingolipid or a glycerol phospholipid using the chemical, monomethylamine. Monomethylamine is a primary amine (strong nucleophile), which reacts with esters to form amides. The reaction is an *O*→*N*-transacylation, with the formation of fatty acid amides or *N*-methyl fatty acids. RdgBβ-bound [^{14}C]-acetate-labelled lipids were first subjected to two-dimensional TLC to purify the lipids (Figure 5.7 A). The PI and mystery lipid spots were identified by comparison with 2D plates run using the same solvent system by other members of the laboratory, the silica scraped and the lipids re-extracted. The extracted lipids were divided into two eppendorf tubes and treated without or with monomethylamine reagent for 30 min at 53°c. Both PI and mystery lipid spots migrated to the top of the plate after treatment (Figure 5.7 B), indicating that both phospholipids contain two ester linages.

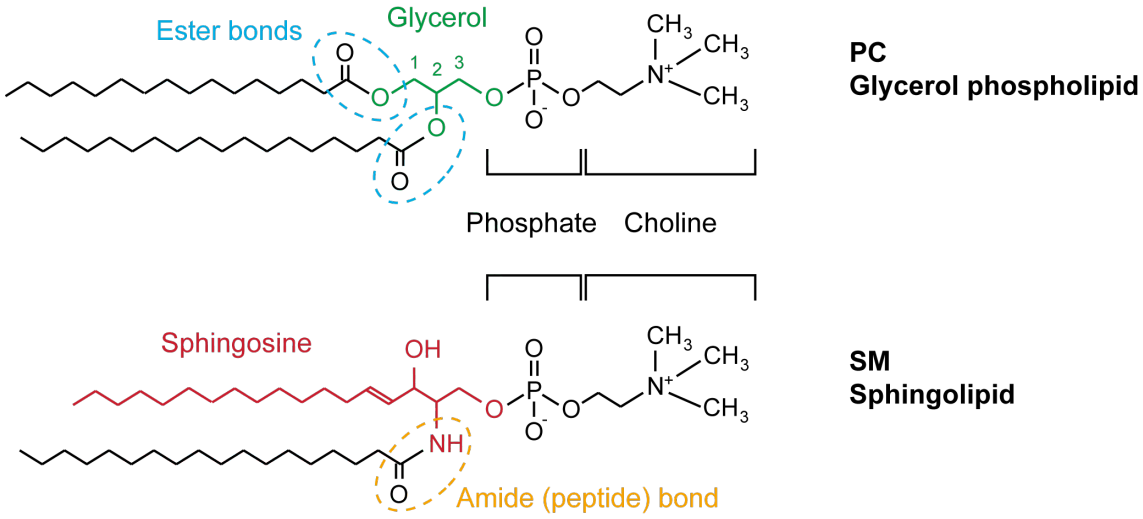

Figure 5.6: The structures of glycerol phospholipids and sphingolipids
Both PC and SM have a phosphate group and a choline group, yet their fatty acid groups are attached in different ways: two fatty acid groups are attached to the glycerol backbone in glycerol phospholipids via ester bonds; a single fatty acid connects to sphingosine in sphingolipids via an amide bond.

(Facing page) Figure 5.7: The mystery lipid is a glycerol phospholipid

(A) Two-dimensional TLC analysis using the solvent systems indicated. *Left panel*: Total [^{14}C]-acetate HL60 cellular lipids (10 µL, 2,400,000 dpm, equivalent to 4 mL cells). *Right panel*: RdgBβ-bound lipids (300 µg recombinant protein), spiked with lipids extracted from 4 mL unlabelled HL60 cells, so that approximately the same amount of lipid was run on both 2D plates. (B) The PI and mystery lipid spots were excised and the lipids re-extracted from the silica. The PI and mystery lipid were treated with monomethylamine reagent for 30 min at 53°c. The lipids were then re-extracted and run on a TLC plate adjacent to untreated samples. (Solvent system: Chloroform: Methanol: Acetic Acid: Water (75: 45: 3: 1 (*v*/*v*)).

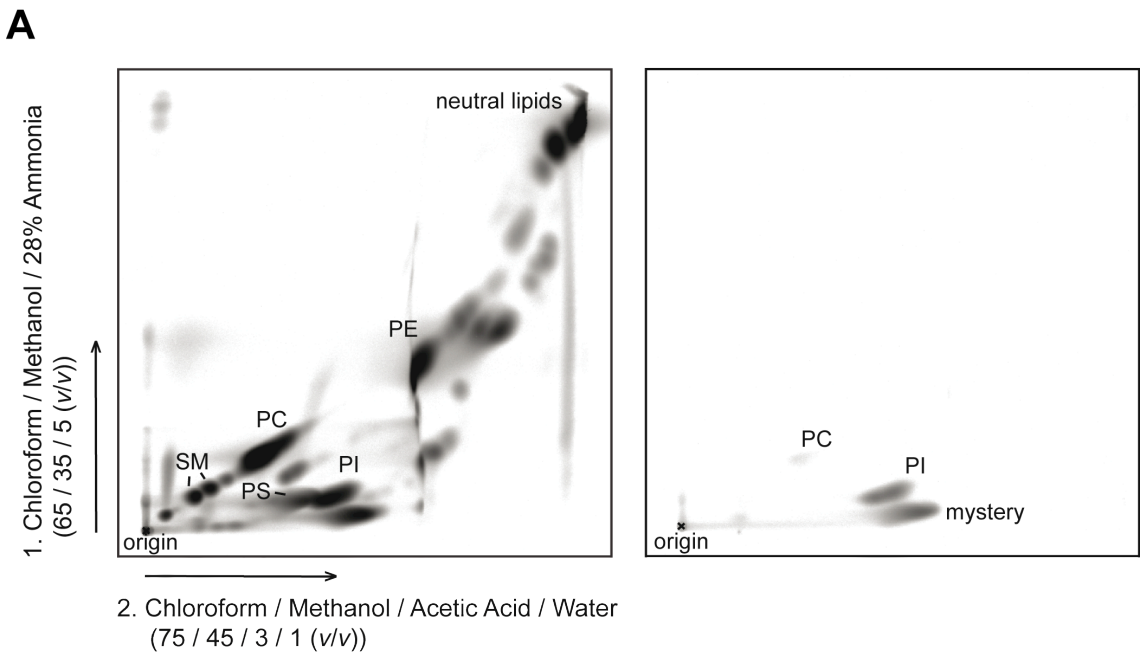
A
1. Chloroform / Methanol / 28% Ammonia
(65 / 35 / 5 (v/v))
neutral lipids
PE
PC
SM
PI
PS
origin
PC
PI
mystery
origin
2. Chloroform / Methanol / Acetic Acid / Water
(75 / 45 / 3 / 1 (v/v))

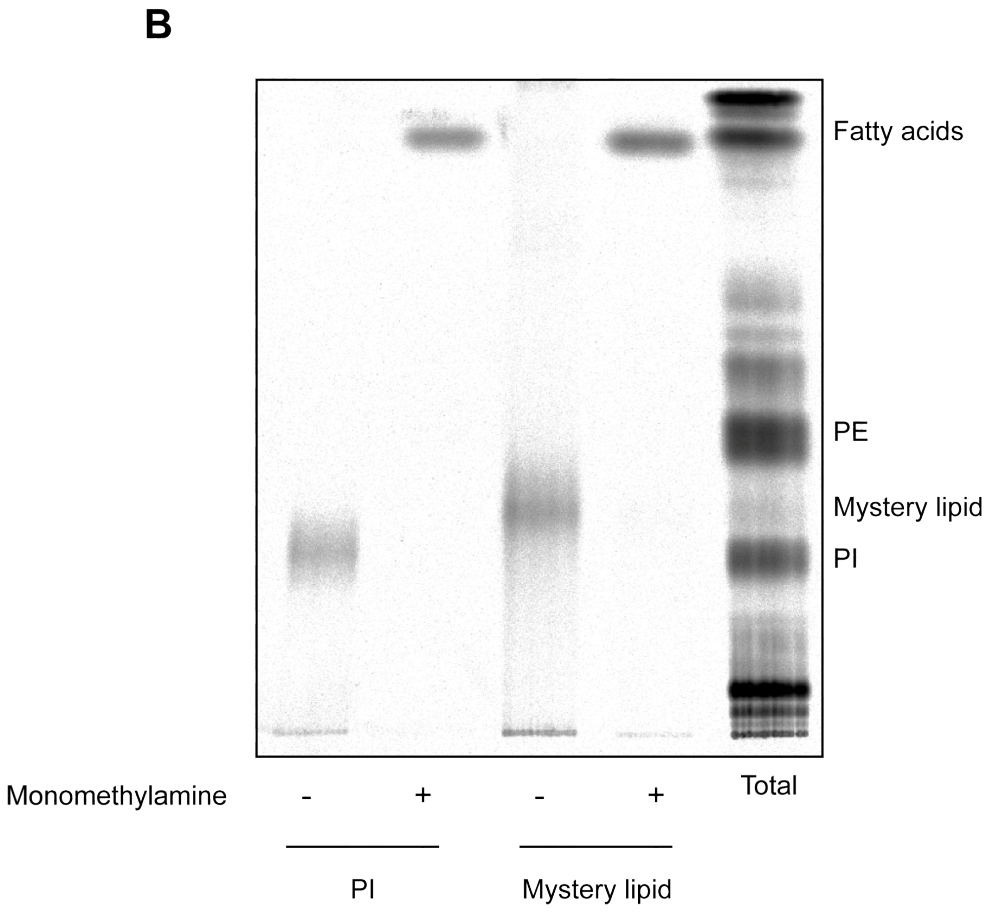
B
Fatty acids
PE
Mystery lipid
PI
Monomethylamine
-
+
-
+
Total
PI
Mystery lipid

5.5: Could the mystery lipid be a PE derivative?

Whereas the major route of PC synthesis is through the Kennedy (CDP-choline) pathway, a minor route comprises the step-wise methylation of PE to PC by two PE *N*-methyltransferase (PEMT) enzymes. The methylated intermediates, phosphatidyl-*N*-monomethyl-ethanolamine (PMME) and phosphatidyl-*N*,*N*-dimethylethanolamine (PDME), would therefore migrate between PE and PC on a TLC plate. I therefore wondered whether the mystery lipid would label with [^{3}H]-ethanolamine.

I carried out a lipid binding assay, this time using HL60 cells labelled with [^{3}H]-ethanolamine. An [^{3}H]-ethanolamine-labelled lipid was observed in material bound by RdgBβ (Figure 5.8), and I hypothesised that this lipid was PMME. The Kennedy pathway can synthesise PC or PE, and involves the activity of three enzymes, whose substrate specificity overlaps between ethanolamine and choline (Gibellini and Smith, 2010). In addition, monomethyl- and dimethyl-ethanolamine can be used as substrates in the Kennedy pathway (Ishidate, 1997), to yield PMME and PDME, respectively. To increase the concentration of [^{14}C]-PMME in the HL60 cells, I labelled cells with [^{14}C]-acetic acid in two flasks, and supplemented one of the cultures with 400 μM 2-(methylamino)ethanol (monomethyl-ethanolamine). The lipid binding assay was performed using these cells, and the bound lipids separated by TLC alongside an unlabelled PMME standard (Figure 5.9).

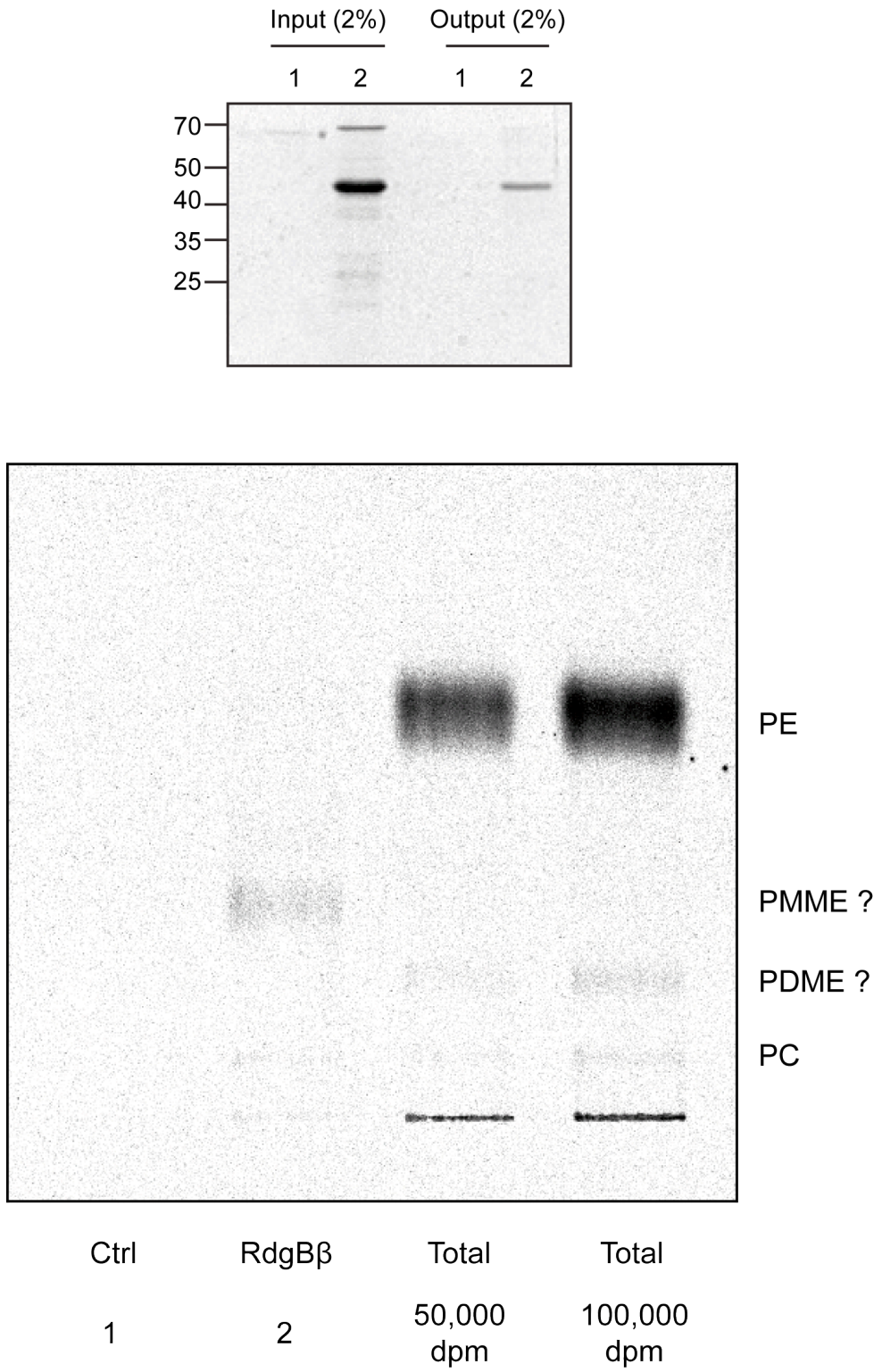

Figure 5.8: RdgBβ binds a [^{3}H]-ethanolamine-labelled lipid

HL60 cells were labelled with [^{3}H]-ethanolamine for 72 hrs, permeabilised, and then incubated with 120 µg recombinant RdgBβ-sp1 for 20 mins. The recombinant protein was re-captured using its His-tag, and the lipids bound extracted and separated by TLC. *Upper panel*: Coomassie-stained SDS-PAGE gel showing input and output protein. *Lower panel*: TLC plate.

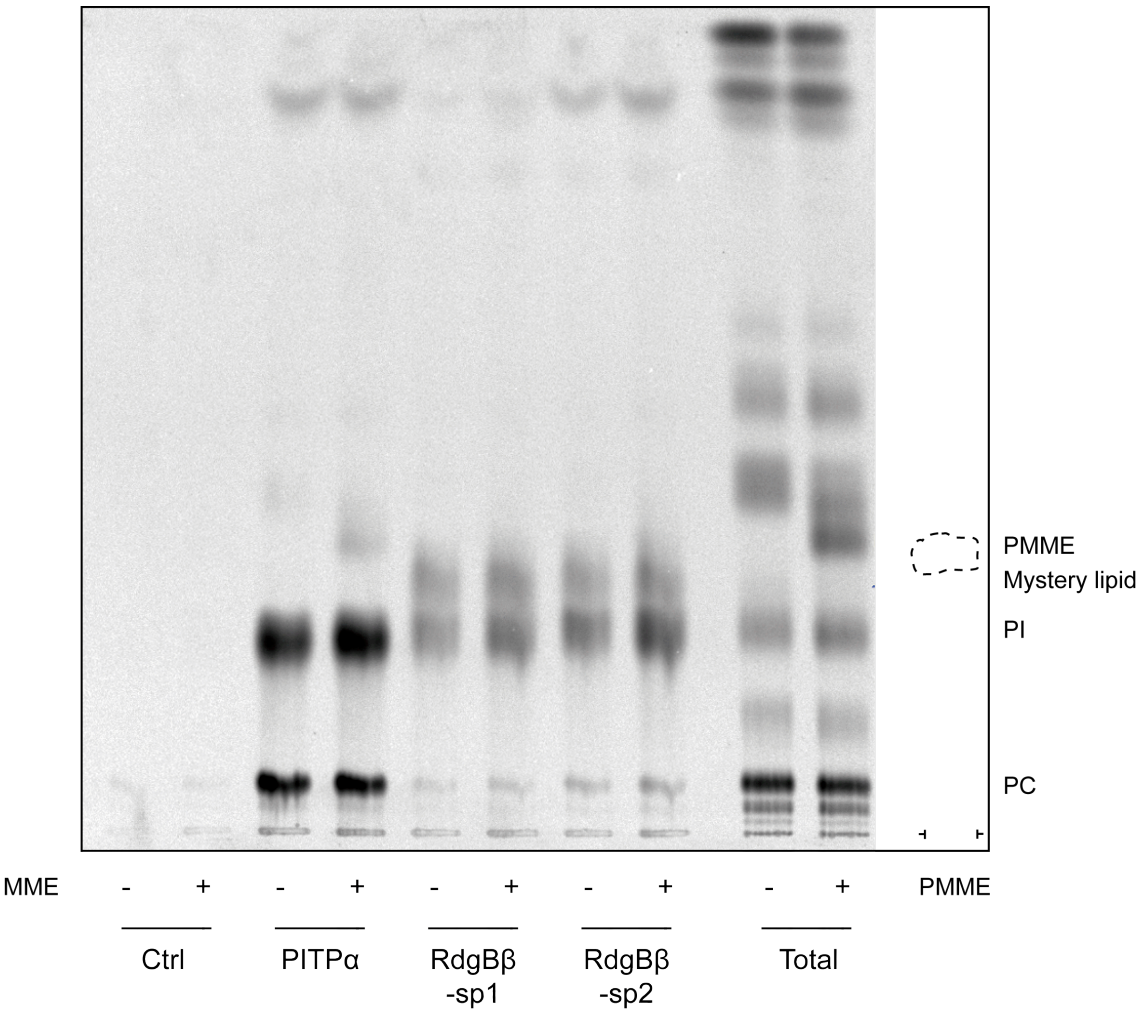

Figure 5.9: The mystery lipid is not PMME

HL60 cells were labelled with 1 μCi.mL^{-1} [^{14}C]-acetic acid +/- 400 μM 2-(methylamino) ethanol ('MME') for 72 hrs, prior to permeabilisation and use in the lipid binding assay. Recombinant proteins, PITPα, RdgBβ-sp1, RdgBβ-sp2, were exposed to the permeabilised cells before being re-captured using their His tags. The bound lipids were extracted and separated by TLC. The unlabelled lipid, PMME, was run alongside the radioactive lipids. 100,000 dpm total HL60 lipids were spotted into the 'Total' lanes. TLC plate shown.

A clear enrichment of PMME in the Total lipids lane was observed just below PE (Figure 5.9). The unlabelled PMME standard partially overlaps with both the radioactive PMME and the mystery lipid. Crucially, however, no enrichment in the mystery lipid was observed when RdgBβ was exposed to the cells with the PMME enrichment, indicating that the mystery lipid is not PMME. By contrast, PITPα does bind a small amount of radioactive PMME.

RdgBβ-sp2 was omitted from the lipid binding assays on the whole, since recombinant RdgBβ-sp2 protein preparations were less pure than those of RdgBβ-sp1, and consequently produced a lower yield. In Figure 5.9, RdgBβ-sp2 was observed to bind the same lipids as RdgBβ-sp1, in the same proportions.

Lyso-PE is another lipid that would label with [^{3}H]-ethanolamine and as it only has a single fatty acid chain, would migrate less far than PE on a TLC plate. Purified HL60 cell lipids labelled with [^{3}H]-ethanolamine from previous experiments were combined and treated with phospholipase A_2 (PLA_2) from bee venom. PLA_2 removes the fatty acid from the *sn*2 position of the glycerol backbone of phospholipids to yield the lyso-phospholipid and free fatty acid. PLA_2-treated PE was resolved on a TLC plate alongside unlabelled PE, PMME and PI standards (Figure 5.10). The solvent-soluble product (lyso-PE) migrates less far than PI, indicating that the mystery lipid is not lyso-PE.

The PI standard used was that from Sigma-Aldrich (P6636). The manufacturers report that this phospholipid sample is ~50% pure, with PE and possibly PA contaminants. In Figure 5.3, a lipid corresponding to PE only was observed. In Figure 5.10, an additional lipid migrating to between PI and PE is observed. In Figure 5.3, I also noted that PA migrates slightly further than PE, and therefore the identity of the additional PI contaminant in Figure 5.10 is unclear.

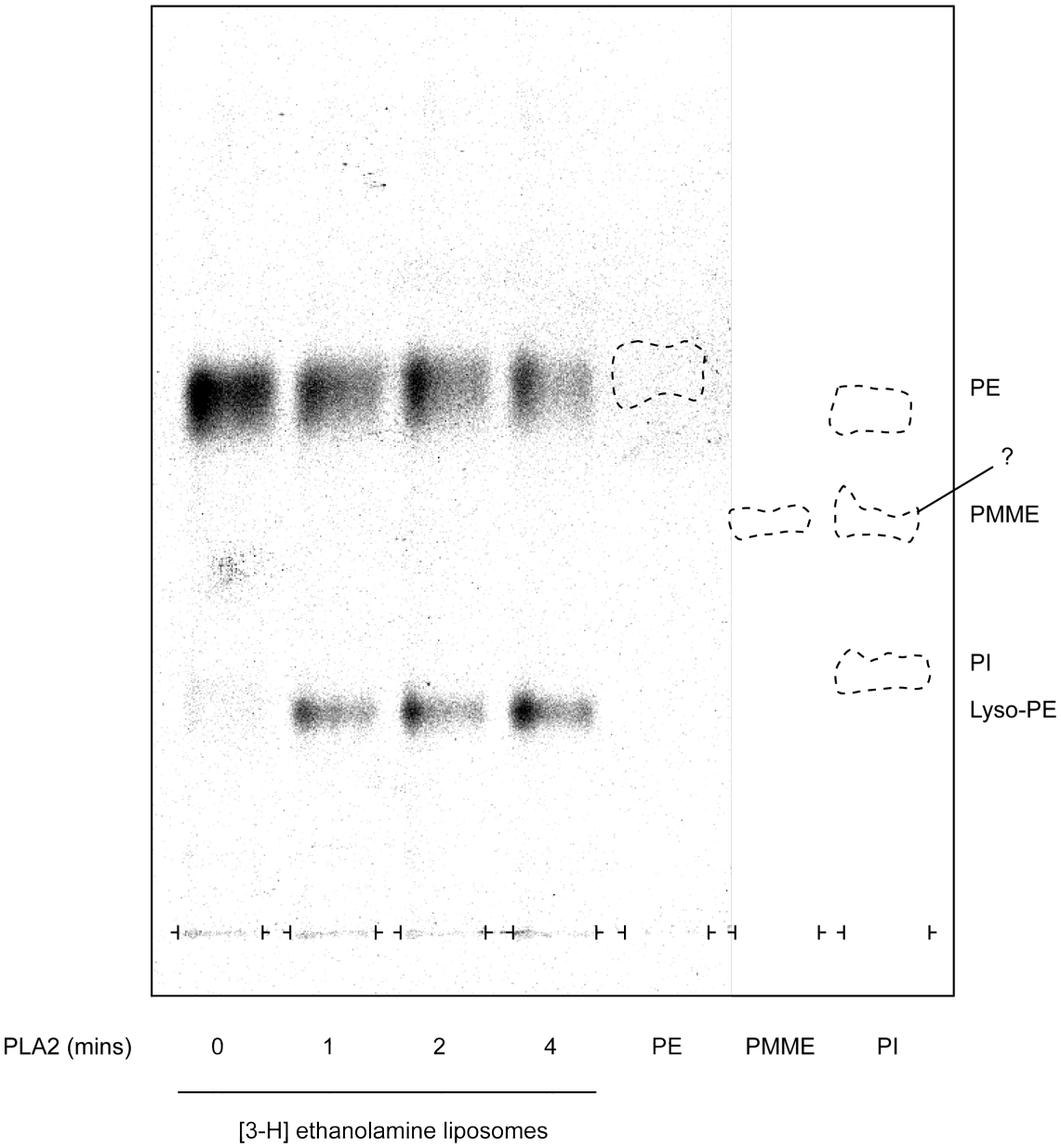

Figure 5.10: The mystery lipid is not lyso-PE

[^{3}H]-ethanolamine-labelled liposomes were treated with PLA_2 for the time periods indicated. The solvent-soluble product (lyso-PE) was resolved using TLC (100,000 dpm) alongside 20 µg of each unlabelled phospholipid standard (PE, PMME, PI). TLC plate shown.

Meanwhile, lipid binding experiments were carried out using [^{3}H]-choline- and [^{3}H]-inositol-labelled HL60 cells. The cells were labelled exactly as for the experiment using [^{3}H]-ethanolamine-labelled HL60 cells, i.e. for 72 hrs. RdgBβ bound some PI, as expected, which was less than the PITPα-bound PI (Figure 5.11). RdgBβ was not observed to bind PC, whereas PITPα clearly bound PC. In addition, in the lipids extracted from PITPα, a [^{3}H]-choline-labelled lipid was observed above PC, approximately in line with the PI labelled with [^{3}H]-inositol, and a [^{3}H]-inositol-labelled lipid was seen below PI, in line with PC labelled with [^{3}H]-choline.

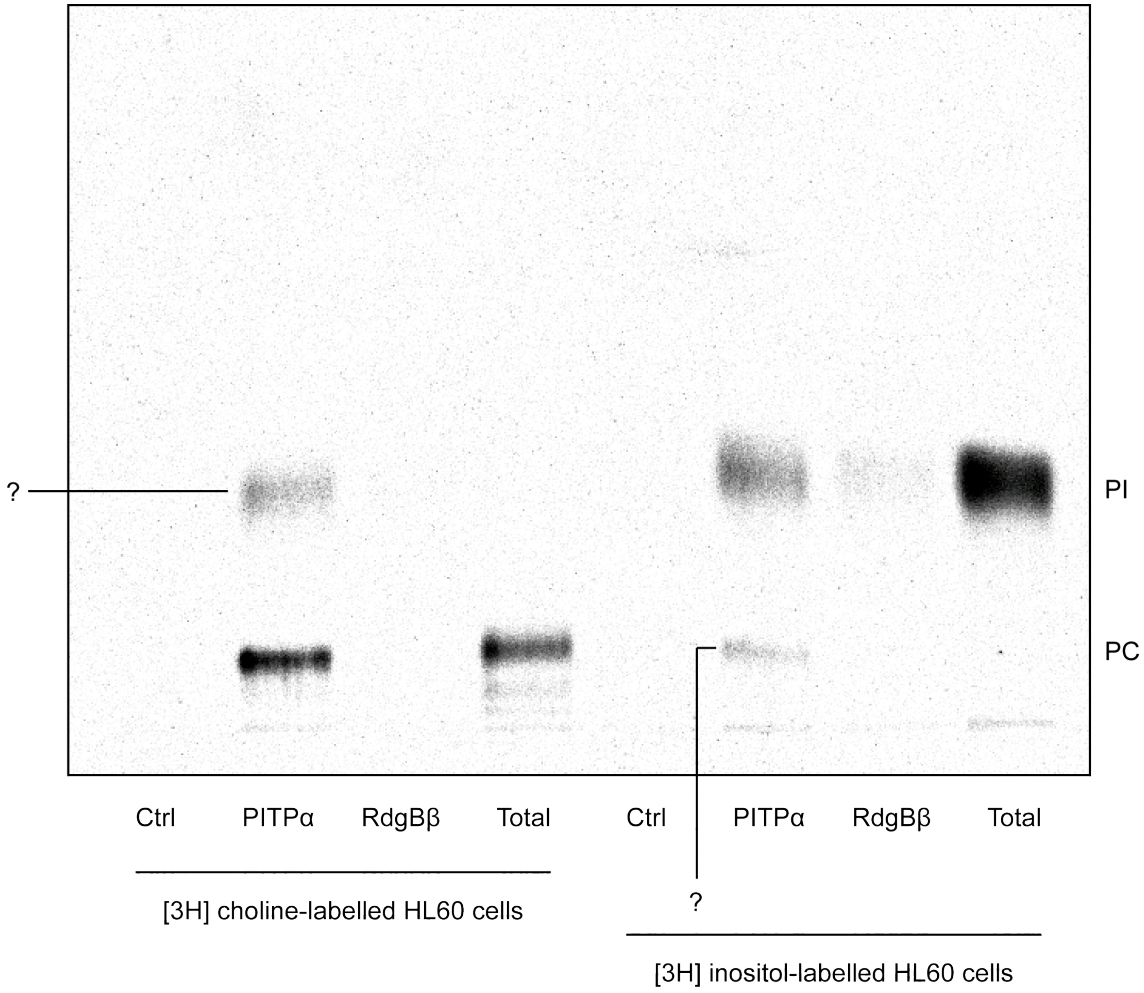

Figure 5.11: Binding of [^{3}H]-choline and [^{3}H]-inositol-labelled lipids by PITPα

HL60 cells labelled with either [^{3}H]-choline chloride (1 μCi.mL^{-1}, 72 hrs) or [^{3}H]-inositol (2 μCi.mL^{-1} M199 medium, 72 hrs), were permeabilised and used in the lipid binding assay. Lipids bound by PITPα and RdgBβ-sp1 were resolved by TLC alongside 50,000 dpm total labelled lipids. TLC plate shown.

5.6: RdgBβ binds PA

The mystery lipid did not co-migrate with any known lipid standards, and although it was observed to label with [^{3}H]-ethanolamine, further experiments ruled out PE derivatives, PMME and lyso-PE, as possible mystery lipid candidates. I therefore sought the assistance of our collaborators, Dr. Alan Hunt and Grielof Koster at the University of Southampton. The lipid binding assay was scaled up to 600 μg recombinant protein and 50 mL (unlabelled) HL60 cells, and the lipids extracted from RdgBβ-sp1 for analysis by mass spectrometry. The molecular species of PI and PC have previously been identified using the same method for PITPα (Hunt et al., 2004), and therefore PITPα was used here as a control. Mass spectrometric analysis revealed that the mystery lipid picked up by RdgBβ was phosphatidic acid (PA).

The acyl chains of PI and PA vary according to the source of the phospholipid: the dominant species of PI in mammalian cells is long chain, polyunsaturated, C18:0/20:4 (*sn*-1-stearoyl-2-arachidonyl), whereas the dominant PC is short-chain, mono-unsaturated or saturated species. PA can be produced either by the hydrolysis of PI(4,5) P_2 by PLC, yielding DAG, which is subsequently phosphorylated to PA by DGK, or by the hydrolysis of PC by PLD, to PA and choline. Analysis of the molecular species of PA bound by RdgBβ using precursor scans of the *m*/*z* -153 fragment revealed that RdgBβ-bound lipids were enriched in short-chain monounsaturated or saturated PA species, specifically C16:0/16:1 (*m*/*z* 645, ~27%) and C16:1/18:1 (*m*/*z* 671, ~23%) species. These species made up ~15% and ~10% of the cellular PA pool, respectively (Figure 5.12 and Table 5.1). By contrast, cellular PA contained a higher proportion of the C16:0/16:0 species (*m*/*z* 647, ~17%), than the RdgBβ-bound PA (~7%). PA molecular species were not observed in the lipid sample extracted from PITPα by mass spectrometry.

Whereas RdgBβ bound short-chain, saturated or monounsaturated PA species (C16:0/16:1 and C16:1/18:1), the PI molecular species bound were long-chain, polyunsaturated species. These are also the most common PI species in mammalian cells. A representative trace of PI species bound by RdgBβ looks remarkably similar to

the profile of PI molecular species in mammalian cells (Figure 5.13, Upper panel and inset).

By comparison, the PI species bound by PITPα were enriched in short-chain, saturated or monounsaturated species, C16:0/16:1 and C16:1/18:1, as previously reported (Hunt et al., 2004).

(Facing page) Figure 5.12: Analysis of PA species bound by RdgBβ and in HL60 cell extracts

(A) Recombinant RdgBβ protein (600 µg) was exposed to permeabilised HL60 cell membranes for 20 mins at 37°c, then recaptured using its His-tag. The lipids bound were extracted and analysed by mass spectrometry. A representative ESI-MS/MS precursor scan of the *m*/*z* -153 fragment in negative ionisation is shown. (B) A second example of a precursor scan of *m*/*z* -153 fragment of the PA species bound by RdgBβ (*upper panel*), together with a scan showing the total PA species present in HL60 cells. Dashed ellipses indicate enriched PA species. (Mass spectrometry and data analysis carried out by Dr. Alan Hunt and Grielof Koster at the University of Southampton.)

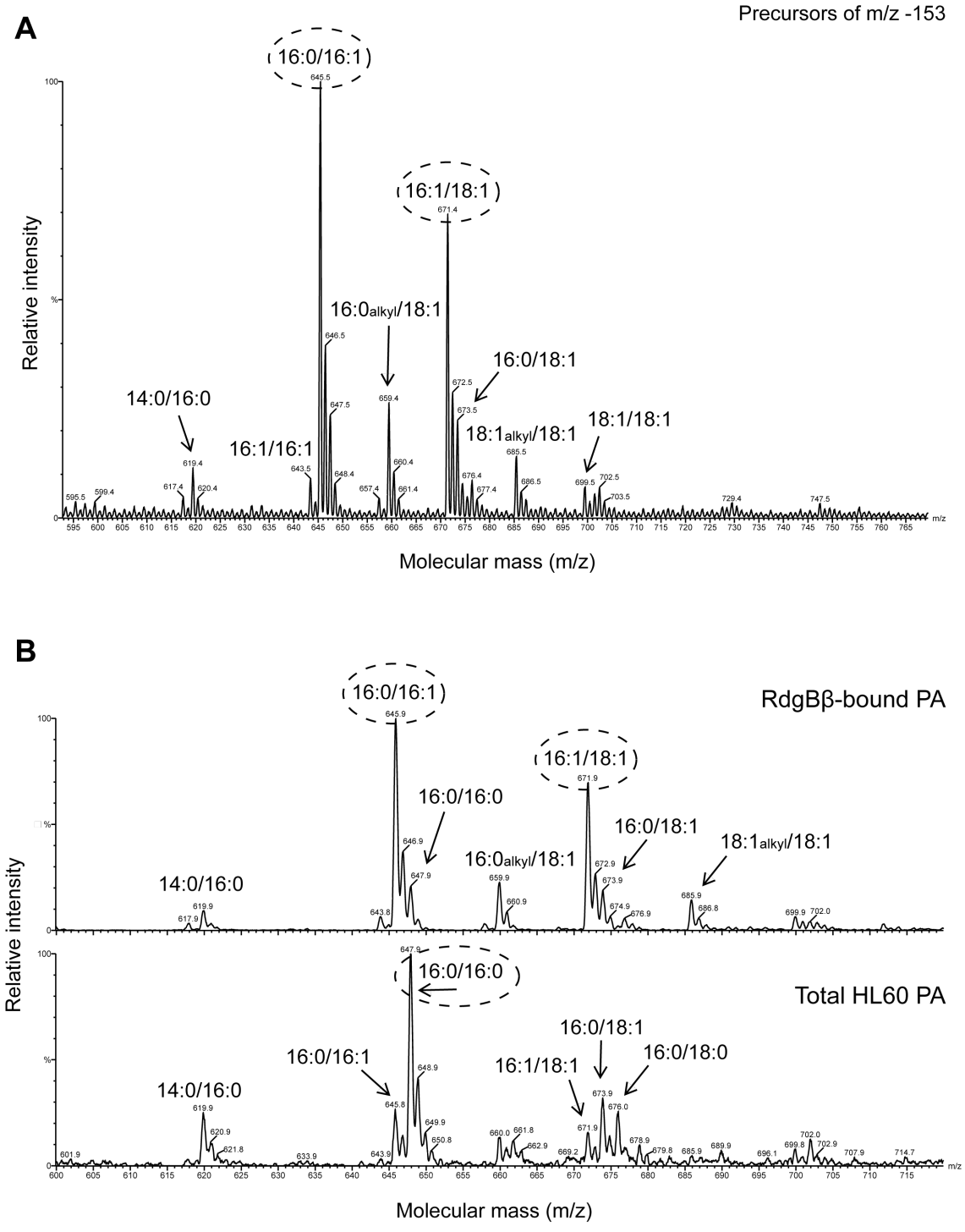
A
Precursors of m/z -153
16:0/16:1
16:1/18:1
16:0alkyl/18:1
16:0/18:1
14:0/16:0
16:1/16:1
18:1alkyl/18:1
18:1/18:1
Relative intensity
Molecular mass (m/z)
B
RdgBβ-bound PA
16:0/16:1
16:1/18:1
16:0/16:0
16:0/18:1
18:1alkyl/18:1
16:0alkyl/18:1
14:0/16:0
Total HL60 PA
16:0/16:0
16:0/18:1
16:0/18:0
16:0/16:1
16:1/18:1
14:0/16:0
Relative intensity
Molecular mass (m/z)

Mass (*m/z*)	Total Carbon: double bonds	Dominant molecular species	Total HL60 PA (%)	PA bound by RdgBβ
619	C30:0	14:0/16:0	10.00 ± 1.47	5.02 ± 0.63 *
643	C32:2	16:1/16:1	4.74 ± 0.70	6.14 ± 0.93
645	C32:1	16:0/16:1	14.59 ± 1.59	26.90 ± 5.27 *
647	C32:0	16:0/16:0	16.77 ± 4.18	7.09 ± 0.58 *
671	C34:2	16:1/18:1	9.94 ± 0.97	23.09 ± 2.80 **
673	C34:1	16:0/18:1	10.82 ± 0.57	7.32 ± 0.59 **
699	C36:2	18:1/18:1	11.52 ± 2.20	6.09 ± 1.14 *
701	C36:1	18:0/18:1	7.56 ± 0.65	6.02 ± 1.61

Table 5.1: PA species bound by RdgBβ

Comparison of the molecular species of PA present in whole HL60 cells with PA bound by RdgBβ. The species identified represent the dominant species from ESI-MS/MS fragmentation analysis. Errors are SEM, n=6. The significance of the fraction of individual PA species bound by RdgBβ compared with the fraction of that species present in whole HL60 cells has been assessed, and p values are indicated: * $p<0.05$, ** $p<0.005$. (Mass spectrometry and data analysis carried out by Dr. Alan Hunt and Grielof Koster at the University of Southampton.)

(Facing page) Figure 5.13: Molecular PI species bound by RdgBβ and PITPα

Recombinant RdgBβ or PITPα protein (600 µg) was exposed to permeabilised HL60 cell membranes for 20 mins at 37°c, then recaptured using its His-tag. The lipids bound were extracted and analysed by mass spectrometry. Representative ESI-MS/MS precursor scans of *m*/*z* -241 precursor in negative ionisation showing PI species bound by RdgBβ (*upper panel*) and PITPα (*lower panel*). *Inset*: Relative quantities of total PI species present in HL60 cells (taken from Hunt et al., 2004 (Fig. 2)). (Mass spectrometry and data analysis carried out by Dr. Alan Hunt and Grielof Koster at the University of Southampton.)

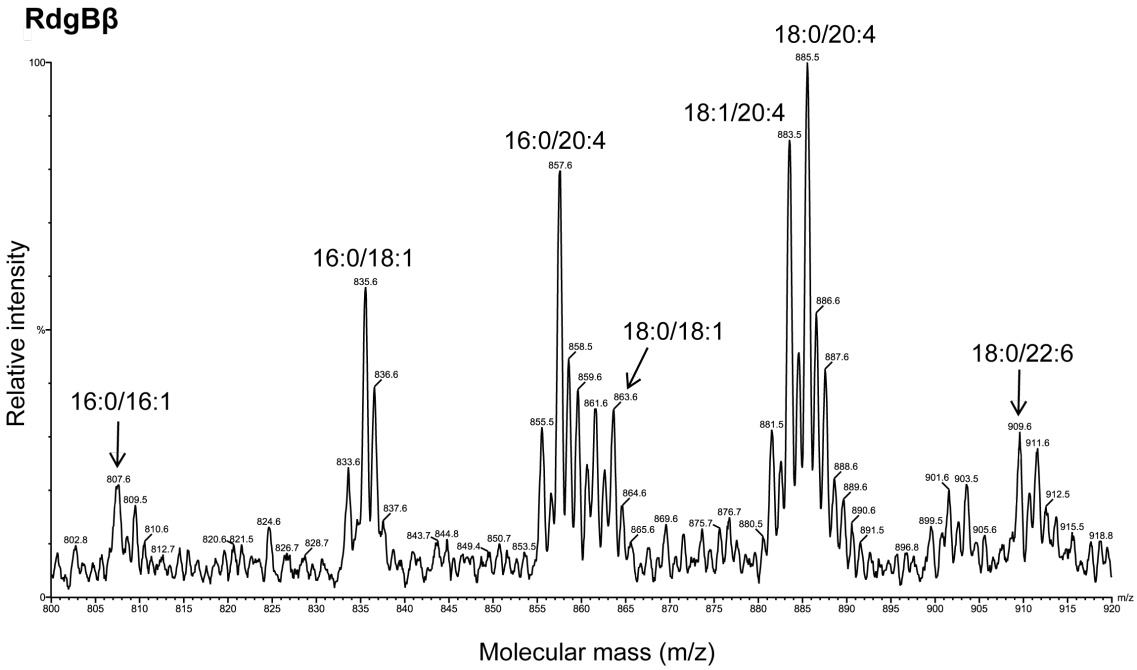
RdgBβ
Relative intensity
Molecular mass (m/z)
16:0/16:1
16:0/18:1
16:0/20:4
18:1/20:4
18:0/20:4
18:0/18:1
18:0/22:6

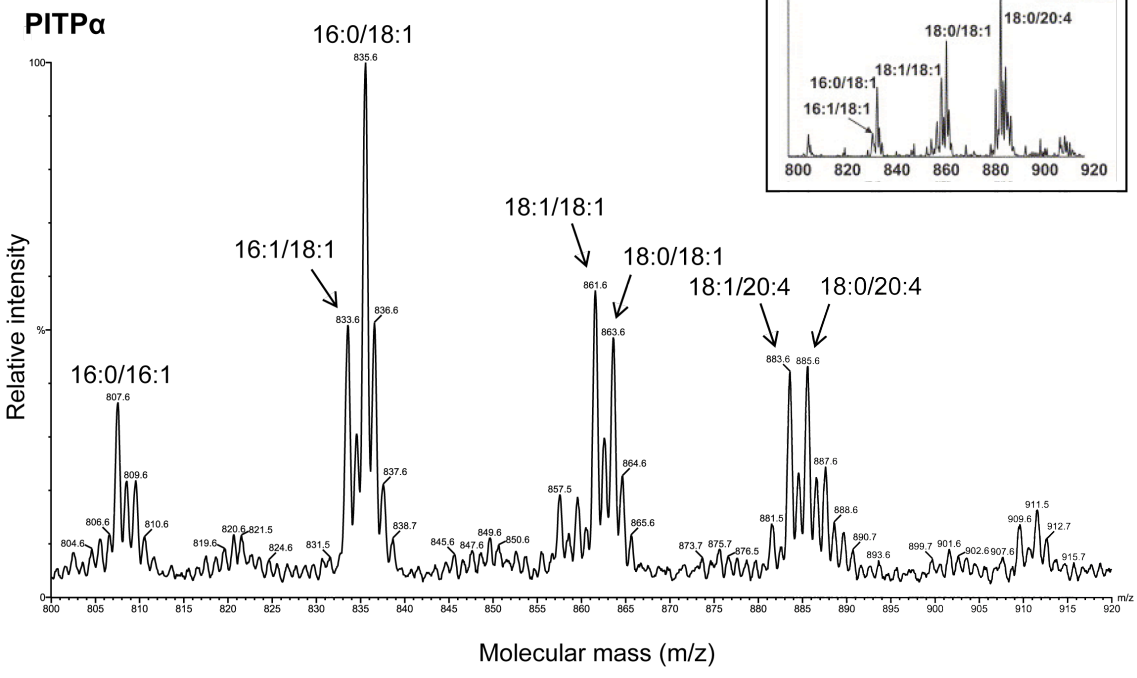
PITPα
Relative intensity
Molecular mass (m/z)
16:0/16:1
16:0/18:1
16:1/18:1
18:1/18:1
18:0/18:1
18:1/20:4
18:0/20:4

Total HL60 cell PI
Precursors of m/z -241
16:0/18:1
16:1/18:1
18:1/18:1
18:0/18:1
18:0/20:4

PA was previously rejected as a candidate for the mystery lipid as the standard did not co-migrate with the lipid bound by RdgBβ, but instead migrated past PE. It now seemed possible that PA species with different acyl chains might migrate differently during TLC. To explore this notion further I sourced additional PA samples and spotted them side-by-side on a TLC plate. A wide difference was observed: the long chain, polyunsaturated C18:0/20:4 PA species migrated noticeably further than the short-chain, saturated C16:0 PA species (Figure 5.14). PA derived from hydrolysis of [^{14}C]-PC by peanut PLD migrated just above PI on another TLC plate (Figure 5.15). ([^{14}C]-PI is not a substrate of PLD, but instead appears to be contaminated here with PA and PC.)

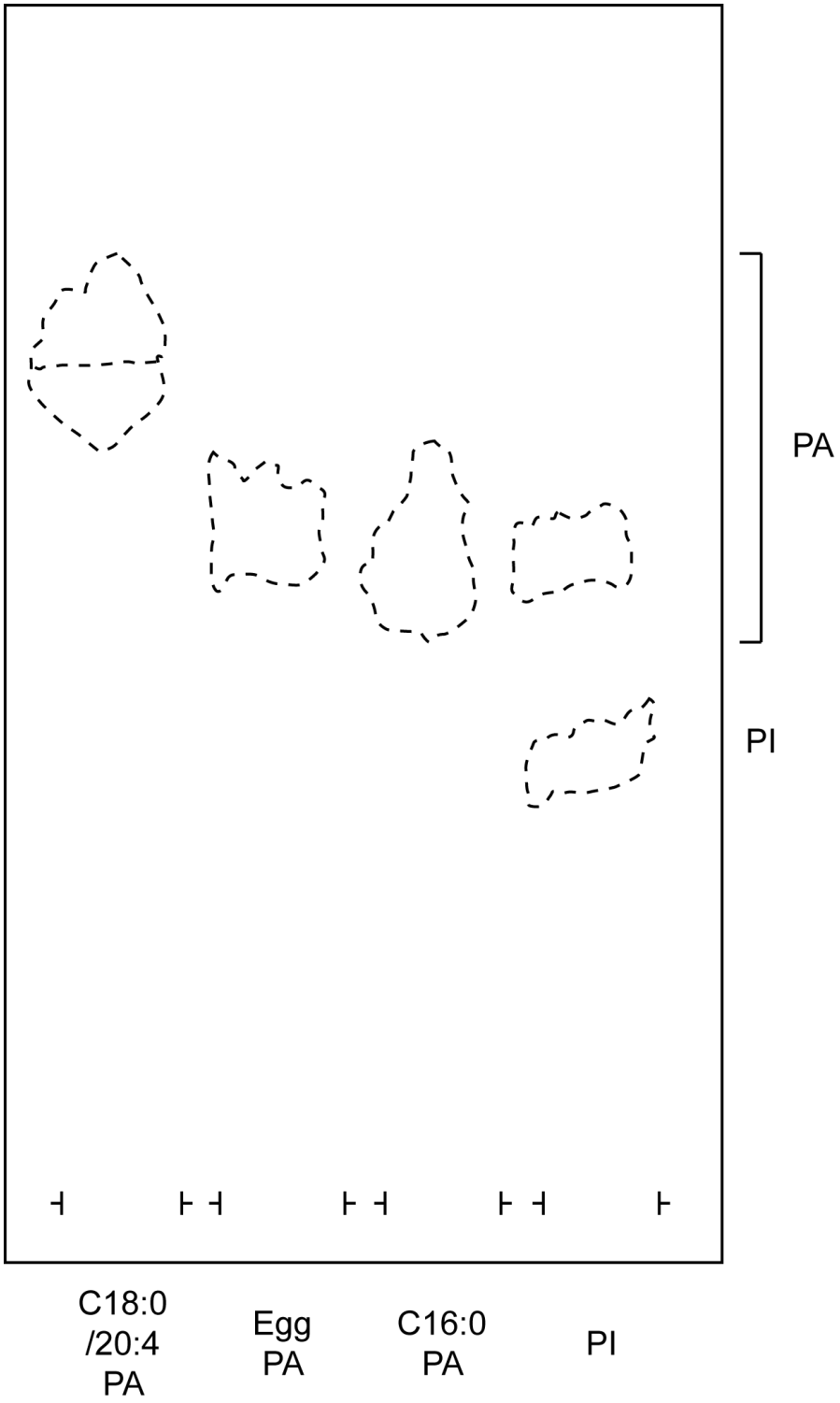

Figure 5.14: Long-chain and short-chain PA standards

C18:0/20:4 PA (P1293, Sigma-Aldrich), egg PA (P9511), dipalmitoyl PA (C16:0) (P9388) samples were spotted onto a TLC plate alongside PI. The lipids were migrated in the solvent system, Chloroform: Methanol: Acetic acid: Water (75: 45: 3: 1, *v*/*v*), then stained in an iodine tank for visualisation of the lipid spots. The edges of the lipids were traced in pencil, and the plate scanned using a flat-bed scanner.

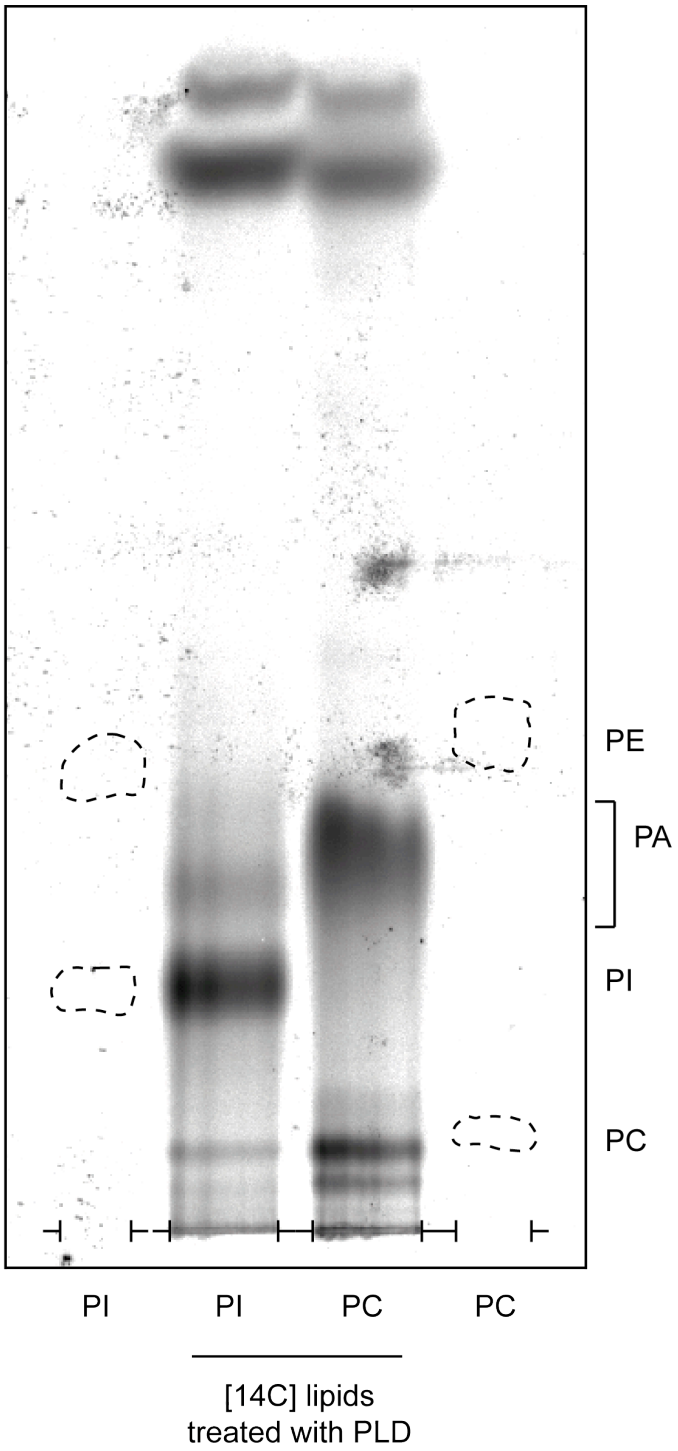

Figure 5.15: Treatment of [^{14}C]-PI and [^{14}C]-PC with PLD

Total HL60 [^{14}C] lipids from previous experiments were combined and separated by TLC. The [^{14}C] PI and [^{14}C] PC lipids were identified and silica scraped. The lipids were re-extracted and treated with PLD for 16 hrs. The lipids were again purified and 100,000 dpm of each run on a TLC plate (shown) alongside 20 µg of PI and PC unlabelled standards.

5.7: PA transfer

The lipid binding assay monitors a single round of lipid exchange. The next step is to ask whether the PITP is able to pick up a radioactive lipid from a donor membrane and deposit it into an unlabelled, acceptor membrane. In a lipid transfer assay, multiple rounds of docking and lipid exchange have taken place. To assess whether RdgBβ is able to transfer PI, I included unlabelled PC:PI (98:2, molar ratio) liposomes in a lipid binding assay. Rather than re-capturing the PITP, the HL60 cell membranes and proteins were denatured and precipitated using 0.2 M sodium acetate/0.25 M sucrose pH 5.0, and the radioactive lipids transferred to the unlabelled liposomes assessed by TLC.

A high background transfer of lipids was observed in the control lane (no PITP) (Figure 5.16). However, this was subtracted from the quantities of particular [^{14}C]-lipids transferred in the presence of PITPα or RdgBβ-sp1. The data are expressed as a percentage of the total PC+PI+PA transferred to the liposomes. PC transfer by RdgBβ is absent, as is PA transfer by PITPα. RdgBβ clearly transfers PA, although considerably less than PI by proportion (20.4 ±0.9% SD PA, compared with 79.6 ±0.9% SD PI). In this assay, PITPα transfers more PC than PI (61.0 ±0.3% SD PC, compared with 38.7 ±0.4% SD PI).

(Facing page) Figure 5.16: RdgBβ transfers [^{14}C]-PA to unlabelled liposomes

Recombinant PITPα or RdgBβ-sp1 proteins were incubated with permeabilised [^{14}C]-HL60 cells and unlabelled PC:PI (98:2, molar ratio) liposomes for 20 min at 37°c (in duplicate). The cells were precipitated using 0.2 M sodium acetate/0.25 M sucrose pH 5.0, and transferred lipids extracted from the liposomes (supernatant). The lipids were spotted onto two TLC plates (one per replicate) and migrated in the solvent system, Chloroform: Methanol: Acetic acid: Water (75: 45: 3: 1 (*v*/*v*)). (A) Single TLC plate shown. (B) Lipids transferred (PC, PI, PA) quantified using densitometry, and background transfer subtracted (control lane). Lipid transfer is expressed as a percentage of the total PC+PI+PA transferred. Error bars are SD (single experiment shown).

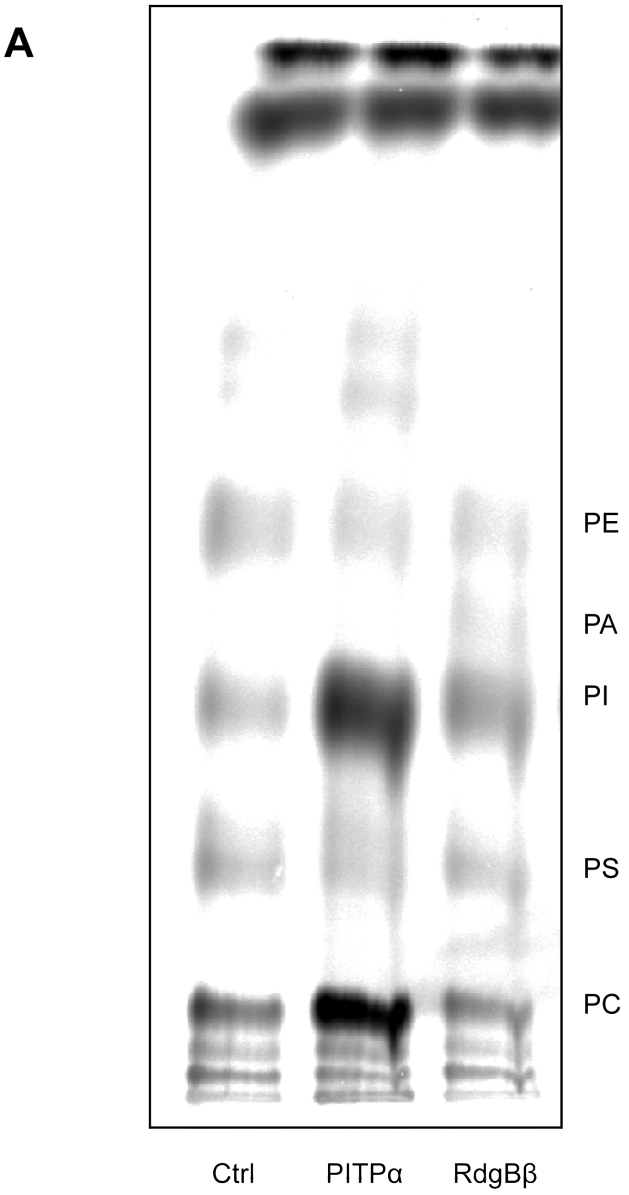
A
PE
PA
PI
PS
PC
Ctrl
PITPα
RdgBβ

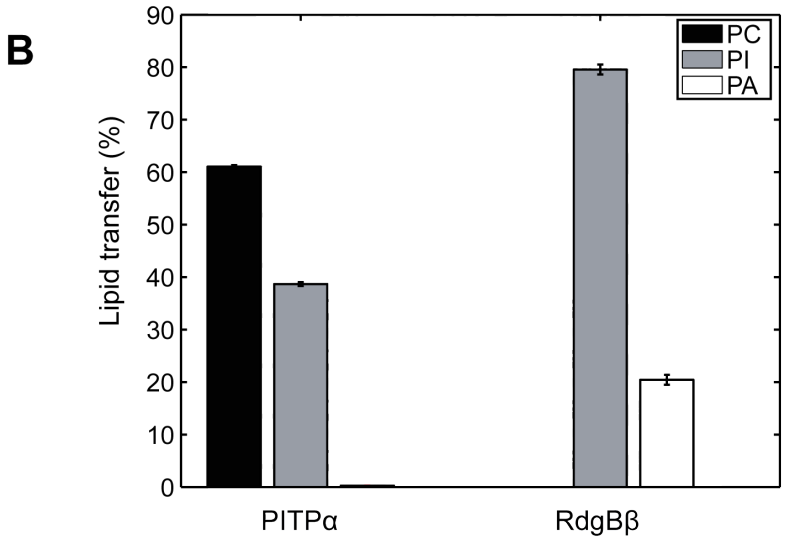
B
Lipid transfer (%)
90
80
70
60
50
40
30
20
10
0
PC
PI
PA
PITPα
RdgBβ

5.8: Lipid binding by RdgBβ in stimulated cells

The availability of PA can be increased by stimulation of cells with GTPγS, PMA or by increasing the Ca^{2+} concentration to 10 μM. I next assessed whether PA binding by RdgBβ was enhanced by these treatments by adapting the lipid binding assay so that the permeabilisation of the cells with SLO was combined with the addition of PITP. This retained the cytosol yet permeabilisation still enabled the recombinant PITPs to enter the cells.

Most notably, PA binding by RdgBβ increased three-fold when cells were stimulated by GTPγS at pCa5 (10 μM Ca^{2+}) (1.1 ±0.6 SD at pCa7 (100 nM Ca^{2+}), rising to 3.3 ±0.2 SD at pCa5, GTPγS), and total lipid binding doubled compared with unstimulated conditions at 100 nM Ca^{2+} (Figure 5.17 A & B). In comparison to PI bound by PITPα at pCa7, PA binding increased considerably, from 12.6 ±3.7% SD at pCa7 to 41.3 ±9.1% SD at pCa5, GTPγS (Table 5.2). A moderate increase in PA binding by RdgBβ was observed when the calcium Ca^{2+} was raised from 100 nM (pCa7) to 10 μM (pCa5), without the addition of stimulus, and PMA treatment did not modify this response further. By contrast, lipid binding by PITPα did not vary greatly upon increase in Ca^{2+} or by treatment of the cells with GTPγS or PMA (Figure 5.17 A & C).

(Facing page) Figure 5.17: RdgBβ PA binding increases upon stimulation with GTPγS

(A) The lipid binding assay was adapted so that SLO was added to permeabilise the [^{14}C]-acetate-labelled HL60 cells during the 20 min incubation with recombinant proteins, RdgBβ or PITPα, calcium buffer (pCa7 (100 nM Ca^{2+}) or pCa5 (10 μM Ca^{2+})), and 100 μM GTPγS or 100 nM PMA to stimulate the cells, as appropriate. Single representative experiment shown. A-H throughout correspond to the lanes on the TLC plate (*right panel*). *Left panel*: Coomassie-stained SDS-PAGE gel loaded with 'Input' and 'Output' recombinant protein. Rβ=RdgBβ; Pα=PITPα. (B) Quantification of phospholipids bound by RdgBβ under the different assay conditions indicated on the TLC image in (A). The amount of lipid bound has been adjusted relative to the amount of recombinant protein recovered in the assay. To compare two independent experiments, the quantity of lipid bound has been adjusted relative to the amount of PI bound at 100 nM Ca^{2+}. * indicates significance of quantity of PA bound by RdgBβ at pCa5 with GTPγS compared to pCa7, $p<0.05$. *Inset*: Total lipid bound (PC+PI+PA) adjusted relative to the total lipid bound at 100 nM Ca^{2+}. (C) As (B) but for PITPα. Error bars are SD, $n=2$.

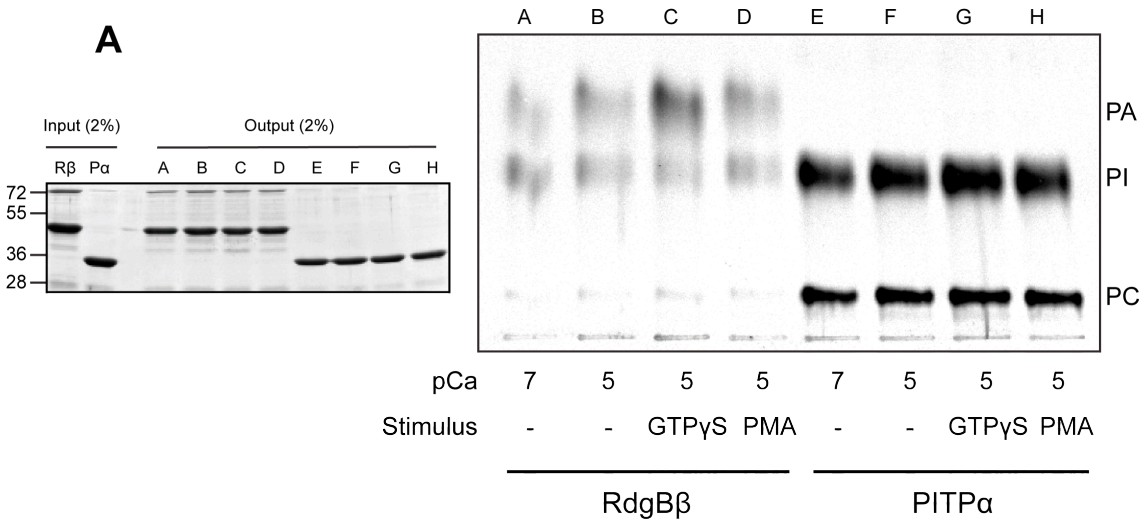
A
Input (2%)
Output (2%)
Rβ Pα A B C D E F G H
72
55
36
28
A B C D E F G H
PA
PI
PC
pCa 7 5 5 5 7 5 5 5
Stimulus - - GTPγS PMA - - GTPγS PMA
RdgBβ
PITPα

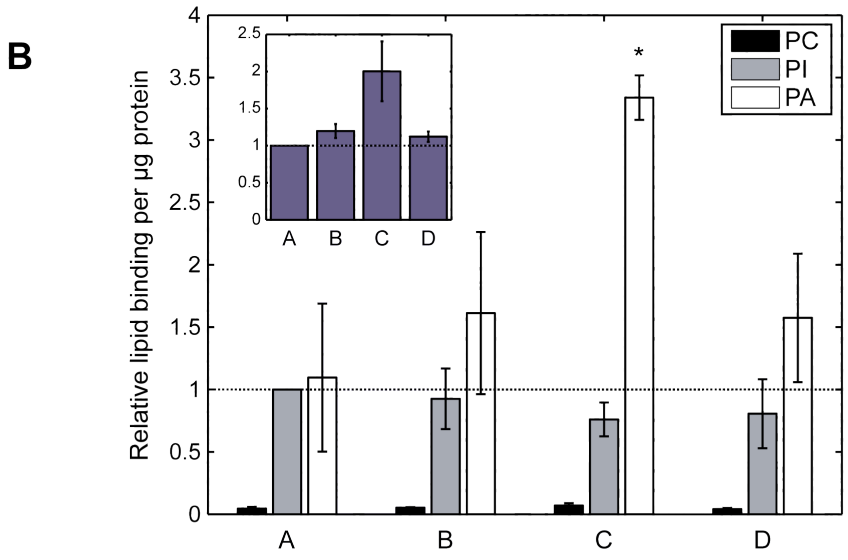
B
Relative lipid binding per µg protein
PC
PI
PA
*
A B C D

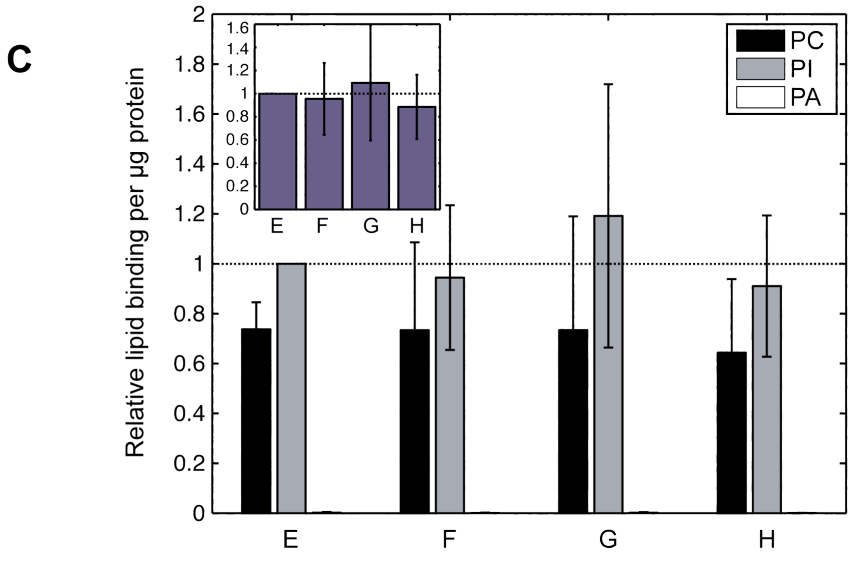
C
Relative lipid binding per µg protein
PC
PI
PA
E F G H

PITP	Condition	PC	PI	PA
RdgBβ	pCa7	0.6 ± 0.3	12.5 ± 3.4	**12.6 ± 3.7**
	pCa5	0.7 ± 0.1	11.1 ± 0.1	19.0 ± 2.6
	GTPγS, pCa5	0.9 ± 0.5	9.2 ± 0.9	**41.3 ± 9.1**
	PMA, pCa5	0.5 ± 0.0	9.6 ± 0.7	18.7 ± 1.1
PITPα	pCa7	73.7 ± 10.8	**100.0 ± 0.0**	0.2 ± 0.3
	pCa5	73.3 ± 35.2	94.4 ± 29.0	0.1 ± 0.1
	GTPγS, pCa5	73.4 ± 45.5	119.1 ± 52.7	0.2 ± 0.2
	PMA, pCa5	64.4 ± 29.4	90.99678198	0.1 ± 0.1

Table 5.2: Lipid binding under stimulated conditions

Data represented in Figure 5.20 expressed as a percentage of PI binding at pCa7 by PITPα. Errors are SD, *n*=2.

5.9: Discussion

I have demonstrated that RdgBβ binds PI and a second lipid in approximately equal proportions; PC binding by RdgBβ is negligible. I analysed the migration patterns of common phospholipids by TLC, employing lipid binding assays with HL60 lipids labelled with a variety of [^{3}H]-radionucleotides, and eventually, upon collaboration with Dr. Alan Hunt at the University of Southampton, the mystery lipid was identified as PA by mass spectrometry. Furthermore, it was revealed that RdgBβ selects for short-chain monounsaturated or saturated PA species, yet is non-selective in its preference of PI species. Modification of the lipid binding assay to manipulate calcium levels with the addition of GTPγS vastly increased PA binding by RdgBβ.

5.9.1: RdgBβ binds PA

The most striking result to emerge from the analysis of the lipid binding properties of RdgBβ was the observation that RdgBβ binds PA. The class I PITPs, PITPα and PITPβ, share ~41% identical residues with RdgBβ, yet PA binding and transfer is specific to RdgBβ.

In the lipid binding assay, where a single round of lipid exchange is assessed by analysing the lipid picked up by PITP proteins, the amount of PI and PA bound across the RdgBβ population was approximately 50:50. When the same assay was used to monitor lipid transfer, with the addition of unlabelled PC:PI liposomes, the proportion of PA transferred relative to PI was 20:80. This latter observation may be due to the amount of PA actually available, rather than the willingness of RdgBβ to transfer the lipid. This notion is consolidated by the observation that PA binding by RdgBβ is increased 3-fold by stimulation (10 μM Ca^{2+}, GTPγS), since under these conditions the availability of PA will be increased by the action of PLC and PLD. It has previously been shown that high intracellular calcium (10 μM) stimulates both PLC and PLD activity to some extent, but the addition of GTPγS causes a robust activation of both phospholipases (Stutchfield and Cockcroft, 1988; Geny and Cockcroft, 1992). In the presence of 10 μM Ca^{2+}, a small increase in PA binding by RdgBβ was observed, which

increased substantially upon addition of GTPγS. Under these conditions PI re-synthesis does not take place since inositol is diluted out of the permeabilised cells.

In retrospect, much of the evidence pointed to the identification of PA as the mystery lipid, but the fact that the PA standard ran higher than PE on the TLC plate led me to disregard PA (Figure 5.5). In Figure 5.5, the CL 'contaminant' that ran in the right place was clearly PA, since PA is one of the intermediates in CL biosynthesis. The PI standard used was ~50% pure, with PE and PA contaminants reported by the manufacturer (seen in Figure 5.10).

The observation that the mystery lipid labelled with [^{3}H]-ethanolamine, with hindsight, was clearly a red herring. A binding assay with [^{3}H]-inositol- and [^{3}H]-choline-labelled revealed that, for either radionucleotide, PITPα bound lipids corresponding in migration distance to PI and PC. The labelling time was the same in this experiment as it was for [^{3}H]-ethanolamine-labelling (72 hrs). This indicates that metabolism of the [^{3}H]-radionucleotide has occurred in this time period, and therefore indicates that the [^{3}H]-ethanolamine lipid bound by RdgBβ in the experiment shown in Figure 5.10 was likely to be PI.

5.9.2: RdgBβ-bound PA and PI acyl chain selectivity

Mass spectrometric analysis indicated that RdgBβ selects short-chain saturated or monounsaturated PA species, particularly C16:0/16:1 and C16:1/18:1. These molecular species were enriched in the RdgBβ-bound material relative to the total cellular lipids. By contrast, RdgBβ was non-selective in its binding of PI, as its profile of bound PI species reflected that present in the total cellular lipids. PA can be produced in cells from PLC hydrolysis of PI(4,5)P_2 to DAG and the subsequent phosphorylation of DAG to PA by DGK. The common PI species in cells is C18:0/20:4 (Figure 5.13, inset), and therefore the PA species produced by this pathway is long-chain, polyunsaturated. An alternative pathway to PA is through the hydrolysis of PC by PLD. The most common PC species in cells is short-chain, saturated or monounsaturated (C16:0/16:1, C16:0/18:1 and C18:1/18:1 (Hunt et al., 2004)), and likewise the PA derived from this

route is short-chain, unsaturated or monounsaturated. Therefore, the PA preferred by RdgBβ is most likely the PLD-derived PA, rather than the PLC-derived species.

The PI and PC molecular species picked by PITPα are identical (in the order, 16:1 > 16:0 > 18:1 > 18:0 (Hunt et al., 2004)), and in the X-ray crystal structure, PI and PC acyl chains occupy the same positions (Yoder et al., 2001; Tilley et al., 2004). Therefore, it is curious that RdgBβ selects short-chain, unsaturated or monounsaturated PA species, yet is non-selective in its PI-binding, binding the most common PI species, long-chain polyunsaturated species. This might indicate that the PI and PA acyl chains occupy different binding sites in RdgBβ, and therefore could indicate the possibility that RdgBβ mutants could be created to differentiate between the PI-bound and PA-bound forms.

5.9.3: Can RdgBβ exist without a lipid bound?

In the unstimulated lipid binding assays, RdgBβ binds only one tenth of the amount of lipid bound. The two tryptophan residues, WW203/204 in PITPα and PITPβ, have been shown to be essential for membrane docking (Shadan et al., 2008), and mutation of these residues to alanines, WW203/204AA, leads to a loss of lipid transfer activity (Tilley et al., 2004). In RdgBβ these residues are a valine and a tryptophan, VW203/204. This may indicate that RdgBβ interacts with membranes less well than PITPα and PITPβ, or that it employs different residues for membrane interaction. During the binding assay only one tenth of the RdgBβ population might successfully exchange their bound lipid.

However, during synthesis in *E. coli*, PITPα is loaded with bacterial lipid, PG and PE in the ratio 8:2 (Hara et al., 1997), and mass spectrometry of the lipids bound by RdgBβ found no trace of un-exchanged, bacterial lipid, indicating that the whole RdgBβ population has exchanged its bound lipid. The lipid binding assay for TLC analysis differs from that for mass spectrometric analysis in that, (1) in the former the cells are metabolically labelled with [^{14}C]-acetic acid, whereas in the latter experiment the cells are unlabelled, (2) the former uses 120 μg recombinant protein per incubation, whereas the latter uses 600 μg, and (3) the former uses 10 mL cells per incubation, whereas the

latter uses 50 mL. None of these three differences can explain why only one tenth of the amount of lipid binding is seen for RdgBβ compared with PITPα. Neither PITPα nor PITPβ have been observed without ligand bound - during X-ray crystallography only the apo-form is devoid of ligand, and this structure is proposed to exist when the protein is docked onto a membrane in the process of lipid exchange.

Two residues are observed to bind the PI or PC acyl chains in the crystal structures of PITPα and PITPβ, Y63 and E218 (Yoder et al., 2001; Tilley et al., 2004; Vordtriede et al., 2005). In RdgBβ, these residues are both valines, and might indicate that the lipid bound in RdgBβ is not nestled so tightly as it is in PITPα and PITPβ: perhaps some lipid is lost during the experimental procedure.

Relevant here also is the observation that PA-binding by RdgBβ was increased by stimulation of PA production by raising the calcium concentration to 10 μM, together with the addition of GTPγS. If lipid is lost during the process of protein capture and lipid extraction, then PA must be more tightly bound in the RdgBβ lipid-binding pocket than PI.

5.9.4: RdgBβ does not bind PC

In contrast to the class I PITPs, I have demonstrated that PC binding by RdgBβ is largely absent. Residues important for PC binding are much harder to predict than for PI, since no residues directly contact the PC head group in the PC-bound X-ray crystal structure of PITP (Yoder et al., 2001). It has been reported that mutation of C95 in PITPβ to either an alanine or a threonine residue causes a loss of PC transfer, leaving PI transfer unaffected (Carvou et al., 2010). In addition, F225 has also been shown to be important for PC transfer (Vordtriede et al., 2005). RdgBβ has a threonine residue at position 95 and a glycine residue at position 225 (Figure 5.1 A), and it is therefore not surprising that RdgBβ does not bind PC.

CHAPTER 6: Discussion

6.1: Summary of results

RdgBβ is the third soluble PITP to be discovered, and is a member of the class II PITPs, also known as the RdgB proteins. Like the other PITPs, RdgBβ-sp1 carries the defining PITP domain at its N-terminus, yet has a unique ~80 aa C-terminal domain. Using bioinformatics tools and protease digestion I have demonstrated that this domain is disordered or unstructured.

The RdgBβ-sp1 C-terminus contains two PEST sequences, and when expressed in COS-7 cells, RdgBβ-sp1 is ubiquitinated and undergoes a moderate rate of turnover. Furthermore, RdgBβ-sp1 interacts with 14-3-3 via two phosphorylated serine residues, Ser274 and Ser299, in its C-terminal domain. Mutation of Ser299 to alanine destabilised RdgBβ-sp1, increasing its rate of turnover, indicating that binding to 14-3-3 might protect RdgBβ from protease digestion. RdgBβ-sp1 interacts with 14-3-3 under basal conditions, and the amount of 14-3-3 present in the FLAG-RdgBβ-immunoprecipitate was reduced by ~50% following 16 hrs treatment with the PKC inhibitor, BIM-I. In addition, PKC inhibition reduced the expression of RdgBβ-sp1 protein in the lysate, and together these observations support a role for 14-3-3 in protecting RdgBβ-sp1 from degradation. This also indicates that PKC is responsible for one or both of the serine phosphorylations mediating the RdgBβ-14-3-3 interaction. However, treatment of the recombinant protein with rat brain PKC was insufficient to promote 14-3-3 binding in the far western assay, indicating that at least one other kinase is required to facilitate the RdgBβ-14-3-3 interaction.

Chronic PMA treatment has been shown to down-regulate PKC, and therefore would be expected to mimic the effect of PKC inhibition. However, the reverse effect was observed: PMA promoted an increase in RdgBβ-sp1 protein expression, which reached a maximal level at 4 hr treatment. Furthermore, PMA treatment increased the amount of 14-3-3 present in the FLAG-RdgBβ-immunoprecipitate relative to the amount of RdgBβ, indicating that, under basal conditions, a small portion of the RdgBβ-sp1 is not bound to 14-3-3. It was reasoned that PMA stimulates PKC at early time points to

phosphorylate RdgBβ-sp1 and promote 14-3-3 binding. As new RdgBβ-sp1 is synthesised, protein expression is stabilised, increasing the size of the RdgBβ pool. That the PMA-induced increase in RdgBβ-sp1 protein expression reached a plateau after 4 hrs likely reflects the eventual down-regulation of PKC.

Two yeast two-hybrid screens reported that RdgBβ interacts with ATRAP (Rual et al., 2005; Venkatesan et al., 2009), and using co-immunoprecipitation experiments I confirmed that this interaction occurs in COS-7 cells between over-expressed, tagged proteins. Surprisingly, this association was not observed under basal conditions, but required 4-16 hrs PMA treatment before HA-ATRAP was resolved in the FLAG-RdgBβ-immunoprecipitate. The combined treatment of cells with PMA and the Ca^{2+} ionophore, ionomycin, for 4 hrs had an additive effect on the RdgBβ-ATRAP interaction. Conversely, the PMA-induced association was blocked by inhibition of PKC or protein synthesis. Since maximal RdgBβ-sp1 concentration was reached by 4 hrs PMA treatment, and the PMA-induced RdgBβ-ATRAP interaction was blocked by inhibition of protein synthesis, I suggested that a certain threshold quantity of RdgBβ was required before interaction with ATRAP was observed. The RdgBβ-ATRAP interaction was not observed when AT_1R-expressing cells were stimulated with Angiotensin II, likely because the Angiotensin II dose used did not optimally increase RdgBβ protein expression.

RdgBβ interacts with ATRAP via its PITP domain, and despite RdgBβ sharing ~40% identical residues with the class I PITPs, neither PITPα nor PITPβ interact with ATRAP when cells are stimulated with PMA. From this information I was able to pinpoint 37 candidate residues, organised into 10 distinct patches on the RdgBβ surface. Notably, 19 candidate residues lie in the regulatory loop, proposed to be a site of protein interactions. Ser119, in the β6-αC section of the regulatory loop, has been reported to be phosphorylated in the mouse brain (Huttlin et al., 2010; Wiśniewski et al., 2010), and lies in a consensus site for phosphorylation by PKC. I therefore suggested that the β6-αC loop mediates the RdgBβ-ATRAP interaction, regulated by PKC.

A role for other members of the PITP family has been established in PLC signalling (Thomas et al., 1993; Xie et al., 2005; Adachi et al., 2010), and by over-expression of

RdgBβ in HEK-293 cells along with the AT_1R, I observed a ~3.8-fold increase in Angiotensin II-stimulated inositol phosphate production by PLC. 10 nM, 100 nM or 1 μM Angiotensin II for 20 min produced little difference in inositol phosphates, indicating maximal activity at all three doses. Consistent with previous reports, ATRAP reduced Angiotensin II-induced inositol phosphate production by PLC, as did PMA pre-treatment.

Lastly, an analysis of the lipids bound by RdgBβ by TLC indicated that whereas the class I proteins bind PI and PC in approximately equal quantities, RdgBβ binds PI and a second lipid in similar amounts, and PC binding by RdgBβ is almost negligible. Further biochemical analysis of the unknown lipid, and finally mass spectrometry, revealed its identity to be PA. Whereas RdgBβ displayed non-selective binding of PI, the PA molecular species bound were enriched in short-chain saturated and mono-unsaturated species. The most common species of PC are short-chain, monounsaturated and saturated species, whereas the most common species of PI are long-chain, polyunsaturated species. Since RdgBβ preferentially binds short-chain, monounsaturated or saturated species, I reasoned that the PA selected by RdgBβ is derived from PLD hydrolysis of PC, rather that the hydrolysis of $PI(4,5)P_2$ by PLC and subsequent phosphorylation by DGK. Unlike the PI and PC species selected by PITPα, the PI and PA bound by RdgBβ differ in their acyl chain composition. I therefore proposed that these two phospholipids occupy distinct sites within RdgBβ, and that the PA-binding site is more secure than that for PI.

In a modification of the lipid-binding assay, RdgBβ was observed to transfer [^{14}C]-PA to unlabelled liposomes. PA binding by RdgBβ was significantly increased by the addition of GTPγS to the lipid binding assay, likely due to the increased availability of PA under these conditions.

6.2: RdgBβ ubiquitination and protein turnover

Inhibition of protein synthesis with cycloheximide and immunoprecipitation experiments with proteasome inhibition indicated that unphosphorylated RdgBβ is rapidly degraded in cells, targeted to the proteasome by the addition of ubiquitin.

Disordered regions of a protein are highly susceptible to proteolytic degradation, particularly if they occur at one of the termini of the protein sequence. Such regions are flexible, permitting interaction with proteases, and give a point for the proteasome to unravel the protein from. The transplantation of a disordered region from one protein to another can increase the rate of degradation of a protein (Prakash et al., 2008), however the disordered region itself is not sufficient for proteasomal degradation, ubiquitination is also required. Ubiquitin may be used as a tag for functions other than degradation, for example regulation of DNA repair, enzyme recruitment or vesicular trafficking (Liu and Walters, 2010). In the absence of MG-132 treatment to inhibit the proteasome, RdgBβ-sp1 ubiquitination is only weakly detectable, indicating that the protein is rapidly degraded as soon as ubiquitin is attached. The ubiquitin smear associated with RdgBβ in untreated cells closely resembles the pattern seen in the MG-132-treated cells, and together these observations indicate an exclusively degradative function for ubiquitin tagging of RdgBβ-sp1.

Three enzymes are necessary for the ubiquitination of a substrate protein: an E1 activating enzyme to activate ubiquitin, an E2 conjugating or ubiquitin carrier enzyme, and an E3 ubiquitin ligase. It is the E3 enzyme that binds to the target protein and thus confers substrate specificity. Phosphorylation of the substrate protein may promote E3 ubiquitin ligase recruitment or displace it. Alternatively, phosphorylation may affect the binding of other proteins to the substrate protein which stabilise the protein or promote its degradation. p53 is bound by Mdm2 which exports it from the nucleus and targets it for ubiquitin-dependent proteolysis in the cytoplasm. However, in response to DNA damage, p53 is phosphorylated preventing its association with Mdm2 and promoting its accumulation in the nucleus to promote gene transcription (Böttger et al., 1999; Chehab et al., 1999). For RhoA GTPase the reverse is true: phosphorylation of the GTP-bound

form of RhoA increases its interaction with its binding partner RhoGDI, preventing its degradation (Rolli-Derkinderen et al., 2005).

For RdgBβ-sp1, mutation of any of its C-terminal phosphorylation sites, Ser274, Thr278 or Ser299, had no effect on the ubiquitination of RdgBβ-sp1. Several other sites had been reported as phosphorylated in the RdgBβ protein, but were omitted from my investigation as they had <5 reports associated with them (Figure 3.4), and it is possible that there are other RdgBβ phosphorylation sites that have not been reported. Any of these sites may be relevant for the ubiquitination of RdgBβ-sp1.

6.3: The RdgBβ-sp1 C-terminal protein-interaction domain

In addition to providing access to proteases, unstructured regions of a protein are commonly used as protein-protein interaction domains for similar reasons: they are flexible, provide a large surface area for interaction and are readily accessible.

6.3.1: PEST sequences

The RdgBβ-sp1 C-terminus contains two PEST sequences, rich in proline, glutamate, serine and threonine residues. PEST sequences were originally identified as degradation signals due to their abundance in rapidly degraded proteins (Rogers et al., 1986; Rechsteiner and Rogers, 1996), yet some researchers have found that the PEST sequence can be deleted from their protein of interest without (or with minimal) stabilising effect, as has been demonstrated for the c-Fos transcription factor (Carillo et al., 1996; Acquaviva et al., 2001). A wider use of this region appears to be in mediating protein-protein interactions. This is indeed a more all-encompassing model. It has been known for a long time that components of large protein complexes are more susceptible to degradation when dissociated from their binding partners (Goldberg and Dice, 1974). PEST sequences may therefore lie in the region mediating binding and will therefore be exposed when the subunits dissociate. The presence of serine and threonine residues amenable to phosphorylation provides a means by which such protein-protein

interactions can be regulated. All three of the RdgBβ-sp1 C-terminal phosphorylation sites (Ser274, Thr278 and Ser299) lie within its PEST sequences.

6.3.2: The RdgBβ-sp1 C-terminus is a proline-rich domain

The PEST sequence itself is a proline-rich domain, as is the rest of the C-terminus of RdgBβ-sp1. Proline-rich domains make common protein-protein interaction domains, for example WW and SH3 domains bind to proline-rich domains and have been hypothesised to compete for binding partners (Sudol, 1996; Macias et al., 2002). The identification of the C-terminal region of RdgBβ-sp1 as a disordered region and a proline-rich domain therefore indicates a high propensity towards multiple binding partners for RdgBβ-sp1.

6.4: The RdgBβ-sp1-14-3-3 interaction

6.4.1: 14-3-3

I have identified one binding partner of the disordered C-terminus of RdgBβ-sp1, 14-3-3. 14-3-3 proteins are 28-33 kDa cytosolic proteins present in all eukaryotes, originally described by Moore and Perez in 1967. The name '14-3-3' refers to their elution position on DEAE-cellulose chromatography and gel electrophoresis during a systematic attempt at classifying bovine brain proteins. There are seven isoforms in the mammalian genome, β, γ, ε, σ, ζ, τ and η, which homo- or heterodimerise, depending on the isoform. Each monomer in a 14-3-3 dimer recognises and binds a single phospho-serine or phospho-threonine motif; together the two monomers making up a 14-3-3 dimer may bind two phosphorylated motifs on the same protein, or on different proteins, bringing two proteins together into a protein complex. The phosphorylated motif generally conforms to the sequence RSXpSXP (mode 1) or RX(Y/F)XpSXP (mode 2) (Yaffe et al., 1997), where 'X' is any amino acid and 'pS' represents the phosphorylated serine (or threonine) residue, although there are exceptions and the interaction is not always phosphorylation-dependent. Where the two 14-3-3-binding sites appear on the same protein, it has been postulated that one binding site might act as a 'gatekeeper',

whose phosphorylation is necessary for 14-3-3 binding, but not necessarily sufficient for the full binding of 14-3-3 and hence for the full biological activity of the interaction (Yaffe, 2002).

Each 14-3-3 subunit consists of nine anti-parallel α-helices that form a 'palisade' around a large, negatively charged ligand-binding groove (Liu et al., 1995; Xiao et al., 1995). Although once believed to be a rigid cup-shaped structure, referred to as a 'molecular anvil' which deformed its bound ligands to induce a conformational change and alteration in protein function (Yaffe, 2002), later work indicated that the 14-3-3 dimer is in fact a flexible structure, enabling 14-3-3 proteins to bind to diverse peptides and a wide variety of proteins of different size and sequence (Yang et al., 2006).

More than two hundred 14-3-3 target proteins have been identified, and analysis of target protein structures indicated that the majority of 14-3-3 binding partners contain regions of disorder, like the RdgBβ-sp1 C-terminal domain. Indeed, ~70-94% of the target proteins contained unstructured regions, depending on the disorder prediction program used (Bustos and Iglesias, 2006). This again indicates a propensity for unstructured regions of a protein to form protein-interaction domains, due to their intrinsic flexibility, and it has been proposed that 14-3-3-binding induces a disorder-to-order transition in the target protein (Bustos and Iglesias, 2006).

Binding partners of 14-3-3 include transcription factors, biosynthetic enzymes, cytoskeletal proteins, signalling molecules, apoptosis factors and tumour suppressors. The precise function of the 14-3-3 interaction varies depending on the protein and site of interaction. There is much discussion as to whether 14-3-3 is an adaptor protein with a passive function or phospho-dependent chaperone protein with an active function in intracellular signalling. Functions of 14-3-3 binding have been classified into three categories, one or more of which may be used at any one time: (i) directed conformational changes of the target protein; (ii) physical occlusion of sequence-specific or structural features (which may alter intracellular localisation, for example); and (iii) scaffolding (Bridges, 2004). 14-3-3 proteins have been described as more than just adaptor proteins, able to 'finish the job' started by phosphorylation to effect changes in the activities of intracellular proteins (MacKintosh, 2004).

6.4.2: The function of the RdgBβ-sp1-14-3-3 interaction

I have demonstrated that 14-3-3 binds directly to RdgBβ-sp1, via phosphorylated residues Ser274 and Ser299, which lie in consensus sites for 14-3-3 recognition. Mutation of either one of these residues abolishes 14-3-3 binding, which was unexpected. As the sequence surrounding Ser274 would be considered to be a low affinity, or degenerate 14-3-3 recognition sequence, one might expect mutation of this residue to have less effect on 14-3-3-binding. I would have expected that Ser299 would be the 'gatekeeper' binding site, whose phosphorylation is necessary for 14-3-3 binding but not sufficient for the full binding of 14-3-3 (Yaffe, 2002). Therefore mutation of Ser299 would abrogate 14-3-3 binding, whereas mutation of Ser274 would only partially reduce binding. This was not the case, however. This discrepancy can be explained if the two phosphorylation events (for Ser274 and for Ser299) are not independent but are in some way linked: if prior phosphorylation of Ser274 is required for phosphorylation of Ser299 (directly or indirectly), the fact that mutation of Ser274 also abolishes 14-3-3 binding rather than merely reducing it, can be accounted for.

The disordered C-terminus of RdgBβ-sp1 permits the access of proteases and gives the proteasome a point from which to unravel the protein from. Recombinant RdgBβ-sp1 is susceptible to digestion by trypsin, and RdgBβ-sp1 expressed in COS-7 cells is subject to a moderate rate of turnover. The majority of the protein in COS-7 cells is bound to 14-3-3 under basal conditions via its C-terminal disordered region. The RdgBβ-sp1 S299A mutant, unable to bind 14-3-3, is more rapidly degraded, with a half-life of ~2 hrs. It is therefore plausible that 14-3-3 masks this unstructured region from access by proteases by physically masking the C-terminus, and possibly promoting a disorder-to-order transition in the structure. The interaction of 14-3-3 with RdgBβ-sp1 therefore can be classified as the physical occlusion of sequence-specific or structural features (Bridges, 2004). It is clear that 14-3-3 does not prevent ubiquitination, however, since mutation of Ser274 or Ser299, the residues responsible for binding 14-3-3, has no effect on the ubiquitination of RdgBβ-sp1.

Biochemical and structural analyses of PITPα indicate that the protein is in a closed conformation, resistant to proteases (Tremblay et al., 1996; Prosser et al., 1997), when in the process of lipid transport. Upon membrane interaction, the αG helix swings out from the main structure and the C-terminal residues become disordered, exposing the lipid-binding cavity to the membrane interface for lipid exchange (Schouten et al., 2002). Unlike PITPα, the longer RdgBβ-sp1 C-terminus is susceptible to protease digestion in the absence of membranes. If 14-3-3-binding does promote a disorder-to-order transition in the RdgBβ-sp1 C-terminus, perhaps 14-3-3 is a co-factor for lipid transport. Binding of 14-3-3 might be required for compaction of RdgBβ to enable its transit through the cytosol. If 14-3-3-binding is required for efficient lipid transport, this could provide another reason for RdgBβ performing less well than PITPα in the lipid transfer assays, where neither RdgBβ phosphorylation, nor 14-3-3, is present.

Upon membrane-binding the C-terminus of PITPα becomes disordered, required so that it doesn't interfere with lipid exchange. Likewise, with 14-3-3 bound, the ordered RdgBβ-sp1 C-terminus would prevent lipid exchange by forming a rigid lid. Therefore it is plausible that as RdgBβ approaches the membrane, 14-3-3 receives a signal to dissociate and the C-terminus of RdgBβ-sp1 resumes its disordered state. RdgBβ would then be able to interact with the membrane for lipid exchange, and its long C-terminus, now flexible, would now not occlude the lipid-binding cavity.

6.5: RdgBβ basal activity: non-selective PI transfer

In the PLC assay, co-expression of RdgBβ and the AT_1R in HEK-293 cells increased inositol phosphate production by PLC stimulated by Angiotensin I for 20 min, 3.8-fold. There was little difference in response between the three Angiotensin II concentrations used, 10 nM, 100 nM and 1 μM, indicating that PLC was operating maximally at all three, limited only by substrate availability. It is possible that RdgBβ prepares the substrate by transporting PI to the agonist-sensitive pool in the absence of stimulation. RdgBβ binds PI without selecting for PI with particular acyl chains, supporting a model in which, under basal conditions, RdgBβ transfers PI from regions of high concentration (the ER, the site of PI synthesis), down its concentration gradient to distal intracellular

membranes. Since the majority of RdgBβ-sp1 is bound to 14-3-3 under basal conditions, this supports the hypothesis that 14-3-3 acts as a co-factor for lipid transport by RdgBβ.

6.6: RdgBβ stimulated activity: membrane localisation and PA binding

6.6.1: The possibility of a distinct RdgBβ function in stimulated cells

For PITPα, several lines of evidence support a model in which activity in stimulated cells differs from its activity in unstimulated cells. A reduced mobility of PITPα at the plasma membrane was observed in response to EGF stimulation in COS-7 cells (Larijani et al., 2003). In A431 cells, PITP was detected in an endogenous signalling complex with the EGF receptor, PI4K and PLCγ, and this association increased following stimulation with 100 nM EGF for 5 mins (Kauffmann-Zeh et al., 1995). In the developing nervous system, PITPα interacts with the DCC and neogenin transmembrane cell surface receptors, and this association increased 4-fold by addition of the agonist, netrin-1 (Xie et al., 2005). These studies indicate that upon cellular stimulation, PITPα is re-localised to membranes through protein-protein interactions.

6.6.2: The PMA-stimulated RdgBβ-ATRAP interaction

RdgBβ interacts with ATRAP when cells are stimulated by PMA. Since ATRAP is a three-pass transmembrane protein, this association would function to localise RdgBβ to the membrane. I found that the PMA-induced RdgBβ-ATRAP interaction could be blocked by treatment with BIM-I, indicating that the direct target of PMA could be PKC. PKC may then directly phosphorylate either RdgBβ or ATRAP to permit the interaction. A candidate residue is Ser119 on the RdgBβ regulatory loop, which has been identified as being phosphorylated in the mouse brain (Huttlin et al., 2010; Wiśniewski et al., 2010), and lies in a consensus site for phosphorylation by PKC.

However, PKC is activated rapidly upon PMA addition (within minutes), yet the RdgBβ-ATRAP interaction is not observed until 4 hrs PMA treatment. This could

indicate that direct phosphorylation of RdgBβ or ATRAP is insufficient for mediating the interaction. In addition to PKC inhibition, I observed that the PMA-induced RdgBβ-ATRAP complex could be blocked by inhibition of protein synthesis. This might imply that a certain threshold concentration of RdgBβ must be synthesised and stabilised prior to interaction with ATRAP. This mechanism of stabilisation of protein expression now appears to be distinct from 14-3-3-binding, since RdgBβ-sp1 1-250 and S299A and RdgBβ-sp2, all unable to bind 14-3-3, undergo a similar increase in protein expression in response to PMA as the wild-type RdgBβ-sp1 (Figure 4.6). In this experiment, ATRAP expression is also observed to increase upon PMA treatment, in fact indicating a global upregulation of protein expression in response to PMA. Whether RdgBβ-sp1 expression needs to be stabilised by post-translational modification or binding a co-factor, or whether merely increased RdgBβ protein synthesis is required for the RdgBβ-ATRAP interaction to take place is therefore unclear.

Perhaps RdgBβ binding to ATRAP only occurs when all of the available 14-3-3 proteins are bound to target proteins. This possibility could be assessed by manipulating 14-3-3 levels by over-expression or RNAi, and monitoring the effect on the RdgBβ-ATRAP interaction. As over two hundred binding partners of 14-3-3 have been identified, the relative state of each of these would determine whether RdgBβ interacts with ATRAP, and therefore represent a very complex form of regulation of the RdgBβ-ATRAP interaction.

6.6.3: Binding of PA under stimulated conditions

RdgBβ binds short-chain, monounsaturated or saturated PA species, and using a modified lipid binding assay, I demonstrated that PA-binding by RdgBβ was increased to some extent by 10 μM Ca^{2+}, but was profoundly increased by stimulation with GTPγS. It has previously been shown that high intracellular calcium (10 μM) stimulates both PLC and PLD activity to some extent, but the addition of GTPγS causes a robust activation of both phospholipases (Stutchfield and Cockcroft, 1988; Geny and Cockcroft, 1992). The PA selected by RdgBβ is more similar to the common PC species than the common PI species, which are enriched in long-chain, polyunsaturated

molecular species, and therefore RdgBβ-PA is likely to be derived from the hydrolysis of PC by PLD.

PLD is also activated by PMA, and it is therefore unclear why the addition of PMA appeared to have no effect on PA-binding by RdgBβ. Since the target of PMA is PKC, it is possible that the high Ca^{2+} conditions have already stimulated PKC, and that the rate-limiting step is therefore activation of PLD by PKC. GTPγS, however, produces an additive effect on top of increased Ca^{2+}. PLD is also directly, activated by the small GTPase ARF, and it is likely to be activation of ARF as well as PLD that produces the additive effect on PA production, and therefore PA-binding by RdgBβ.

6.6.4: PA binding as a signal regulating protein interactions

PITPα binds short-chain, monounsaturated or saturated PI and PC molecular species, and X-ray crystal structures of PI- and PC-bound PITPα indicate that PI and PC acyl chains occupy the same space in the PITPα lipid-binding cavity. Since the PI and PA acyl chains are different, this may imply that PI and PA occupy slightly different sites in the RdgBβ cavity. RdgBβ lacks the Y63 and E218 residues, that in PITPα, make hydrogen bond contact with the acyl chains. Therefore the sites of the phospholipid chains in RdgBβ are difficult to predict. Perhaps the binding of one of these phospholipids deforms the lipid in a particular way, in contrast to the other, making it possible to 'sense' whether RdgBβ has bound PI or PA from interaction with the protein surface.

Alternatively, PI and PA carry different amounts of negative charge. The original purification of PITP from bovine brain yielded two subforms that could be distinguished on the basis of their isoelectric points (Helmkamp et al., 1974). Subsequent analysis revealed that these two subforms were the PI- and PC-loaded forms of PITP (van Paridon et al., 1987b), due to the different charges on the phospholipid molecules: PI is negatively charged due to the phospholipid phosphate group, whereas in PC this negative charge is cancelled out by a single positive charge in the choline head group. Likewise, PI and PA could impart different charges on the RdgBβ protein, which could be sensed by a protein interacting with the RdgBβ surface: PI carries a single negative

charge on its phosphate, whereas PA carries two (in PI the second negative charge is removed through covalent interaction with the inositol head group).

It is possible that both PKC phosphorylation of the regulatory loop at Ser119, which occurs constitutively, and the binding of PA, which only occurs when PLD activity is stimulated sufficiently to increase PA production, could promote ATRAP-binding and targeting of RdgBβ to the membrane. If PA-binding is the signal for ATRAP-binding then the conditions under which Angiotensin II promotes an increase in PA will be the true determinant of the RdgBβ-ATRAP interaction.

6.7: Function of the RdgBβ-ATRAP interaction

6.7.1: ATRAP down-regulates Angiotensin II signalling

ATRAP has been reported to have a negative effect on Angiotensin II signalling. Over-expression of ATRAP suppresses inositol phosphate production by PLC in response to Angiotensin II stimulation (Daviet et al., 1999; Lopez-Ilasaca et al., 2003), and GTP binding experiments indicated a reduction in GTP binding following Angiotensin II stimulation of membranes prepared from cells over-expressing ATRAP (Lopez-Ilasaca et al., 2003). Together, these observations suggested that ATRAP uncouples the AT_1R from G_q protein, resulting in a reduced G protein activation and therefore GTP binding, and a consequent reduced stimulation of PLC. The possibility that ATRAP affects activation of other membrane-associated GTPases, such as the small GTPase Rho, was not assessed. ARF GTPase would have dissociated from the membranes under the conditions used (Fensome et al., 1996).

ATRAP also interacts with CAML (Guo et al., 2005), and the function of this interaction appears to be related to, but distinct from, the role of ATRAP in suppression of Angiotensin II signalling (Min et al., 2009). Since other PITPs have been implicated in PLC signalling (Thomas et al., 1993; Xie et al., 2005; Adachi et al., 2010), and one of the effects of the ATRAP-AT_1R interaction is the reduction in Angiotensin II-stimulated inositol phosphate production by PLC (Daviet et al., 1999; Lopez-Ilasaca et al., 2003), it

seemed plausible that the RdgBβ-ATRAP interaction functioned to prevent the delivery of PI by RdgBβ to the signalling membrane. Significantly, the conditions under which the RdgBβ-ATRAP interaction was observed, 4-16 hrs PMA, inhibited PLC activity, consistent with negative feedback by PKC on the AT_1R through heterologous desensitisation (Tang et al., 1998). Therefore, it seems unlikely that RdgBβ binding to ATRAP at this time would have a significant effect on PLC activity and the supply of substrate.

In addition to uncoupling the AT_1R from G proteins, ATRAP promotes internalisation of the receptor (Cui et al., 2000; Lopez-Ilasaca et al., 2003). ATRAP appears to perform this function even in unstimulated cells, and has been observed to maintain the AT_1R in internal compartments, even after the removal of Angiotensin II (Tanaka et al., 2005; Azuma et al., 2007). The mechanism by which it promotes receptor internalisation has not been reported, yet the action of ATRAP, to uncouple the receptor from G proteins and promote its internalisation, is comparable to the function of arrestin.

6.7.2: RdgBβ and AT_1R endocytosis

Roles for PITPs have been reported in membrane trafficking (Hay and Martin, 1993; Ohashi et al., 1995; Fensome et al., 1996; Peretti et al., 2008; Carvou et al., 2010), specifically through the formation, fission and fusion of vesicles at membranes, due to the requirement for phosphoinositides in these processes for the assembly of protein effector molecules at the membrane.

PA is small, and since it lacks a head group, promotes negative membrane curvature. In this way, PA is important at the neck of a developing membrane vesicle. PLD itself is activated by Gβγ subunits in response to Angiotensin II stimulation (Ushio-Fukai et al., 1999). PLD2 localises to the plasma membrane and has been observed to facilitate endocytosis of the EGF receptor by acting as a GTPase-activating protein for dynamin (Lee et al., 2006), which is responsible for scission of the newly-formed endocytosing vesicle from the plasma membrane. PLD2 has also been shown to be important in AT_1R endocytosis: in PLD2-knockdown HEK-293 cells, or cells transfected with the inactive

PLD2-K758A mutant, the stably expressed AT_1R did not endocytose in response to Angiotensin II (Du et al., 2004).

A role for RdgBβ in AT_1R endocytosis seems possible. In unstimulated cells, RdgBβ re-distributes PI from the ER to other intracellular membranes, down its concentration gradient. This ensures that a certain quantity of PI is present at the membranes when a stimulus is received. $PI(4,5)P_2$ is required for the full activation of PLD, and re-localisation of RdgBβ binding to ATRAP upon stimulation could focus RdgBβ activity to the membrane, close to PLD. Here, RdgBβ might be required for the local re-organisation of PI and PA into distinct patches for vesicle formation and the assembly of coat proteins. PA has been shown to activate type 1 PI4P-5-K (Jenkins et al., 1994), producing positive feedback to concentrate the formation of $PI(4,5)P_2$ at the membrane.

6.8: RdgBβ-sp2

The short splice variant, RdgBβ-sp2, was largely omitted from my study as it had a low yield when expressed in COS-7 cells, or in *E. coli* for synthesis of the recombinant protein. In an analysis of the localisation of *PITPNC1* transcripts in the mouse brain, mRNA encoding RdgBβ-sp2 was seen mainly in the embryonic brain (weak expression in the ventricular and mantle zones of the cerebral cortex), which declined after birth (Takano et al., 2003). RdgBβ-sp2 expression was also observed in the P49 heart and small intestine, indicating that this protein has a very restricted expression, and probably a specific function in those cells. Since RdgBβ-sp2 is unable to bind to 14-3-3 and due to its instability, it seems likely that RdgBβ-sp2 has its own co-factor, required to stabilise its expression. This factor could be specific to a restricted number of cell types, where RdgBβ-sp2 is expressed.

Despite not carrying the 14-3-3-binding site, RdgBβ-sp2 does share the ATRAP-binding site with RdgBβ-sp1, and may be ubiquitinated by the same method, targeting it for degradation. Therefore, unwelcome RdgBβ-sp2 might be degraded unless co-expressed with its own stabilising partner.

6.9: Conclusion

Unmodified RdgBβ (-sp1 or -sp2) is susceptible to ubiquitination and targeting to the proteasome. Unmasked, the protein C-terminus is unstructured and therefore accessible to proteases, giving the proteasome a point from which to unravel the protein from.

Alternatively, RdgBβ-sp1 is phosphorylated at Ser274 and Ser299 in its C-terminus by the concerted activity of PKC and at least one other kinase. These serine phosphorylations mediate interaction with 14-3-3, which masks and orders the protein C-terminus, protecting it from degradation by the proteasome. RdgBβ-sp1 is not protected from ubiquitination, however. 14-3-3 acts as a co-factor for lipid transport, making the RdgBβ-sp1 protein into a compact heterodimer. Interaction between RdgBβ and the membrane encourages 14-3-3 to dissociate from RdgBβ, removing the order from the C-terminus and permitting lipid exchange.

In addition, PKC might phosphorylate RdgBβ-sp1 and -sp2 on residue Ser119 in the regulatory loop. Phosphorylation of RdgBβ occurs under basal conditions and is increased by activation of PKC, for example with PMA and/or ionomycin and/or 10 μM Ca^{2+}.

PMA also activates PLD, which hydrolyses PC and increases the concentration of PA at the membrane. PA binding targets RdgBβ to the membrane and permits its interaction with ATRAP, mediated by the phosphorylated Ser119 residue in its regulatory loop. In this way, ATRAP localises RdgBβ to the membrane to enrich it in the negatively charged phospholipid, PA, required for endocytosis of the AT_1R. Alternatively, RdgBβ might enhance the activity of PI4P-5-K for production of $PI(4,5)P_2$ for assembly of endocytic vesicle coat proteins at the membrane (Figure 6.1).

6.10: Future work

- The production of the RdgBβ-14-3-3 *in vitro* complex will aid in establishing whether 14-3-3 is a co-factor for lipid transport by RdgBβ-sp1, and whether association with 14-3-3 protects RdgBβ-sp1 from protease digestion.

- PITPs are clearly involved in the delivery of PI, but whether they have an active role in stimulation of PI4K or PI3K activity is not always clear. My experiments indicate that RdgBβ enhances the basal incorporation of [^{3}H]-inositol, probably due to the removal of PI from the ER, promoting flux through the PI cycle. Whether RdgBβ is able to stimulate the PI4K activity *in vitro* should therefore be assessed. Since PA has been shown to activate type 1 PI4P-5-K, the ability of RdgBβ to stimulate the activity of this lipid kinase should also be examined. Each of these experiments should be performed in the presence and absence of PI and PA vesicles, with and without recombinant RdgBβ.

- PLD requires PI(4,5)P_2 for its activity, and therefore the ability of RdgBβ to promote PLD activity in the presence and absence of PI vesicles *in vitro* should be assessed to further understand the function of RdgBβ.

- The interaction between RdgBβ and ATRAP was only observed when cells were stimulated with PMA for 4-16 hr, which may be due to its ability to promote an increase in RdgBβ protein expression or to promote an increase in PA production by PLD. By contrast, an interaction was not observed when cells were stimulated by Angiotensin II, either because Angiotensin II is unable to activate the same downstream effectors as PMA, or the incorrect dose was administered. If the latter is correct, the effect of a variety of different Angiotensin II concentrations and times could be administered to HEK-293-AT1 cells, and assessed for their ability to increase RdgBβ protein concentration by western blotting or PA concentration using TLC. The Angiotensin II doses promoting the highest increase in RdgBβ expression and PA concentration should then be assessed to establish whether they promote the RdgBβ-ATRAP interaction. Assessment of whether the RdgBβ-ATRAP interaction occurs under chronic Angiotensin II stimulation (>72 hrs) will require methods to analyse

either the endogenous interaction or a stable cell line expressing the tagged proteins. It should be borne in mind that ATRAP expression is down-regulated by chronic Angiotensin II treatment (14 days) (Wakui et al., 2010a; 2010b), and so an interaction between RdgBβ and ATRAP is unlikely at this time point.

- The existing anti-RdgBβ polyclonal antibody #101 is unable to recognise endogenous RdgBβ, probably because the concentration of RdgBβ is low in unstimulated cells, but also because the antibody is not very sensitive. In addition, monoclonal antibodies seem to work much better for immunoprecipitation since they recognise a single epitope and so give a sharper signal. For analysis of RdgBβ-sp1 alone, a monoclonal antibody could be raised against part of the protein C-terminus. Although an antibody could be designed that would avoid the 14-3-3-binding site, the RdgBβ-sp1 C-terminus demonstrates a high propensity towards protein-protein interactions, some amount of trial-and-error might be required to make an antibody that recognises the endogenous, native protein by immunofluorescence microscopy and immunoprecipitation. The availability of a good antibody able to recognise endogenous RdgBβ would permit analysis of the RdgBβ-ATRAP interaction in specialised cell lines or primary cells, such as those derived from the heart or kidney.

- Confocal immunofluorescence microscopy should be employed to establish where in cells the RdgBβ-ATRAP interaction occurs, and how the association reacts to stimulation in real time. Moreover, this method will be required to analyse whether RdgBβ is required for endocytosis of the AT_1R, and how the membrane trafficking events unfold in real time.

(Facing page) Figure 6.1: Model of RdgBβ regulation

Nascent RdgBβ may either be ubiquitinated, targeting the protein for degradation, or phosphorylated. Phosphorylation at Ser274 and Ser299 by PKC and one or more other kinases permits 14-3-3 binding to the RdgBβ-sp1 C-terminus. This interaction orders the C-terminus and protects the protein from proteasomal degradation, irrespective of ubiquitin modification. In this state, under basal conditions, RdgBβ participates in the non-selective re-distribution of PI from the ER, using 14-3-3 as a co-factor for transport. Meanwhile, PKC also phosphorylates the regulatory loop of RdgBβ at Ser119. When PLD is stimulated, PA concentration at the membrane is increased, targeting RdgBβ to the membrane for binding to ATRAP via the phosphorylated regulatory loop. Membrane interaction signals the dissociation of 14-3-3, removing order from the C-terminus and permitting lipid exchange. (The RdgBβ PITP domain structure used is the comparative model, with PI from PDB: 1uw5. The atoms of the inositol head group were removed for visualisation of PA. C-terminus manually added in dark blue. Regulatory loop coloured brown. Ub, ubiquitin.)

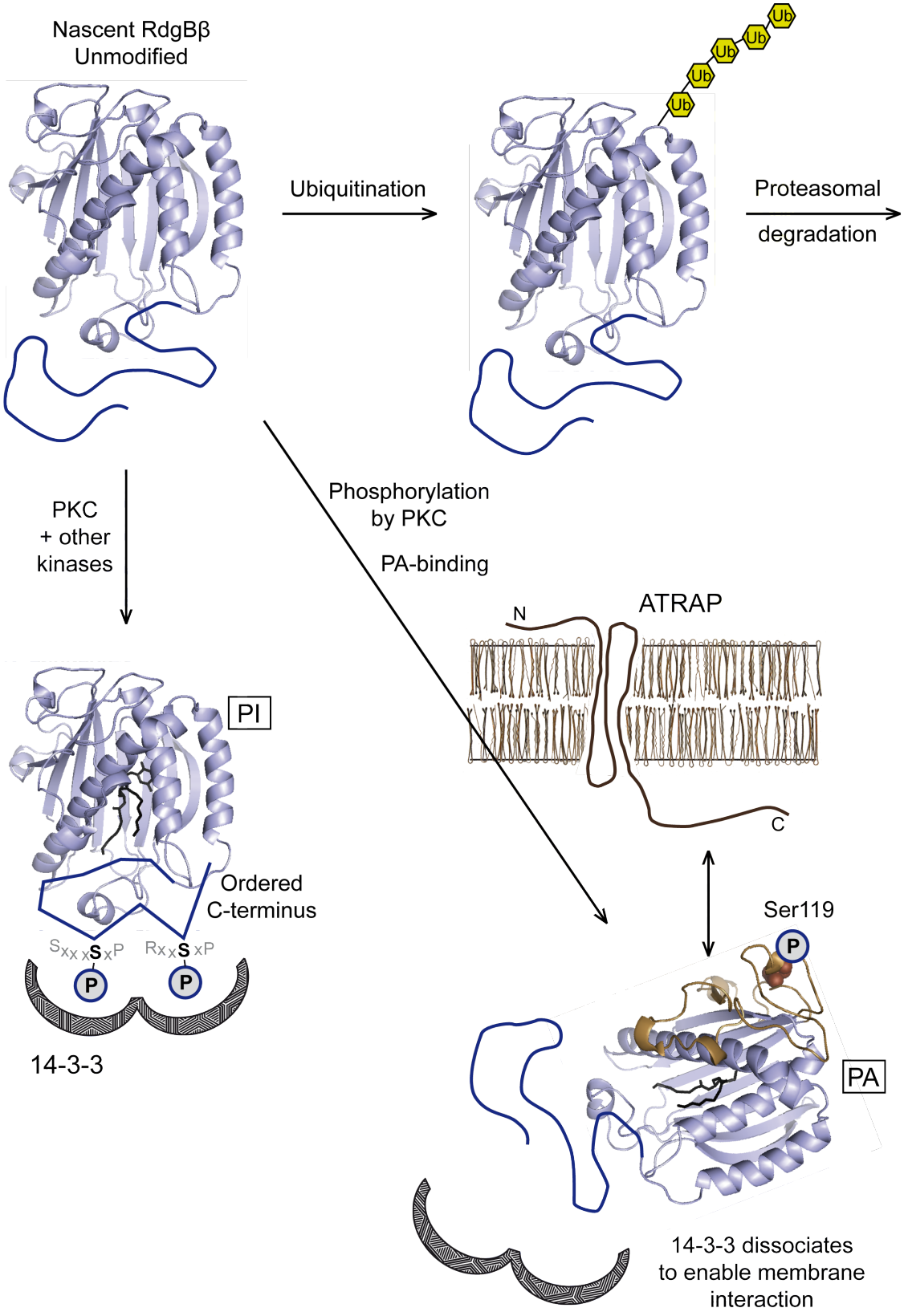
Nascent RdgBβ
Unmodified
Ubiquitination
Ub
Ub
Ub
Ub
Ub
Proteasomal
degradation
PKC
+ other
kinases
Phosphorylation
by PKC
PA-binding
ATRAP
N
C
PI
Ordered
C-terminus
SXX XSXP
RXXSXP
P
P
14-3-3
Ser119
P
PA
14-3-3 dissociates
to enable membrane
interaction

References

Acquaviva, C., Brockly, F., Ferrara, P., Bossis, G., Salvat, C., Jariel-Encontre, I., and Piechaczyk, M. (2001). Identification of a C-terminal tripeptide motif involved in the control of rapid proteasomal degradation of c-Fos proto-oncoprotein during the G(0)-to-S phase transition. Oncogene *20*, 7563–7572.

Adachi, T., Kunitomo, H., Tomioka, M., Ohno, H., Okochi, Y., Mori, I., and Iino, Y. (2010). Reversal of Salt Preference Is Directed by the Insulin/PI3K and Gq/PKC Signaling in Caenorhabditis elegans. Genetics *186*, 1309–1319.

Aikawa, Y., Kuraoka, A., Kondo, H., Kawabuchi, M., and Watanabe, T. (1999). Involvement of PITPnm, a mammalian homologue of Drosophila rdgB, in phosphoinositide synthesis on Golgi membranes. J Biol Chem *274*, 20569–20577.

Alb, J.G., Gedvilaite, A., Cartee, R.T., Skinner, H.B., and Bankaitis, V.A. (1995). Mutant rat phosphatidylinositol/phosphatidylcholine transfer proteins specifically defective in phosphatidylinositol transfer: implications for the regulation of phospholipid transfer activity. Proc Natl Acad Sci USA *92*, 8826–8830.

Alb, J.G., Phillips, S.E., Rostand, K., Cui, X., Pinxteren, J., Cotlin, L., Manning, T., Guo, S., York, J.D., Sontheimer, H., et al. (2002). Genetic ablation of phosphatidylinositol transfer protein function in murine embryonic stem cells. Mol Biol Cell *13*, 739–754.

Alessi, D.R. (1997). The protein kinase C inhibitors Ro 318220 and GF 109203X are equally potent inhibitors of MAPKAP kinase-1beta (Rsk-2) and p70 S6 kinase. FEBS Lett *402*, 121–123.

Altschul, S.F., Madden, T.L., Schäffer, A.A., Zhang, J., Zhang, Z., Miller, W., and Lipman, D.J. (1997). Gapped BLAST and PSI-BLAST: a new generation of protein database search programs. Nucleic Acids Res *25*, 3389–3402.

Amanchy, R., Periaswamy, B., Mathivanan, S., Reddy, R., Tattikota, S.G., and Pandey, A. (2007). A curated compendium of phosphorylation motifs. Nat Biotechnol *25*, 285–286.

Amarilio, R., Ramachandran, S., Sabanay, H., and Lev, S. (2005). Differential regulation of endoplasmic reticulum structure through VAP-Nir protein interaction. J Biol Chem *280*, 5934–5944.

Azuma, K., Tamura, K., Shigenaga, A.-I., Wakui, H., Masuda, S.-I., Tsurumi-Ikeya, Y., Tanaka, Y., Sakai, M., Matsuda, M., Hashimoto, T., et al. (2007). Novel regulatory effect of angiotensin II type 1 receptor-interacting molecule on vascular smooth muscle cells. Hypertension *50*, 926–932.

Ballif, B.A., Villén, J., Beausoleil, S.A., Schwartz, D., and Gygi, S.P. (2004). Phosphoproteomic analysis of the developing mouse brain. Mol Cell Proteomics *3*, 1093–1101.

Bose, H.S., Whittal, R.M., Baldwin, M.A., and Miller, W.L. (1999). The active form of the steroidogenic acute regulatory protein, StAR, appears to be a molten globule. Proc Natl Acad Sci USA *96*, 7250–7255.

Böttger, V., Böttger, A., Garcia-Echeverria, C., Ramos, Y.F., van der Eb, A.J., Jochemsen, A.G., and Lane, D.P. (1999). Comparative study of the p53-mdm2 and p53-MDMX interfaces. Oncogene *18*, 189–199.

Bridges, D. (2004). 14-3-3 Proteins: A Number of Functions for a Numbered Protein. Sci STKE *2004*, re10–re10.

Brill, L.M., Xiong, W., Lee, K.-B., Ficarro, S.B., Crain, A., Xu, Y., Terskikh, A., Snyder, E.Y., and Ding, S. (2009). Phosphoproteomic analysis of human embryonic stem cells. Cell Stem Cell *5*, 204–213.

Bryson, K., McGuffin, L.J., Marsden, R.L., Ward, J.J., Sodhi, J.S., and Jones, D.T. (2005). Protein structure prediction servers at University College London. Nucleic Acids Res *33*, W36–W38.

Bustos, D.M., and Iglesias, A.A. (2006). Intrinsic disorder is a key characteristic in partners that bind 14-3-3 proteins. Proteins *63*, 35–42.

Carillo, S., Pariat, M., Steff, A.M., Jariel-Encontre, I., Poulat, F., Berta, P., and Piechaczyk, M. (1996). PEST motifs are not required for rapid calpain-mediated proteolysis of c-fos protein. Biochem J *313*, 245–251.

Carvou, N., Holic, R., Li, M., Futter, C., Skippen, A., and Cockcroft, S. (2010). Phosphatidylinositol- and phosphatidylcholine-transfer activity of PITP is essential for COPI-mediated retrograde transport from the Golgi to the endoplasmic reticulum. J Cell Sci *123*, 1262–1273.

Chang, J.T., Milligan, S., Li, Y., Chew, C.E., Wiggs, J., Copeland, N.G., Jenkins, N.A., Campochiaro, P.A., Hyde, D.R., and Zack, D.J. (1997). Mammalian homolog of Drosophila retinal degeneration B rescues the mutant fly phenotype. J Neurosci *17*, 5881–5890.

Chehab, N.H., Malikzay, A., Stavridi, E.S., and Halazonetis, T.D. (1999). Phosphorylation of Ser-20 mediates stabilization of human p53 in response to DNA damage. Proc Natl Acad Sci USA *96*, 13777–13782.

Choudhary, C., Olsen, J.V., Brandts, C., Cox, J., Reddy, P.N.G., Bohmer, F.D., Gerke, V., Schmidt-Arras, D.-E., Berdel, W.E., Muller-Tidow, C., et al. (2009). Mislocalized Activation of Oncogenic RTKs Switches Downstream Signaling Outcomes. Mol Cell *36*, 326–339.

Clarke, N.G., and Dawson, R.M. (1981). Alkaline O leads to N-transacylation. A new method for the quantitative deacylation of phospholipids. Biochem J *195*, 301–306.

Cook, J.L., Mills, S.J., Naquin, R.T., Alam, J., and Re, R.N. (2006). Cleavage of the angiotensin II type 1 receptor and nuclear accumulation of the cytoplasmic carboxy-terminal fragment. AJP: Cell Physiology *292*, C1313–C1322.

Cosker, K.E., Shadan, S., van Diepen, M., Morgan, C., Li, M., Allen-Baume, V., Hobbs, C., Doherty, P., Cockcroft, S., and Eickholt, B.J. (2008). Regulation of PI3K signalling by the phosphatidylinositol transfer protein PITP during axonal extension in hippocampal neurons. J Cell Sci *121*, 796–803.

Cuff, A.L., and Martin, A.C.R. (2004). Analysis of void volumes in proteins and application to stability of the p53 tumour suppressor protein. J Mol Biol *344*, 1199–1209.

Cui, T., Nakagami, H., Iwai, M., Takeda, Y., Shiuchi, T., Tamura, K., Daviet, L., and Horiuchi, M. (2000). ATRAP, novel AT1 receptor associated protein, enhances internalization of AT1 receptor and inhibits vascular smooth muscle cell growth. Biochem Biophys Res Commun *279*, 938–941.

Cunningham, E., Tan, S.K., Swigart, P., Hsuan, J., Bankaitis, V., and Cockcroft, S. (1996). The yeast and mammalian isoforms of phosphatidylinositol transfer protein can all restore phospholipase C-mediated inositol lipid signaling in cytosol-depleted RBL-2H3 and HL-60 cells. Proc Natl Acad Sci USA *93*, 6589–6593.

Cunningham, E., Thomas, G.M., Ball, A., Hiles, I., and Cockcroft, S. (1995). Phosphatidylinositol transfer protein dictates the rate of inositol trisphosphate production by promoting the synthesis of PIP2. Curr Biol *5*, 775–783.

Currie, R.A., MacLeod, B.M., and Downes, C.P. (1997). The lipid transfer activity of phosphatidylinositol transfer protein is sufficient to account for enhanced phospholipase C activity in turkey erythrocyte ghosts. Curr Biol *7*, 184–190.

Daviet, L., Lehtonen, J.Y., Tamura, K., Griese, D.P., Horiuchi, M., and Dzau, V.J. (1999). Cloning and characterization of ATRAP, a novel protein that interacts with the angiotensin II type 1 receptor. J Biol Chem *274*, 17058–17062.

de Vries, K.J., Heinrichs, A.A., Cunningham, E., Brunink, F., Westerman, J., Somerharju, P.J., Cockcroft, S., Wirtz, K.W., and Snoek, G.T. (1995). An isoform of the phosphatidylinositol-transfer protein transfers sphingomyelin and is associated with the Golgi system. Biochem J *310*, 643–649.

de Vries, K.J., Westerman, J., Bastiaens, P.I., Jovin, T.M., Wirtz, K.W., and Snoek, G.T. (1996). Fluorescently labeled phosphatidylinositol transfer protein isoforms (alpha and beta), microinjected into fetal bovine heart endothelial cells, are targeted to distinct intracellular sites. Exp Cell Res *227*, 33–39.

Deng, Y., Golinelli-Cohen, M.-P., Smirnova, E., and Jackson, C.L. (2009). A COPI coat subunit interacts directly with an early-Golgi localized Arf exchange factor. EMBO Rep. *10*, 58–64.

Du, G., Huang, P., Liang, B.T., and Frohman, M.A. (2004). Phospholipase D2 localizes to the plasma membrane and regulates angiotensin II receptor endocytosis. Mol Biol Cell *15*, 1024–1030.

Dumaresq-Doiron, K., Savard, M.-F., Akam, S., Costantino, S., and Lefrancois, S. (2010). The phosphatidylinositol 4-kinase PI4KIIIalpha is required for the recruitment of GBF1 to Golgi membranes. J Cell Sci *123*, 2273–2280.

Elia, A.E.H., Cantley, L.C., and Yaffe, M.B. (2003a). Proteomic Screen Finds pSer/pThr-Binding Domain Localizing Plk1 to Mitotic Substrates. Science *299*, 1228–1231.

Elia, A.E.H., Rellos, P., Haire, L.F., Chao, J.W., Ivins, F.J., Hoepker, K., Mohammad, D., Cantley, L.C., Smerdon, S.J., and Yaffe, M.B. (2003b). The molecular basis for phosphodependent substrate targeting and regulation of Plks by the Polo-box domain. Cell *115*, 83–95.

Eswar, N., Webb, B., Marti-Renom, M.A., Madhusudhan, M.S., Eramian, D., Shen, M.-Y., Pieper, U., and Sali, A. (2006). Comparative protein structure modeling using Modeller. Current Protocols in Bioinformatics / Editoral Board, Andreas D Baxevanis [Et Al] *Chapter 5*, Unit 5.6.

Fensome, A., Cunningham, E., Prosser, S., Tan, S.K., Swigart, P., Thomas, G., Hsuan, J., and Cockcroft, S. (1996). ARF and PITP restore GTP gamma S-stimulated protein secretion from cytosol-depleted HL60 cells by promoting PIP2 synthesis. Curr Biol *6*, 730–738.

Fullwood, Y., Santos, dos, M., and Hsuan, J.J. (1999). Cloning and characterization of a novel human phosphatidylinositol transfer protein, rdgBbeta. J Biol Chem *274*, 31553–31558.

Garner, K., Li, M., Ugwuanya, N., and Cockcroft, S. (2011). The phosphatidylinositol transfer protein RdgBβ binds 14-3-3 via its unstructured C-terminus, whereas its lipid-

binding domain interacts with the integral membrane protein ATRAP (angiotensin II type I receptor-associated protein). Biochem J *439*, 97–111.

Gasteiger, E. (2003). ExPASy: the proteomics server for in-depth protein knowledge and analysis. Nucleic Acids Res *31*, 3784–3788.

Geny, B., and Cockcroft, S. (1992). Synergistic activation of phospholipase D by protein kinase C- and G-protein-mediated pathways in streptolysin O-permeabilized HL60 cells. Biochem J *284*, 531–538.

Giansanti, M.G., Bonaccorsi, S., Kurek, R., Farkas, R.M., Dimitri, P., Fuller, M.T., and Gatti, M. (2006). The class I PITP giotto is required for Drosophila cytokinesis. Curr Biol *16*, 195–201.

Gibellini, F., and Smith, T.K. (2010). The Kennedy pathway-De novo synthesis of phosphatidylethanolamine and phosphatidylcholine. IUBMB Life *62*, 414–428.

Gillooly, D.J., Morrow, I.C., Lindsay, M., Gould, R., Bryant, N.J., Gaullier, J.M., Parton, R.G., and Stenmark, H. (2000). Localization of phosphatidylinositol 3-phosphate in yeast and mammalian cells. Embo J *19*, 4577–4588.

Glickman, M.H., and Ciechanover, A. (2002). The ubiquitin-proteasome proteolytic pathway: destruction for the sake of construction. Physiol Rev *82*, 373–428.

Goldberg, A.L., and Dice, J.F. (1974). Intracellular protein degradation in mammalian and bacterial cells. Annu Rev Biochem *43*, 835–869.

Gu, Y.-M., Jin, Y.-H., Choi, J.-K., Baek, K.-H., Yeo, C.-Y., and Lee, K.-Y. (2006). Protein kinase A phosphorylates and regulates dimerization of 14-3-3 epsilon. FEBS Lett *580*, 305–310.

Guo, S., Lopez-Ilasaca, M., and Dzau, V.J. (2005). Identification of calcium-modulating cyclophilin ligand (CAML) as transducer of angiotensin II-mediated nuclear factor of activated T cells (NFAT) activation. J Biol Chem *280*, 12536–12541.

Hamilton, B.A., Smith, D.J., Mueller, K.L., Kerrebrock, A.W., Bronson, R.T., van Berkel, V., Daly, M.J., Kruglyak, L., Reeve, M.P., Nemhauser, J.L., et al. (1997). The

vibrator mutation causes neurodegeneration via reduced expression of PITP alpha: positional complementation cloning and extragenic suppression. Neuron *18*, 711–722.

Hara, S., Swigart, P., Jones, D., and Cockcroft, S. (1997). The first 5 amino acids of the carboxyl terminus of phosphatidylinositol transfer protein (PITP) alpha play a critical role in inositol lipid signaling. Transfer activity of PITP is essential but not sufficient for restoration of phospholipase C signaling. J Biol Chem *272*, 14908–14913.

Hardie, R.C., Raghu, P., Moore, S., Juusola, M., Baines, R.A., and Sweeney, S.T. (2001). Calcium influx via TRP channels is required to maintain PIP2 levels in Drosophila photoreceptors. Neuron *30*, 149–159.

Hay, J.C., and Martin, T.F. (1993). Phosphatidylinositol transfer protein required for ATP-dependent priming of Ca(2+)-activated secretion. Nature *366*, 572–575.

Hay, J.C., Fisette, P.L., Jenkins, G.H., Fukami, K., Takenawa, T., Anderson, R.A., and Martin, T.F. (1995). ATP-dependent inositide phosphorylation required for Ca(2+)-activated secretion. Nature *374*, 173–177.

Helmkamp, G.M., Harvey, M.S., Wirtz, K.W., and Van Deenen, L.L. (1974). Phospholipid exchange between membranes. Purification of bovine brain proteins that preferentially catalyze the transfer of phosphatidylinositol. J Biol Chem *249*, 6382–6389.

Hornbeck, P.V., Chabra, I., Kornhauser, J.M., Skrzypek, E., and Zhang, B. (2004). PhosphoSite: A bioinformatics resource dedicated to physiological protein phosphorylation. Proteomics *4*, 1551–1561.

Hotta, Y., and Benzer, S. (1969). Abnormal electroretinograms in visual mutants of Drosophila. Nature *222*, 354–356.

Huang, F.L., Yoshida, Y., Cunha-Melo, J.R., Beaven, M.A., and Huang, K.P. (1989). Differential down-regulation of protein kinase C isozymes. J Biol Chem *264*, 4238–4243.

Hunt, A.N., Skippen, A.J., Koster, G., Postle, A.D., and Cockcroft, S. (2004). Acyl chain-based molecular selectivity for HL60 cellular phosphatidylinositol and of

phosphatidylcholine by phosphatidylinositol transfer protein alpha. Biochim Biophys Acta *1686*, 50–60.

Hunyady, L., Baukal, A.J., Gaborik, Z., Olivares-Reyes, J.A., Bor, M., Szaszak, M., Lodge, R., Catt, K.J., and Balla, T. (2002). Differential PI 3-kinase dependence of early and late phases of recycling of the internalized AT1 angiotensin receptor. J Cell Biol *157*, 1211–1222.

Huttlin, E.L., Jedrychowski, M.P., Elias, J.E., Goswami, T., Rad, R., Beausoleil, S.A., Villén, J., Haas, W., Sowa, M.E., and Gygi, S.P. (2010). A Tissue-Specific Atlas of Mouse Protein Phosphorylation and Expression. Cell *143*, 1174–1189.

Ishidate, K. (1997). Choline/ethanolamine kinase from mammalian tissues. Biochim Biophys Acta *1348*, 70–78.

Iwata, R., Oda, S., Kunitomo, H., and Iino, Y. (2011). Roles for class IIA phosphatidylinositol transfer protein in neurotransmission and behavioral plasticity at the sensory neuron synapses of Caenorhabditis elegans. Proc Natl Acad Sci U S A *108*, 7589-94.

Jenkins, G.H., Fisette, P.L., and Anderson, R.A. (1994). Type I phosphatidylinositol 4-phosphate 5-kinase isoforms are specifically stimulated by phosphatidic acid. J Biol Chem *269*, 11547–11554.

Kauffmann-Zeh, A., Thomas, G.M., Ball, A., Prosser, S., Cunningham, E., Cockcroft, S., and Hsuan, J.J. (1995). Requirement for phosphatidylinositol transfer protein in epidermal growth factor signaling. Science *268*, 1188–1190.

Kostelecky, B., Saurin, A.T., Purkiss, A., Parker, P.J., and McDonald, N.Q. (2009). Recognition of an intra-chain tandem 14-3-3 binding site within PKCepsilon. EMBO Reports *10*, 983–989.

Kular, G., Loubtchenkov, M., Swigart, P., Whatmore, J., Ball, A., Cockcroft, S., and Wetzker, R. (1997). Co-operation of phosphatidylinositol transfer protein with phosphoinositide 3-kinase gamma in the formylmethionyl-leucylphenylalanine-dependent production of phosphatidylinositol 3,4,5-trisphosphate in human neutrophils. Biochem J *325*, 299–301.

Lal, A., Haynes, S.R., and Gorospe, M. (2005). Clean Western blot signals from immunoprecipitated samples. Mol Cell Probes *19*, 385–388.

Larijani, B., Allen-Baume, V., Morgan, C.P., Li, M., and Cockcroft, S. (2003). EGF regulation of PITP dynamics is blocked by inhibitors of phospholipase C and of the Ras-MAP kinase pathway. Curr Biol *13*, 78–84.

Laskowski, R.A. (2009). PDBsum new things. Nucleic Acids Res *37*, D355–D359.

Lee, C.S., Kim, I.S., Park, J.B., Lee, M.N., Lee, H.Y., Suh, P.-G., and Ryu, S.H. (2006). The phox homology domain of phospholipase D activates dynamin GTPase activity and accelerates EGFR endocytosis. Nat Cell Biol *8*, 477–484.

Lee, S.-J., Xu, H., Kang, L.-W., Amzel, L.M., and Montell, C. (2003). Light Adaptation through Phosphoinositide-Regulated Translocation of Drosophila Visual Arrestin. Neuron *39*, 121–132.

Lev, S., Hernandez, J., Martinez, R., Chen, A., Plowman, G., and Schlessinger, J. (1999). Identification of a novel family of targets of PYK2 related to Drosophila retinal degeneration B (rdgB) protein. Mol Cell Biol *19*, 2278–2288.

Litvak, V., Dahan, N., Ramachandran, S., Sabanay, H., and Lev, S. (2005). Maintenance of the diacylglycerol level in the Golgi apparatus by the Nir2 protein is critical for Golgi secretory function. Nat Cell Biol *7*, 225–234.

Litvak, V., Shaul, Y.D., Shulewitz, M., Amarilio, R., Carmon, S., and Lev, S. (2002). Targeting of Nir2 to lipid droplets is regulated by a specific threonine residue within its PI-transfer domain. Curr Biol *12*, 1513–1518.

Liu, D., Bienkowska, J., Petosa, C., Collier, R.J., Fu, H., and Liddington, R. (1995). Crystal structure of the zeta isoform of the 14-3-3 protein. Nature *376*, 191–194.

Liu, F., and Walters, K.J. (2010). Multitasking with ubiquitin through multivalent interactions. Trends Biochem Sci *35*, 352–360.

Loewen, C.J.R., Roy, A., and Levine, T.P. (2003). A conserved ER targeting motif in three families of lipid binding proteins and in Opi1p binds VAP. Embo J *22*, 2025–2035.

Lopez-Ilasaca, M., Liu, X., Tamura, K., and Dzau, V.J. (2003). The angiotensin II type I receptor-associated protein, ATRAP, is a transmembrane protein and a modulator of angiotensin II signaling. Mol Biol Cell *14*, 5038–5050.

Lu, C., Peng, Y.W., Shang, J., Pawlyk, B.S., Yu, F., and Li, T. (2001). The mammalian retinal degeneration B2 gene is not required for photoreceptor function and survival. Neuroscience *107*, 35–41.

Lu, C., Vihtelic, T.S., Hyde, D.R., and Li, T. (1999a). A neuronal-specific mammalian homolog of the Drosophila retinal degeneration B gene with expression restricted to the retina and dentate gyrus. J Neurosci *19*, 7317–7325.

Lu, P.-J., Zhou, X.Z., Shen, M., and Lu, K.P. (1999b). Function of WW Domains as Phosphoserine- or Phosphothreonine-Binding Modules. Science *283*, 1325–1328.

Macias, M.J., Wiesner, S., and Sudol, M. (2002). WW and SH3 domains, two different scaffolds to recognize proline-rich ligands. FEBS Lett *513*, 30–37.

MacKintosh, C. (2004). Dynamic interactions between 14-3-3 proteins and phosphoproteins regulate diverse cellular processes. Biochem J *381*, 329–342.

Martiny-Baron, G., Kazanietz, M.G., Mischak, H., Blumberg, P.M., Kochs, G., Hug, H., Marmé, D., and Schächtele, C. (1993). Selective inhibition of protein kinase C isozymes by the indolocarbazole Gö 6976. J Biol Chem *268*, 9194–9197.

Matsuda, M., Tamura, K., Wakui, H., Dejima, T., Maeda, A., Ohsawa, M., Kanaoka, T., Haku, S., Azushima, K., Yamasaki, H., et al. (2011). Involvement of Runx3 in the basal transcriptional activation of the mouse angiotensin II type 1 receptor-associated protein gene. Physiol Genomics *43*, 884–894.

McCahill, A., Warwicker, J., Bolger, G.B., Houslay, M.D., and Yarwood, S.J. (2002). The RACK1 scaffold protein: a dynamic cog in cell response mechanisms. Mol Pharmacol *62*, 1261–1273.

Miller, K.G., Emerson, M.D., and Rand, J.B. (1999). Goalpha and diacylglycerol kinase negatively regulate the Gqalpha pathway in C. elegans. Neuron *24*, 323–333.

Milligan, S.C., Alb, J.G., Elagina, R.B., Bankaitis, V.A., and Hyde, D.R. (1997). The phosphatidylinositol transfer protein domain of Drosophila retinal degeneration B protein is essential for photoreceptor cell survival and recovery from light stimulation. J Cell Biol *139*, 351–363.

Min, L.-J., Mogi, M., Tamura, K., Iwanami, J., Sakata, A., Fujita, T., Tsukuda, K., Jing, F., Iwai, M., and Horiuchi, M. (2009). Angiotensin II type 1 receptor-associated protein prevents vascular smooth muscle cell senescence via inactivation of calcineurin/nuclear factor of activated T cells pathway. J Mol Cell Cardiol *47*, 798–809.

Ming, G., Song, H., Berninger, B., Inagaki, N., Tessier-Lavigne, M., and Poo, M. (1999). Phospholipase C-gamma and phosphoinositide 3-kinase mediate cytoplasmic signaling in nerve growth cone guidance. Neuron *23*, 139–148.

Mochly-Rosen, D., Khaner, H., and Lopez, J. (1991). Identification of intracellular receptor proteins for activated protein kinase C. Proc Natl Acad Sci USA *88*, 3997–4000.

Mogensen, J.E., Ferreras, M., Wimmer, R., Petersen, S.V., Enghild, J.J., and Otzen, D.E. (2007). The Major Allergen from Birch Tree Pollen, Bet v 1, Binds and Permeabilizes Membranes †. Biochemistry *46*, 3356–3365.

Moorhead, G., Douglas, P., Cotelle, V., Harthill, J., Morrice, N., Meek, S., Deiting, U., Stitt, M., Scarabel, M., Aitken, A., et al. (1999). Phosphorylation-dependent interactions between enzymes of plant metabolism and 14-3-3 proteins. Plant J *18*, 1–12.

Morgan, C.P., Allen-Baume, V., Radulovic, M., Li, M., Skippen, A., and Cockcroft, S. (2006). Differential expression of a C-terminal splice variant of phosphatidylinositol transfer protein β lacking the constitutive-phosphorylated Ser262 that localizes to the Golgi compartment. Biochem J *398*, 411.

Morgan, C.P., Skippen, A., Segui, B., Ball, A., Allen-Baume, V., Larijani, B., Murray-Rust, J., McDonald, N.Q., Sapkota, G., Morrice, N., et al. (2004). Phosphorylation of a Distinct Structural Form of Phosphatidylinositol Transfer Protein at Ser166 by Protein Kinase C Disrupts Receptor-mediated Phospholipase C Signaling by Inhibiting Delivery

of Phosphatidylinositol to Membranes. Journal of Biological Chemistry *279*, 47159–47171.

Moritz, A., Li, Y., Guo, A., Villen, J., Wang, Y., MacNeill, J., Kornhauser, J., Sprott, K., Zhou, J., Possemato, A., et al. (2010). Akt-RSK-S6 Kinase Signaling Networks Activated by Oncogenic Receptor Tyrosine Kinases. Science Signaling *3*, ra64–ra64.

Nurrish, S., Ségalat, L., and Kaplan, J.M. (1999). Serotonin inhibition of synaptic transmission: Galpha(0) decreases the abundance of UNC-13 at release sites. Neuron *24*, 231–242.

Obenauer, J.C., Cantley, L.C., and Yaffe, M.B. (2003). Scansite 2.0: Proteome-wide prediction of cell signaling interactions using short sequence motifs. Nucleic Acids Res *31*, 3635–3641.

Ohashi, M., and Huttner, W.B. (1994). An elevation of cytosolic protein phosphorylation modulates trimeric G-protein regulation of secretory vesicle formation from the trans-Golgi network. J Biol Chem *269*, 24897–24905.

Ohashi, M., Jan de Vries, K., Frank, R., Snoek, G., Bankaitis, V., Wirtz, K., and Huttner, W.B. (1995). A role for phosphatidylinositol transfer protein in secretory vesicle formation. Nature *377*, 544–547.

Oppermann, M., Gess, B., Schweda, F., and Castrop, H. (2010). Atrap deficiency increases arterial blood pressure and plasma volume. Journal of the American Society of Nephrology *21*, 468–477.

Oshita, A., Iwai, M., Chen, R., Ide, A., Okumura, M., Fukunaga, S., Yoshii, T., Mogi, M., Higaki, J., and Horiuchi, M. (2006). Attenuation of inflammatory vascular remodeling by angiotensin II type 1 receptor-associated protein. Hypertension *48*, 671–676.

Panaretou, C., Domin, J., Cockcroft, S., and Waterfield, M.D. (1997). Characterization of p150, an adaptor protein for the human phosphatidylinositol (PtdIns) 3-kinase. Substrate presentation by phosphatidylinositol transfer protein to the p150.Ptdins 3-kinase complex. J Biol Chem *272*, 2477–2485.

Peretti, D., Dahan, N., Shimoni, E., Hirschberg, K., and Lev, S. (2008). Coordinated lipid transfer between the endoplasmic reticulum and the Golgi complex requires the VAP proteins and is essential for Golgi-mediated transport. Mol Biol Cell *19*, 3871–3884.

Perry, R.J., and Ridgway, N.D. (2006). Oxysterol-binding protein and vesicle-associated membrane protein-associated protein are required for sterol-dependent activation of the ceramide transport protein. Mol Biol Cell *17*, 2604–2616.

Phillips, S.E., Ile, K.E., Boukhelifa, M., Huijbregts, R.P.H., and Bankaitis, V.A. (2006). Specific and nonspecific membrane-binding determinants cooperate in targeting phosphatidylinositol transfer protein beta-isoform to the mammalian trans-Golgi network. Mol Biol Cell *17*, 2498–2512.

Pike, L.J., and Casey, L. (1996). Localization and turnover of phosphatidylinositol 4,5-bisphosphate in caveolin-enriched membrane domains. J Biol Chem *271*, 26453–26456.

Prakash, S., Inobe, T., Hatch, A.J., and Matouschek, A. (2008). Substrate selection by the proteasome during degradation of protein complexes. Nat Chem Biol *5*, 29–36.

Prosser, S., Sarra, R., Swigart, P., Ball, A., and Cockcroft, S. (1997). Deletion of 24 amino acids from the C-terminus of phosphatidylinositol transfer protein causes loss of phospholipase C-mediated inositol lipid signalling. Biochem J *324*, 19–23.

Rechsteiner, M., and Rogers, S.W. (1996). PEST sequences and regulation by proteolysis. Trends Biochem Sci *21*, 267–271.

Rodriguez, M., Yu, X., Chen, J., and Songyang, Z. (2003). Phosphopeptide Binding Specificities of BRCA1 COOH-terminal (BRCT) Domains. Journal of Biological Chemistry *278*, 52914–52918.

Rogers, S., Wells, R., and Rechsteiner, M. (1986). Amino acid sequences common to rapidly degraded proteins: the PEST hypothesis. Science *234*, 364–368.

Rogers, T.B., Gaa, S.T., Massey, C., and Dösemeci, A. (1990). Protein kinase C inhibits Ca2+ accumulation in cardiac sarcoplasmic reticulum. J Biol Chem *265*, 4302–4308.

Rolli-Derkinderen, M., Sauzeau, V., Boyer, L., Lemichez, E., Baron, C., Henrion, D., Loirand, G., and Pacaud, P. (2005). Phosphorylation of serine 188 protects RhoA from ubiquitin/proteasome-mediated degradation in vascular smooth muscle cells. Circ Res *96*, 1152–1160.

Rual, J.-F., Venkatesan, K., Hao, T., Hirozane-Kishikawa, T., Dricot, A., Li, N., Berriz, G.F., Gibbons, F.D., Dreze, M., Ayivi-Guedehoussou, N., et al. (2005). Towards a proteome-scale map of the human protein–protein interaction network. Nature *437*, 1173–1178.

Sadoshima, J., and Izumo, S. (1993). Signal transduction pathways of angiotensin II--induced c-fos gene expression in cardiac myocytes in vitro. Roles of phospholipid-derived second messengers. Circ Res *73*, 424–438.

Sambrook, J. (2001). Molecular Cloning: A Laboratory Manual, Third Edition (3 Volume Set) (Cold Spring Harbor Laboratory Press).

Schäffer, A.A., Aravind, L., Madden, T.L., Shavirin, S., Spouge, J.L., Wolf, Y.I., Koonin, E.V., and Altschul, S.F. (2001). Improving the accuracy of PSI-BLAST protein database searches with composition-based statistics and other refinements. Nucleic Acids Res *29*, 2994–3005.

Schermoly, M.J., and Helmkamp, G.M. (1983). The inactivity of brain phospholipid transfer protein toward phosphatidylinositol 4-phosphate. Brain Res. *268*, 197–200.

Schouten, A., Agianian, B., Westerman, J., Kroon, J., Wirtz, K.W.A., and Gros, P. (2002). Structure of apo-phosphatidylinositol transfer protein alpha provides insight into membrane association. Embo J *21*, 2117–2121.

Shadan, S., Holic, R., Carvou, N., Ee, P., Li, M., Murray-Rust, J., and Cockcroft, S. (2008). Dynamics of lipid transfer by phosphatidylinositol transfer proteins in cells. Traffic *9*, 1743–1756.

Skippen, A., Jones, D.H., Morgan, C.P., Li, M., and Cockcroft, S. (2002). Mechanism of ADP ribosylation factor-stimulated phosphatidylinositol 4,5-bisphosphate synthesis in HL60 cells. J Biol Chem *277*, 5823-5831.

Smith, R.D., Baukal, A.J., Zolyomi, A., Gaborik, Z., Hunyady, L., Sun, L., Zhang, M., Chen, H.C., and Catt, K.J. (1998). Agonist-induced phosphorylation of the endogenous AT1 angiotensin receptor in bovine adrenal glomerulosa cells. Mol Endocrinol *12*, 634–644.

Speed, C.J., and Mitchell, C.A. (2000). Sustained elevation in inositol 1,4,5-trisphosphate results in inhibition of phosphatidylinositol transfer protein activity and chronic depletion of the agonist-sensitive phosphoinositide pool. J Cell Sci *113*, 2631–2638.

Speed, C.J., Neylon, C.B., Little, P.J., and Mitchell, C.A. (1999). Underexpression of the 43 kDa inositol polyphosphate 5-phosphatase is associated with spontaneous calcium oscillations and enhanced calcium responses following endothelin-1 stimulation. J Cell Sci *112*, 669–679.

Stutchfield, J., and Cockcroft, S. (1988). Guanine nucleotides stimulate polyphosphoinositide phosphodiesterase and exocytotic secretion from HL60 cells permeabilized with streptolysin O. Biochem J *250*, 375–382.

Sudol, M. (1996). The WW module competes with the SH3 domain? Trends Biochem Sci *21*, 161–163.

Takano, N., Owada, Y., Suzuki, R., Sakagami, H., Shimosegawa, T., and Kondo, H. (2003). Cloning and characterization of a novel variant (mM-rdgBbeta1) of mouse M-rdgBs, mammalian homologs of Drosophila retinal degeneration B gene proteins, and its mRNA localization in mouse brain in comparison with other M-rdgBs. J Neurochem *84*, 829–839.

Tanaka, S., and Hosaka, K. (1994). Cloning of a cDNA encoding a second phosphatidylinositol transfer protein of rat brain by complementation of the yeast sec14 mutation. J Biochem *115*, 981–984.

Tanaka, Y., Tamura, K., Koide, Y., Sakai, M., Tsurumi, Y., Noda, Y., Umemura, M., Ishigami, T., Uchino, K., Kimura, K., et al. (2005). The novel angiotensin II type 1 receptor (AT1R)-associated protein ATRAP downregulates AT1R and ameliorates cardiomyocyte hypertrophy. FEBS Lett *579*, 1579–1586.

Tang, H., Guo, D.F., Porter, J.P., Wanaka, Y., and Inagami, T. (1998). Role of cytoplasmic tail of the type 1A angiotensin II receptor in agonist- and phorbol ester-induced desensitization. Circ Res *82*, 523–531.

Thomas, G.M., Cunningham, E., Fensome, A., Ball, A., Totty, N.F., Truong, O., Hsuan, J.J., and Cockcroft, S. (1993). An essential role for phosphatidylinositol transfer protein in phospholipase C-mediated inositol lipid signaling. Cell *74*, 919–928.

Thomas, G.M., Geny, B., and Cockcroft, S. (1991). Identification of a novel cytosolic poly-phosphoinositide-specific phospholipase C (PLC-86) as the major G-protein-regulated enzyme. Embo J *10*, 2507–2512.

Tilley, S.J., Skippen, A., Murray-Rust, J., Swigart, P.M., Stewart, A., Morgan, C.P., Cockcroft, S., and McDonald, N.Q. (2004). Structure-function analysis of human phosphatidylinositol transfer protein alpha bound to phosphatidylinositol. Structure *12*, 317–326.

Touyz, R.M., and Berry, C. (2002). Recent advances in angiotensin II signaling. Braz. J. Med. Biol. Res. *35*, 1001–1015.

Tremblay, J.M., Helmkamp, G.M., and Yarbrough, L.R. (1996). Limited proteolysis of rat phosphatidylinositol transfer protein by trypsin cleaves the C terminus, enhances binding to lipid vesicles, and reduces phospholipid transfer activity. J Biol Chem *271*, 21075–21080.

Tremblay, J.M., Voziyan, P.A., Helmkamp, G.M., and Yarbrough, L.R. (1998). The C-terminus of phosphatidylinositol transfer protein modulates membrane interactions and transfer activity but not phospholipid binding. Biochim Biophys Acta *1389*, 91–100.

Tsurumi, Y., Tamura, K., Tanaka, Y., Koide, Y., Sakai, M., Yabana, M., Noda, Y., Hashimoto, T., Kihara, M., Hirawa, N., et al. (2006). Interacting molecule of AT1 receptor, ATRAP, is colocalized with AT1 receptor in the mouse renal tubules. Kidney Int. *69*, 488–494.

Turu, G., Szidonya, L., Gaborik, Z., Buday, L., Spat, A., Clark, A.J., and Hunyady, L. (2006). Differential β-arrestin binding of AT1 and AT2 angiotensin receptors. FEBS Lett *580*, 41–45.

Ushio-Fukai, M., Alexander, R.W., Akers, M., Lyons, P.R., Lassègue, B., and Griendling, K.K. (1999). Angiotensin II receptor coupling to phospholipase D is mediated by the betagamma subunits of heterotrimeric G proteins in vascular smooth muscle cells. Mol Pharmacol *55*, 142–149.

van Paridon, P.A., Gadella, T.W., Somerharju, P.J., and Wirtz, K.W. (1987a). On the relationship between the dual specificity of the bovine brain phosphatidylinositol transfer protein and membrane phosphatidylinositol levels. Biochim Biophys Acta *903*, 68–77.

van Paridon, P.A., Gadella, T.W., Somerharju, P.J., and Wirtz, K.W. (1988). Properties of the binding sites for the sn-1 and sn-2 acyl chains on the phosphatidylinositol transfer protein from bovine brain. Biochemistry *27*, 6208–6214.

van Paridon, P.A., Visser, A.J., and Wirtz, K.W. (1987b). Binding of phospholipids to the phosphatidylinositol transfer protein from bovine brain as studied by steady-state and time-resolved fluorescence spectroscopy. Biochim Biophys Acta *898*, 172–180.

van Tiel, C.M., Westerman, J., Paasman, M.A., Hoebens, M.M., Wirtz, K.W.A., and Snoek, G.T. (2002). The Golgi localization of phosphatidylinositol transfer protein beta requires the protein kinase C-dependent phosphorylation of serine 262 and is essential for maintaining plasma membrane sphingomyelin levels. J Biol Chem *277*, 22447–22452.

van Tiel, C.M., Westerman, J., Paasman, M.A., Wirtz, K.W.A., and Snoek, G.T. (2000). The Protein Kinase C-dependent Phosphorylation of Serine 166 Is Controlled by the Phospholipid Species Bound to the Phosphatidylinositol Transfer Protein alpha. J Biol Chem *275*, 21532–21538.

Venkatesan, K., Rual, J.-F., Vazquez, A., Stelzl, U., Lemmens, I., Hirozane-Kishikawa, T., Hao, T., Zenkner, M., Xin, X., Goh, K.-I., et al. (2009). An empirical framework for binary interactome mapping. Nat Methods *6*, 83–90.

Vihtelic, T.S., Goebl, M., Milligan, S., O'Tousa, J.E., and Hyde, D.R. (1993). Localization of Drosophila retinal degeneration B, a membrane-associated phosphatidylinositol transfer protein. J Cell Biol *122*, 1013–1022.

Vihtelic, T.S., Hyde, D.R., and O'Tousa, J.E. (1991). Isolation and characterization of the Drosophila retinal degeneration B (rdgB) gene. Genetics *127*, 761–768.

Vordtriede, P.B., Doan, C.N., Tremblay, J.M., Helmkamp, G.M., and Yoder, M.D. (2005). Structure of PITPbeta in complex with phosphatidylcholine: comparison of structure and lipid transfer to other PITP isoforms. Biochemistry *44*, 14760–14771.

Wakui, H., Tamura, K., Matsuda, M., Bai, Y., Dejima, T., Shigenaga, A.-I., Masuda, S.-I., Azuma, K., Maeda, A., Hirose, T., et al. (2010a). Intrarenal suppression of angiotensin II type 1 receptor binding molecule in angiotensin II-infused mice. AJP: Renal Physiology *299*, F991–F1003.

Wakui, H., Tamura, K., Tanaka, Y., Matsuda, M., Bai, Y., Dejima, T., Masuda, S.-I., Shigenaga, A.-I., Maeda, A., Mogi, M., et al. (2010b). Cardiac-specific activation of angiotensin II type 1 receptor-associated protein completely suppresses cardiac hypertrophy in chronic angiotensin II-infused mice. Hypertension *55*, 1157–1164.

Walev, I., Bhakdi, S.C., Hofmann, F., Djonder, N., Valeva, A., Aktories, K., and Bhakdi, S. (2001). Delivery of proteins into living cells by reversible membrane permeabilization with streptolysin-O. Proc Natl Acad Sci USA *98*, 3185–3190.

Wallace, A.C., Laskowski, R.A., and Thornton, J.M. (1995). LIGPLOT: a program to generate schematic diagrams of protein-ligand interactions. Protein Eng *8*, 127–134.

Wang, W., Huang, Y., Zhou, Z., Tang, R., Zhao, W., Zeng, L., Xu, M., Cheng, C., Gu, S., Ying, K., et al. (2002). Identification and characterization of AGTRAP, a human homolog of murine Angiotensin II Receptor-Associated Protein (Agtrap). Int J Biochem Cell Biol *34*, 93–102.

Wang, Y.-T., Tsai, C.-F., Hong, T.-C., Tsou, C.-C., Lin, P.-Y., Pan, S.-H., Hong, T.-M., Yang, P.-C., Sung, T.-Y., Hsu, W.-L., et al. (2010). An Informatics-assisted Label-free Quantitation Strategy that Depicts Phosphoproteomic Profiles in Lung Cancer Cell Invasion. J. Proteome Res. *9*, 5582–5597.

Ward, J.J., Sodhi, J.S., McGuffin, L.J., Buxton, B.F., and Jones, D.T. (2004). Prediction and functional analysis of native disorder in proteins from the three kingdoms of life. J Mol Biol *337*, 635–645.

Weimar, W.R., Lane, P.W., and Sidman, R.L. (1982). Vibrator (vb): a spinocerebellar system degeneration with autosomal recessive inheritance in mice. Brain Res. *251*, 357–364.

Westphal, S., Perwitz, N., Iwen, K.A.H., Kraus, D., Schick, R., Fasshauer, M., and Klein, J. (2008). Expression of ATRAP in adipocytes and negative regulation by beta-adrenergic stimulation of JAK/STAT. Horm Metab Res *40*, 165–171.

Wirtz, K.W.A., Schouten, A., and Gros, P. (2006). Phosphatidylinositol transfer proteins: From closed for transport to open for exchange. Advances in Enzyme Regulation *46*, 301–311.

Wiśniewski, J.R., Nagaraj, N., Zougman, A., Gnad, F., and Mann, M. (2010). Brain Phosphoproteome Obtained by a FASP-Based Method Reveals Plasma Membrane Protein Topology. J. Proteome Res. *9*, 3280–3289.

Wu, L., Niemeyer, B., Colley, N., Socolich, M., and Zuker, C.S. (1995). Regulation of PLC-mediated signalling in vivo by CDP-diacylglycerol synthase. Nature *373*, 216–222.

Xiao, B., Smerdon, S.J., Jones, D.H., Dodson, G.G., Soneji, Y., Aitken, A., and Gamblin, S.J. (1995). Structure of a 14-3-3 protein and implications for coordination of multiple signalling pathways. Nature *376*, 188–191.

Xie, Y., Ding, Y.-Q., Hong, Y., Feng, Z., Navarre, S., Xi, C.-X., Zhu, X.-J., Wang, C.-L., Ackerman, S.L., Kozlowski, D., et al. (2005). Phosphatidylinositol transfer protein-α in netrin-1-induced PLC signalling and neurite outgrowth. Nat Cell Biol *7*, 1124-1132.

Yaffe, M.B. (2002). How do 14-3-3 proteins work?-- Gatekeeper phosphorylation and the molecular anvil hypothesis. FEBS Lett *513*, 53–57.

Yaffe, M.B., Rittinger, K., Volinia, S., Caron, P.R., Aitken, A., Leffers, H., Gamblin, S.J., Smerdon, S.J., and Cantley, L.C. (1997). The structural basis for 14-3-3:phosphopeptide binding specificity. Cell *91*, 961–971.

Yang, X., Lee, W.H., Sobott, F., Papagrigoriou, E., Robinson, C.V., Grossmann, J.G., Sundström, M., Doyle, D.A., and Elkins, J.M. (2006). Structural basis for protein-

protein interactions in the 14-3-3 protein family. Proc Natl Acad Sci USA *103*, 17237–17242.

Yau, W.M., Wimley, W.C., Gawrisch, K., and White, S.H. (1998). The preference of tryptophan for membrane interfaces. Biochemistry *37*, 14713–14718.

Yoder, M.D., Thomas, L.M., Tremblay, J.M., Oliver, R.L., Yarbrough, L.R., and Helmkamp, G.M. (2001). Structure of a multifunctional protein. Mammalian phosphatidylinositol transfer protein complexed with phosphatidylcholine. J Biol Chem *276*, 9246–9252.

Zanivan, S., Gnad, F., Wickström, S.A., Geiger, T., Macek, B., Cox, J., Fässler, R., and Mann, M. (2008). Solid Tumor Proteome and Phosphoproteome Analysis by High Resolution Mass Spectrometry. J. Proteome Res. *7*, 5314–5326.